2012

DIFFUSE TRAUMATIC AXONAL INJURY WITHIN THE VISUAL SYSTEM: IMPLICATIONS FOR VISUAL PATHWAY REORGANIZATION

Jiaqiong Wang
Virginia Commonwealth University

DIFFUSE TRAUMATIC AXONAL INJURY WITHIN THE VISUAL SYSTEM: IMPLICATIONS FOR VISUAL PATHWAY REORGANIZATION

A dissertation submitted in partial fulfillment of the requirement of the degree of Doctor of Philosophy at Virginia Commonwealth University.

by

Jiaqiong Wang
M.B., Tongji Medical College of Huazhong University of Science and Technology, 2003
M.S., Nanjing Medical University, 2006

Director: John T. Povlishock, Ph.D.
Professor and Chairman
Department of Anatomy and Neurobiology

Virginia Commonwealth University
Richmond, VA
December, 2012

ACKNOWLEDGEMENT

This research project was carried out under the supervision and guidance of Dr. John T Povlishock. I am grateful to his insights, guidance and encouragement. Since English is not my mother tongue, Dr. Povlishock was very patient with me. He put in much effort to make sure that I reached beyond the level of mediocrity. His generosity gave me the privilege to attend various scientific meeting such as the National Neurotrauma Society and the Society for Neuroscience annual meetings, to learn new knowledge and to meet scientists from other laboratories. I also appreciate his humor in impacting his criticism to me. For example, when I transferred my topic without good transitional sentence, he pointed it out that it was like that travelling in Beijing in one minute and then jumped to New York the next minute. I consider him as a father to me, supporting me all the way, from the time I entered his program to my seeking employment today.

All the people in Dr. Povlishock's lab have been very kind to me and given me tremendous support. For example, Dr. Wei has helped me be a better person. Dr. Melissa McGinn Greer and Dr. John Greer have taught me how to do the craniotomy, the injury, the sacrifice and the perfusion of the animal. Additionally, Dr. John Greer has helped me with phospho-c-Jun immunostaining. Dr. Audrey Lafrenaye has been like a sister, helped me with the preparation of my poster and the presentation on the neurotrauma meetings. Susan A Walker helped me with the immunohistochemical staining and the preparation of electron microscopic samples. Carol Lynn Davis helped me order animals and immunohistochemical staining. Judy C Williamson helped me with electron microscopy. Jesse Sims helped me with the cryosection of tissue and the immunohistochemical staining.

Besides Dr. Povlishock and his lab's support, other professors and doctors also gave me a lot of help during the course of my graduate program.

Specifically, I would like to thank Dr. Scott Henderson, who has given me invaluable instruction with the use of confocal microscope and the guidance of the image analysis.

I would like to thank Dr. Raymond Colello, who taught me the dissection of the optic nerve out of the skull and the cryosection of the optic nerve.

I would like to thank Dr. Michael Fox, who helped me with the preparation of the retina and the immunohistochemical staining of the retina, and the analysis of retinal ganglion cells response to TAI within the optic nerve.

I would like to thank Dr. Michelle Block, who spent a lot of time in guiding me through the immunohistochemical staining of microglia/macrophage and the analysis of their activity following TAI within the optic nerve.

I would like to thank Dr. Robert Hamm, who helped me through the data analysis, specifically the utilization of SPSS software.

I would like to thank all the professors serving as my dissertation committee, specifically Dr. Dong Sun, Dr. Galia R. Abdrakhmanova, Dr. Scott Henderson and Dr. Thomas M. Reeves, for helping me with the accomplishment of this research project.

I would also like to thank Dr. John Bigbee, our current neuroscience program director. Dr. Bigbee was always kind to me in guiding me through the whole Ph.D. training in neuroscience. Whenever I had to make decision on course work at the beginning of each semester, he always gave me good advice.

I would like to thank Dr. Leslie Satin, our previous neuroscience program director, who did a phone interview with me and recruited me from China into our neuroscience program in 2006. In the first year of my Ph.D. training, he guided me through the laboratory rotations. It was Dr. Satin's wise recommendation that I ended up working in Dr. Povlishock's laboratory.

Lastly, I would like to thank my parents. They are in China. They have sent me to America for Ph.D. education since 2006. Every time when I talk with them on the phone, they always encourage me to work hard and to cooperate well with people. They never stop to make me a better person.

This work was supported by grants from the National Institutes of Health, grant number HD055813 and 5P30NS047463.

TABLE OF CONTENTS

LIST OF TABLES

LIST OF FIGURES

LIST OF ABBREVIATIONS

AAD	acute axonal degeneration
ABC	avidin-biotin complex
ANOVA	analysis of variance
ANT	adenine nucleotide translocator
APP	β-amyloid precursor protein
AQP	aquaporin
AST	ascending sensory tract
ATF-3	activating transcription factor 3
atm	atmospheres
ATP	adenosine triphosphate
BBB	blood-brain barrier
BDNF	brain-derived neurotrophic factor
BSA	bovine serum albumin
Ca^{2+}	calcium ion
$[Ca^{2+}]_i$	intracellular calcium ion concentration
CAP	compound action potential
CAP-23	cytoskeleton-associated protein-23
CDC	Centers for Disease Control and Prevention
cFPI	central fluid percussion injury
CMSP	calpain-mediated spectrin proteolysis
CNS	central nervous system
CNTF	ciliary neurotrophic factor
CREB	cAMP response element binding protein
CsA	cyclosporin A
CSF	cerebrospinal fluid
CSPG	chondroitin sulfate proteoglycans
CST	corticospinal tract
CyP-D	cyclophilin D
DAB	diaminobenzidine
DAI	diffuse axonal injury
DBI	diffuse brain injury
DNA	deoxyribonucleic acid
DRG	dorsal root ganglion
DVBIC	the Defense Veterans Brain Injury Center
DVI	diffuse vascular injury
EIF2α	alpha subunit, eukaryotic translation initiation factor 2
EM	electron microscopy (-e, -ic)
FA	fractional anisotropy

FDA	the Food and Drug Administration
GDNF	glial cell derived neurotrophic factor
GFP	green fluorescent protein
H_2O_2	hydrogen peroxide
HRP	horseradish peroxidase
Hsp27	heat shock protein 27
IACUC	the Institutional Animal Care and Use Committee
IFN	interferon
IL	interleukin
IP3	inositol trisphosphate
JIP	JNK interacting protein
JNK	c-Jun N-terminal kinase
kDa	kilodalton
LM	light microscopy (-e, -ic)
LGN	lateral geniculate nucleus
M	molar
µM	micromolar
mM	millimolar
nM	nanomolar
µm	micrometer
mm	millimeter
mg	milligram
µg	microgram
mL	milliliter
M1	macrophage subset, proinflammatory type
M2	macrophage subset, anti-inflammatory type
MAG	myelin-associated glycoprotein
MAP	microtubule-associated protein
MAP1A	microtubule-associated protein 1A
MAP1B	microtubule-associated protein 1B
MAP2	microtubule-associated protein 2
MAPK	mitogen activated protein kinase
MCU	mitochondrial Ca^{2+} uniporter
MEKK	mitogen activated protein kinase kinase kinase
MKK	mitogen activated protein kinase kinase
MLK	mixed lineage kinase
MMP	matrix metalloproteinase
MPT	mitochondrial permeability transition
MPTP	mitochondrial permeability transition pore
mTOR	mammalian target of rapamycin
Na^+	sodium ion
NAA	N-Acetylaspartate
NF	neurofilament
NFC	neurofilament compaction
NGF	nerve growth factor
NGS	normal goat serum

NLS	nuclear localization signal
NO	nitric oxide
O_2	oxygen
OCT	optimal cutting temperature compound
OMgp	oligodendrocyte-myelin glycoprotein
PBS	phosphate buffered saline
p-c-Jun	phosphorylated (Ser63) c-Jun
PiC	the mitochondrial phosphate carrier
PKA	protein kinase A
PKN1	protein kinase N 1
PLC	phospholipase C
PMT	photon multiply tube
PNS	peripheral nervous system
PPAR	peroxisome proliferator activated receptor
PPIase	peptidyl-prolyl cis–trans isomerase
PTEN	phosphatase and tensin homologue
RAG	regeneration associated genes
RER	rough endoplasmic reticulum
RGC	retinal ganglion cell
SBDP	spectrin breakdown product
SCI	spinal cord injury
SEM	standard error of the mean
SER	smooth endoplasmic reticulum
SOCS	suppressor of cytokine signaling
SPRR1A	small proline-repeat protein 1A
TAI	traumatic axonal injury
TBI	traumatic brain injury
TBS	Tris-buffered saline
TdT	terminal deoxynucleotidyl transferase
TEM	transmission electron microscopy
TTX	tetrodotoxin
TUNEL	terminal deoxynucleotide transferase mediated d-UTP nick end labeling
VDAC	voltage dependent anion channel
VGCC	voltage-gated calcium channel
VGSC	voltage-gated sodium channel
WT	wild type
WldS	the slow Wallerian degeneration mutant gene
YFP	yellow fluorescent protein
YFP-16	B6.Cg-Tg(Thy1-YFP)16Jrs/J mouse strain (Jackson Labs)

ABSTRACT

DIFFUSE TRAUMATIC AXONAL INJURY WITHIN THE VISUAL SYSTEM: IMPLICATIONS FOR VISUAL PATHWAY REORGANIZATION

By Jiaqiong Wang, Ph.D. Candidate

A dissertation submitted in partial fulfillment of the requirements for the degree of Doctor of Philosophy at Virginia Commonwealth University

Virginia Commonwealth University, 2012

Major Director: John T. Povlishock, Ph.D.
Professor and Chairman
Department of Anatomy and Neurobiology

Traumatic brain injury is a major health problem with much of its morbidity associated with traumatic axonal injury (TAI). To date, significant insight has been gained into the initiating pathogenesis of TAI. However, the specific anterograde and retrograde sequelae of TAI are poorly understood because the diffuse nature of TAI complicates data analysis. To overcome this limitation, we subjected transgenic mice expressing yellow fluorescent protein (YFP) within the visual system to central fluid percussion injury, and consistently generated diffuse TAI within the optic nerve that could easily be followed in the organized YFP positive fibers. We

demonstrated progressive axonal swelling, disconnection and proximal and distal axonal dieback, with regression and reorganization of the proximal swellings, and the persistence of the distal disconnected and degenerating swellings. Antibodies targeting the C-terminus of amyloid precursor protein, a marker of TAI, mapped to the proximal axonal segments without distal targeting. Antibodies targeting microglia/macrophages, revealed activated microglia/ macrophages closely encompassing the distal disconnected, degenerating axonal segments at 7 - 28 days post injury, suggesting their role in the delayed axonal degeneration. In contrast, in the proximal reorganizing axonal segments, microglia/macrophages appeared less reactive with their processes paralleling preserved axonal profiles. Concomitant with these events, YFP fluorescence quenching also occurred, complicating data analysis. This quenching mapped to Texas-Red-conjugated-IgG immunoreactive loci, suggesting that blood–brain barrier disruption and its attendant edema participated in fluorescence quenching. This was confirmed through antibodies targeting endogenous YFP, which identified the retention of intact axons despite YFP fluorescent loss. Paralleling these events, TAI was not accompanied by retrograde retinal ganglion cell (RGC) death. Specifically, no TUNEL+ or cleaved caspase-3 immunoreactive RGCs were observed from 2 days to 3 months post-TBI. Further, Brn3a immunoreactive RGC quantification revealed no significant RGC loss. This RGC preservation was accompanied by the persistent phospho-c-Jun expression for up to 3 months post-TBI, a finding linked to neuronal survival and potential axonal repair. Parallel ultrastructural study again failed to identify RGC death. Collectively, this study provides unprecedented insight into the evolving pathobiology associated with TAI, and offers advantages for future studies focusing on its therapeutic management and neuronal reorganization.

CHAPTER ONE

GENERAL INTRODUCTION

Traumatic brain injury

Traumatic brain injury (TBI) is a major national and global health problem which leads to death and serious neurological dysfunction. According to Centers for Disease Control and Prevention (CDC), each year in the United States, approximately 1.7 million people suffer from a TBI, resulting in 52,000 deaths, 275,000 hospitalization, and 1,365 million emergency rooms visits. The cost of TBI reached $76.5 billion in the United States in 2000 both directly and indirectly (Coronado et al., 2012; Finkelstein et al., 2006). Similarly, TBI has the high incidence in United Kingdom, Australia, France, Sweden and China (Fearnside and Simpson, 1997). Both males and females are affected by TBI at different ages. These sobering statistics mandate the call for intensive research to increase our understanding of TBI while developing therapeutic strategies to ameliorate the deficits associated with TBI.

TBI is acquired when sudden trauma damages the brain. According to CDC, falls are the primary cause of TBI, which account for 35.2% of injuries. Motor vehicle accidents involving motorcycles, bicycles and pedestrians, compose of 17.3% of total TBI, and they are the biggest cause of TBI-related deaths (31.8%). Other causes originate from blasts (war, terrorism), sports-related accidents (horseback riding, boxing, football and basketball) (Fearnside and Simpson, 1997), suicide, homicide, child abuse, domestic abuse, elder abuse, and natural disasters (Chu et al., 2011; Heather et al., 2012; Lee et al., 2003).

Pathology of Traumatic Brain Injury

Most investigators consider the pathobiology of TBI in the context of focal as well as diffuse change, with the diffuse pathologies being recognized as the major determinants of the adverse outcomes associated with TBI (Povlishock and Katz, 2005). It is accepted that focal brain injury is more likely due to direct contact, while the diffuse brain damage is more likely caused by rapid acceleration / deceleration of the brain during motor vehicle accidents or falls (Graham and Gennarelli, 2000). Focal TBI include cerebral contusion, laceration and hemorrhage (Adams et al., 1980; Gennarelli and Thibault, 1985; Granacher RP, 2007; Hardman and Manoukian, 2002; Huang et al., 2011; Jamieson and Yelland, 1968; Zimmerman and Bilaniuk, 1982). Diffuse TBI refers to non-localized, scattered damage in the brain, including diffuse traumatic axonal injury (TAI), diffuse vascular injury (DVI)(Adams et al., 1980; Iwamura et al., 2012, Pittella and Gusmao, 2003), diffuse hypoxic-ischemic damage (Dietrich et al., 1994; Maxwell et al., 1988 and 1991), and diffuse brain swelling (Aldrich et al., 1992; Donkin and Vink, 2010; Jayakumar et al., 2011; Lang, et al., 1994; Liang et al., 2007; Marmarow, 2007; Unterberg et al., 2004).

Much of the morbidity and mortality associated with TBI are associated with diffuse traumatic axonal injury (Christman et al., 1994; Li et al, 2009; Li et al., 2010; Zemlan et al., 1999). TBI patients who have cognitive impairment, particularly difficulty with memory and information processing, typically reveal the evidence of TAI (Lipton et al., 2008), with the demonstration of TAI in subcortical white matter, corpus callosum and internal capsule in addition to other brain sites (Blumbergs et al., 1989; Graham et al., 2002).

Pathogenesis of Diffuse Traumatic Axonal Injury

Diffuse traumatic axonal injury (TAI) presents in the form of damaged axons scattered throughout the central nervous system (CNS) (Buki and Povlishock, 2006). Despite traditional thought that the diffusely injured axons were torn at the injury moment (Strich, 1956), more recent findings do not support this premise. Rather, it has been demonstrated that diffuse axotomy is associated with transient focal changes in axolemmal permeability (Pettus and Povlishock, 1996), which are related to local calcium dysregulation and subsequent protease-mediated cytoskeletal disruption (Buki et al., 1999) and mitochondrial dysfunction (Buki et al., 2000). Together, these events compromise local axonal transport, result in the focal accumulation of organelles and proteins with progressive axonal swelling, leading to delayed disconnection and downstream Wallerian degeneration (Kelley et al., 2006; Pettus et al., 1994; Povlishock, 1992).

Alteration in axolemmal permeability and calcium dysregulation in TAI

Traditionally, it has been believed that increased axolemmal permeability is the direct result of the shear and tensile injury forces. Early experiments showed that horseradish peroxidase (HRP, molecular weight 40kDa), a tracer normally excluded by axolemma, was present in injured axons which also revealed local neurofilament compaction and microtubule loss as early as 5 minutes post injury (Pettus et al., 1994; Pettus and Povlishock, 1996). These findings supported the premise that axolemmal mechanoporation is responsible for this process with transient membrane pore formation in the initial pathogenesis of axonal damage. In addition to overt local membrane disruption, Kilinc et al (2008, 2009) applied fluid shear stress on cultured CNS neurons, and observed an increased flux of Ca^{2+} as early as 5-30 minutes post injury, which led to the activation of calpain as well as local axonal beading. Interestingly, these events were blocked by Poloxamer 188, a membrane sealing material (Kilinc et al., 2007;

Serbest et al., 2005; Serbest et al., 2006), again suggesting that altered axolemmal permeability precipitated axonal damage.

As noted, increased axonal membrane permeability has been linked to an increased intracellular calcium ion concentration ($[Ca^{2+}]_i$) following injury (Fineman et al., 1993; LaPlaca et al., 1998). One explanation of the rise of intracellular calcium is the influx of calcium from the extracellular space through the axolemmal pores generated at the moment of injury (Büki and Povlishock, 2006; Gennarelli, 1993; Gennarelli et al., 1998). Alternatively, another source for the increased intra-axonal ($[Ca^{2+}]_i$ maybe related to the dysfunction of the calcium store - smooth endoplasmic reticulum (SER) and mitochondrial (Nikolaeva et al., 2005; Stys, 2005; Weber et al., 1999 and 2001). *In vitro* studies using the stretch injured cortical neurons, showed that $[Ca^{2+}]_i$ increased rapidly after injury, the neuronal calcium stores did not respond 15 min after injury, which was prevented by phospholipase C (PLC) inhibitor (Weber et al., 1999 and 2001). *In vitro* ischemia of optic nerve axons has also demonstrated that the release of intra-axonal Ca^{2+} was from the inositol trisphosphate (IP3) receptors and ryanodine receptors on SER, as well as the mitochondrial Na^+/ Ca^{2+} exchanger, all of which were Na^+ - dependent (Nikolaeva et al., 2005; Stys, 2005).

In addition to calcium influx from the mechanoporation and the calcium release from SER and mitochondrial, the observed $[Ca^{2+}]_i$ increase following axonal injury may also be related to an injury induced channelopathy. Employing an *in vitro* unmyelinated axonal stretch injury model, Wolf et al. (2001) observed an immediate increase in intra-axonal calcium after injury that was completely reversed by either tetrodotoxin(TTX) - the sodium channel blocker, ω–conotoxin MVIIC, a voltage-gated calcium channel(VGCC) blocker, or bepridil, a blocker of the Na^+- Ca^{2+} exchanger also participate in decreasing intra-axonal Ca^{2+}. All these studies

indicated that mechanically sensitive Na^+ channels, the VGCCs and the Na^+- Ca^{2+} exchanger are involved in calcium dysregulation. Using the same model, Iwata et al. (2004) observed proteolysis of the NaCh α-subunit at 5 and 20 min after trauma, resulting in persistent elevations in $[Ca^{2+}]_i$. Further, von Reyn et al. (2009) proved that this proteolysis was dependent on Ca^{2+} and calpain activity at 6h after mechanical injury, which is relatively late compared to the early loss of NaCh (Iwata et al., 2004). Despite the proteolysis, there was no fragment formation or internalization, which may contribute to further calcium elevation, subsequent calpain activation and probably later axonal degeneration (Iwata et al., 2004; von Reyn et al., 2009). Of note is the fact that all the results originating from the stretch injury model employed unmyelinated axons *in vitro*. *In vitro*, Reeves et al. (2005) showed significant and sustained depression of the compound action potentials (CAP) associated with the unmyelinated axon population within the rat corpus callosum following fluid percussion injury. This suppression in unmyelinated axons persisted 7 days post injury, while in myelinated axons the CAP recovered to control levels 7 days post injury, suggesting that unmyelinated axons may be more vulnerable to TBI than myelinated axons, and that the corresponding pathogenesis mechanism may be different (Reeves et al., 2005; Reeves et al., 2007). Further investigation is required to determine whether the mechanically sensitive Na^+ channels, the VGCCs and the Na^+- Ca^{2+} exchanger play a role in the pathological change of these *in vivo* unmyelinated axons, similar to those described in the *in vitro* stretch injured unmyelinated fibers.

Calcium-induced calpain-mediated spectrin proteolysis, microtubule disorganization and neurofilament compaction in TAI

Irrespective of the initial causative mechanisms, it is now well appreciated that Ca^{2+} overloading and subsequent activation of proteases and phosphatases, Ca^{2+} -induced proteolytic pathways are pivotal players in the ensuing axonal pathology. Ca^{2+}-activated neutral protease,

calpain, exclusively cleaves the axonal membrane cytoskeleton protein, spectrin. To date, μ-calpain and m-calpain have been identified, although no known difference has been found between their role in trauma. Physiologically, calpain participates in remodeling of cytoskeletal/membrane attachment, cell signaling and synaptic activity (Goll et al., 2003; Wu and Lynch, 2006). Calpain breakdown products have been observed in rat axons of damaged white matter tracts following lateral fluid percussion brain injury (Saatman et al., 1996), in rat spinal cord from contusion injury (Springer et al., 1997), in rat pyramidal tract and medial lemnisci at the level of pontomedullary and cervicolmedullary junction sustaining weight drop injury (Buki et al., 1999), in the rat neocortex, subcortical white matter, corpus callosum, thalamus and hippocampus sustaining moderate midline fluid percussion injury (McGinn et al., 2009; Reeves et al., 2010), as well as in mice optic nerves from stretch injury (Saatman et al., 2003; Serbest et al., 2007). Besides animal studies, calpain-mediated breakdown of the cytoskeleton has also been found in the corpus callosum from patients died of close head injury (McCracken et al., 1999).

In addition to the brain parenchyma, calpain-specific spectrin breakdown products (SBDPs), 150kDa and 145kDa fragments were also found to be elevated in cerebrospinal fluid (CSF). Specifically, the 145kDa SBDPs were increased in rat CSF following moderate midline fluid percussion injury (McGinn et al., 2009). 150kDa and 145kDa SBDPs were found in CSF from severe TBI patients (Farkas et al., 2005; Mondello et al., 2010; Pineda et al., 2007). The mean SBDP densitometry values obtained shortly after TBI were correlated with the severity of injury and the outcome half a year post-injury, suggesting that SBDPs were meaningful clinical biomarker of severe TBI patients (Pineda et al., 2007).

Of note is the fact that the calpain mediated spectrin proteolysis (CMSP) has been identified in the subaxolemmal domain as early as 15min post injury, and then transferred to the axoplasm proper at 30-120 min post injury, supporting the role of local CMSP in the pathogenesis of DAI (Buki et al., 1999). Interestingly, Saatman and coworkers (2003) observed biphasic calpain activation in traumatic injured axons in mice optic nerve after stretch injury. Calpains were acutely activated in the first 20 minutes to hours post injury, followed by a delayed phase of calpain-mediated proteolysis at 4 days post injury possibly participating in axonal degeneration and neuronal death (Saatman et al., 2003).

Further evidence to support the involvement of calpain is found in the protective function of calpain inhibitors in attenuating axonal damage. For example, calpain inhibitor CEP-4143, given before spinal cord injury, inhibited calpain activation, decreased neurofilament NF200 dephosphorylation, attenuated axonal damage, and improved behavior (Schumacher et al., 2000). Similarly, the calpain inhibitor SJA6017, when administered at 20 min or delayed to 4 h post injury, improved mice functional outcome after diffuse brain injury (Kupina et al., 2001). Lastly, the calpain inhibitor MDL-28170, when given intravenously before an impact acceleration TBI, also reduced the number of damaged axons in the rat brainstem (Buki et al., 2003).

In addition to calpain-mediated spectrin proteolysis, calpain can also proteolize tubulin, GAP-43, microtubule-associated proteins (MAP), such as MAP1A, MAP1B and MAP2 (Saatman et al., 1998; Saatman et al., 2010; Taft et al., 1992; Thompson et al., 2006). Calpain also cleaves tau protein and generates a toxic 17-kDa tau fragment in cultured hippocampal neurons (Park et al., 2005).

Calpain also mediates degradation of neurofilaments. For example, in the corpus callosum, NF200 and NF68 were found to be decreased in head-injured patients compared to

control patients (McCracken et al., 1999; Saatman et al., 1998). Serbest et al (2007) also observed the decrease of NF200 and NF68 in the mice optic nerve following stretch injury.

In addition to the above calpain-mediated events, Ca^{2+} can also activate calcineurin, which dephosphorylates both neurofilament (NF) subunits and microtubule associated protein-tau, thereby altering the interaction between adjacent NFs and between NFs and microtubules (Mata et al., 1997). Consequently, the repelling forces between the NF side-arms are decreased, resulting in neurofilament compaction (NFC), disrupting the organization of microtubules, and compromising axonal transport (Buki and Povlishock 2006; Mata et al., 1997; Okonkwo et al., 1998). Neurofilament dephosphorylation was also observed in the optic nerve following stretch injury (Saatman et al., 2003). Okonkwo et al. (1998) showed that NFC was spatially and temporally correlated with intra-axonal calpain-mediated spectrin-proteolysis (CMSP). NFC was also observed in optic nerve stretch model (Maxwell et al., 2003).

Collectively, the increased intra-axonal calcium promotes spectrin-proteolysis, disruption of microtubules and neurofilament compaction.

Mitochondrial damage in TAI

Concomitant with above changes, local mitochondrial swelling has been observed in the injured axonal segment in diffuse TBI models (Büki et al., 1999; Büki et al., 2000; Büki and Povlishock, 2006; Povlishock et al., 1997; Wang et al., 2011). Mitochondria also are found to accumulate abnormally in swollen axonal segments in cultured primary chick forebrain neurons following fluid shear stress injury (Kilinc et al., 2008). In a rat lateral head rotation model, axonal damage was observed in medulla oblongata, associated with Ca^{2+} overloading with many axons revealing an abundance of Ca^{2+} associated with swollen mitochondria (He et al., 2004). These findings suggest that Ca^{2+} overloading by itself may lead to mitochondrial dysfunction.

Physiologically, the level of total mitochondrial calcium within neurons is approximately 0.1 mM and the level of free mitochondrial calcium approximates 100 nM (Babcock and Hille, 1998; Pivovarova and Andrews 2010; Pozzo-Miller et al., 1997). When stimulated, mitochondria accumulate large amounts of calcium (Montero et al., 2000; Pivovarov et al., 1999), which maybe mediated by the mitochondrial ryanodine receptor, the mitochondrial uncoupling proteins, the Letm1 Ca^{2+}/H^{+} exchanger, as well as the mitochondrial Ca^{2+} uniporter (MCU) and its Ca^{2+} sensing regulatory subunit MICU1(Pan et al., 2011). Mitochondria release Ca^{2+} primarily by Na^{+}/Ca^{2+} exchanger (Crompton and Costi, 1978; Nicholls, 2005) and Na^{+}/H^{+} exchanger (Nicholls, 2005; Starkov, 2010). Normal oscillation of Ca^{2+} in mitochondria participates in ATP production, axonal transport, excitability and synaptic transmission (MacAskill et al., 2010; Pivovarova and Andrews 2010; Starkov, 2010). However, when Ca^{2+} overloading is so severe, it depolarizes mitochondria, opening mitochondrial permeability transition pores (MPTP), resulting in neuronal degeneration (Bezprozvanny, 2009) as well as axonal damage. Further, this axonal damage was attenuated by agents providing mitochondrial protection via their targeting of MPTP. Specifically cyclosporin A (CsA) and FK506 have been shown to preserve mitochondria, attenuate axonal injury and improve axonal function (Büki et al., 1999; Marmarow and Povlishock, 2006; Okonkwo and Povlishock, 1999; Reeves et al., 2007; Singleton et al., 2001).

Although the exact molecular components of MPTP are unclear, several different components have been identified, including cyclophilin D (CyP-D), adenine nucleotide translocator (ANT), the mitochondrial phosphate carrier (PiC), and the voltage-dependent anion channel (VDAC) (Halestrap, 2009; Leung and Halestrap, 2008). As noted previously, the opening of MPTP is triggered by mitochondria matrix Ca^{2+}. The addition of Ca^{2+} *in vitro* has been shown to open the MPTP while Ca^{2+} chelation can induce the closure of MPTP (Crompton

et al., 1987; Crompton and Costi, 1988 and 1990; Haworth and Hunter, 1979). This Ca^{2+} triggered MPTP opening was facilitated by cyclophilin D, a matrix peptidyl-prolyl cis–trans isomerase (PPIase) (Connern and Halestrap, 1992; Johnson et al., 1999). CsA and its analogues bind to cyclophilin D and inhibit MPTP opening (Griffiths and Halestrap, 1995; Waldmeier et al., 2002), without interfering with the activity of calcineurin.

The opening of MPTP and subsequent mitochondrial depolarization can also be induced and/or facilitated by free radicals (Brustovetsky et al., 2003) as well as the activity of proteinase, calpain (Aguilar et al., 1996). Besides cytosolic calpain, there have also been reports that mitochondrial calpain is involved in mitochondrial dysfunction. Arrington et al (2006) reported that calpain 10, a mitochondrial calpain, could cleave Complex I subunit NDUFV2 and ND6, activate MPTP, and result in mitochondrial dysfunction, which were blocked by calpain inhibitors.

Upon the opening of MPTP, Ca^{2+} influx becomes unregulated, resulting in mitochondria depolarization. Concomitantly, water is drawn in by the colloidal osmotic pressure, related to the high concentration of proteins and Ca^{2+} within the mitochondrial matrix. Collectively, this leads to mitochondrial swelling and dysfunction (Halestrap et al., 1998; 2004; Halestrap and Pasdois 2009).

Ultimately, the failure of mitochondrial function results in local bioenergetic deficiency together with impairment of local axonal transport. Ahmed and coworkers (2000) reported that mitochondrial membrane potentials decreased in cultured neurons 15 min after severe stretch injury, and ATP content declined 22–28% in mixed cultures of neuron and astrocytes 15 min following stretch. *N*-Acetylaspartate (NAA), which is synthesized by the mitochondria, was

reduced gradually based on the severity of the impact acceleration insult on adult rats (Signoretti et al., 2001).

Activation of the caspase cascade and corresponding cytoskeletal damage in TAI

Following the MPTP formation and the subsequent mitochondria dysfunction, the apoptosis activating factor, cytochrome-c and caspase enzymes are released into the axonal cytosol, activating the caspase cascade in the traumatically injured axonal segments (Buki and Povlishock, 2006; Buki et al., 2000). Cytochrome-c release increases parallel to caspase-3 activation over time after injury (Buki et al., 2000). Caspase-3 cleaves spectrin into 120kDa segment (SBDP-120-kDa), the signature protein of caspase-3 activation. SBDP-120-kDa has been found to colocalize with cytochrome-c release and calpain activation in severely damaged segments, suggesting that cytochrome-c, caspase-3 and calpain are involved in the terminal cascade of TAI. Compared to calpain-mediated spectrin proteolysis, which targets the alpha chain of spectrin, caspase-3 also degrades the beta chain of subaxolemmal spectrin followed by changes in axonal morphology and axolemmal permeability (Buki and Povlishock, 2006; Wang et al., 1998).

Besides the proteolysis of spectrin, active caspase-3 cleaves tau into a 50-kDa truncated tau segment (Gamblin et al., 2003), which is different from calpain mediated 17-kDa toxic tau fragments. All these truncated tau proteins probably facilitate microtubule disorganization, disrupting axonal transport.

Additionally, it has been reported that caspase-3 also mediates the cleavage of protein kinase N 1 (PKN1), which has been recognized to be important in neurofilament organization and transport (Manser et al., 2008). Collectively, these findings indicate that activation of

caspase-3 may contribute to disrupting NF organization and axonal transport. Thus, caspase-inhibitors may be a potential therapeutic approach in TAI.

In sum, following diffuse axon injury, axolemmal permeability increases followed by calcium influx. This leads to calcium overloading, which activates proteinase calpain mediated spectrin proteolysis and tau cleavage. Also proteolytic NF-sidearm modification or Ca^{2+} -induced activation of calcineurin alters the NF-sidearm phosphorylation state, both promotes neurofilament compaction. Concomitantly, Ca^{2+} overloading damages mitochondria both morphologically and functionally, followed by the release of pro-apoptotic factors which trigger caspase mediated proteolysis of spectrin, tau and PKN1. These sequences of events ultimately destroy axonal cytoskeleton and disrupt axonal transport.

Impairment of axonal transport, organelle accumulation and axonal swelling

As discussed above, in diffuse axonal injury animal and humans suffering from brain trauma, calcium-activated proteases calpain and caspase, destroy cytoskeletal proteins tubulin, neurofilament polypeptides and spectrin, consequently blocking axonal transport and resulting in organelle and protein accumulation, triggering axonal swelling.

Focal axonal swellings are the morphological hallmarks of altered axonal transport. Proteins and organelles, such as β-amyloid precursor protein (APP), mitochondria, microtubules, and profiles of smooth endoplasmic reticulum, accumulate in the swollen axonal segment (Povlishock and Christman, 1995). The development of axonal swelling is a time-dependent process. From initiation up to 1 hour post-injury, some axons show initial focal swellings, some containing swollen mitochondria, and others NFs revealing oblique to the axon long axis, precipitating impaired axonal transport (Yaghmai and Povlishock, 1992). In 2-3 h following injury, axonal swelling continues, with a total blockage of axonal transport in the proximal and

distal segments, suggesting focal axonal dysfunction and disconnection (Pettus et al., 1994; Povlishock et al., 1983). At 3 h post-injury, most axons appear disconnected with continued expansion to form a mature swollen bulb due to accumulation of organelles (Pettus et al., 1994). By 12–48 h post-injury, axonal swellings became more mature and expanded with axonal disconnection now dominant (Pettus et al., 1994).

Maxwell and Graham (1997) demonstrated that the sites of microtubule loss correlated with the sites of axonal swellings in the stretch injured optic nerve. Further, positive staining of antibody specific to kinesin, a motor protein important for anterograde axonal transport, was identified in swollen axonal bulbs in all cases of TBI patients of both the short-term survival period (mean 64 h post injury) and long-term survival period (mean 245 days post injury) (Chen et al., 2009), confirming that these axonal swellings were due to the blockage of vesicles transported anterogradely at the injured axonal segment.

Further evidence of the axonal disconnection is found in the work of Saatman et al (2003) who showed decreased retrograde labeling of the RGCs by fluorescent tracer placed in the superior colliculi after the optic nerve stretch injury. Utilizing YFP-H transgenic mice, Greer et al (2011) observed both proximal and distal axonal swelling in the cerebral cortex after the central fluid percussion injury. Greer (2011) showed that the antibodies targeting the C terminus of APP labeled only the proximal swollen segment, without labeling of the distal swollen segment. Additionally, the proximal APP immunostaining disappeared at 48 hours post injury, in contrast to the distal endogenous YFP fluorescence positive swellings which persisted days after injury. This disappearance of APP labeling over time could be due to the degradation of APP in the injured axonal segment, but the possibility could not be excluded that anterograde axonal transport is converted into retrograde transport (Martz et al., 1989; Sahenk and Lasek, 1988).

Limitations of current research on the pathogenesis of TAI and new directions

As noted above, majority of previous studies focused on the initial pathological mechanisms associated with TAI, particularly the initiating intraaxonal cellular and subcellular mechanisms. While these studies are important and well established targets for potential therapeutic intervention, they have left unaddressed the important consequences of TAI in terms of the long term fate of those neurons linked to the TAI as well as the potential for anterograde/retrograde dieback of the diffusely damaged axons. This unaddressed information will be vital for future studies exploring the potential for regeneration and repair following TAI. Accordingly, in following passages, we address what limited information exists in relation to these issues in the context of TAI.

Evidence for axonal dieback following TAI

Axonal dieback is a phenomenon whereby axons retract from the initial site of injury. While virtually no information exists on the process of axonal dieback following TAI, some comparisons can be drawn from studies of axonal transection.

Axonal dieback has been reported in spinal cord injury (SCI). Retrograde axonal dieback (of the proximal segment) was observed in the rat corticospinal tract (CST) after thoracic spinal cord transection (Seif et al., 2007), and similarly, in the mice CST after thoracic SCI (Yoshimura et al., 2011). Utilizing time-lapse imaging of green fluorescent protein (GFP) fluorescent axons that run superficially in the dorsal spinal cord of living transgenic mice, Kerschensteiner et al (2005) observed acute axonal degeneration (AAD) over 200-300µm within 30 minutes. The AAD was identical in the proximal and distal axon ends, after transection of selected axons mostly originating from the dorsal root ganglion (DRG). In part, the underling mechanism of

AAD may be similar to Wallerian degeneration since it was significantly decreased in transgenic mice with "Wallerian degeneration slow" mutation (Kerschensteiner et al., 2005). Additionally, AAD was blocked by calpain inhibitors, suggesting the involvement of calpain protease in AAD (Kerschensteiner et al., 2005). Overtime, the proximal end remained stable, or showed early sprouting as early as 6-24 hours after lesion (Kerschensteiner et al., 2005). In contrast, the distal end underwent continued Wallerian degeneration (Kerschensteiner et al., 2005).

Besides the activity of calpain and Wallerian degeneration, axonal dieback after SCI has also in part been linked to chronic macrophage activation (Busch et al., 2009; Busch et al., 2010; Horn et al., 2008). Horn and his colleagues (2008) observed spatiotemporal correlation between macrophage infiltration and injured ascending dorsal column sensory axon retraction from 7 to 28 days after injury, which was reduced by administration of liposomal clodronate - an inhibitor of macrophage infiltration. Using an in vitro model of macrophage-axon interaction, they also demonstrated that there were direct adhesive contacts between activated macrophages and dystrophic axons, and that extensive axonal retraction could be induced only when macrophages were activated (Horn et al., 2008). Further, Busch and his colleagues (2009) tried several methods to attenuate macrophage induced retraction. One approach was through the inactivation of matrix metalloproteinases (MMP), specifically MMP-9, while another approach was to modify substrate, for example, the digestion of the aggrecan substrate by chondroitinase ABC. Both of these two methods have been effective in blocking macrophage-induced axonal retraction (Busch et al., 2009). Taken together, it appears now that axonal dieback is a complex process, involving chronic macrophage activation and attachment to the dystrophic axons, as well as the secretion of MMP and chondroitin sulfate proteoglycans.

In addition to macrophage activation, oligodendrocyte and microglia/macrophage death (Stirling et al., 2004) and myelin degeneration (McPhail et al., 2004) have also been implicated in axonal dieback. Fourteen days after transection of the dorsal columns at the cervical C7-C8 level, apoptotic oligodendrocytes and microglia/macrophages were observed in the proximal descending corticospinal tract (CST) and the distal degenerating, ascending sensory tract (AST) (Stirling et al., 2004). Minocycline, which is an anti-inflammatory and neuroprotective medication, inhibiting microglial activation (Yrjänheikki et al., 1998), attenuated MMPs (Brundula et al., 2002) and inhibited caspase expression (Chen et al., 2000). When administered intraperitoneally, minocycline was effective in reducing the number of ED1-positive microglia/macrophages within the degenerating axonal segments at 7 d after injury. This strategy prevented CST axonal dieback, reducing lesion size, and promoting functional outcome at both 7 and 14 days after spinal cord injury (Stirling et al., 2004).

Of note, distinct macrophage subsets, proinflammatory type (M1) and anti-inflammatory type (M2), were activated differentially following SCI (Kigerl et al., 2009). Previous studies have demonstrated that, by the stimulation of lipopolysaccharide and interferon-γ (IFN- γ), the macrophage differentiated into the M1 phenotype, producing nitric oxide, superoxide and other proinflammatory cytokines, mediating neuronal death (Block et al., 2007; Kigerl et al., 2009). In contrast, via the stimulation of interleukin-4 (IL-4) or IL-13, the macrophage differentiated into the M2 phenotype, promoting axonal growth (Barrette et al., 2008; Kigerl et al., 2009; Yin et al., 2003; Yin et al., 2006), the phagocytosis of myelin (Vallie`res et al., 2006), and the maturation of oligodendrocytes and remyelination (Schonberg et al., 2007). Temporally, the M1 macrophages were activated rapidly and were maintained up to 28d post spinal cord injury, while in contrast, the M2 macrophages were activated transiently and returned to preinjury levels by 14d post

injury (Kigerl et al., 2009). At the lesion site, the ratio of M1/M2 cells shifted from approximately equal at 1–3 dpi, toward an M1 macrophage phenotype dominant phase after the first week (Kigerl et al., 2009). This downregulation of M2 macrophage phenotype has been linked to the lesion-derived factors in the microenvironment, based upon the fact that the percent of M2 phenotype macrophage remained unchanged when injected into intact spinal cord, while they became reduced by 20-40% when injected into the spinal cord contusion lesion (Kigerl et al., 2009). Interestingly, a shift from M1 to M2 macrophages has been observed in equine tendon repair (Dakin et al., 2012), the healing cutaneous wound site (Deonarine et al., 2007) and the healing myocardium (Lambert et al., 2008; Nahrendorf et al., 2007), implicating that inducing M2 macrophage formation is a potential therapeutic strategy to promote axonal regeneration and CNS repair. Supporting evidence has already existed in preclinical models of SCI employing peroxisome proliferator activated receptor (PPAR) agonists, which have been approved by the Food and Drug Administration (FDA) to treat diabetes. It has been shown that PPAR agonists could also facilitate the differentiation of macrophages into the M2 phenotype through IL-4 (Odegaard et al., 2007; Villanueva and Tontonoz, 2010), and promote anatomical and functional repair after SCI (McTigue et al., 2007).

Activation of microglia has also been observed in brain injury. Specifically, in a mice midline closed skull injury model, which induces diffuse axonal injury in the corpus callosum, the activation of different subpopulation of microglia has been observed both acutely and chronically (1d - 28d post injury) (Venkatesan et al., 2010). Particularly, some activated galectin-3/Mac-2 immunoreactive microglia engulfed injured axonal segments, consistent with the role of myelin phagocytosis during CNS inflammation (Reichert and Rotshenker, 1999; Venkatesan et al., 2010; Walther et al., 2000). At the same time, activated galectin-3/Mac-2 immunoreactive

microglia expressed nerve growth factor (Venkatesan et al., 2010), which is believed to have a beneficial role, such as promoting neuronal repair, axon sprouting and oligodendrocyte proliferation (Althaus et al., 1992; Frielingsdorf et al., 2007; Kromer, 1987; Sofroniew et al., 2001). However, a detrimental role of nerve growth factor also exists, such as its association with oligodendrocyte death (Casaccia-Bonnefil et al., 1996; Frade et al., 1996; Yune et al., 2007). Thus, the real function of microglia/macrophage activation in axonal damage is still unclear. Specifically, it is required to study whether they are associated with axonal dieback and/or axonal regeneration/repair following diffuse traumatic axonal injury.

Anterograde degeneration following TAI

Previous experimental animal models of TBI as well as human studies have shown that, following axonal damage and disconnection, the downstream distal axonal segments undergo Wallerian degeneration, with subsequent deafferentation of the target tissue (Kelley et al., 2006; Povlishock 1992; Povlishock et al., 1992). For example, in a rodent model of DAI, the distal segment and its related synaptic terminals manifest an increase in electron density and/or neurofilamentous hyperplasia, with detachment from their normal target sites within 24-48 hours of injury (Povlishock 1992; Povlishock et al., 1992). Such axonal degeneration and deafferentation may be linked to the neurological dysfunction and long-term deficits associated with DAI.

However, other data also suggest that this same diffuse deafferentation may set the stage for the subsequent sprouting of related intact nerve fibers which may be involved in synaptic plasticity (Erb and Povlishock, 1991; Greer et al., 2011) and/or maladaptive modification (Phillips et al., 1994; Reeves et al., 2003). In a feline model of mild to moderate TBI, Erb and

Povlishock reported that the post-TBI diffuse pattern of axon terminal degeneration and subsequent deafferentation in the dorsal lateral vestibular nucleus was followed by a prolonged adaptive recovery process that occurred 2-6 months post injury (Erb and Povlishock, 1991). Utilizing the entorhinal cortical lesion model coupled to TBI, a more severe injury paradigm, Phillip and Reeves observed maladaptive sprouting of the crossed temporodentate fibers and synaptogenesis after the clearance of the axonal debris (Phillips et al., 2001; Reeves et al., 2003). Taken together, these results suggest that in cases of diffuse degeneration and deafferentation induced by mild/moderate TBI, as opposed to more severe injury, the injured brain may in fact harbor a permissive environment for the adaptive sprouting of nerve fibers and resultant synaptic input to the previously deafferented targets.

Retrograde effect of TAI on the neuronal cell body

Again, our understanding of the retrograde consequences of TAI is incomplete. The retrograde response of neuronal cell body to axonal injury is influenced by several factors, (1) the type of the neuron sustaining axotomy, (2) how the axon is injured, transection (primary) versus stretch during acceleration and deceleration (secondary), and (3) the distance from the axonal lesion to the neuronal soma. This issue is of direct relevance to the issue of axonal dieback, in that if the sustaining neuronal cell body dies, the fate of its downstream axonal segment is a forgone conclusion.

The type of the neuron influences the retrograde response to axonal injury

The neuronal response to axonal injury is vastly different between the peripheral nervous system (PNS) and the central nervous system (CNS). The PNS neuron has the capacity to regenerate axons after the peripheral nerve lesion in the growth permissive environment.

Postinjury, the morphology of the cell body of axotomized PNS neurons transitions to "chromatolysis", which includes the restructuring of the granular endoplasmic reticulum and the lateralization of the nucleus, which are related to mRNA synthesis alteration and protein expression modification (Fenrich and Gordon, 2004; Gordon, 1983; Kreutzberg, 1995; Kreutzberg, 1996). Evidence exists as to the up-regulation of the cytoskeletal proteins, such as tubulin and actin (Tetzlaff et al., 1991), and the growth associated proteins, GAP-43, as well as cytoskeleton-associated protein-23 (CAP-23, Bomze et al., 2001), which play an important role in growth cone elongation (Bomze et al., 2001; Bulsara et al., 2002; Igarashi et al, 1995; Piehl et al., 1998; Strittmatter et al., 1994). The denervated Schwann cells, the glial cells in PNS, transition from the myelinating phenotype to the growth supportive nonmyelinating phenotype (Hall, 1999). This is associated with a decrease in the expression of the myelin-associated genes with an increase in the expression of regeneration associated genes (RAG), which include neurotrophic factors, such as the brain-derived neurotrophic factor (BDNF), neurotrophin, glial cell derived neurotrophic factor (GDNF), truncated receptors and the p75 neurotrophic factor receptor (Boyd and Gordon, 2003; Funakoshi et al., 1993; Höke et al., 2002; Ito et al., 1998; Meyer et al., 1992; Naveilhan et al., 1997; Seniuk et al., 1992).

In contrast, the CNS neuron does not mount a regenerative response after axotomy. This could be due to (1) the insufficient ability of CNS neurons to express RAGs (Fernandes et al., 1999; Hiebert et al., 2000; Plunet et al., 2002), (2) the inhibitory proteins that expressed by oligodendrocytes, such as Nogo-A, oligodendrocyte-myelin glycoprotein (OMgp), myelin-associated glycoprotein (MAG) (Atalay et al., 2007; Giger et al., 2008; McDonald et al., 2011), as well as (3) the proliferation of astrocytes, the formation of the glial scar and its release of

inhibitory molecules, especially chondroitin sulfate proteoglycans (CSPGs) (Holmberg et al., 2008; Ito et al., 2009; Susarla et al., 2011; Toyooka et al., 2011).

The pattern of axonal injury results in different fates for the neuronal cell body

Following axotomy, CNS neurons undergo cell death or somatic atrophy. Axonal injury due to direct transection is commonly followed by neuronal death. Dale et al (1995) reported that only 30 - 40% of corticospinal motor neurons in layer V of the adult rat cerebral cortex survived 13 days after the intracortical transection at 200µm ventral to the layer V cortex. The number of corticospinal neurons decreased 5 and 10 weeks after complete thoracic spinal cord transection at T-6/T-7 level (Feringa et al., 1983). Similarly, the number of corticospinal and rubrospinal neurons decreased at 10 or 20 weeks after complete thoracic spinal cord transection at T-9 level (McBride et al., 1990). Apoptosis of the primary cortical motor neurons was observed at 1 week after transection of the dorsal funiculus at T-9 level (Hains et al., 2003). Galindo-Romero and colleagues (2011) observed significant retinal ganglion cell (RGC) loss at 5 days and 21 days following optic nerve transection 0.5mm from the optic disc.

In contrast to neuronal death seen with transection, neuronal survival and atrophy has been described following diffuse traumatic axonal injury in animal models. Povlishock and colleagues demonstrated that the neuronal cell bodies affected by perisomatic axonal injury sustained atrophy rather than cell death (Greer et al., 2011; Lifshitz et al., 2007; Singleton et al., 2002). Specifically, in a rat midline fluid percussion injury model, a diffuse TBI model, Singleton (2002) observed that diffuse axonal swellings occurred within the mediodorsal neocortex, with the neocortical neurons sustaining traumatic axonal injury from 30 minutes to 48 hours post injury. These axotomized somata demonstrated the increased expression of eIF2α, while ultrastructurally these somata showed reactive response, the dispersion and loss of rough

endoplasmic reticulum, without evidence of overt organelle or cytoskeletal change, not supporting a cell death cascade (Singleton et al., 2002). Utilizing the same animal model, Lifshitz (2007) observed that the number of neurons in the ventral basal complex suffering perisomatic axotomy, did not decrease significantly from 1 day through 28 days post injury, suggesting no significant cell death following diffuse traumatic axonal injury (Lifshitz et al., 2007). The nuclear volume of thalamic neurons of the ventral basal complex, however, decreased at 1 day and 7 days post injury compared to sham animals, consistent with atrophy (Lifshitz et al., 2007). By modifying this midline fluid percussion injury model to mice, Greer (2011) showed evidence that the neurons in layer V of cerebral cortex demonstrated atrophy at 28 days after diffuse TBI, without evidence of neuronal death, and over time the downstream axon showed a significant elongation, suggesting a regenerative response.

The distance from the axonal lesion to the neuronal soma affects the neuronal response

In addition, the proximity of the axonal injury to their neuronal cell bodies of origin may influence the neuronal cell body response. More cell death occurs when the axonal lesion is near to the neuronal cell body of origin, with more neuronal sparing seen with more distal lesions (Dale et al., 1995; Liu et al., 2003; Liu et al., 2004). For example, the number of surviving corticospinal motor neurons in layer V of the adult rat cerebral cortex was 70% at 13 days after the intracortical transection 400μm below the layer V cortex, and decreased to 30-40% during the same period when the intracortical transection was 200μm below the layer V cortex (Dale et al., 1995). After infusion of ciliary neurotrophic factor (CNTF), the number of surviving corticospinal motor neurons increased to 2- fold compared to the number seen with vehicle treatment following the axonal transection at the 200μm depth, while no recognizable CNTF - mediated neuronal protection was observed when the intracortical transection was at the 400μm

depth (Dale et al., 1995). These results suggest that the neuronal survival depends on the retrograde axonal transport of neurotrophic factors to the neuronal cell body and/or other neuronal signaling molecules. The more distant axotomy from the neuronal cell body, the more continued retrograde axonal transport of the neurotrophic factors from the downstream target tissue, and the more likely that the sustaining neuronal cell body will survive.

Similar findings were observed in spinal cord injury. Fifty seven percent cell loss of rat rubrospinal neurons occurred at 2 weeks after the axonal transection at the brain stem level, in contrast to the 7% cell loss during the same period after the axotomy at C2 level (Liu et al., 2003). More swollen mitochondria appeared in rat rubrospinal neurons following axotomy at brainstem than at C2 level, with more increased expression of nitric oxide (NO) synthase after axotomy at brainstem than at C2 level, and no significant change after axotomy at T10 level, and the mitochondrial Mn-superoxide dismutase was significantly reduced after axotomy at brainstem in contrast to no alteration following C2 axotomy (Liu et al., 2004). These findings suggest that the distance between the axonal lesion and the neuron soma is one of the determinants of the response on the neuronal body and the neuronal fate, probably through the NO-mediated toxicity and superoxide -mediated mitochondrial damage (Liu et al., 2004).

The signal transmission process from the axonal lesion to the neuron body

Since different neurons have different fates following different patterns/locations of axotomy, as described above, it is meaningful to address how the axonal injury signal transfers to the neuronal cell body. The current view regarding retrograde response of neuronal cell body to axonal injury is based on physical transection model (Bonatz et al., 2000; Giehl and Tetzlaff 1996; Merline and Kalil 1990). The transection of CNS axons exposes the axonal cylinder to different extracellular electrical and chemical environment, and activates a complex series of

responses. The early phase is mediated by the electrical signal from the axonal lesion site back to the soma (Mandolesi et al., 2004), the second phase is the alteration of biochemical signal, followed by the third phase of modulating gene expression and protein translation.

The first signal from axotomy event is the electrophysiological response. In an *in vitro* study, following the axotomy (~100μM from cell body) of neurons cultured from rodent visual cortex, influx of calcium was initially observed at the lesion site, and then this increase of calcium transferred along the axon toward the soma. This axotomy induced calcium increase was associated with the activation of the voltage-gated calcium channels and Na^{+}/Ca^{2+} exchange (Mandolesi et al., 2004).

The second signal involves the interruption of the supply of trophic factors conveyed to the cell body by retrograde axonal transport, which are essential for neuronal survival and regeneration (Ben-Yaakow and Fainzilber, 2009; Shadiack et al., 2001).

Another system of signaling involves the retrograde transport of activated proteins originating from the injury site (Ambron and Walters, 1996; Ben-Yaakow and Fainzilber, 2009; Hanz et al., 2003; Perlson et al., 2004; Zhang and Ambron, 2000). De novo synthesis of importin β at the axon lesion site was observed 30 minutes to 1 hour after lesioning by local translation of axonal mRNA (Hanz et al., 2003). Then importin α and importin β formed a high-affinity heterodimer and associated with the motor protein dynein 2 hours after lesion (Hanz et al., 2003). Further, nuclear localization signal (NLS) – bearing signaling protein bond to the high-affinity binding site on the α/β importin (Hanz et al., 2003). Then, NLS-binding complex was transferred retrogradely toward the cell body at about 1h/mm, through the interaction of importin α with dynein (Hanz et al., 2003; Hanz and Fainzilber, 2004). Any disruption of NLS complex slowed the regeneration of injured sensory neurons (Hanz and Fainzilber, 2004). These findings

implicated the connection between retrogradely transported NLS by importins in periphery and the nuclear import of NLS by importins in cell bodies, and probably this is a potential retrograde intrinsic mechanism to promote neuronal regeneration in CNS.

The activation of CREB-cAMP pathway in neuron cell body after axotomy

After receiving the retrograde transported injury signal, the neuronal cell body regulates transcription factors and alters translation of related protein. It has been documented that cAMP level was elevated in the DRG neurons following a conditioning lesion, in which the sciatic nerve and the dorsal column were injured simultaneously, or the sciatic nerve was injured before the dorsal column (Hannila and Filbin, 2008; Qiu et al., 2002). This cAMP elevation was dependent on the activation of protein kinase A (PKA) (Qiu et al., 2002). Following cAMP elevation, the transcription factor cAMP response element binding protein (CREB) was activated, promoting neurite outgrowth and axon regeneration (Gao et al., 2004). Several cAMP-regulated genes have been identified, such as arginase I, polyamines (Abe and Cavalli, 2008; Cai et al., 2002; Gao et al., 2004) and interleukin-6 (IL-6; Cao et al., 2006).

The activation of c-Jun and the induction of ATF-3 in neuron cell body after axotomy, and their relation to axon regeneration

In addition to the activation of CREB-cAMP pathway, the c-Jun N-terminal kinase (JNK) pathway is also activated following axotomy (Kenney and Kocsis, 1998; Greer et al., 2011; Itoh et al., 2011; Lindwall and Kanje, et al., 2005). Greer et al (2011) demonstrated that at 1 and 3 days following midline fluid percussion injury, phospho-c-Jun was expressed in atrophic neurons within the layer V cortex that sustained traumatic axonal injury, and this expression persisted through 28 day following injury. Similarly, activating transcription factor 3 (ATF-3), was also upregulated in axotomized neurons in layer V cortex at 3 day and 7 day post-injury, although its

expression was reduced at 14 day and 28 day post-injury (Greer et al., 2011). Concomitant with these findings, reactive sprouting from the truncated axon was observed as early as 1 day post-injury, and long, thin axonal profiles originated from phospho-c-Jun positive neurons was observed at 14 and 28 day post-injury (Greer et al., 2011). These results support the axonal regeneration function of JNK pathway following axotomy (Broude et al., 1997; Raivich et al., 2004; Raivich, 2008). Lindwall and Kanje (2005) observed in a rat sciatic nerve ligation model, the retrograde axonal transport of JNK upstream kinases, including mitogen activated protein kinase (MAPK) kinase kinases (MEKKs) MEKK1, MAPK kinases (MKK) MKK7 and p-MKK4, mixed lineage kinase (MLK) 3, p-JNK, p-ATF2, and the scaffolding protein JNK interacting protein (JIP) (Whitmarsh et al., 2001; Yasuda et al., 1999). On the contrary, the retrograde transport of c-Jun and p-c-Jun was minimal (Cavalli et al., 2005; Lindwall and Kanje, et al., 2005). Additionally, they revealed the anterograde axonal transport of Hsp27, a protein upregulated after the activation of c-Jun and the induction of ATF3 in the nucleus, and transported and coupled with p-c-Jun and ATF3 (Lindwall and Kanje, et al., 2005; Nakagomi et al., 2003). These facts indicate that JNK signaling molecules are transported retrogradely toward the neuronal cell body, where they activate the phosphorylation of c-Jun and the induction of ATF3 (Lindwall and Kanje, et al., 2005). Interestingly, NLS motifs, as described before which were transferred retrogradely toward the cell body via the coupling of importin α with dynein (Hanz et al., 2003), were found located within the basic region of the DNA binding domain of ATF proteins (Hai et al., 1989), suggesting that ATF3 could be induced after the reception of the retrogradely transported NLS signal from the axon lesion site.

JNKs have 3 isoforms, JNK1, JNK2 and JNK3. It has been demonstrated that JNK2 and JNK3 are necessary for neuritogenesis, JNK1 and JNK2 are related to neurite elongation and the

phosphorylation of microtubule-associated protein MAP1B which plays function in axonal regeneration, and JIP1 is associated with neurite initiation and extension (Barnat et al., 2010; Bogovevitch 2006; Bouquet et al., 2004; Dajas-Bailador et al., 2008; Mack et al., 2000). These JNKs functions are further supported by the fact that axonal outgrowth was reduced when c-Jun phosphorylation was inhibited by the selective JNK inhibitors SP600125 and (D)-JNKI1 (Lindwall et al., 2004).

The phosphorylation of c-Jun is involved in axonal regeneration. Upregulation of phospho-c-Jun was observed in the rat layer V cortex neuron after central fluid percussion brain injury (Greer et al., 2011), the rat mammillaris neurons up to 150 days after the transection of the medial forebrain bundle and mammillothalamic tract (Herdegen et al., 1993), bulbospinal and rubrospinal neurons after cervical spinal hemisection (Vinit et al., 2011). In a sciatic nerve crush injury model, when the expression of c-Jun was depleted in adult DRGs by siRNA technique, the size of the growth cone of the regenerating axons reduced, suggesting the role of c-Jun in regulating growth cone morphology (Saijilafu et al., 2011).

ATF-3 expression is also associated with axon regeneration. It has been demonstrated that ATF-3 facilitated peripheral nerve regeneration by increasing the expression of growth-associated genes small proline-repeat protein 1A (SPRR1A) in the DRG neurons (Huebner et al., 2009; Seijffers, et al., 2007). When pieces of peripheral nerve were transplanted into the thalamus of adult rats, axonal regeneration was observed originating from the thalamic reticular nucleus and medial geniculate nuclear that contained ATF-3 positive cells, which concomitantly expressed c-Jun (Campbell et al., 2005). Again, Greer (2011) also observed ATF-3 expression in axotomized neurons in layer V cortex at 1 - 7 day post-injury. These results indicate the initiation of a somatic gene expression program promoting neuronal recovery and/or axon regeneration.

In summary, the CNS neurons undergo cell loss due to primary transection of the axon, or survive and /or undergo atrophic change following diffuse axonal injury induced by the stretch at the acceleration/deceleration event. This divergent neuronal response could be due to different electrical and biochemical signals transferred from the axon terminal retrogradely toward the cell body of CNS neuron, which then initiates the synthesis and/or modification of corresponding molecules and factors, determining whether the neuron should die or survive and promote axon regeneration and/or repair. This response could be further influenced by the distance from the axonal lesion to the neuronal soma (perisomatic versus remote from the cell body).

Visual dysfunction in TBI

As noted above, there are limitations in our understanding of the mechanisms involved in axonal dieback in TAI, its anterograde/downstream degeneration and potential synaptic plasticity, as well as the differential response of the CNS neuronal cell body to axonal injury. In addition to these limitations, the majority of previous TAI studies have been conducted in neocortex, thalamus, corpus callosum, internal capsule and brainstem, and focused on motor and memory function, without sufficient consideration of the special sensory pathways involved in TBI, such as the visual system.

This issue is of merit as visual dysfunction occurs frequently following TBI and can include decreased visual acuity, loss of color perception and contrast sensitivity, visual field loss, diplopia, blurred vision, photophobia, convergence insufficiency, saccade and disorientation (Atkins et al., 2008; Barker et al., 1997; Hoyt, 2007). In a study on the incidence of combat-related eye injuries, the Defense Veterans Brain Injury Center (DVBIC) reported that 80 percent of the 3,900 troops sustaining TBI had visual problems (Zampieri, 2007). These could be due to

traumatic optic nerve damage or the disturbance of the intracranial visual pathways associated with TBI (Atkins et al., 2008). Traumatic optic nerve damage may be directly due to optic canal fracture (Matsuzaki et al., 1982; Sarkies 2004) during TBI which results in optic nerve compression/crush (Chen et al., 2004; Rumiantsev et al., 1981; Zhilin et al., 2011) or transection (Sarkies 2004). Optic nerve may also be injured indirectly from compression and contusion in closed head injury (Anderson et al., 1982; Sarkies, 2004). The intracanalicular optic nerve is unmovable within the optic canals, making this segment susceptible to shearing and/or stretching forces from the orbital and intracranial segments during rapid acceleration-deceleration movements (Rubin, 2005). In addition to the optic nerve, the optic chiasm, the optic radiation, the occipital cortex, as well as cranial nerves III, IV and VI may also be damaged during TBI (Cockerham et al., 2009).

Diffuse traumatic axonal injury in the visual system

Several human and animal studies have demonstrated diffuse axonal injury within the visual system after traumatic brain injury. With diffusion tensor imaging, Palmer et al (2010) showed that fractional anisotropy (FA) decreased in the optic radiation in patients sustaining severe TBI, consistent with axonal damage in that area. In a study on infants sustaining the shaken baby syndrome, Gleckman et al (2000) observed axonal swellings in the optic nerve caudal to the lamina cribrosa utilizing beta-amyloid precursor protein immunostaining. Foda and Marmarou (1994) found diffuse axonal injury in the optic tract in a rat weight drop model. Similarly, in a rat weight drop injury model, Ding et al (2001) observed diffuse axonal injury in the optic chiasm, optic tract, lateral geniculate nuclei and superior colliculus with silver staining.

Besides the occurrence of TAI within the visual system after TBI, several researchers have utilized an optic nerve stretch model to generate diffuse axonal injury in the optic nerve (Gennarelli et al., 1989; Maxwell et al., 1994; Maxwell and Graham, 1997; Sulaiman et al., 2011; Saatman et al., 2003; Serbest et al., 2007). As early as 1989, Gennarelli and colleagues stretched the optic nerve of albino guinea pigs, and observed beaded axons and terminal bulbs in the optic nerve, as well as impaired axonal transport of HRP from the vitreous to the superior colliculus. Saatman and colleagues (2003) modified this optic nerve stretch model in the albino guinea pig to mice, and observed axonal swellings and bulbs in the optic nerve, as well as impaired retrograde axonal transport from the superior colliculus to the retina.

Summary and Statement of the Problem

In sum, we have discussed TBI and TAI as a major contributor to TBI mortality and morbidity. Previous work on TAI has provided critical insight into the initiating mechanisms associated with TAI, involving alterations in axolemmal permeability, calcium dysregulation, and the subsequent activation of the proteases calpain and caspase, which then alter the cytoskeleton to ultimately impair axonal transport to result in organelle / protein accumulation, with the formation of axonal swelling and disconnection. However, following axonal swelling and disconnection, little is known in terms of the subsequent axonal dieback overtime post TAI, as well as its ongoing anterograde/downstream changes or the retrograde response of neuronal cell body to TAI. These issues are important from several perspectives in that such information is critical to future studies targeting neuroprotection and repair. Further, in that the visual system provides a highly organized projection system to follow these events, its choice for continued investigation seems both reasonable and rational. Lastly, given the prevalence of visual

dysfunction following TBI, and the evidence of TAI within the visual system in human and animal studies, the current thesis attempts to address TAI within the optic nerve/visual pathway following TBI, and its anterograde and retrograde change take on further significance.

In this dissertation (Chapter 3), using a mice central fluid percussion diffuse brain injury model, we describe the development of TAI within the optic nerve, its disconnection and associated axonal dieback both proximally and distally overtime post injury. We compare and contrast the morphological differences between the proximal and distal disconnected axonal segments. Specifically, we describe the regression and reorganization of the proximal swellings, and the persistence of the distal disconnected and degeneration swellings. We also demonstrate that this pathological TAI within the optic nerve is accompanied by transient and subtle breakdown of the blood-brain-barrier with the formation of edema and YFP fluorescence quenching in the early phases post injury.

In this communication (Chapter 4), we also address the fate of retinal ganglion cell layer following TAI within the optic nerve from 2 to 90 days post injury. Utilizing multiple qualitative and quantitative methods as well as ultrastructure analysis, we find no evidence of RGC loss following TAI. Rather, we demonstrate RGC survival, together with the persistent expression of phospho-c-Jun, which has been linked to neuronal survival and potential axonal repair in other injury paradigms.

Further, in Appendix I (Chapter 5), we demonstrate a differential microglia/macrophage response in the disconnected proximal and distal axonal segments. Specifically, we demonstrate that activated microglia/macrophages closely envelop/encompass the distal disconnected, degenerating axonal segments. In contrast, the microglia/macrophages appear less reactive in the

proximal axonal segments, with their processes paralleling these axonal profiles undergoing reorganization/repair.

Lastly, in Appendix II (Chapter 6), we demonstrate the resolution of edema in the interstitial space within the optic nerve, and the recovery of intact YFP fluorescent axonal fibers overtime in the region of previously demonstrating fluorescent loss (Chapter 3). This recovery of the intact YFP fibers is consistent with the reversal of fluorescence quenching.

Collectively, the data provided in both Appendix I and II support the reparative processes ongoing in the optic nerve at the site of injury as well as in its upstream/retrograde sites, while supporting the persistence of downstream/anterograde scattered Wallerian degeneration.

CHAPTER TWO

GENERAL MATERIALS AND METHODS

Breeding and genotyping of YFP-16 transgenic mice.

The Thy1-YFP-16 transgenic mice [B6.Cg-Tg(Thy1-YFP)16Jrs/J, stock number 003709] were obtained from the Jackson Laboratory (Bar Harbor, ME) and maintained as heterozygotes. Inheritance of the YFP gene was identified from an ear punch taken at weaning (approximately postnatal day 21). The ear tissue was mounted onto a glass slide and examined using a FITC filter on an Olympus DP71 digital camera (Olympus, Center Valley, PA), where YFP-positive axons could be easily identified.

Surgery and animal model of traumatic brain injury.

All protocols used in this study were approved by the Institutional Animal Care and Use Committee (IACUC) of Virginia Commonwealth University. Adult male C57/BL6 mice and Thy1-YFP-16 transgenic mice (20–25 g) were subjected to central fluid percussion TBI to produce traumatic axonal injury in the optic nerve. The fluid percussion injury model was modified from that previously described in detail by Dixon (1987). Briefly, animals were anesthetized with 4% isoflurane in 100% O_2, and maintained via nosecone with 2% isoflurane in 100% O_2 during surgery, with the body temperature controlled at 37^{o}C via a feedback-controlled heating pad (Harvard Apparatus, Holliston, MA). A midline 3.0 mm circular craniotomy was made over the sagittal suture halfway between the bregma and the lambda, taking care not to

damage the underlying dura. A Luer-Loc syringe hub was cut away from a 20 gauge needle and affixed to the craniotomy site. Dental acrylic was applied around the hub to enhance stability. As the dental acrylic dried and the injury hub became stable, saline was applied to blunt any exothermic reaction from the cured acrylic. The skin was then sutured over the hub, with lidocaine and bacitracin ointment applied to the wound. The animal was allowed to recover for 1 hour in a warmed cage prior to injury. Before the induction of injury, each animal was again anesthetized for 4 min (100% O_2 and 4% isoflurane). The craniotomy site was exposed and the injury hub was connected to the fluid percussion device. The animal was then injured at a magnitude of 1.40±0.05 atmospheres. The pressure pulse was measured by a storage oscilloscope (Tektronix 5111; Tektronix, Beaverton, OR). Injury preparation and induction were completed prior to the animal's recovery from anesthesia. The hub and dental acrylic were then removed, and the incision was rapidly sutured. The duration of transient unconsciousness was determined by measuring the time it took for the animal to recover the following reflexes: toe pinch, tail pinch, corneal blink, pinna, and righting reflex. After recovery of the righting reflex, the animals were placed in an incubator with a heating pad to maintain normothermia and monitored during recovery. For animals receiving sham injury, all of the above steps were followed with the exclusion of the injury pulse. All injured animals had righting reflex recovery times of 4–5 min, compared with less than 2 min for sham-injured animals, indicating injuries of comparable severity.

Animals Utilized for Specific Studies.

For the characterization of the diffuse traumatic axonal injury within the optic nerve following TBI, YFP-16 and wild type (WT) mice were allowed to survive 5 min, 15 min, 1 hour,

3 hour, 12 hour, 24 hour and 48 hour following injury (for each time point, 1 WT and 6 YFP-16 mice were utilized in the injured group, with 1 WT and 2 YFP-16 mice was used in the sham group). For the study of the retinal ganglion cell response to diffuse traumatic axonal injury, as well as the activation of microglia/macrophage in the optic nerve, YFP-16 mice were allowed to survive 2 day, 7 day, 14 day, 28 day and 90 day following injury (for each time point, 9 YFP-16 mice were utilized in the injured group, with 6 YFP-16 mice were utilized in the sham group).

Animal perfusion

At the predetermined survival times, mice were intraperitoneally injected with an overdose of sodium pentobarbital and then transcardially perfused with 100 ml heparinized normal saline followed by 200 ml 4% paraformaldehyde in Millonig's buffer (135.8mM Na Phosphate monobasic/108.8mM NaOH). For electron microscopy, animals were perfused with 4% paraformaldehyde/0.2% glutaraldehyde or 2% paraformaldehyde/2.5% glutaraldehyde for optimal processing.

Optic nerve preparation

After above perfusion and overnight incubation in the perfusion fixative solution, the optic nerve, chiasm and optic tract, together with the brain were removed from the skull for routine fluorescence and confocal analysis. The optic nerves were blocked to include the entire optic nerve, the chiasm, the initial part of the optic tract, and related brain tissue, and post-fixed in the same fixative solution overnight. Following post-fixation, this optic nerve block was cryoprotected and then cut longitudinally into 10µm sections with a cryotome (Shandon Scientific Ltd., Cheshire, U.K.). Serial sections revealing the entire length of the optic nerve

(from the globe to the chiasm) were then collected in a serial order in Millonig's buffer in 24 well culture plates (Falcon, Newark, DE), and stored at 4^{o}C for further use.

Retinal whole-mount preparations

After 15 minutes fixation, the extraocular muscles were cut from the globe, the optic nerve was transected immediately behind the globe, and the globe was dissected out from the orbit. The cornea was punctured with an 18 gauge needle, cut into 4 quadrants, and torn to the limbus using two sets of forceps. The lens was removed. The retina was separated from the pigmented layer, and immersed in 4% paraformaldehyde in Millonig's buffer for 4 hours. Then the retina was washed with phosphate buffered saline (PBS) for 5 x 10 minutes. Then each retina was cut into 4 quadrants, and mounted flat on a glass slide with Vectashield Hardset Mounting Medium with DAPI (Vector Laboratories), and cover-slipped for image capture with a Leica TCS-SP2 AOBS confocal microscope (Wetzlar, Germany).

Retinal cryostat section preparation

After the retina was separated from the pigmented layer as described above, it was fixed in 4% paraformaldehyde in Millonig's buffer overnight. After 5 x 10 minutes thorough wash in PBS, the retina was immersed in 30% sucrose in PBS overnight. The pair of retinal cups from the same animal was then embedded side to side and frozen to -20^{o}C in optimal cutting temperature (OCT) compound (Electron Microscopy Sciences, Cat No.62550-01, Hatfield, PA, U.S.A.), and cut into 12µm sections with a cryotome. Serial sections were collected on Superfrost®/Plus microscopic glass slides (Fisher Scientific, catalog no.12-550-15, U.S.A.), with

4 serial sections of each eye on each slide (8 sections for 2 eyes), and stored at -20^{o}C for further use.

Single and double immunofluorescence labeling protocol

After optic nerve or retinal sections were selected, they were rinsed 3 x 10 minute in PBS or Tris-buffered saline (TBS) (for antibodies targeting phosphorylated antigens), sections were treated with blocking solution 10% normal goat serum (NGS) with 0.5% Triton X-100 and 2% bovine serum albumin (BSA) in PBS (or TBS) for 2 hours. When employing primary antibodies produced from a mouse host, endogenous mouse IgG was blocked by Mouse on Mouse Kit (MOM™; Vector Laboratories; Burlingame, CA). The sections were then incubated in primary antibodies in 10% NGS with 0.5% Triton X-100 and 2% BSA in PBS (or TBS) at 4°C overnight. On the second day, the sections were rinsed in 1% NGS with 0.2% Triton X-100 and 1% BSA in PBS (or TBS) 6 x 10 minutes, then incubated in the appropriate Alexa fluor-conjugated secondary antibodies (Alexa 568, Alexa 594 or Alexa 633) in 1% NGS with 0.2% Triton X-100 and 1% BSA in PBS (or TBS) solution for 2 hours at room temperature. Then tissue sections were rinsed in PBS (or TBS), mounted onto gelatin-coated glass slides, and cover slipped with Vectashield Hardset Mounting Medium with DAPI (Vector Laboratories). Antibody concentrations are listed in Table 1.

For double labeling, the same protocols were utilized, with the specific attention that different primary antibodies were added at the same time for the overnight incubation, followed by the reaction with secondary antibodies that were conjugated to different Alexa fluors with binding specifically to different primary antibodies.

Table 1. Antibodies for immunofluorescence labeling

Antibodies		Host	Vendor	Dilution
1st	Anti-β-APP (c-terminus)	rabbit	Zymed, San Francisco, CA	1:1000
2nd	Alexa 594-conjugated goat anti-rabbit IgG	goat	Vector Laboratories, Burlingame, CA	1:200
1st	Texas-Red conjugated goat anti-mouse IgG	goat	Molecular probes, Invitrogen	1:200
1st	Anti-GFP	rabbit	Chemicon, Temecula, CA	1:8000
2nd	Alexa 594-conjugated goat anti-rabbit IgG	goat	Vector Laboratories	1:500
1st	Anti-Digoxigenin	mouse	Roche Applied Science, Germany	1:250
2nd	Alexa 594-conjugated goat anti-mouse IgG	goat	Invitrogen; Eugene, Oregon	1:250
1st	cleaved-caspase-3(Asp175)	rabbit	Cell Signaling Technology	1:500
2nd	Alexa 594-conjugated goat anti-rabbit IgG	goat	Molecular probes, Invitrogen	1:250
1st	Anti-Brn3a	mouse	Chemicon and Linco, Millipore	1:125
2nd	Alexa 568-conjugated goat anti-mouse IgG	goat	Molecular probes, Invitrogen	1:500
1st	phospho-c-Jun (Ser63)	rabbit	Cell Signaling Technology, Danvers, MA	1:100
2nd	Alexa 633-conjugated goat anti-rabbit IgG	goat	Molecular probes, Invitrogen	1:200
1st	Anti-Iba1	rabbit	Wako Pure Chemical Industries, Ltd	1:1000
2nd	Alexa 568-conjugated goat anti-rabbit IgG	goat	Molecular probes, Invitrogen	1:500

Confocal Microscopy and Image Acquisition

Images of YFP positive retina and optic nerve were acquired with a Leica TCS-SP2 AOBS confocal microscope (Leica Microsystems, Wetzlar, Germany). Targeted optic nerves or retina were imaged with a scan resolution of 1024 × 1024 pixels. DAPI fluorescence was excited using a 405nm laser, and emission was detected over a range of 410-550 nm with the intensity at 25%. YFP fluorescence was excited using the 514 nm line of an argon laser, and emission was detected over a range of 520-554 nm with the intensity at 50%. Texas-Red fluorescence was excited using a 594 nm helium–neon laser, and emission was detected over a range of 605-700 nm with the intensity at 50%. Alexa 568 fluorescence was excited using a 594 nm helium–neon

laser, and emission was detected over a range of 599-628 nm with the intensity at 100%. Alexa 594 fluorescence was excited using a 594 nm helium–neon laser, and emission was detected over a range of 600-652 nm with the intensity at 100%. Alexa 633 fluorescence was excited using a 633 nm helium–neon laser, and emission was detected over a range of 640-685 nm with the intensity at 100%. During scanning, the "Offset" of PMT (photon multiply tube) which adjusts the background was set to show a few green spots, and the "Gain" of PMT which adjusts the bright points was set to show a few blue spots using the color gradient to avoid pixel intensity saturation. To minimize noise, the line averaging was always set at 4. A sequential scan was performed to avoid the potential for crosstalk between the YFP fluorophore, DAPI and Alexa dyes. For the study of the spatial-temporal relationship between the axon and macrophage/microglia, their three-dimensional reconstruction was obtained via the Volocity Software package (Improvision, version 4.3.2, Perkin Elmer; Waltham, MA).

Electron microscopy

For electron microscopic (EM) analysis, two different perfusion protocols were employed to achieve: (1) optimal ultrastructure detail, or (2) the optimal visualization of the YFP-positive axons.

To achieve optimal ultrastructure detail, wild type mice or the YFP-16 transgenic mice were first perfused with 100ml heparinized normal saline, followed by 200ml 2% paraformaldehyde and 2.5% glutaraldehyde in Millonig's buffer. After 15 minutes fixation, the retina was removed as described above, and immersed in 2% paraformaldehyde and 2.5% glutaraldehyde in Millonig's buffer overnight, together with the brain and the optic nerve. Then these fixation prepared retina and optic nerves were osmicated, dehydrated, and flat embedded in epoxy resin (Embed-812; Electron Microscopy Sciences, Hatfield, PA) as detailed below.

For the optimal EM analysis of the YFP positive axons, the YFP-16 transgenic mice were first perfused with 100ml heparinized normal saline, followed by 200ml 4% paraformaldehyde and 0.2% glutaraldehyde in Millonig's buffer in order to maintain the structure of YFP fluorescent protein and optimize immunoreactivity. Again, the brain and the optic nerves were post-fixed and blocked as described above. Then the optic nerve sections were cut longitudinally at 16µm with a vibratome (Leica VT1000 S; Leica Microsystems GmbH, Nussloch, Germany), and then prepared for immunocytochemistry using a primary antibody rabbit anti-GFP (1:8000; Chemicon) followed by the secondary antibody, biotinylated goat anti-rabbit IgG (1:1000; Vector). Next, the tissue was incubated in avidin-biotin complex (1:200, Vectastain ABC Standard Elite Kit; Vector Laboratories), and visualized by diaminobenzidene (DAB; Sigma-Aldrich, St. Louis, MO) for subsequent EM analysis.

Briefly, the above-prepared retina, optic nerves and the immunoreactive YFP-expressing optic nerve sections were osmicated in 1% OsO4, dehydrated, embedded in epoxy resins, mounted on plastic slides (Thomas Scientific Co., Swedesboro, NJ) and cover-slipped. After resin curing, the plastic slides were examined via routine light microscopy to identify RGCs, or the injured axonal segments within the optic nerve based on the patterns of distribution seen in the YFP-expressing mice evaluated by confocal microscopy. Once identified, these sites were excised, mounted on plastic studs, and thick sectioned to the RGC layer, or the depth of the immunoreactive sites of interest using an ultramicrotome (Leica Ultracut R; Leica, Wien, Austria). Serial 40nm sections were cut and mounted onto Formvar-coated single-slotted grids. The grids were then stained with 5% uranyl acetate in 50% methanol for 2 minutes and 0.5% lead citrate for 1 minute, and visualized using a JEM 1230 electron microscope (JEOL Ltd., Tokyo, Japan).

Quantification of YFP fluorescent axonal swellings and statistical analysis

At the 12, 24 and 48 hours post injury time points, quantitative analysis of any observed axonal swelling detected by confocal imaging was conducted. The randomly selected YFP optic nerve sections were analyzed via the placement of 12 serial grids (each grid = 200 µm x 200 µm) along the optic nerve, six of which were placed proximally and labeled P1–P6 moving from the initial locus of TAI (approximately 1 mm rostral to the chiasm) to the globe, and the other six grids were located distally and labeled D1–D6 moving from the initial locus of TAI to the chiasm(Figure 3.6). Each 200 µm x 200 µm grid was aligned over the center of the optic nerve. For each individual grid, the number of axonal swellings per unit area, the total area of axonal swellings per unit area, and the percentage of the total area of axonal swellings per unit area, as well as the size of axonal swellings per unit area were measured using the Imaging Processing (IP) Lab 3.7 image analysis system (Scanalytics, Inc., Fairfax, VA). Only those swellings over 5 µm in diameter were analyzed (Gao et al., 2010). Any swellings overlapping either the top, the bottom, or the left line of the grid were included, while those overlapping the right grid line were excluded from analysis. All results were presented as mean ± standard error of the mean (SEM). Each dependent variable was analyzed separately by a split-plot analysis of variance [ANOVA; 3 (Time) x 12 (Location)]. To examine the specific effect of time for each dependent variable at each of the locations, subsequent one-factor (time) ANOVAs and posthoc Fisher LSD tests were conducted for each grid location. Statistical significance was set at $p < 0.05$ for all tests.

Quantification of RGC and statistical analysis

To quantify the number of RGCs, the Brn3a immunofluorescently labeled retinal sections were captured using routine epifluorescent microscopy. Specifically, Brn3a retinal section (4 sections per eye, with each slide containing 8 sections from both eyes) was digitally acquired at 20 x magnification moving from side to side of the retina covering its entire extent, parallel to its curvature. Each retinal section was reconstructed using 7-9 images taken along the extent of the retina (Figure 4.4 A). To quantify the number of RGCs, the central image of those acquired was selected together with the other next adjacent image from both sides (Figure 4.4 A arrow). For each selected image, the number of Brn3a positive RGCs was counted in a 0.05 mm^2 grid expanding along the image parallel to the alignment of the RGCs (Figure 4.4 B). This process of acquisition and counting was repeated for each of the retinal sections on the slide for a total of 72 retinal images per animal (3 images/section x 8 sections/slide x 3 slides/animal = 72 images/animal). For each animal, the number of Brn3a positive RGCs was calculated by summating the number of Brn3a positive RGCs from the 72 images, expressing them as mean ± standard deviation. To test the difference of the number of Brn3a positive RGCs overtime post injury, one way ANOVA was conducted. Statistical significance was set at $p < 0.05$ for all tests.

CHAPTER THREE

TRAUMATIC AXONAL INJURY IN THE OPTIC NERVE: EVIDENCE FOR AXONAL SWELLING, DISCONNECTION, DIEBACK, AND REORGANIZATION

Abstract

Traumatic axonal injury (TAI) is a major feature of traumatic brain injury (TBI) and is associated with much of its morbidity. To date, significant insight has been gained into the initiating pathogenesis of TAI. However, the nature of TAI within the injured brain precludes the consistent evaluation of its specific anterograde and retrograde sequelae. To overcome this limitation, we used the relatively organized optic nerve in a central fluid percussion injury (cFPI) model. To improve the visualization of TAI, we utilized mice expressing yellow fluorescent protein (YFP) in their visual pathways. Through this approach, we consistently generated TAI in the optic nerve and qualitatively and quantitatively evaluated its progression over a 48-h period in YFP axons via confocal microscopy and electron microscopy. In this model, delayed axonal swelling with subsequent disconnection were the norm, together with the fact that once disconnected, both the proximal and distal axonal segments revealed significant dieback, with the proximal swellings showing regression and reorganization, while the distal swellings persisted, although showing signs of impending degeneration. When antibodies targeting the C-terminus of amyloid precursor protein (APP), a routine marker of TAI were employed, they mapped exclusively to the proximal axonal segments without distal targeting, regardless of the

survival time. Concomitant with this evolving axonal pathology, focal YFP fluorescence quenching occurred and mapped precisely to immunoreactive loci positive for Texas-Red-conjugated-IgG, indicating that blood–brain barrier disruption and its attendant edema contributed to this phenomenon. This was confirmed through the use of antibodies targeting endogenous YFP, which demonstrated the retention of intact immunoreactive axons despite YFP fluorescence quenching. Collectively, the results of this study within the injured optic nerve provide unprecedented insight into the evolving pathobiology associated with TAI.

Key words: anterograde and retrograde axonal change; amyloid precursor protein; axonal dieback; brain edema; traumatic brain injury; YFP mice

Introduction

Traumatic axonal injury (TAI) is a major feature of human traumatic brain injury (TBI) (Povlishock and Katz 2005), and has been associated with much of its morbidity (Graham et al., 2002). This has recently been reaffirmed by the use of modern imaging tools, including diffusion tensor imaging, which consistently demonstrates the presence of axonal injury across the spectrum of mild to severe TBI (Belanger et al., 2007; Kumar et al., 2010; Wang et al., 2008). In human postmortem studies, as well as in experimental animal investigations, significant insight has been gained into its initiating pathogenesis (Blumbergs et al., 1989; Buki et al., 2000; Christman et al., 1994; Farkas and Povlishock, 2007; Kelley et al., 2006; Maxwell et al., 1997; Pettus and Povlishock, 1996; Povlishock, 1992; Povlishock and Katz, 2005; Saatman et al., 2003; Saatman et al., 2009), and its potential therapeutic management (Buki et al., 2003; Deng-Bryant et al., 2008; Hall et al., 2010; Kilinc et al., 2007; Koizumi and Povlishock, 1998;

Marmarou and Povlishock, 2006; Mbye et al., 2009; Maxwell et al., 2005; Oda et al., 2011; Okonkwo et al., 1999; Saatman et al., 2010).

Despite this progress, however, a fully comprehensive appreciation of TAI has been limited by both technical and animal modeling issues that have precluded the possibility of experimentally analyzing the course of a single nerve fiber from its initial injury to its ultimate axotomy. Further, although various antibodies have been widely embraced in both humans and animals to target such evolving axonal pathology, it is unclear if these antibodies, many of which target amyloid precursor proteins (APP; Blumbergs et al., 1995; Hortobagyi et al., 2007; Sherriff et al., 1994a, 1994b; Stone et al., 2000), universally detect axonal change within the proximal disconnected axonal segment versus the more distal, disconnected segment, or both. This issue is of more than academic interest in that these antibodies are routinely used in human forensic analysis (Gleckman et al., 1999; Reichard et al., 2005).

To better follow the proximal and distal progression of traumatically-induced axonal injury, we assessed in the current study the relationship of known biological markers of axonal injury in an animal central fluid percussion injury (cFPI) model that evokes TAI within the optic nerve, whose axons manifest a relatively organized alignment. Further, to better follow the fate of these damaged axonal segments and their relation to known immunocytochemical markers of axonal injury, we utilized transgenic animals expressing yellow fluorescent protein (YFP), a variant of green fluorescent protein (GFP), in the optic nerve. Through the use of qualitative and quantitative imaging approaches examining the YFP expressing injured axons, we confirm and significantly extend previous data supporting the delayed pathogenesis of TAI. Importantly, we also provide unprecedented insight into this complex pathology, demonstrating post-TBI axonal swelling and disconnection, with proximal and distal axonal dieback accompanied by the

regression and reorganization of the proximal axonal swellings, and the degeneration and delayed clearance of the distal swellings.

Methods

To visualize axonal damage within the optic nerve, we utilized C57/BL6 wild-type mice and Thy1-YFP-16 transgenic mice which express YFP under the promoter Thy1 within over 80% of the optic nerve fibers (Feng et al., 2000). We posited that within such a YFP-positive fiber population, any potential axonal change induced by the traumatic event could be easily and consistently visualized via routine fluorescence and/or confocal microscopy.

Breeding and genotyping of YFP-16 transgenic mice

The Thy1-YFP-16 transgenic mice [B6.Cg-Tg(Thy1-YFP)16Jrs/J, stock number 003709] were obtained from the Jackson Laboratory (Bar Harbor, ME) and maintained as heterozygotes. Inheritance of the YFP gene was identified from an ear punch taken at weaning (approximately postnatal day 21). The ear tissue was mounted onto a glass slide and examined using a FITC filter on an Olympus DP71 digital camera (Olympus, Center Valley, PA), where YFP-positive axons could be easily identified.

Surgery and animal model of traumatic brain injury

All protocols used in this study were approved by the Institutional Animal Care and Use Committee (IACUC) of Virginia Commonwealth University. Adult male C57/BL6 mice and Thy1-YFP-16 transgenic mice (20–25g) were subjected to central fluid percussion TBI to produce TAI in the optic nerve. The fluid percussion injury model was modified from that

previously described in detail by Dixon (1987). Briefly, animals were anesthetized with 4% isoflurane in 100% O_2, and maintained via nosecone with 2% isoflurane in 100% O_2 during surgery, with the body temperature controlled at 37^{o}C via a feedback-controlled heating pad (Harvard Apparatus, Holliston, MA). A midline 3.0mm circular craniotomy was made over the sagittal suture halfway between the bregma and the lambda, taking care not to damage the underlying dura. A Luer-Loc syringe hub was cut away from a 20 gauge needle and affixed to the craniotomy site. Dental acrylic was applied around the hub to enhance stability. As the dental acrylic dried and the injury hub became stable, saline was applied to blunt any exothermic reaction from the cured acrylic. The skin was then sutured over the hub, with lidocaine and bacitracin ointment applied to the wound. The animal was allowed to recover for 1h in a warmed cage prior to injury. Before the induction of injury, each animal was again anesthetized for 4min (100% O_2 and 4% isoflurane). The craniotomy site was exposed and the injury hub was connected to the fluid percussion device. The animal was then injured at a magnitude of 1.40 ± 0.05 atmospheres. The pressure pulse was measured by a storage oscilloscope (Tektronix 5111; Tektronix, Beaverton, OR). Injury preparation and induction were completed prior to the animal's recovery from anesthesia. The hub and dental acrylic were then removed, and the incision was rapidly sutured. The duration of transient unconsciousness was determined by measuring the time it took for the animal to recover the following reflexes: toe pinch, tail pinch, corneal blink, pinna, and righting reflex. After recovery of the righting reflex, the animals were placed in an incubator with a heating pad to maintain normothermia and monitored during recovery. For animals receiving sham injury, all of the above steps were followed with the exclusion of the injury pulse. All injured animals had righting reflex recovery times of 4 - 5min, compared with less than 2min for sham-injured animals, indicating injuries of comparable

severity. The animals were allowed to survive 5min, 15min, 1h, 3h, 12h, 24h, and 48h following injury.

Optic nerve preparation

At the appropriate survival times, Thy1-YFP-16 transgenic mice and wild-type mice were euthanized via an intraperitoneal overdose of sodium pentobarbital, and then transcardially perfused with 100ml heparinized normal saline, followed by 200ml 4% paraformaldehyde in Millonig's buffer. After overnight incubation in the perfusion fixative solution, the optic nerve, chiasm, and optic tract, together with the brain were removed from the skull for routine fluorescence and confocal analysis. The optic nerves were blocked to include the entire optic nerve, the chiasm, the initial part of the optic tract, and related brain tissue, and post-fixed in the same solution overnight. Following post-fixation, this optic nerve block was cryoprotected and then cut longitudinally into 10µm sections with a cryotome (Shandon Scientific Ltd., Cheshire, U.K.). Serial sections revealing the entire length of the optic nerve (from the globe to the chiasm) were then collected in a serial order. All sections were collected beginning at a randomly generated starting point in Millonig's buffer in 24-well culture plates (Falcon, Newark, DE). Beginning at a random starting point, every fourth serial section was then prepared for the visualization of the YFP. These sections were directly mounted on glass slides with ProLong-Gold antifade reagent (Invitrogen, Carlsbad, CA), and cover-slipped for image capture with a Leica TCS-SP2 AOBS confocal microscope (Wetzlar, Germany) under the same setting. The adjacent serial sections were used for immunohistochemical staining via antibodies targeting APP. Next, the adjacent serial sections were prepared for the evaluation of potential blood–brain barrier (BBB) disruption via antibodies targeting IgG. Lastly, the subsequent adjacent serial

sections were used for determining axonal integrity via antibodies targeting the endogenous YFP (see below).

Immunohistochemistry

To study the relationship between the YFP-linked axonal change and an established biological marker of axonal pathology, antibodies targeting APP were used. YFP fluorescent optic nerve sections were microwaved for antigen retrieval (Stone et al., 1999; Stone et al., 2000), incubated with the primary antibody rabbit anti-C-terminus APP (1:1000; Zymed, San Francisco, CA), washed, and then incubated in the secondary antibody Alexa 594-conjugated goat anti-rabbit IgG (1:200, Vector Laboratories, Burlingame, CA). Then the sections were washed and mounted for analysis via confocal microscopy.

Additionally, to determine if these axonal changes were related to blood-brain barrier (BBB) disruption, with the formation of edema and its potential quenching of the YFP fluorescence, we probed the adjacent optic nerve sections with the antibody Texas-Red conjugated goat anti-mouse IgG (1:200; Invitrogen), targeting mouse serum proteins, and mapping any potential changes in BBB status with any related loss of YFP fluorescence.

Lastly, to determine the potential for axonal preservation despite the loss of YFP fluorescence due to YFP fluorescence quenching, we reacted the subsequent adjacent segments with antibodies targeting the endogenous YFP. Briefly, after antigen retrieval in a microwave, YFP-expressing optic nerve sections were incubated with a primary antibody rabbit anti-GFP (1:8000; Chemicon, Temecula, CA). This was done because YFP and GFP share the same structure (Shagin et al., 2004). Thus, antibodies to GFP also recognize the YFP antigen (Sprecher and Desplan, 2008). Next, the sections were washed, followed by incubation in the secondary

antibody Alexa 594-conjugated goat anti-rabbit IgG (1:500; Vector Laboratories) for confocal microscopic analysis. In these immunocytochemical/confocal studies 5 injured mice were evaluated per time point, with the evaluation of 1 sham injured control per time point.

Electron microscopy

For electron microscopic (EM) analysis, additional mice were employed to include 1 injured wild-type mouse, 1 injured YFP-expressing mouse, and their appropriate sham injured controls per time point. In these animals, two different perfusion protocols were employed to achieve: (1) optimal ultrastructure detail, or (2) the optimal visualization of the YFP-positive axons. To achieve optimal ultrastructure detail, wild-type mice were first perfused with 100mL heparinized normal saline, followed by 200ml 2% paraformaldehyde and 2.5% glutaraldehyde in Millonig's buffer. For EM analysis of the Thy1-YFP-16 transgenic mice, the animals were first perfused with 100ml heparinized normal saline, followed by 200ml 4% paraformaldehyde and 0.2% glutaraldehyde in Millonig's buffer in order to maintain the structure of YFP fluorescent protein and optimize immunoreactivity. Again, the brain and the optic nerves were post-fixed and blocked as described above. For routine EM study the whole optic nerve was osmicated, dehydrated, and flat embedded in epoxy resin (Embed-812; Electron Microscopy Sciences, Hatfield, PA) as detailed below. In contrast, for the YFP-expressing mice, the optic nerve sections were cut longitudinally at 16µm with a vibratome (Leica VT1000 S; Leica Microsystems GmbH, Nussloch, Germany), and then prepared for immunocytochemistry using a primary antibody rabbit anti-GFP (1:8000; Chemicon) followed by the secondary antibody, biotinylated goat anti-rabbit IgG (1:1000; Vector). Next, the tissue was incubated in avidin-biotin complex (1:200, Vectastain ABC Standard Elite Kit; Vector Laboratories), and visualized by

diaminobenzidene (DAB; Sigma-Aldrich, St. Louis, MO) for subsequent EM analysis.

Briefly, the above-prepared immunoreactive YFP-expressing sections were osmicated in 1% OsO4, dehydrated, embedded in epoxy resins, mounted on plastic slides (Thomas Scientific Co., Swedesboro, NJ) and cover-slipped. After resin curing, the plastic slides were examined via routine light microscopy to identify the injured axonal segments within the optic nerve based on the patterns of distribution seen in the YFP-expressing mice previously evaluated by confocal microscopy. Once identified, these sites were excised, mounted on plastic studs, and thick sectioned to the depth of the immunoreactive sites of interest using an ultramicrotome (Leica Ultracut R; Leica, Wien, Austria). Serial 40nm sections were cut and mounted onto Formvar-coated single-slotted grids. The grids were then stained with 5% uranyl acetate in 50% methanol for 2 min and 0.5% lead citrate for 1 min, and visualized using a JEM 1230 electron microscope (JEOL Ltd., Tokyo, Japan).

Confocal microscopic data analysis

At the 12-, 24-, and 48-h time points, quantitative analysis of any observed axonal swelling detected by confocal imaging was conducted. The randomly selected YFP optic nerve sections were analyzed via the placement of 12 serial grids (each grid = 200 µm x 200 µm) along the optic nerve, six of which were placed proximally and labeled P1–P6 moving from the initial locus of TAI (approximately 1 mm rostral to the chiasm) to the globe, and the other six of which were located distally and labeled D1–D6 moving from the initial locus of TAI to the chiasm. Each 200 µm x 200 µm grid was aligned over the center of the optic nerve. For each individual grid, the number of axonal swellings per unit area, the total area of axonal swellings per unit area, and the percentage of the total area of axonal swellings per unit area, as well as the size of

axonal swellings per unit area were measured using the Imaging Processing (IP) Lab 3.7 image analysis system (Scanalytics, Inc., Fairfax, VA). Only those swellings over 5 μm in diameter were analyzed (Gao et al., 2010). Any swellings overlapping either the top, the bottom, or the left line of the grid were included, while those overlapping the right grid line were excluded from analysis. All results were presented as mean ± standard error of the mean (SEM). Each dependent variable was analyzed separately by a split-plot analysis of variance [ANOVA; 3 (Time) x 12 (Location)]. To examine the specific effect of time for each dependent variable at each of the locations, subsequent one-factor (time) ANOVAs and posthoc Fisher LSD tests were conducted for each grid location. Statistical significance was set at $p < 0.05$ for all tests.

Results

Macroscopic changes in the mouse brain and optic nerve

Using this model system, which was modified from that previously used in rats (Dixon et al., 1987), we consistently generated microscopic injury in the optic nerve (see below), without overt damage to the brain tissue. As shown in Figure 3.1A, the injured brain revealed no significant contusion, parenchymal hemorrhage, or overt damage of the optic nerve and/or the globe. Macroscopic brain sectioning again revealed no damage within the brain parenchyma, either in terms of intraparenchymal petechial hemorrhage or blood in the intraventricular space.

Qualitative fluorescent microscopic change within the optic nerve following TBI

Despite the lack of macroscopic damage in this model, axonal damage was evoked in a scattered fashion throughout the brain parenchyma as well as the optic nerve of Thy1-YFP-16 transgenic mice following TBI. While not the focus of the current communication, within the

brain parenchyma itself, scattered axonal damage could be identified within both the superficial and deep layers of the neocortex, as well as the dorsolateral thalamus and subcortical white matter. These findings are entirely consistent with those recently reported in the same mouse injury model using a YFP-H mouse (Greer et al., 2011). Importantly, in the current study these axonal changes occurred without any evidence of local petechial hemorrhage and/or any other form of tissue disruption, consistent with a mild TBI. Within the optic nerve, the traumatic axonal injury typically was induced approximately 1mm proximal to the chiasm. As will be detailed below, within this locus, scattered reactive axonal change could be observed in YFP-expressing axons, while adjacent YFP axons maintained normal structural detail. These findings stood in stark contrast to the sham-injured animals, wherein numerous linear/non-swollen YFP-expressing axonal profiles (Fig.3.1B) could be seen spanning the length of the optic nerve, consistent with the initial characterization of the Thy1-YFP-16 transgenic mouse (Feng et al., 2000).

Consistent with previous descriptions of traumatically induced axonal damage, the injured YFP-expressing axons demonstrated a progression of reactive change over time. At 1h post-TBI, the majority of axons manifested normal morphology, with only scattered axons demonstrating punctuate, focal YFP-fluorescent axonal swellings (Fig. 3.1C), as well as some evidence of initial axonal disconnection (Fig. 3.1D). These scattered punctuate swellings were typically found at only one locus along the axon's length, without any evidence of additional proximal to distal involvement.

By 3h post-TBI, focal axonal disconnection was now prominent together with a significant increase in the number and the size (8.32±0.69μm) of the YFP-expressing axonal swellings, which now capped both the proximal and distal disconnected segments. Again, these

damaged axons were interspersed among adjacent intact fibers (Fig. 3.1E). At this time point, those proximal axonal swellings maintaining continuity with the retina (arrow in Fig. 3.1E) appeared bulbous/spheroidal in shape. The distal axonal swellings on those axons projecting to the chiasm were also spheroidal (arrowhead in Fig. 3.1E). As now both the proximal and distal swellings were frequently separated, this suggested axonal retraction or dieback, an issue further detailed below.

By 12h post-TBI, the above described YFP-expressing axonal swellings exhibited further maturation (Fig. 3.2A), with axonal disconnection now predominating. The proximal axonal swellings had expanded to an area of 28.26±2.00μm^2, and now revealed a more truncated configuration (Fig. 3.2C and 3.2E). In contrast, the distal axonal swellings continued to expand (25.53±1.38μm^2), yet maintained their more rounded/spheroidal shape (Fig. 3.2B and 3.2D). From 24h to 48h post-TBI, the distal axonal swellings underwent further expansion (42.78±5.88μm^2 at 24h post-TBI, and 50.84±2.48μm^2 at 48h post-TBI), with their distribution shifted more distally toward the chiasm. Similarly, the proximal axonal swellings now redistributed from the initial site of injury to the more proximal segments of the optic nerve approaching the globe. In contrast to the distal segments, however, these proximal truncated segments showed continued evidence of shrinkage and resorption.

While these axonal findings at 12, 24, and 48h post-TBI were scattered, routine confocal analysis revealed that these reactive axonal changes and dieback were accompanied by an apparent focal loss of fluorescence in the region between the detached proximal and distal axonal segments. At first, this was interpreted to reflect total fiber loss in this now nonfluorescent domain. However, as will be explicated below, this apparent fluorescent fiber loss was not the

result of actual fiber dissolution. Rather it was the result of local fluorescence quenching, a sequelae of local BBB disruption discussed below.

Electron microscopic evaluation of the traumatic axonal damage

EM analysis confirmed and supplemented the above described fluorescence analysis. Via EM analysis of the wild type mice, we observed as early as 5 to 15 min post-TBI, scattered axons located approximately 1mm rostral to the optic chiasm demonstrating initial axonal swelling, associated with an accumulation of mitochondria (M in Fig. 3.3). Despite these local reactive changes, adjacent axons remained intact and displayed normal ultrastructural detail, all of which was consistent with previous descriptions of TAI. In these same regions, edematous-like change could also be identified via the expansion of the interstitial space (asterisk in Fig. 3.3). Additionally, by 1h post-TBI, there was local dissolution of some damaged axons, consistent with the process of disconnection and separation (arrowhead in Fig. 3.3).

By 3h post-TBI, axonal detachment was common in the Thy1-YFP-16 mice, with both the proximal and distal axonal swellings now easily recognized. As observed via confocal microscopy above, both proximal and distal swellings were spheroidal, with obvious separation between the proximal and distal swellings. Although it proved difficult to follow the course of one individual separated axon via electron microscopy, examination of numerous serial sections revealed that the proximal and distal swellings were separated by highly vacuolated and organelle-devoid axonal cylinders, suggesting that they were the residual axonal segments that once joined both the proximal and distal swellings. The proximal swelling appeared reminiscent of previous descriptions of TAI in that the swelling itself contained numerous profiles of smooth endoplasmic reticulum and vesicles which were interspersed with intact mitochondria and

multiple vesicular profiles embedded in an electron-lucent axoplasm (Povlishock et al., 1983). This proximal organelle cap typically encompassed a disorganized cytoskeletal core containing misaligned neurofilaments and microtubules. The distal swellings also showed organelle accumulation and a disorganized cytoskeletal core (Fig. 3.4). However, unlike the proximal segments, these swellings were typically electron dense, and they contained numerous dilated mitochondria with disorganized cristae (M in Fig. 3.4), all of which appeared consistent with an ongoing degenerative process.

By 24h post-TBI of the Thy1-YFP-16 mice, the distal swellings enlarged further, once again containing numerous mitochondria with disordered cristae, as well as occasional autophagic vacuoles and lysosomal debris (Fig. 3.5C and D). In contrast to the distal swellings, the proximal axonal swellings, similarly to those observed via confocal fluorescence microscopy, were now truncated (Fig. 3.5A and B). Typically, these truncated segments were encompassed by an intact myelin sheath, and contained numerous organelles, all of which appeared intact (Fig. 3.5B). Specifically, these truncated appendages contained numerous mitochondria, profiles of smooth endoplasmic reticulum and vesicles, as well as cytoskeletal constituents, all of which revealed normal morphological detail. In contrast to the distal swellings, not only did these proximal swellings reveal intact mitochondria, but importantly, these organelles were found in an electron-lucent environment, with no evidence of increased electron density.

Quantitative analysis of the progressive axonal swellings and dieback in the proximal and distal segments

As noted, the quantitative analysis conducted in the current investigation employed confocal microscopy to assess the number of axonal swellings per unit area, the total area of

axonal swellings per unit area, the percentage of the total area of axonal swellings per unit area, as well as the size of axonal swellings per unit area. As noted, these measures were examined along the proximal to distal extent of the optic nerve, with a grid analysis (Fig. 3.6) that moved both proximally and distally from the point of injury initiation.

While examining the total number of axonal swellings within each grid, a split-plot ANOVA on these data yielded a significant main effect of location ($F_{11, 66} = 81.31$, $p<0.001$), and a Time x Location interaction ($F_{22, 66} = 22.44$, $p<0.001$). Figure 3.7 displays a line graph (Fig. 3.7A) and a bar graph (Fig. 3.7B) of the same data set, along with the results of the Fisher LSD tests that examined significant group differences at each axonal location. In the proximal portion of the optic nerve, the peak number of axonal swellings per unit area revealed significant redistribution from 200µm – 400µm (grid P2) at 12 h post-TBI (97.44±7.61), to 400µm – 600µm (grid P3) at 24 h post-TBI (53.22±9.56), and approaching 600µm – 800µm (grid P4) at 48h post-TBI (46.55±4.05). These data suggested a dieback of the proximal disconnected axons over time. Similarly, axonal swellings in the distal segment moved in the opposite direction toward the chiasm. Specifically, here the peak number of axonal swellings per unit area moved from 200µm – 400µm (grid D2) at 12 h post-TBI (87.56±13.36), to 400µm – 600µm (grid D3) at 24h post-TBI (87.11±8.78), and approaching 600µm – 800µm (grid D4) at 48 h post-TBI (103.78±1.73). These quantitative findings confirmed those qualitative impressions of proximal swelling and regression as well as distal expansion and retention, all of which were associated with dieback.

Comparable to the data discussed in terms of the number of axonal swellings, a similar relationship was found in the total area of the axonal swellings per unit area over time along the length of the optic nerve. As shown in Figure 3.8, a split-plot ANOVA on these data again revealed a significant main effect of location ($F_{11, 66} = 68.85$, $p<0.001$), and a Time x Location

interaction ($F_{22, 66}$ = 19.27, $p<0.001$). In the proximal segment, the peak total area of axonal swellings was redistributed from 200µm – 400µm proximal to the lesion (grid P2) at 12h post-TBI (2203.67±216.93µm^2), to 400µm – 600µm proximal to the lesion (grid P3) at 24h post-TBI (1502.28±42.09µm^2), and further to 600µm –800µm proximal to the lesion (grid P4) at 48h post-TBI (1006.01±137.07µm^2). In the distal segment, the peak total area of axonal swellings migrated from 200µm – 400µm distal to the lesion (grid D2) at 12h post-TBI (2271.54±451.63µm^2), to 400µm – 600µm distal to the lesion (grid D3) at 24h post-TBI (3689.21±294.12µm^2), and further to 600µm – 800µm distal to the lesion (grid D4) at 48h post-TBI (5267.26±209.76µm^2). This again demonstrated progressive axonal dieback in both the proximal and distal directions along the optic nerve post-TBI.

Similarly, the analysis on the percentage of the total area of axonal swellings per unit area revealed a statistically significant relationship comparable to that described above over time along the length of the optic nerve (data not shown). In contrast, the analysis of the size of axonal swellings per unit area did not reveal robust significant changes over time along the length of the optic nerve (data not shown).

Relationship between the above-described YFP-linked changes and established markers of TAI (APP)

To compare the above results of progressive proximal and distal axonal swellings obtained from the YFP-16 transgenic mice to the previous data gained from the use of biological markers of axonal pathology, including those targeting APP, a dual fluorescence approach was employed. At all time points post-TBI, the use of antibodies to APP alone revealed immunoreactive axonal swellings consistent with previous descriptions (Fig. 3.9). However,

when these same nerve segments were examined via confocal microscopy to visualize both the endogenous YFP as well as the antibodies to the C-terminus of APP, an unanticipated response was seen. Specifically, in this approach, we noted that the antibodies to the C-terminus of APP mapped exclusively to proximal swellings, with no evidence of distal immunoreactivity, despite the presence of numerous large and well-formed distal YFP-positive swellings (Fig. 3.9).

Evidence for blood–brain barrier disruption and the retention of axons in the region of YFP fluorescence quenching

As noted previously, the delayed regional loss of YFP fluorescence observed in the current study was potentially related to fluorescence quenching and not to the over-loss of fiber coursing through this region. To assess this potential and its impact upon our data analysis, we probed the injured YFP optic nerve sections with antibodies to assess the BBB integrity (antibodies to endogenous IgG), as well as antibodies targeting the retention of potentially YFP fluorescence-quenched axons (the antibody to GFP recognizes the endogenous YFP; Sprecher and Desplan, 2008). As early as 1h post-TBI, Texas-Red fluorescent IgG mapped to the region of YFP fluorescent loss in the damaged optic nerve (Fig. 3.10A, B, and C), with the caveat that this IgG penetrance was not seen in sham YFP expressing animals. The zone of IgG Texas-Red fluorescence expanded further at 3h post-TBI (Fig. 3.10D, E, and F), and again mapped to the now expanded locus of YFP fluorescence loss. This extravasation of IgG was interpreted to reflect a focal perturbation of the BBB, with the passage of serum proteins into the interstitial space. Further, it was assumed that this protein passage most likely involved the concomitant movement of water, with the formation of edema, all of which were also consistent with our EM observations of edematous-like change occurring in the expanding interstitium (Fig. 3.3). It is

important to note that this barrier disruption, associated with IgG passage into the optic nerve, was not linked to the presence of either overt or petechial hemorrhage, suggesting a more subtle form of BBB perturbation.

Despite the breakdown of the BBB and the loss of YFP fluorescence, we also observed the persistence of intact/unaltered axons, as well as detached and fragmented axons, in these same regions via the use of antibodies targeting endogenous YFP. Specifically, as shown in Figure 3.11, through the anti-GFP antibody's positive immunoreactive staining of the endogenous YFP, the optic nerve at 24h post-TBI revealed the existence of unaltered axons coursing through the locus of fluorescence quenching, together with scattered damaged axonal profiles again consistent with TAI.

Discussion

This study illustrates that a model of traumatic brain injury is capable of evoking traumatic axonal change within the optic nerve that can be evaluated in a consistent fashion. The current study's use of YFP-expressing mice provides an unprecedented view into the pathogenesis of traumatic induced axonal injury, allowing for the precise identification of the initiation of axonal injury and the subsequent progression of axonal swelling and disconnection, as well as the ongoing proximal and distal axonal response. To date, others have studied traumatic axonal injury using optic nerve stretch (Maxwell et al., 1990; Maxwell and Graham, 1997; Mohammed Sulaiman et al., 2011; Saatman et al., 2003; Serbest et al., 2007), and these studies have provided important information on the progressive changes associated with traumatically-induced axonal injury. While one could argue that the reactive changes seen within the optic nerve following cFPI mirror those observed with the optic nerve stretch model,

differences do exist. Although both injury models involve predominantly the prechiasmatic region, cFPI, in contrast to optic nerve stretch (Gennarelli, et al., 1989), involves less prominent axonal damage over the length of the optic nerve. Further, following cFPI, blood–brain barrier disruption is seen within the optic nerve. This appears consistent with the brain parenchymal barrier disruption seen following fluid-percussion brain injury that has been linked to concomitant brain deformation and compression (Povlishock et al., 1978). Such differences between the optic nerve injury induced by cFPI versus optic nerve stretch suggest that unlike optic nerve stretch models, cFPI involves a stretch as well as a compression/deformation component that participates in the subsequent pathological response. Irrespective of the causative factors and their specific relationship to the pathobiology of TBI, the current animal model offers another important characteristic that further distinguishes it from the optic nerve stretch model. Specifically, unlike optic nerve stretch, cFPI also evokes TAI throughout the related brain parenchyma, which is entirely consistent with our recent finding of TAI within the neocortex, hippocampus, and thalamus of comparably injured YFP-H mice (Greer et al., 2011). This is of more than academic interest in that we envision that the currently described optic nerve injury model via its routine quantitative assessment of axonal damage will allow for rapid preclinical therapeutic screening using either intravenous, intraperitoneal, or intrathecal routes of therapy administration. The perceived benefit of this current cFPI-induced optic nerve injury model resides in the fact that if any therapy is judged to be protective within the optic nerve, such protection could then be easily screened in the brain parenchyma of these same animals, thereby providing more compelling evidence of generalized therapeutic efficacy.

In the current investigation using a model of brain and optic nerve injury, we demonstrated within the optic nerve, the involvement of multiple axons typically found in

relation to other unaltered axons. Consistent with previous descriptions of the pathogenesis of TAI, our studies confirmed that this optic nerve involvement did not involve physical transection of the axon or the concomitant involvement of local destructive vascular lesions (Maxwell et al., 1997; Povlishock et al., 1983; Povlishock and Kontos, 1985). Rather, the injury evoked in YFP-expressing axons was scattered swellings that underwent lobulation, leading to disconnection over a 1 to 3h post-TBI period. Particularly significant in the current communication was the parallel finding of the relatively rapid dieback of both the proximal and distal disconnected segments, together with the rapid regression of the proximal swollen axonal segment, and the persistence of the degenerating distal swelling. To our knowledge, these findings have not been previously described in either the experimental TBI animal or human forensic literature. As seen in the data provided, relatively significant dieback occurred in both the proximal and distal segments within 48h following injury, wherein the injured segments moved approximately 0.4–0.8mm in both the proximal and distal directions. While such dieback has not been previously described in the context of TBI, spatially and temporally similar dieback has been described following spinal cord injury (Horn et al., 2008; Kerschensteiner et al., 2005; Oudega et al., 1999), and laser induced in vitro axonal damage (Hellman et al., 2010). With spinal cord injury such dieback has been linked to macrophage infiltration and possible substrate modification (Busch et al., 2009; Horn et al., 2008), while in vitro studies suggest that calcium dysregulation plays an important role (Hellman et al., 2010). Given the differences between TBI and in vivo spinal cord injury and in vitro laser injury, the actual mechanisms involved in this dieback remain unclear, and perhaps may involve a combination of all the above factors. In relation to this process of axonal dieback, it is also of note that the singular distal swellings observed in the current study are at variance with the Wallerian changes described following physical transection of the optic

nerve, wherein Wallerian degeneration was associated with relatively dramatic axonal beading along the continuous axonal segment distal to the transection (Beirowski et al., 2010). This difference is most likely consistent with the nature of TAI, which does not evoke the dramatic local destructive change typically associated with the studies of Wallerian degeneration evoked by optic nerve transection (Beirowski et al., 2010), and/or the fiber damage seen with optic nerve ligation or crush (Knöferle et al., 2010). Although it is difficult to directly extrapolate from a static image the actual progression of a dynamic process, our parallel EM analysis proved useful in assessing the fate of the proximal and distal swellings. As noted, the distal swellings routinely demonstrated increased electron density, together with significant mitochondrial disruption, all of which are consistent with their degeneration and subsequent dieback.

In concert with the above observations focusing on the distal swellings, our evaluation of the proximal axonal swellings also provided significant, previously unreported insight into the progression of TAI. Our quantitative and qualitative studies confirmed the dieback of the proximal axonal swellings that moved proximally over time. As noted, such injured axons were seen adjacent to other intact fibers, although this relationship was somewhat obscured by the presence of local tissue edema and fluorescence quenching, an issue which will be discussed below. While the proximal segment, like its distal stump, revealed dramatic dieback, it also manifested a previously unappreciated response in which it underwent a relatively rapid transition from an enlarged and swollen to a thinned and truncated appendage. Parallel ultrastructural studies substantiated this finding and suggested that the dieback of the axonal swelling and its formation of the truncated appendage were not related to overt degeneration, but rather some form of axonal reorganization. In fact, this dynamic reorganization appeared

consistent with the conversion of anterograde to retrograde axonal transport, which has been suggested in other experimental studies (Martz et al., 1989; Sahenk and Lasek, 1988).

In concert with the above observations, another unanticipated finding centered on the observation that antibodies targeting C-terminus APP mapped exclusively to the proximal axonal segments, with virtually no evidence of distal swelling immunoreactivity at all the delayed time points assessed. Antibodies to APP have been widely used in animal studies and human forensic analysis (Hortobagyi et al., 2007; Sherriff et al., 1994a, 1994b; Stone et al., 2000), yet there has been no widespread appreciation of what component of the injured axon is delineated by APP. Further complicating this issue is also the fact that there has been no consideration of the potential that different antibodies targeting different APP epitopes may yield different responses. Our antibodies which target APP's C-terminus consistently mapped to the proximal swelling, without targeting to the distal swelling. In contrast, in studies of Wallerian degeneration within the optic nerve, using antibodies targeting the N-terminus of APP, Beirowski and colleagues (2010) demonstrated APP targeting of the distal swelling, although in these studies there was no attempt to evaluate the immunoreactivity of the proximal axonal segment. The difference between our study and that of Beirowski and colleagues most likely reflects epitope specificity, with the caveat that the degenerative change ongoing in the distal degenerating segment may undergo proteolytic cleavage of the C-terminus with the exposure of the N-terminus, an issue which will obviously require further evaluation. This observation also takes on increased importance in the context of human forensic studies, wherein the use of antibodies to the N-terminus is the norm, raising the issue as to whether the use of such antibodies may lead to either an over- or under-appreciation of the overall burden of axonal injury both in studies of adult brain injury and child abuse.

Although we have emphasized the scattered nature of axonal change occurring within the optic nerve, we have also observed that this phenomenon was negatively influenced by the presence of local CNS BBB disruption and edema, which correlated with local quenching of the endogenous YFP fluorescence. Such non-hemorrhagic BBB disruption is a well-recognized feature of mild TBI, and our lab has previously identified comparable barrier disruption and protein extravasation within the brainstem and neocortex following TBI (Kelley et al., 2007; Povlishock et al., 1978). The linkage of BBB disruption to fluorescent quenching is supported by the observation that all zones of local fluorescence loss mapped precisely to concomitant alterations in BBB status, as assessed by the passage of the endogenous immunoglobulin IgG. The suggestion here is that the parallel movement of water with the IgG participated in the fluorescent quenching. While this phenomenon has not been described in the context of fluorescently-expressing transgenic animals, it has been demonstrated that water and solvent properties of water can result in fluorescence quenching by multiple mechanisms such as hydrogen-bond interactions (Oshima et al., 2006), photoionization (Sadkowski and Fleming, 1980), the transition to a close-lying energy level (Tobita et al., 2001), intersystem crossing (Seliskar and Brand, 1971), and specific solute–solvent interactions (Ebbesen and Ghiron, 1989). Since optic nerve edema most likely involves significant water generation (Donkin and Vink, 2010), it is not unreasonable to assume that this water can participate in fluorescence quenching via either one or several of the above-described mechanisms. The correctness of this assumption is further supported by our parallel investigations using antibodies to the endogenous YFP, which consistently labeled fibers independent of their YFP fluorescence, via our reliance on a chromogen-based approach. This strategy confirmed that the loss of fluorescence was most likely due to quenching, and not associated with actual fiber loss.

In summary, this study reveals TBI-induced TAI within the optic nerve. Further, these observations within the optic nerve provide unique insight into the pathobiology associated with TAI, particularly in terms of axonal swelling, disconnection, and proximal and distal dieback changes not well appreciated in the highly complex brain environment. We also demonstrate that this optic nerve approach provides via its regional specificity, the opportunity for rigorous quantification. This provides the potential for multiple future applications utilizing the rigorous assessment to evaluate various therapeutic interventions in attenuating axonal damage, while also permitting the evaluation of anterograde downstream neuronal and/or synaptic plasticity, and/or the assessment of retrograde upstream neuronal injury.

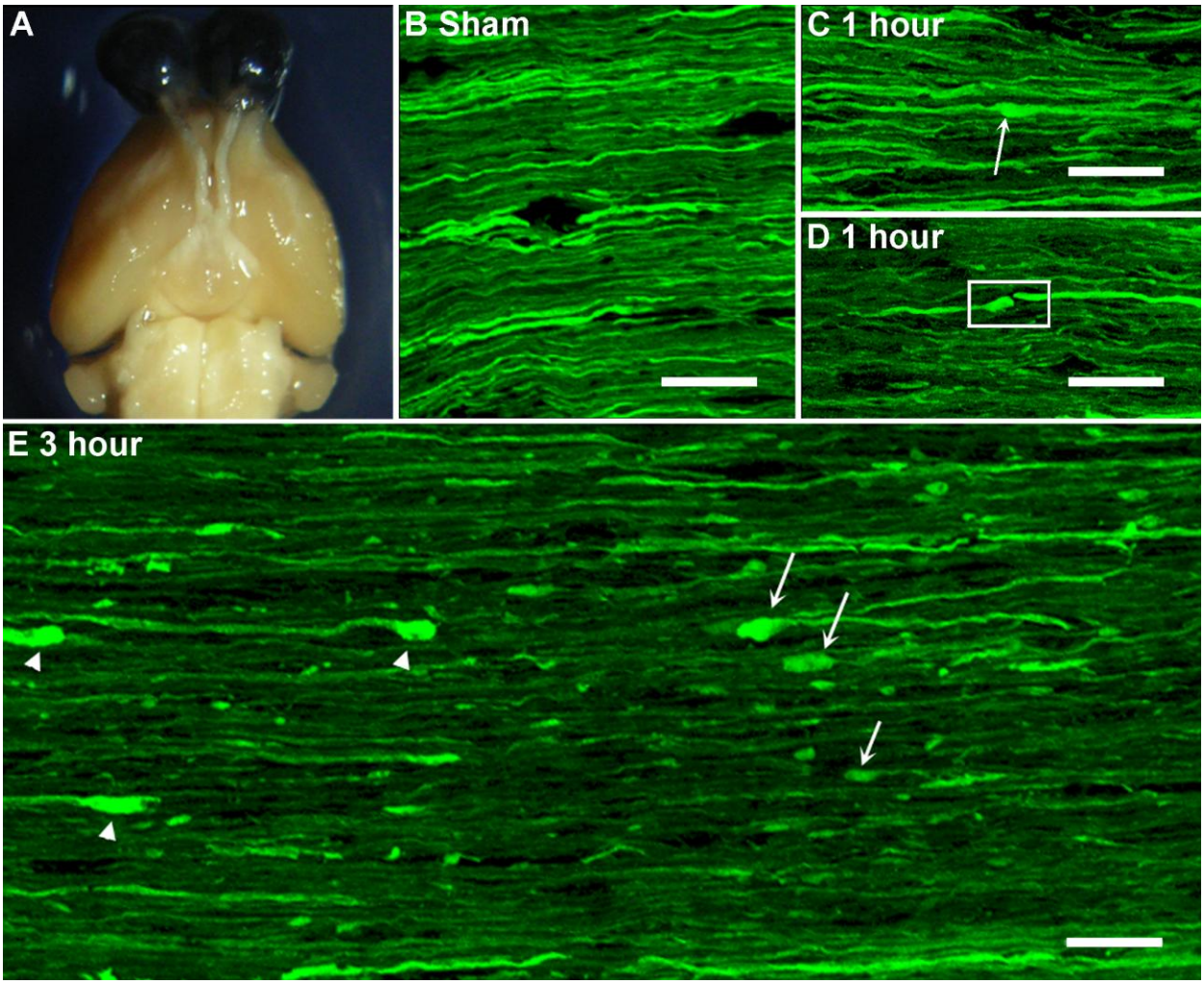

Figure 3.1 A macroscopic view of the injured brain and the optic nerve together with the microscopic evidence of axonal damage in the optic nerve of Thy1-YFP-16 mice. Note that upon macroscopic examination, no significant contusion, mass lesion or hemorrhage can be identified within either the brain or the optic nerve following TBI (A). Via confocal microscopy, the optic nerve of the sham injured mice reveals a robust distribution of YFP positive axons maintaining continuity with no evidence of axonal swelling (B). At 1 hour post TBI, the majority of YFP positive axons manifest normal morphology, with only scattered, punctate axonal swelling (arrow in C) and isolated axonal disconnection (grid in D). At 3 hours post TBI, note the increase in both the number and the size of axonal swellings in both the proximal (arrow in E) and distal segments (arrow heads in E). Also note that the disconnection of many damaged axons occurs interspersed among adjacent intact fibers. In this image, the chiasm is to the left and the globe lies to the right. All scale bars, 20μm.

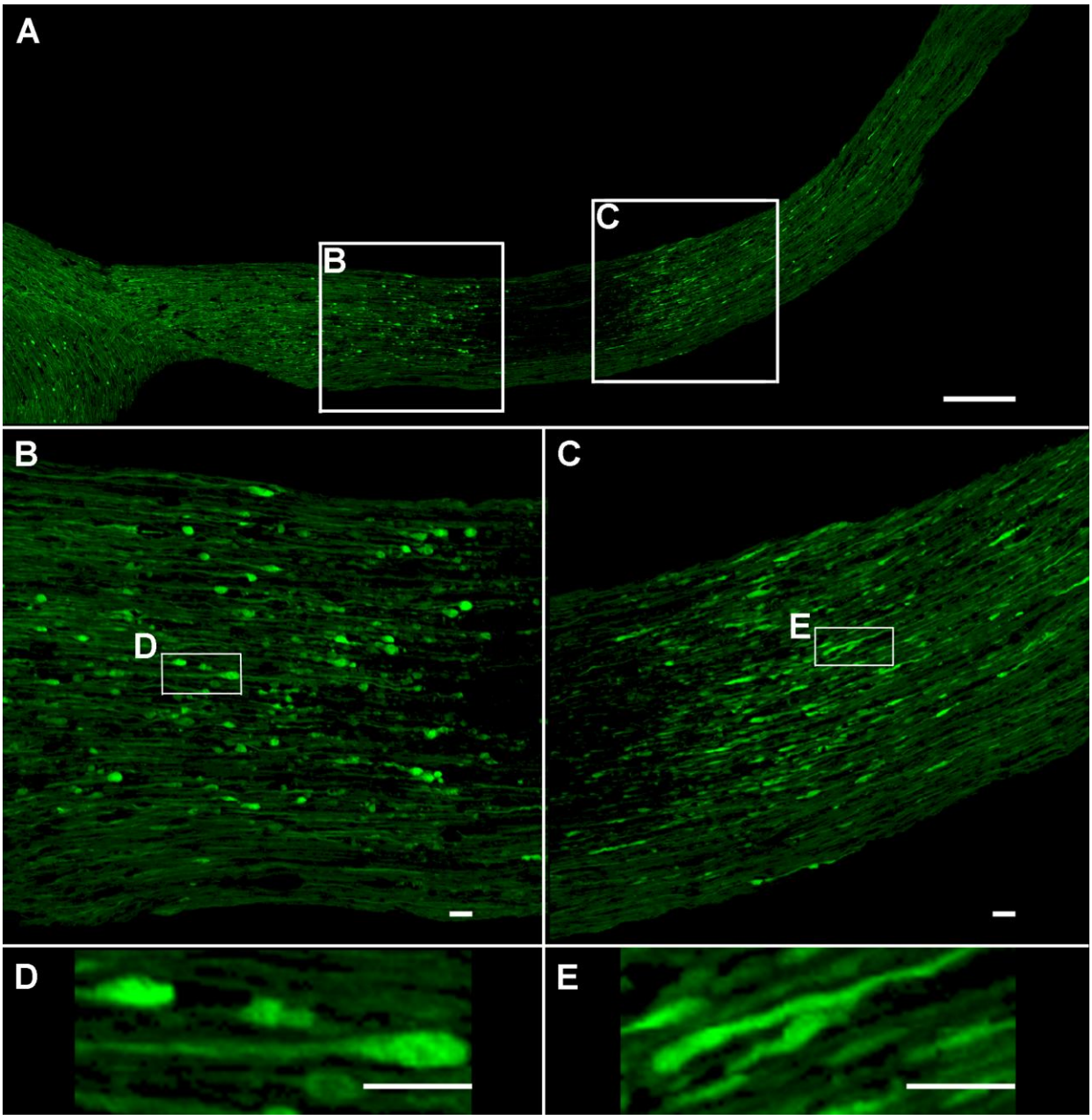

Figure 3.2 Confocal microscopic evidence of axonal swellings within the optic nerve of Thy1-YFP-16 mice at 12 hours post TBI. Note that the axonal swellings now manifest further maturation (A). Additionally note that the distal axonal swellings expand to form spheroids (B and D), while the proximal axonal swellings now assume a more truncated form (C and E). Scale bar, 200μm (A), 20μm (B, C, D and E).

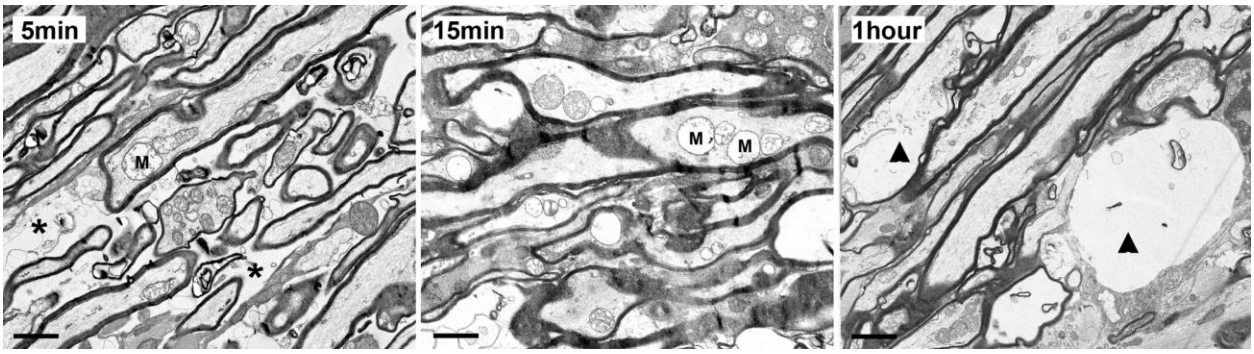

Figure 3.3 Electron microscopic evidence of the progression of axonal damage in the optic nerve of wild type mice from 5 minutes to 1 hour post TBI. Note that at 5 minutes and 15 minutes post TBI the initial axonal swellings are associated with accumulation of mitochondria, some of which are swollen (M). Also note the related expansion of the extracellular space consistent with the presence of edema (asterisk). Lastly, note that at 1hour post TBI damaged axons reveal local dissolution (arrow head) consistent with the process of disconnection which is present in the optic nerve of Thy1-YFP-16 mice. All scale bars, 1μm.

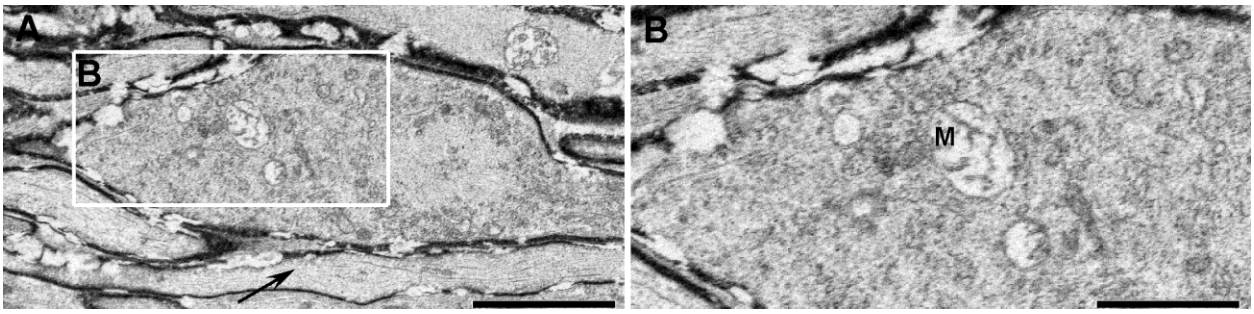

Figure 3.4 Electron microscopic evidence of axonal swelling in the optic nerve of Thy1-YFP-16 mice at 3 hours post TBI. At this time point the distal axonal swellings display continued maturation, with the accumulation of numerous vesicles and organelles which overlie a disorganized cytoskeletal core (A). Note that in the enlarged image (B), the dilated mitochondria exhibit disorganized cristae (M). Also note that in contrast to the swollen damaged axon, the adjacent axon remains intact (arrow in A). Scale bar, 2μm (A), 1μm (B).

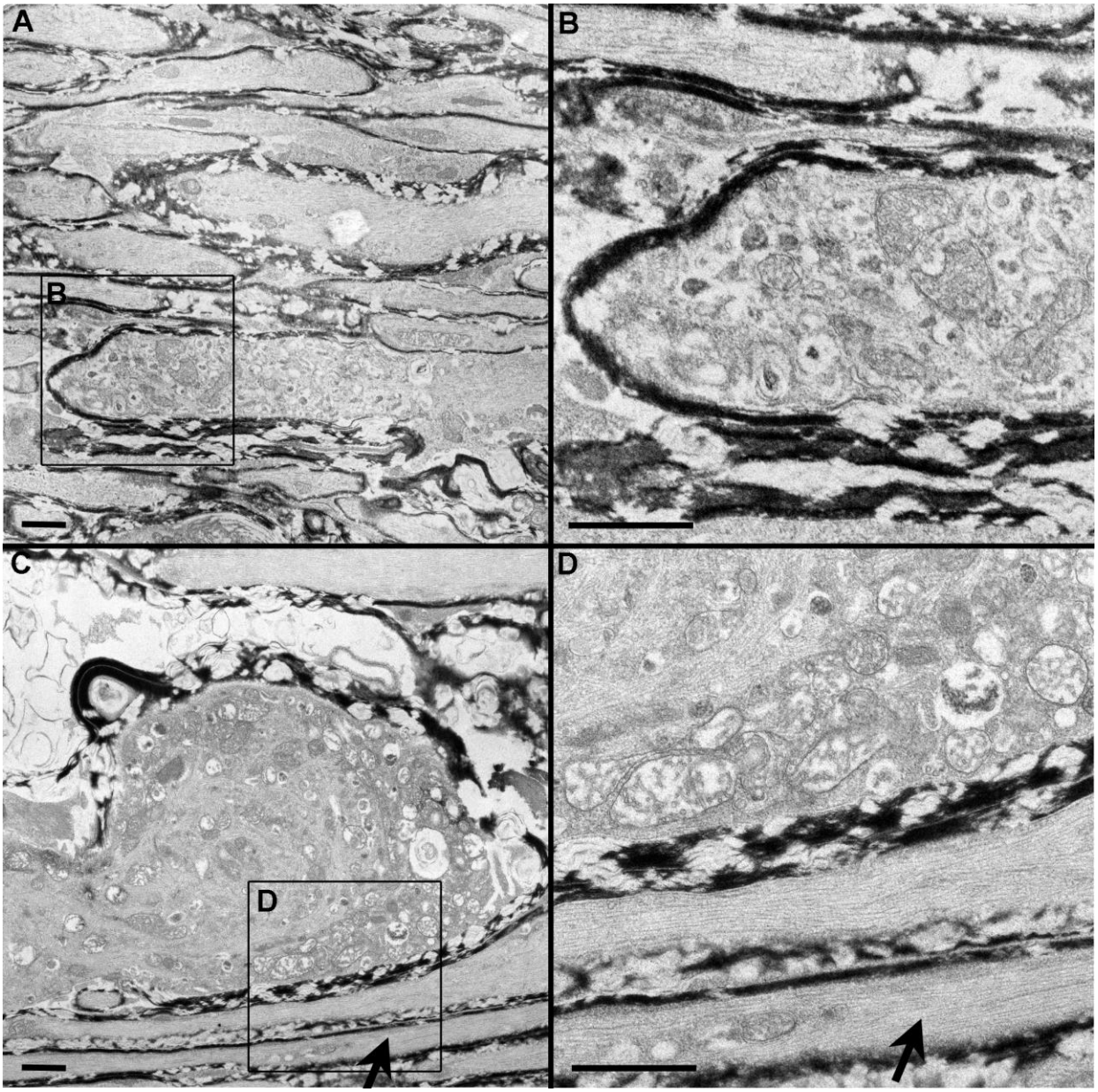

Figure 3.5 Electron microscopic evidence of progressive axonal swelling in the optic nerve of Thy1-YFP-16 mice at 24 hours post TBI. Now the proximal axonal swelling is more truncated (A and B), with numerous vesicles and smooth endoplasmic reticulum accumulating in the swollen axonal segment (B), while the related mitochondria remain intact (B). In contrast, the distal axonal swelling continues to expand and becomes increasingly rounded (C). Note the swollen mitochondria with disordered cristae (D) accumulating within the swollen bulb (C and D). Also note the presence of isolated continuous non-axotomized fibers coursing adjacent to the swollen axons at this time point (C and D arrow). All scale bars, 1µm.

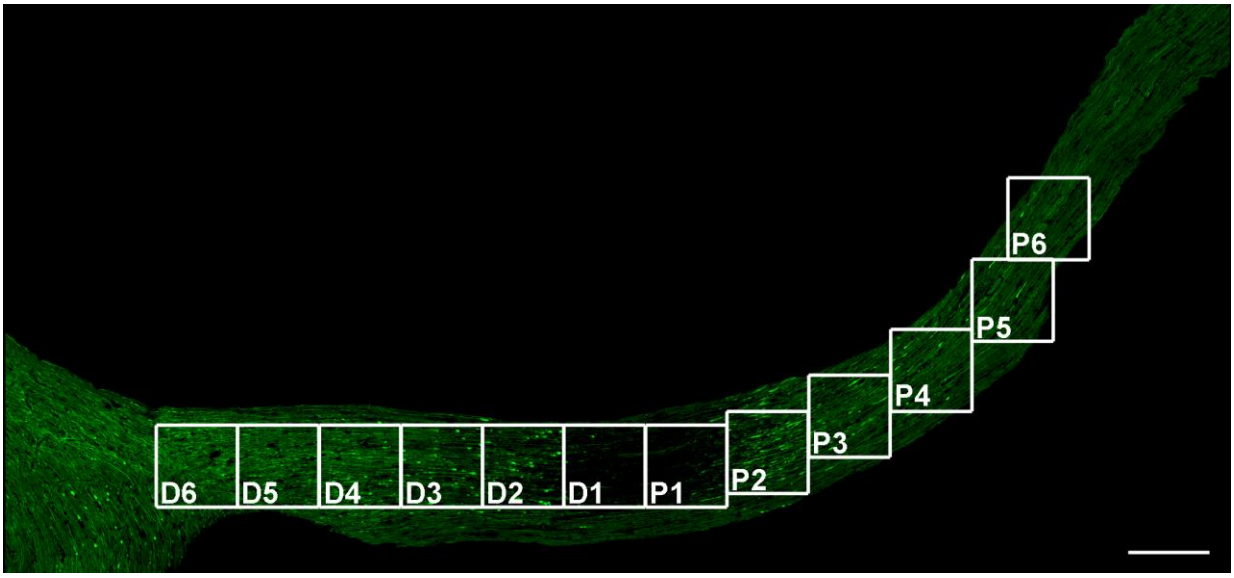

Figure 3.6 The location of 12 grids along the YFP expressing optic nerve for quantitative assessment. In this study, each grid encompasses 200µm x 200µm. From the initial locus of TAI, grids P1 to P6 are placed along the proximal segment approaching the globe, while grids D1 to D6 are located in the distal segment approaching the chiasm. Scale bar: 200µm.

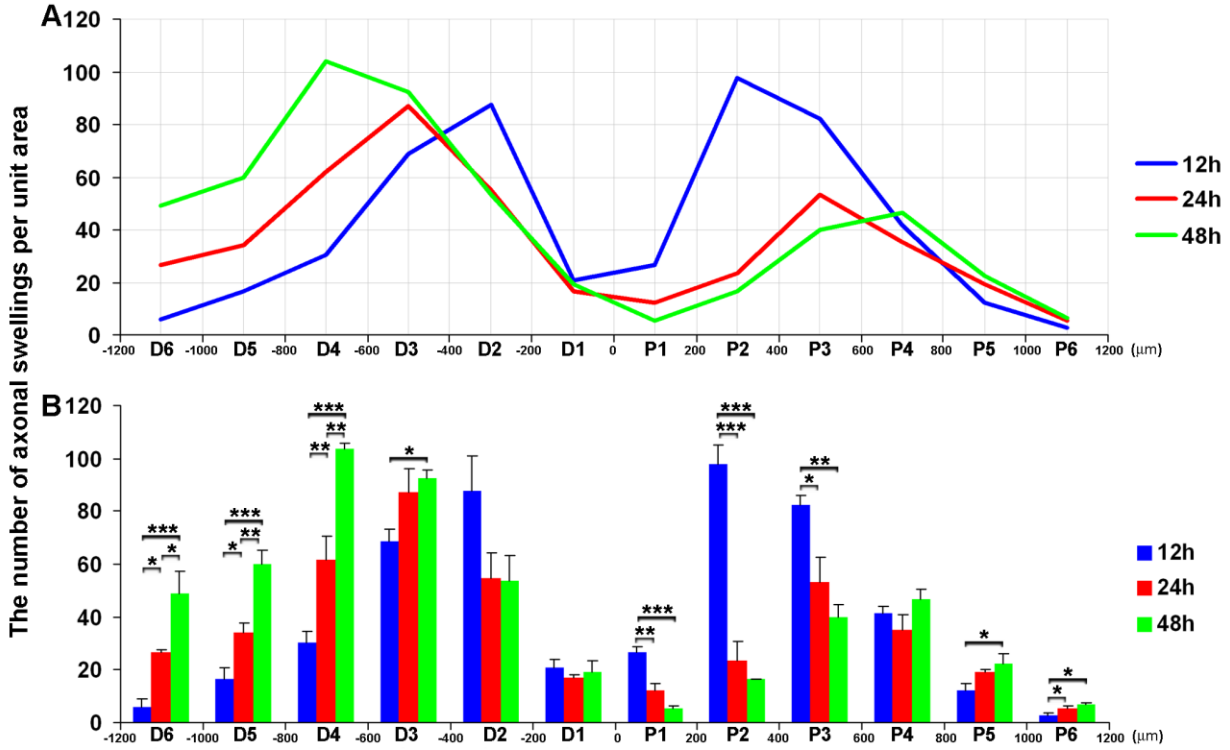

Figure 3.7 A plot of the number of axonal swellings per unit area and their distribution along the optic nerve over time. In both the line (A) and bar (B) graph, significant difference exists between the number of axonal swellings each time point at the related region ($p<0.05$). The line graph (A) best illustrates the change of axonal swelling distribution along the optic nerve over time (blue-12 hour, red-24 hour and green-48 hour). Note that the peak number of proximal axonal swellings moves from P2 to P3 and to P4 from 12 hours to 24 hours and to 48 hours post TBI respectively. The peak number of distal axonal swellings also shows significant redistribution from D2 to D3 and further to D4 from 12 hours to 24 hours and further to 48 hours post TBI respectively. This is consistent with progressive axonal dieback both proximally and distally over time post TBI. The bar graph (B) shows, in more detail, the statistical difference at each location. Specifically, in those segments 200μm-600μm proximal to the initial focus of injury (P2 and P3), the number of axonal swellings at 12 hours post TBI is significantly higher than those of 24 hours and 48 hours post TBI. These confirm the qualitative impression of the regression of proximal axonal swellings. In contrast, at 600μm-1200μm distal to the initial focus of injury (D4, D5 and D6), the number of axonal swellings at 24 hours post TBI is higher than that of 12 hours post TBI, while at 48 hours post TBI the number is again significantly higher than those of 12 hours and 24 hours post TBI. These confirm the qualitative impression of the retention of distal axonal swellings (* $p<0.05$, ** $p<0.01$, *** $p<0.001$).

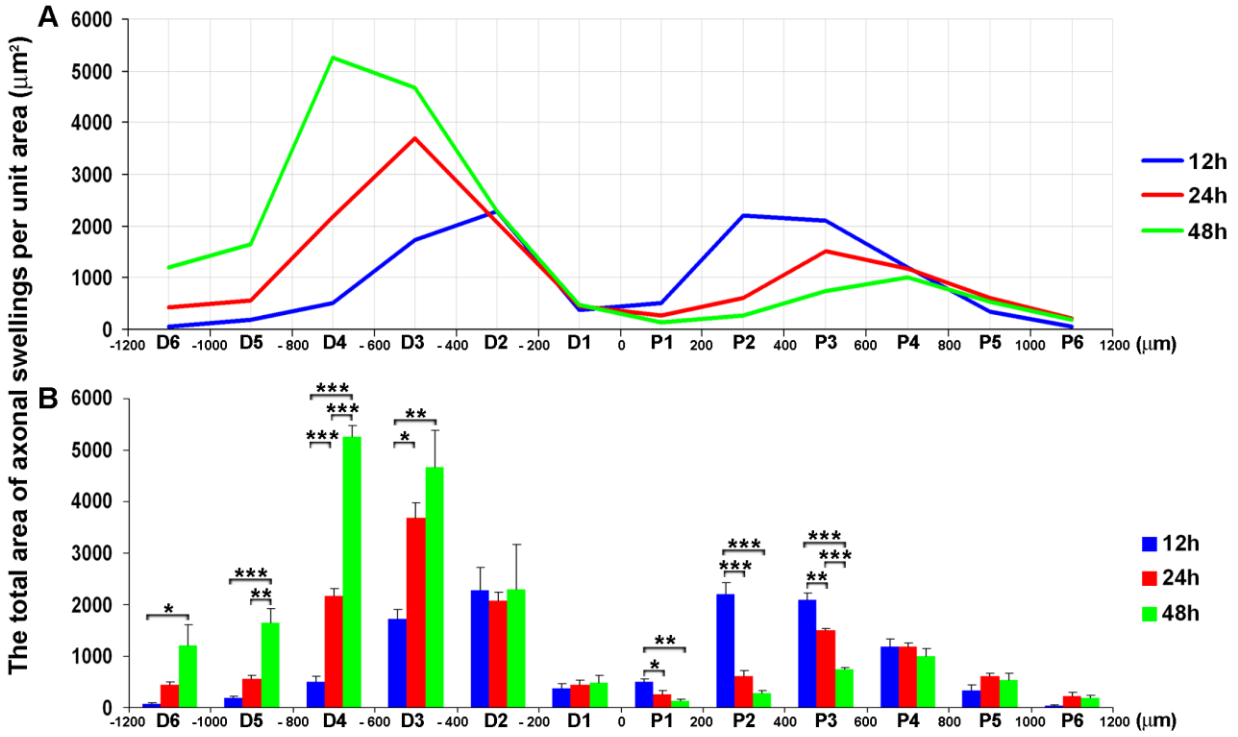

Figure 3.8 A plot of the total area of axonal swellings per unit area and their distribution along the optic nerve over time. Here again we display both in line (A) and bar (B) graph formats the total area of axonal swellings per unit area, which equals the sum of the area of each swellings in each individual grid. The line graph (A) best illustrates the change of the total axonal swelling area and its distribution along the optic nerve over time (blue-12 hour, red-24 hour and green-48 hour). Note that the peak of total area of proximal axonal swellings moves from P2 at 12 hours, to P3 at 24 hours and further to P4 at 48 hours post TBI. The peak of total area of distal axonal swellings shows significant redistribution from D2 at 12 hours, to D3 at 24 hours and further to D4 at 48 hours post TBI. This again demonstrates progressive axonal dieback both proximally and distally post TBI. The bar graph (B) reveals in more detail the statistical deference at each individual location. Specifically, in those segments 200μm-600μm proximal to the initial focus of injury (P2 and P3), the total area of axonal swellings at 12 hours post TBI is significantly higher than those of 24 hours and 48 hours post TBI. These confirm the qualitative impression of the regression of proximal axonal swellings. In contrast, at 400μm-800μm distal to the initial focus of injury (D3 and D4), the total area of axonal swellings at 24 hours post TBI is higher than that of 12 hours post TBI. At 400μm-1200μm distal to the initial focus of injury (D3, D4, D5 and D6), the total area of axonal swellings at 48 hours post TBI is higher than that of 12 hours post TBI. These again suggest the retention of distal axonal swellings over time (*p<0.05, **p<0.01, ***p<0.001).

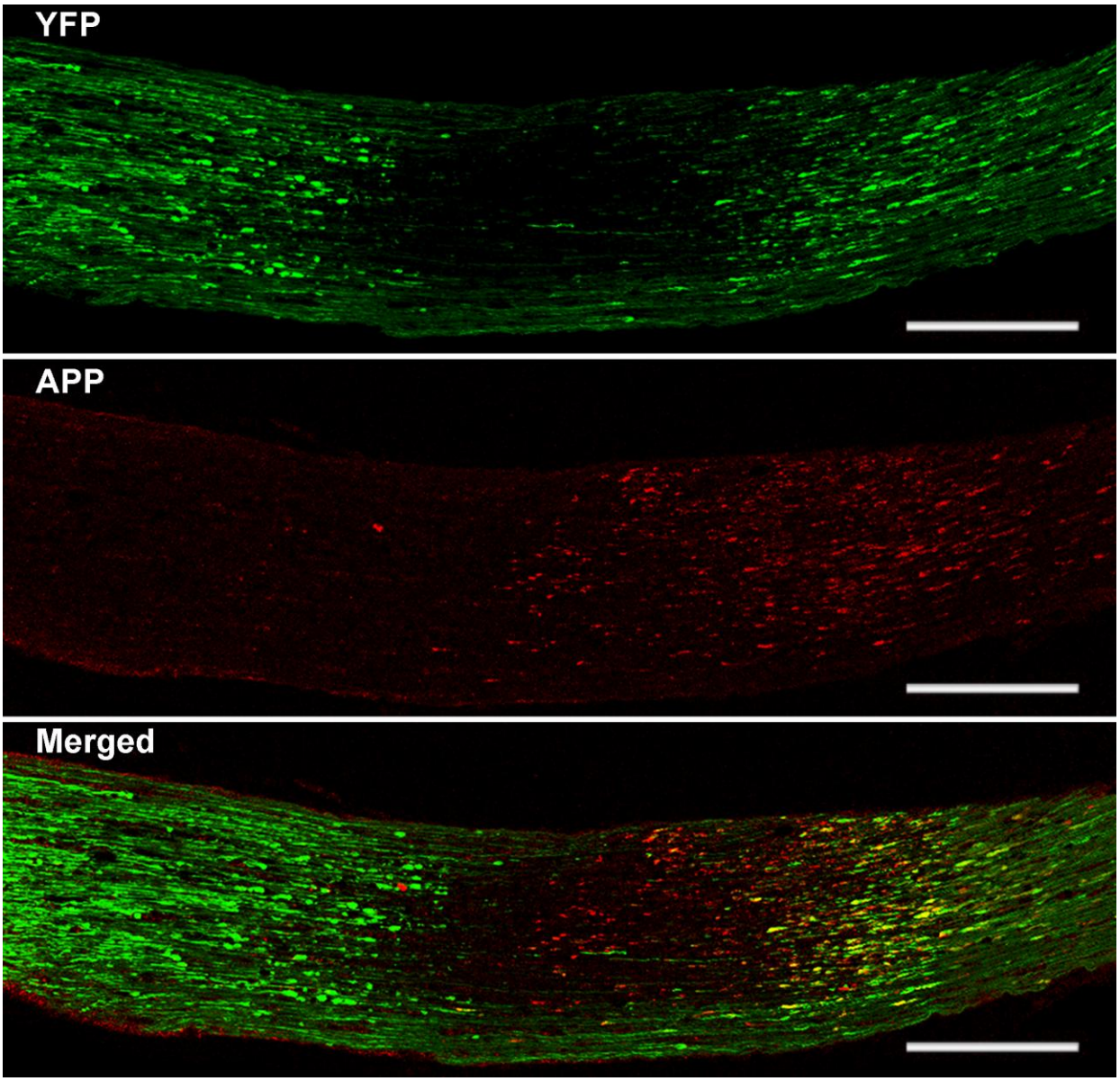

Figure 3.9 The relationship between the YFP-linked axonal changes and the APP immunofluorescent staining via confocal microscopy. As noted above, axonal swellings can be readily visualized by their YFP fluorescence at both the proximal and the distal optic nerve segments at 12 hours post TBI. Note that at this time point the APP immunoreactivity is found exclusively in the proximal segments, where it co-localizes with the YFP fluorescence (yellow in the merged image). In contrast, in the distal segment, there is no APP immunoreactivity despite the presence of numerous YFP positive axonal swellings. Here the chiasm is to the left and the globe is to the right. Scale bar, 200µm.

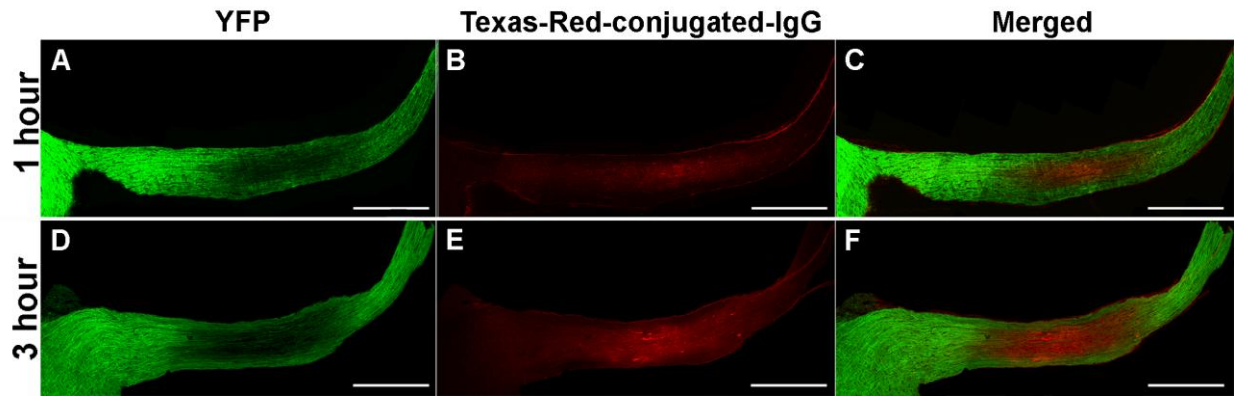

Figure 3.10 Texas-Red-conjugated-IgG maps to the region of YFP fluorescence quenching in the optic nerve of Thy1-YFP-16 mice. Note that at 1 hour post TBI, the region of fluorescent loss (A) directly correlates with the IgG immunoreactivity (B and C). Further, note the locus of YFP fluorescent loss is expanded at 3 hours post TBI (D), which also corresponds to the Texas-Red-conjugated IgG localization (E and F). Scale bar, 500μm.

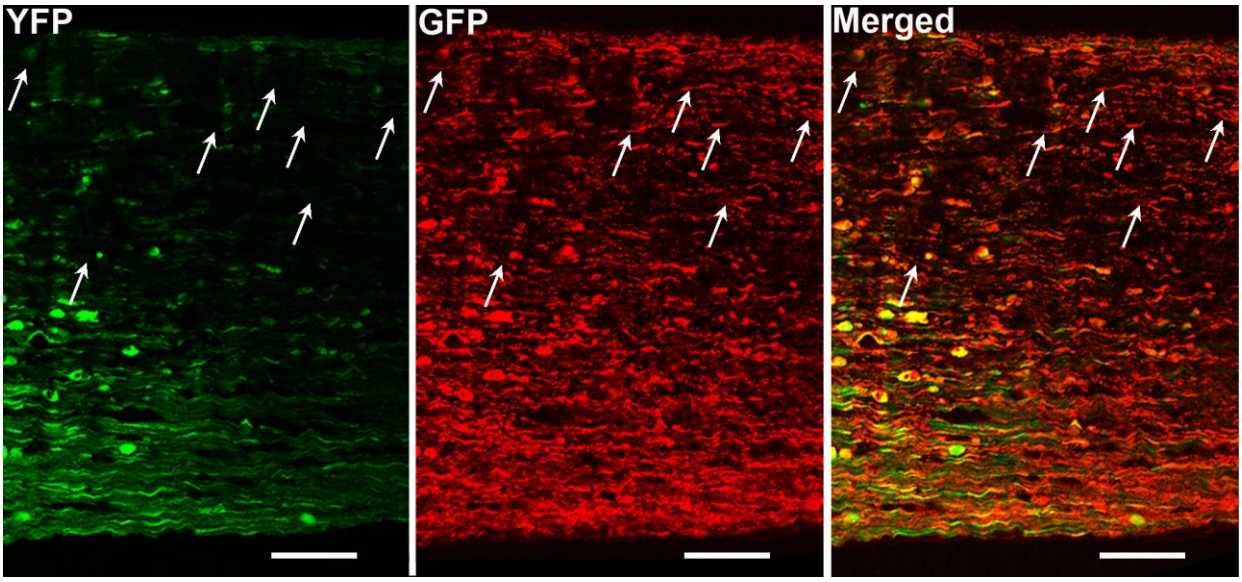

Figure 3.11 The retention of YFP expressing axons in the region of fluorescence quenching. With confocal microscopy, at 24 hours post TBI, the YFP fluorescently-quenched axons can now be visualized by antibodies targeting GFP (arrows) in a distal optic nerve segment. This suggests that despite axonal YFP fluorescence quenching, intact axons are retained in the same field. Scale bar, 50µm.

CHAPTER FOUR

DIFFUSE AXONAL INJURY IN THE OPTIC NERVE IS NOT ASSOCIATED WITH RETINAL GANGLION CELL LOSS

Abstract

Much of the morbidity following traumatic brain injury (TBI) is associated with traumatic axonal injury (TAI). Although most TAI studies focus on the callosal white matter, visual system involvement has been increasingly identified. To assess visual system TAI and probe various therapeutic approaches we developed a mouse model of optic nerve TAI. However, in this model it is unknown if TAI causes retinal ganglion cell (RGC) death, an issue of importance to therapeutic intervention. YFP-16 transgenic mice were subjected to mild TBI and followed from 2 days to 3 months. RGC death was evaluated qualitatively by TUNEL and cleaved caspase-3 immunostaining. RGC survival was quantified by counting Brn3a immunoreactivity and phospho-C-Jun immunolabeling. YFP positive cells in the RGC layer revealed no loss from 2 days to 28 days post-TBI. No TUNEL+ or cleaved caspase-3 immunoreactive RGCs were observed from 2 days to 3 months post-TBI. Brn3a immunoreactive RGC quantification revealed no significant RGC loss with concomitant phospho-c-Jun expression elevated up to 3 months post-TBI. Parallel EM analysis revealed no evidence of RGC death. These findings confirm many of the unique features of TAI, and suggest that this model offers advantages for future studies focusing on visual system TAI, its therapeutic management and its potential reorganization and repair.

Key words: traumatic brain injury; traumatic axonal injury; visual system; YFP-16 transgenic mice; retinal ganglion cell survival

Introduction

Traumatic brain injury (TBI) is a major national and global health problem which can lead to death and serious neurological dysfunction. Much of the mortality and morbidity of TBI is associated with diffuse traumatic axonal injury (TAI) (Christman et al., 1994; Li and Feng, 2009; Li et al., 2010; Zemlan et al., 1999). Although previous studies of TAI have focused on the callosal and rostral subcortical white matter, there is increased recognition that the visual system white matter is equally sensitive to injury (Ding et al., 2001; Foda and Marmarou, 1994; Gleckman et al., 2000; Palmer et al., 2010). This is reflected in both the military and civilian populations. In a study on the incidence of combat-related eye injuries, the Defense Veterans Brain Injury Center (DVBIC) reported that 80 percent of over 3,900 troops sustaining TBI had some form of visual problem (Zampieri, 2007).

To date, few have addressed this issue in either animal models or humans to gain better insight into the pathobiology of this visual damage and/or its potential treatment. To address this issue, we have recently characterized a model of diffuse traumatic axonal injury in the mouse visual system wherein we found diffuse/scattered axonal swellings, together with their disconnection, dieback and reorganization overtime (Wang et al., 2011).

Given the TAI observed in this system, an obvious question relevant to any future investigations including potential therapeutic intervention centers on the fate of the cell bodies of origin of these diffusely damaged optic nerve axons. Historically, it has been reported that virtually any form of damage to optic nerve results in dramatic retinal ganglion cell (RGC) loss. Complete intraorbital optic nerve transection has been shown to result in the loss of the majority of RGCs within 2 weeks (Berkelaar et al., 1994; Kielczewski et al., 2005; Peinado-Ramon et al.,

1996). With rat optic nerve crush, Dibas (2010) reported that the number of RGCs labeled retrogradely from superior colliculus, decreased by 47% at 7 days post injury, reaching a 76% loss at 2 weeks post injury. In a guinea-pig optic nerve stretch model, a model assumed to replicate the important features of TAI, Mohammed Sulaiman (2011) observed a continued loss of RGCs beginning at 1 week and further increasing over the next 12 weeks, with only 60% of RGCs remaining at 12 weeks post TAI. Further they recognized that this cell loss was associated with RGC apoptosis at 2, 3, 8 and 12 weeks, with the peak number of apoptic RGCs occurring at 3 weeks post injury. In a mouse optic nerve stretch model, Saatman (2003) reported that the number of RGCs, retrogradely labeled by Fluorogold injected into the superior colliculus, dramatically decreased by over 50% by 1 day and at 2 weeks after stretch injury, in contrast to the sham animals.

Based upon these studies, it would seem that retinal ganglion cell death would be the foregone conclusion of diffuse axonal injury in the optic nerve. However, our previous work in the diffusely injured optic nerve suggested otherwise (Wang et al., 2011). Specifically, in this TAI model system we demonstrated that once disconnected, the proximal axonal segment underwent a relatively rapid transition from an enlarged and swollen axonal segment to a thinned and truncated appendage. Further this transition was not related to degeneration, but rather axonal reorganization and repair (Wang et al., 2011). Collectively, these observations in the proximal axotomized segment are entirely consistent with an intact axon maintaining continuity with viable RGCs that are capable of continued protein synthesis and organelle stability.

Support for the premise of RGC survival also follows from the work of Povlishock and colleagues who evaluated in the neocortex those neuronal cell bodies linked to diffuse axonal injury (Greer et al., 2011; Lifshitz et al., 2007; Singleton et al., 2002). Specifically, using

multiple experimental approaches, they demonstrated that TAI did not result in either neocortical or thalamic neuronal death. Rather it triggered atrophic change. In these studies, it was assumed that the subtle axonal changes precipitated by TAI, did not trigger the massive ionic influx and dysregulation associated with axonal transection or crushing, thereby protecting the neuronal cell body, a premise that may also carry forward to the diffusely injured optic nerve.

Because of the importance of these issues to our understanding of the pathobiology and treatment of TAI in the visual system and because of the predominance of the literature suggesting that RGC loss is the inevitable consequence of any form of optic nerve damage, the current study comprehensively evaluated the response of RGCs to diffuse TAI. Specifically, using multiple markers of neuronal cell death together with rigorous qualitative and quantitative assessments of RGC integrity, we demonstrate that diffuse traumatic axonal injury within the optic nerve is not associated with significant ganglionic cell death.

Material and methods

To study the cell death or survival of RGCs following diffuse traumatic axonal damage within the optic nerve, we utilized Thy1-YFP-16 transgenic mice which express YFP under the promoter Thy1 within the retina and the optic nerve fibers (Feng et al., 2000). This strategy, as previously described (Wang et al., 2011), was employed to directly visualize the YFP cells in the RGC layer under routine fluorescent and/or confocal microscope, with the endogenous expression of YFP (Feng et al., 2000).

Animal Surgery and Perfusion

All protocols used in this study were approved by the Institutional Animal Care and Use Committee (IACUC) of Virginia Commonwealth University. *Thy1-YFP-16* transgenic mice were obtained from the Jackson Laboratory (Bar Harbor, ME), and were breed, genotyped and maintained as heterozygotes as described previously (Wang et al., 2011). Adult 2 month old Thy1-YFP-16 mice (20–25g) were subjected to mild central fluid percussion injury (1.40±0.05 atmospheres) as previously described (Wang et al., 2011, Dixon et al., 1987). The fluid pressure pulse in this model resulted in a brief deformation of the brain and induced diffuse traumatic axonal injury in the optic nerve approximately 1mm proximal to the chiasm (Wang et al., 2011). Sham-injured animals received the same surgeries, with the absence of the injury. Animals were allowed to survive for either 2 days, 7 days, 14 days, 28 days or 90 days following injury. At the appropriate survival times, animals were euthanized via an intraperitoneal overdose of sodium pentobarbital, and then transcardially perfused with 100ml heparinized normal saline, followed by 200ml 4% paraformaldehyde in Millonig's buffer. For electron microscopy (EM) analysis, animals were perfused with 200ml 2% paraformaldehyde and 2.5% glutaraldehyde in Millonig's buffer. At each time point, 9 animals were injured, of which 2 animals were prepared for retinal whole mount observation to allow for a qualitative assessment of any potential loss of YFP-expressing cells in the RGC layer. Five mice were prepared for serial sectioning on a cryostat to permit immunocytochemical processing for markers of cell death while also allowing for the quantitative assessment of any potential RGC loss. Lastly, 2 animals were prepared for EM analysis to identify any potential neuronal damage or loss in the RGC layer. These injured animals which were evaluated at all time points, were prepared together with 6 sham injured mice per time point (1 for retinal whole mount observation, 3 for qualitative immunocytochemistry and quantitative assessment, and another 2 for EM).

Retinal whole-mount preparation

Following transcardial perfusion, the extraocular muscles were cut from the globe, the optic nerve was transected immediately behind the globe, and the eye was dissected from the orbit. The cornea was punctured with an 18 gauge needle, cut into 4 quadrants, and opened to the limbus using two sets of forceps. The lens was removed and the retina was then separated from the pigmented layer, and immersed in 4% paraformaldehyde in Millonig's buffer for 4 hours. Next, the retina was washed thoroughly with phosphate buffered saline (PBS) 5 x 10 minutes. The retina was then cut into four quadrants, and mounted flat on a glass slide with Vectashield Hardset Mounting Medium with DAPI (Vector Laboratories), and cover-slipped for image capture with a Leica TCS-SP2 AOBS confocal microscope (Wetzlar, Germany).

Retinal cryostat section preparation

After the retina was separated from the pigmented layer as described above, fixation was continued in 4% paraformaldehyde in Millonig's buffer overnight. After washing in PBS 5 x 10 minutes, the retina was immersed in 30% sucrose in PBS overnight. The pair of retinal cups from the same animal was then embedded side to side and frozen to -20^{o}C in optimal cutting temperature (OCT) compound (Electron Microscopy Sciences, Cat No.62550-01, Hatfield, PA, U.S.A.). Twelve micrometer sections were then cut with a cryotome (Shandon Scientific Ltd., Cheshire, U.K.). Serial sections were collected on Superfrost®/Plus microscopic glass slides (Fisher Scientific, catalog no.12-550-15, U.S.A.), with four serial sections of each eye on each slide for a total of 8 sections on each slide, and stored at -20^{o}C for further use.

Immunohistochemistry

TUNEL immunohistochemistry

To detect nuclear fragmentation within RGCs, frozen retinal sections (3 random slides from each injured and sham injured animal) were processed at the designated 2 days, 7 days, 14 days, 28 days and 90 days time points, using a terminal deoxynucleotidyl transferase dUTP nick end labeling (TUNEL) kit (ApoTag In Situ Apoptosis Detection Kit; S7101, S7160 and S7165, Millipore), using modification of the manufacturer's protocol. Frozen retinal sections were obtained and warmed to room temperature for 30 minutes. They were then rinsed 2 x 5 minutes in PBS, and post fixed in precooled ethanol: acetic acid (2:1) solution for 5 minutes at -20^{o}C in a humidified chamber. After washing 2 x 5 minutes in PBS, the sections were incubated in 50μg/ml proteinase K (Invitrogen, Cat No. 25530-015) in PBS for 30 minutes at room temperature. Once again, sections were washed 2 x 5 minutes in PBS, and incubated in the proprietary equilibration buffer for 30 minutes at room temperature. After clearing the equilibration buffer, the sections were incubated with working strength terminal deoxynucleotidyl transferase (TdT) enzyme in a humidified chamber for 1.5 hours at 37°C. The slides were then rinsed by the proprietary stop/wash buffer 2 x 10 minutes at room temperature, and washed in PBS 3 x 5 minutes. The sections were then incubated in the mouse anti-Digoxigenin (1:250, Roche, Cat. No. 11333062910) at 4^{o}C in a humidified chamber overnight. After rinse in PBS 4 x 5 minutes, the sections were incubated with secondary antibody Alexa fluor 594-conjugated goat anti-mouse IgG (1:250, Invitrogen) for 1 hour at room temperature. Then the slides were washed 4 x 2 minutes in PBS, cover-slipped with Vectashield Hardset Mounting Medium with DAPI (Vector Laboratories) for confocal microscopic analysis with a Leica TCS-SP2 AOBS confocal microscope (Wetzlar, Germany). To generate positive control,

sham-injured retinal sections pretreated with deoxyribonuclease (DNAase, 1,000U/ml) at room temperature for 10 minutes were used. To generate a negative control, the TdT enzyme treatment was deleted.

Cleaved-caspase-3 immunohistochemistry

To detect apoptosis within RGCs, frozen retinal slides adjacent to those prepared for TUNEL staining (3 slides per animal), were selected for cleaved-caspase-3 immunofluorescent staining. Sections were warmed to room temperature for 30 minutes, and then rinsed 3 x 10 minutes in PBS. Following pretreatment with 10% normal goat serum (NGS) with 2% bovine serum albumin (BSA) and 0.5% Triton X in PBS at room temperature for 2 hours, they were incubated overnight at 4^{o}C with the primary antibody rabbit anti-cleaved-caspase-3(Asp175) (1:500, Cell Signaling Technology, Cat. no. 9661), in 10% NGS with 2% BSA and 0.5% Triton X in PBS. The sections were washed 6 x 10 minutes with 1% NGS with 1% BSA and 0.2% Triton X in PBS at room temperature, followed by incubation with the secondary antibody Alexa fluor 594-conjugated goat anti-rabbit IgG (1:250, Molecular probes, Invitrogen) in 1% NGS with 1% BSA and 0.2% Triton X in PBS for 2 hours at room temperature. Then the sections were washed 4 x 5 minutes in PBS and 2 x 5 minutes in 0.1M sodium phosphate buffer, and cover-slipped with Vectashield Hardset Mounting Medium with DAPI (Vector Laboratories) for confocal microscopic analysis.

Brn3a immunohistochemistry

Besides the qualitative studies of the RGCs detailed above (TUNEL and caspase-3 immunostaining), quantitative evaluation of the number of RGC was performed using the anti-

Brn3a antibody immunohistochemistry, which has been shown to specifically detect rodent RGCs (Galindo-Romero et al., 2011; Nadal-Nicolas et al., 2009). This approach provided advantages over routine YFP analysis in that unlike the YFP which can be found in RGCs as well as amacrine cells (Feng et al., 2000), Brn3a is confined solely to RGCs (Xiang et al., 1995). For Brn3a immunostaining, three slides from equivalent eccentricity from the optic nerve head, and adjacent to those utilized for TUNEL and Caspase-3 immunostaining were employed. These slides were warmed to room temperature for 30 minutes. Then the sections were rinsed 3 x 10 minutes in PBS, and pretreated with 10% NGS with 2% BSA and 0.5% Triton X in PBS at room temperature for 2 hours. Endogenous mouse IgG was blocked by anti-mouse Ig Reagent derived from a mouse host (Mouse on Mouse Kit, MOM™; Vector Laboratories; Burlingame, CA). Then the sections were washed 3 x 10 minutes in 10% NGS with 2% BSA and 0.5% Triton X in PBS, and then incubated overnight at 4^{o}C with the primary antibody mouse anti-Brn3a monoclonal antibody (1:125, Millipore, MAB1585) in 10% NGS with 2% BSA and 0.5% Triton X in PBS. Then the sections were washed 6 x 10 minutes with 1% NGS with 1% BSA and 0.2% Triton X in PBS at room temperature, followed by incubation with the secondary antibody Alexa fluor 568-conjugated goat anti-mouse IgG (1:500, Molecular probes, Invitrogen) in 1% NGS with 1% BSA and 0.2% Triton X in PBS for 2 hours at room temperature. Then the sections were washed 4 x 5 minutes in PBS and 2 x 5 minutes in 0.1M sodium phosphate buffer, and cover-slipped with Vectashield Hardset Mounting Medium with DAPI (Vector Laboratories) for epifluorescent microscopic analysis. A Nikon Eclipse 800 microscope (Tokyo, Japan) fitted with an Olympus DP71 digital camera (Olympus, Center Valley, PA) was utilized with the appropriate excitation/emission filters.

Phosphorylated c-Jun immunohistochemistry

In addition to assessing markers of neuronal death (TUNEL and caspase 3) as well as survival (Brn3a), we also employed other antibodies linked to potential neuronal survival and repair. Specifically, based on our recent experience with neocortical axonal injury (Greer et al., 2011), we employed antibodies to phospho-c-Jun. Three slides containing eight frozen retinal sections, adjacent to slides used for TUNEL, cleaved-caspase-3 staining and Brn3a staining, were chosen from each animal for immunostaining with the primary antibody polyclonal rabbit anti-phospho-c-Jun (Ser63) (1:100; Cat. no. 9261, Cell Signaling; Danvers, MA), followed by the secondary antibody Alexa fluor 633 or Alexa fluor 594-conjugated goat anti-rabbit IgG (1:200, Molecular probes, Invitrogen). The same protocol for Brn3a immunostaining was utilized, except for the replacement of PBS by Tris-buffered saline (TBS). Further, adjacent slides were chosen for Brn3a and phospho-c-Jun double labeling and the observation under confocal microscopy.

Electron microscopy

For electron microscopic (EM) analysis, additional mice were employed to include 2 injured YFP-16 mice, and their appropriate sham injured controls per time point. To achieve optimal ultrastructure detail, YFP-16 mice were first perfused with 100ml heparinized normal saline, followed by 200ml 2% paraformaldehyde and 2.5% glutaraldehyde in Millonig's buffer. After 15 minutes fixation, the retina was removed as described above, and immersed in 2% paraformaldehyde and 2.5% glutaraldehyde in Millonig's buffer overnight, together with the brain and the optic nerve. Then the fixation prepared retina was osmicated in 2% OsO4 in 0.1M sodium phosphate buffer, dehydrated in alcohol with 1% uranyl acetate, embedded in epoxy

resin (Embed-812; Electron Microscopy Sciences, Hatfield, PA), mounted on plastic slides (Thomas Scientific Co., Swedesboro, NJ) and cover-slipped. After resin curing, the plastic slides were examined via routine light microscopy to identify RGCs, using a Nikon Eclipse E800 microscope fitted with an Olympus DP71 digital camera (Olympus, Center Valley, PA). Once identified, these sites were excised, mounted on plastic studs, and thick sectioned to the RGC layer using an ultramicrotome (Leica Ultracut R; Leica, Wien, Austria). Serial 40nm sections were cut and mounted onto Formvar-coated single-slotted grids. The grids were then stained with 5% uranyl acetate in 50% methanol for 2 minutes and 0.5% lead citrate for 1 minute, and visualized using a JEM 1230 electron microscope (JEOL Ltd., Tokyo, Japan).

Q*uantification of RGC* and statistical analysis

To quantify the number of RGCs, the Brn3a immunofluorescently labeled retinal sections were captured using routine epifluorescent microscopy. Specifically, Brn3a retinal section (4 sections per eye, with each slide containing 8 sections from both eyes) was digitally acquired at 20 x magnification moving from side to side of the retina covering its entire extent, parallel to its curvature. Each retinal section was reconstructed using 7-9 images taken along the extent of the retina (Figure 4.4 A). To quantify the number of RGCs, the central image of those acquired was selected together with the other next adjacent image from both sides (Figure 4.4 A arrow). For each selected image, the number of Brn3a positive RGCs was counted in a 0.05 mm^2 (0.435 mm x 0.115 mm) grid expanding along the image parallel to the alignment of the RGCs (Figure 4.4 B). This process of acquisition and counting was repeated for each of the retinal sections on the slide for a total of 72 retinal images per animal (3 images/section x 8 sections/slide x 3 slides/animal = 72 images/animal). For each animal, the number of Brn3a positive RGCs was

calculated by summating the number of Brn3a positive RGCs from the 72 images, expressing them as mean ± standard deviation. To test the difference of the number of Brn3a positive RGCs overtime post injury, one way ANOVA was conducted.

Results

Whole mount retina YFP assessment following TAI in the optic nerve

The YFP expressing retinal whole mounts were well preserved, with RGC axons converging toward the optic disc, without any evidence of axonal swelling. In the injured animals, the YFP positive cells in the RGC layer from both the center of the retina and its more peripheral regions, did not reveal overt loss or change in fluorescent intensity from 2 days, 7 days to 14 days and 28 days post TBI compared to the retina harvested from the 2 days sham animal (Figure 4.1).

TUNEL and caspase 3 assessment in the RGC layer following TAI in the optic nerve

To assess the potential for any axonal damage-induced death of RGCs, the TUNEL method was utilized to identify nuclear fragmentation within the RGC layer as a consequence of axonal injury. Positive control retinal sections from DNAase treated YFP retinal sections demonstrated positive staining in the nuclei of cells at the different layers of the retina (Figure 4.2). In retina from sham-injured animals, no TUNEL positive cells were observed in the RGC layer (data not shown). Importantly, no TUNEL positive cells were observed within the RGC layer at any time point from 2 days to 90 days assessed post injury (Figure 4.2).

Besides TUNEL analysis, we also assessed the potential for RGC apoptosis induced by diffuse traumatic axonal injury of the optic nerve. Specifically, cleaved caspase-3

immunostaining approach was utilized to identify apoptosis in the RGC layer from 2 days to 90 days after axonal damage. Positive control retinal sections from P2 mice pups demonstrated positive staining of the cleaved caspase-3 (Figure 4.3). In retina from sham-injured animals, no positive staining of the cleaved caspase-3 was observed in the RGC layer (data not shown). Importantly, no cleaved caspase-3 immunoreactive cells were observed within the RGC layer from 2 days to 90 days post-TBI (Figure 4.3).

Quantitative analysis of the RGCs following TAI in the optic nerve

Besides the use of TUNEL and caspase-3 immunostaining to detect RGC death, quantitative analyses utilizing Brn3a immunostaining were performed to evaluate the number of RGCs overtime following TAI. This approach revealed a subtle time dependent decrease of RGCs in the injured animals from 7 days to 28 days post injury (Figure 4.4 C). Of note, however, was the finding of a comparable time dependent decrease of RGCs in the sham animal at 7 days to 28 days post sham injury, which was obviously not related to traumatic axonal injury. Compared to sham injured animals, there was no significant decrease in the number of RGCs at each time point post injury. At 7 days post injury, 2620.6±102.3 (mean ±standard deviation) RGCs survived compared to 2610.7±103.5 in the sham group. At 14 days post injury, 2358.8±148.1 RGCs survived compared to 2509.5±65.8 in the sham group. Further at 28 days post injury, 2378.8±93.2 RGCs survived compared to 2465.5±65.8 in the sham group. Despite the subtle loss of RGCs overtime, majority of RGCs survived at each time point post injury, consistent with the TUNEL and caspase-3 immunostaining which did not support dramatic RGC death following diffuse traumatic axonal injury of the optic nerve.

Persistent expression of phospho-c-Jun overtime following TAI in the optic nerve

As noted above, as no overt RGC loss could be identified post injury, we also employed antibodies to phospho-c-Jun, which has been linked to neocortical neuronal survival and axonal regeneration following diffuse traumatic axonal injury (Greer et al., 2011). In the current study, the expression of phospho-c-Jun was found specifically within the RGCs, based upon its colocalization with Brn3a (Figure 4.5). In this domain, the phospho-c-Jun positive RGCs were interspersed by other RGCs lacking phospho-c-Jun expression. Further, the expression of phospho-c-Jun by RGCs persisted from 2 days to 90 days post-TBI (Figure 4.6). Collaboratively, this persistent expression of phospho-c-Jun is consistent with RGC survival overtime.

Qualitative ultrastructural analysis of RGC following TAI in the optic nerve

Parallel ultrastructural analysis of cells within the RGC layer undertaken from 7 days to 28 days post injury also confirmed the absence of overt cell death. Throughout the period of 7 days, 14 days and 28 days no apoptotic or necrotic RGC profiles were seen (Figure 4.7). Additionally, no evidence of chromatin clumping, nuclear eccentricity or increased neuronal electron density was found, again consistent with neuronal preservation. Although occasional mitochondrial dilation was observed, this dilation did not progress over time, suggesting that this was a fixation artifact. Of note, the cell body appeared smaller at 28 days post injury, suggesting atrophic change overtime (Figure 4.7).

DISCUSSION

In the current communication, both qualitative (TUNEL and caspase-3 immunostaining) and quantitative (Brn3a immunostaining) studies demonstrated no evidence of significant RGCs

death following diffuse traumatic axonal injury in the optic nerve. The parallel finding from 2 days to 90 days post injury of phospho-c-Jun expression, an established marker of neuronal survival and potential axonal repair, further argued for RGC survival rather than death. Lastly, our parallel ultrastructural analysis did not reveal RGC death, again consistent with RGC survival.

As presented the findings of the current study, stand in contrast to numerous studies reporting that virtually any damage to optic nerve results in dramatic RGC loss (Berkelaar et al., 1994; Dibas et al., 2010; Kielczewski et al., 2005; Sulaiman et al., 2011; Peinado-Ramon et al., 1996; Saatman et al., 2003). The reason for this different response to TAI in comparison to other models of optic nerve injury is not entirely clear, however, it most likely resides in the diffuse nature of the injury, together with major differences in the pathogenesis of axonal injury following diffuse traumatic injury vs. crush/transection.

As noted, the survival of RGCs following diffuse axonal injury in the optic nerve varies from the dramatic RGC loss routinely described following the optic nerve transection and crush injury. The major difference between these model systems is that optic nerve transection and crush constitute a primary axonal injury, while TAI involves secondary/delayed processes leading to disconnection over a period of several hours (Büki and Povlishock, 2006). Primary axonal injury (transection) directly disrupts the axolemma, immediately exposing the injured axonal cylinder to the extracellular environment, resulting in sodium and calcium influx and the activation of proteases which then could cause further axonal damage progressing to neuronal death (Emery et al., 1991; Leybaert and de Hemptinne, 1996; Lucas et al., 1990; Rosenberg et al., 2001; Strautman et al., 1990). RGC death has also been observed following optic nerve transection or crush, due to the activation of the superoxide anion-initiated apoptotic signaling

pathway (Catrinescu et al., 2012), caspase-3 induced apoptotic signaling pathway (Agudo et al., 2008), and TNF-α pathway (Lukas et al., 2009). Unlike optic nerve transection/crush injury, the central fluid percussion brain injury used in the current study induces acute transit acceleration-deceleration and compression-decompression of the optic nerve, resulting in diffuse traumatic axonal injury. This injury induces subtle, progressive changes in the axonal cylinder, as reported in our previous publications in the optic nerve as well as other fiber systems (Buki and Povlishock, 2006; Wang et al., 2011). Conceivably, these more subtle and progressive axonal changes do not lead to the massive ionic disruption associated with transection thereby supporting RGC survival.

Besides the differences between optic nerve TAI and transection/crush injury, the survival of RGCs following diffuse traumatic axonal injury of the optic nerve, also differs from the RGCs response to optic nerve stretch injury, which also typically evokes RGC death, involving necrotic and/or apoptotic pathways (Sulaiman et al., 2011; Saatman et al., 2003). The underling mechanisms for this RGC response most likely originates from the mechanical stretch injury itself, during which the globe and optic nerve are stretched by a sling placed behind the globe (Gennarelli et al., 1989; Maxwell et al., 1994; Maxwell and Graham 1997; Sulaiman et al., 2011; Saatman et al., 2003; Serbest et al., 2007). In this model, the force of stretch is applied directly to the globe, and then transferred from the globe to the optic nerve. This approach most likely injures both RGCs and the axons within the optic nerve via the mechanical forces acting on the retina, its intrinsic vasculature and downstream fibers. In contrast, with the central fluid percussion injury used in this study, the fluid injury pulse impacts the dorsal cortex, causing its elastic deformation along a rostral caudal path to reach the brainstem (Dixon et al., 1987; Wang et al., 2011). This deformation compresses the optic nerve transiently, stretching it, inducing the

diffuse traumatic axonal injury approximately 1 mm proximal to the chiasm (Wang et al., 2011). Importantly, in this model, the globe itself is shielded from the injury pulse, most likely sparing the retina while generating DAI in a more remote segment of the optic nerve than that previously assessed by others.

In this regard, the majority of optic nerve transection or crush lesions have been performed in the intraorbital segment of the optic nerve, which directly approximates the RGCs (Alarcón-Martínez et al., 2010; Dibas et al., 2010; Hu et al., 2012). Similarly with optic nerve stretch, the utilized sling triggers axonal damage in the proximal optic nerve segment, with the caveat that the proximity of the axonal injury to the RGC of origin may also be a confounding factor in the fate of the RGC cell body. Previous studies evaluating the survival of rubrospinal neurons following axonal transection at the brain stem vs. the C2 level (Liu et al., 2004; Liu et al., 2003), and the survival of the corticospinal motor neuron after the intracortical axonal transection at different depth below layer V cortex (Dale et al., 1995), have shown that more neuronal sparing occurs as the distance between the neuronal somata and the downstream lesion increases, with proportionally more neuronal death occurs when the primary axonal lesion occurs adjacent to the neuronal cell body of origin (Dale et al., 1995; Liu et al., 2004; Liu et al., 2003). These results are consistent with our observations in more RGCs surviving TAI in the remote intracranial segment of the optic nerve, compared to less RGCs surviving transection/crush or stretch of the more proximal segment of the optic nerve.

While the above described differences in animal modeling as well as our failure to demonstrate evidence of cell loss/death support our conclusions, further direct confirmation of RGC survival can be found in our additional immunocytochemical studies utilizing phospho-c-Jun. Previous studies have demonstrated that the activation of the c-Jun pathway is associated

with scattered RGC survival, axonal sprouting and regeneration in various models of optic nerve injury in fish and rodents (Fitzgerald et al., 2010; Fitzgerald et al., 2009; Herdegen et al., 1993; Hüll and Bähr, 1994; Lu et al., 2003; Robinson 1994 and 1995). Further our RGCs expression of phospho-c-Jun is consistent with its expression in the neocortical neurons sustaining TAI which also do not die (Greer et al., 2011). Importantly, ATF-3, another transcription factor associated with axonal regeneration, is activated in the neocortical neurons following TAI (Greer et al., 2011).

One unexpected finding in the current communication is the subtle decrease of RGC number in the sham and injured animals overtime as detected through the use of antibodies to Brn3a. Importantly, however no difference existed between the number of RGC in the sham and injured animals at each time point. Accordingly we cannot conclude that the subtle RGC loss in the injured group was due to traumatic axonal injury. Rather other factors were at work most likely. Recently, Comley and colleagues (2011) demonstrated that the YFP fluorescent protein expressed in the thy1-YFP mice was not biologically inactive. In fact, it upregulated multiple genes and proteins associated with various cell stress responses, such as apoptosis signaling, DNA damage and repair, inflammation as well as oxidative or metabolic stress (Comley et al., 2011). The high neuronal expression of YFP in YFP-16 transgenic mouse also subtly increased the incidence of the neuronal morphological abnormality and altered the time-course of dying-back pathology (Comley et al., 2011). Thus, these adverse effects of YFP fluorescent protein within the neuron could explain the subtle decrease of RGC currently described in both the sham and injured animal populations.

While the current communication in the visual system significantly extends our understanding of TAI and its implication for concomitant retinal change, it also offers many

other potential applications and benefits. The preservation of the RGCs and their proximal axonal appendages in a relatively intact optic nerve offer an unprecedented opportunity for evaluating possible regeneration and repair. Further, the fact that the optic nerve itself is accessible to both blood-born and CSF applied therapeutic approaches, this model should prove invaluable in multiple drug screening approaches. Accordingly, in light of the current finding on the preservation of the RGCs in response to TAI, our model system takes on increased utility and importance.

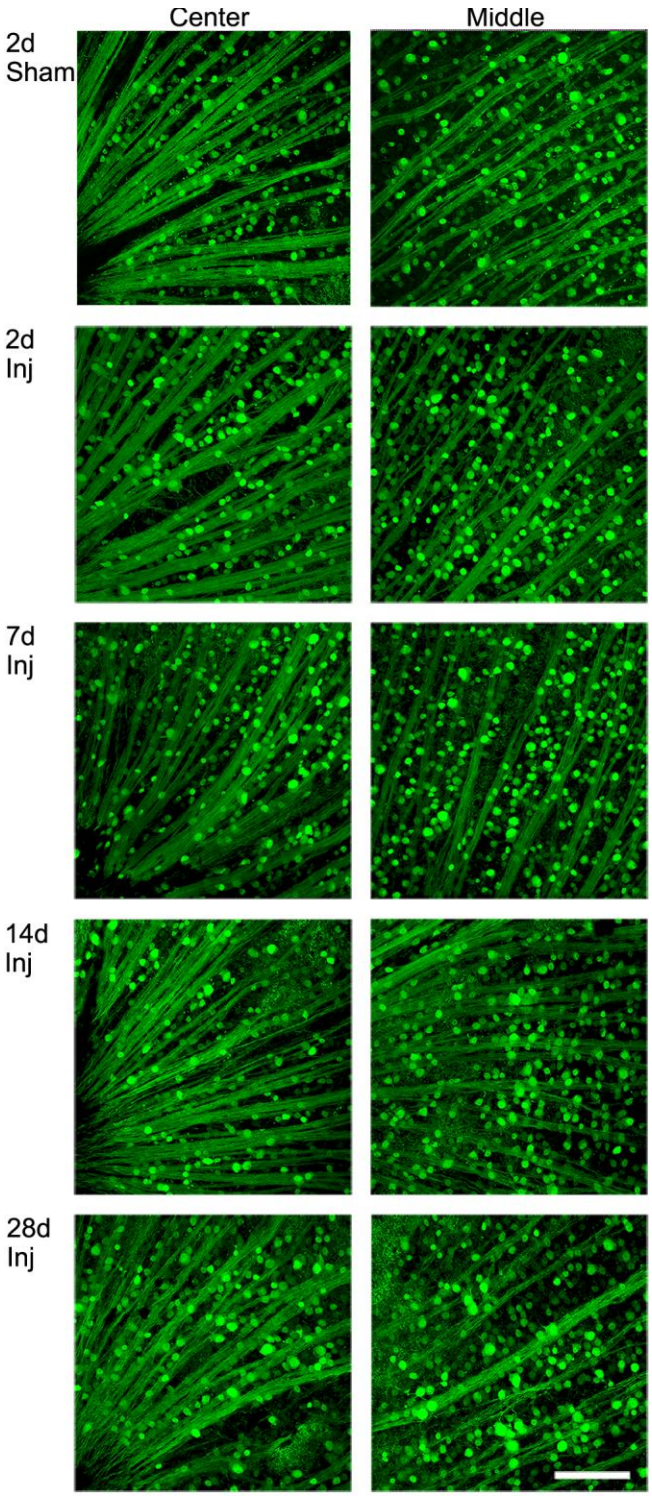

Figure 4.1 No overt loss of YFP positive cells in the retinal ganglion cell (RGC) layer overtime post injury. These retinal whole mounts demonstrate comparable YFP distribution in the sham as well as the injured animals at all time points post TBI. The axons in the retina maintain intact, without any axonal swellings. Compared to the retina of the 2 day sham animal, the center and the middle region of the retina reveal no overt loss of YFP positive cells in the retinal ganglion cell (RGC) layer (the same layer of RGC axons) at 2, 7, 14 and 28 days post injury. Scale bar: 100μm.

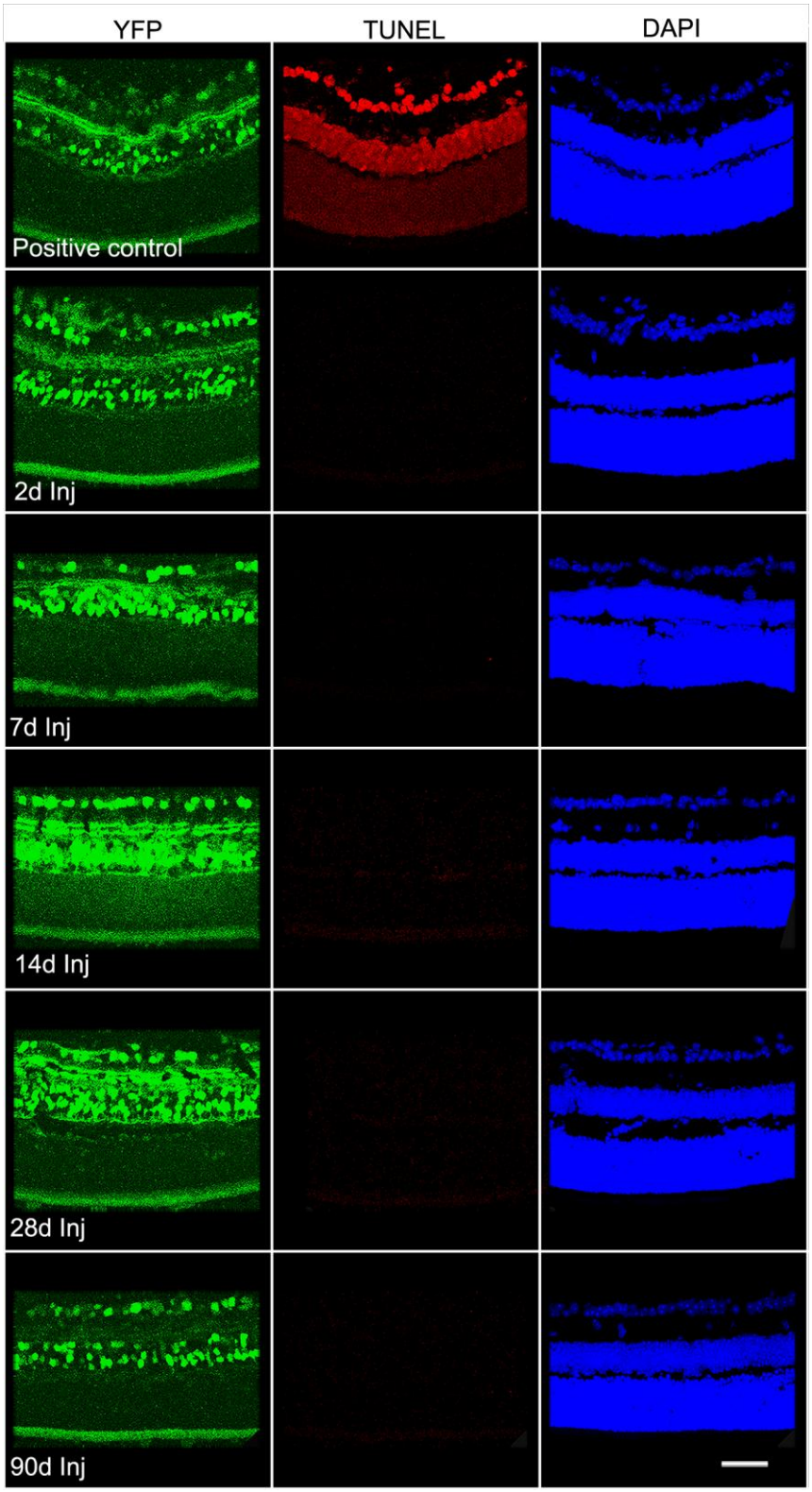

Figure 4.2 This figure reveals negative TUNEL staining of retinal ganglion cells from 2 days to 90 days post TBI, in contrast to the positive control section treated by DNAase, which shows positive TUNEL staining within different layers of the retina. Scale bar: 50 µm.

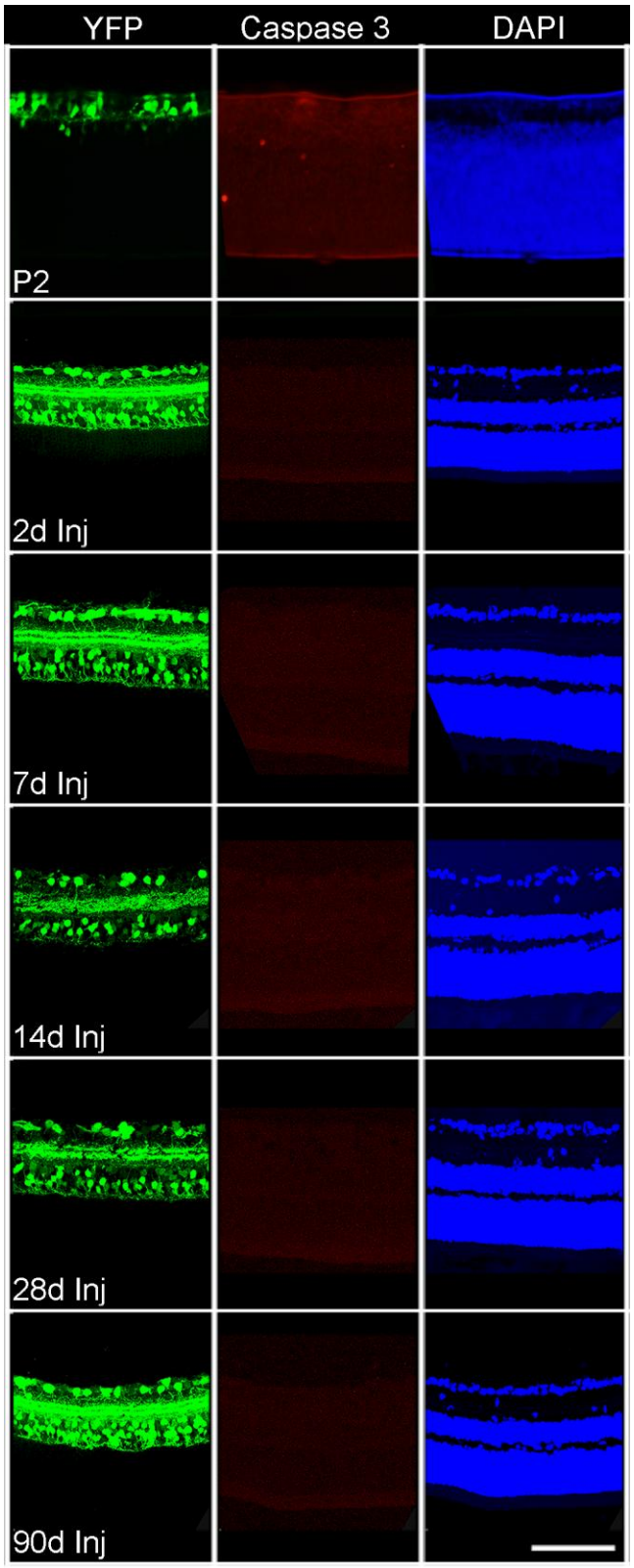

Figure 4.3 This figure demonstrates the absence of the cleaved caspase-3 expression in the retinal ganglion cell layer from 2 days to 90 days post injury. This finding contrasts to the positive control retinal section from a P2 pup, which shows positive expression of the cleaved caspase-3 in different layers of the retina. Scale bar: 100 µm.

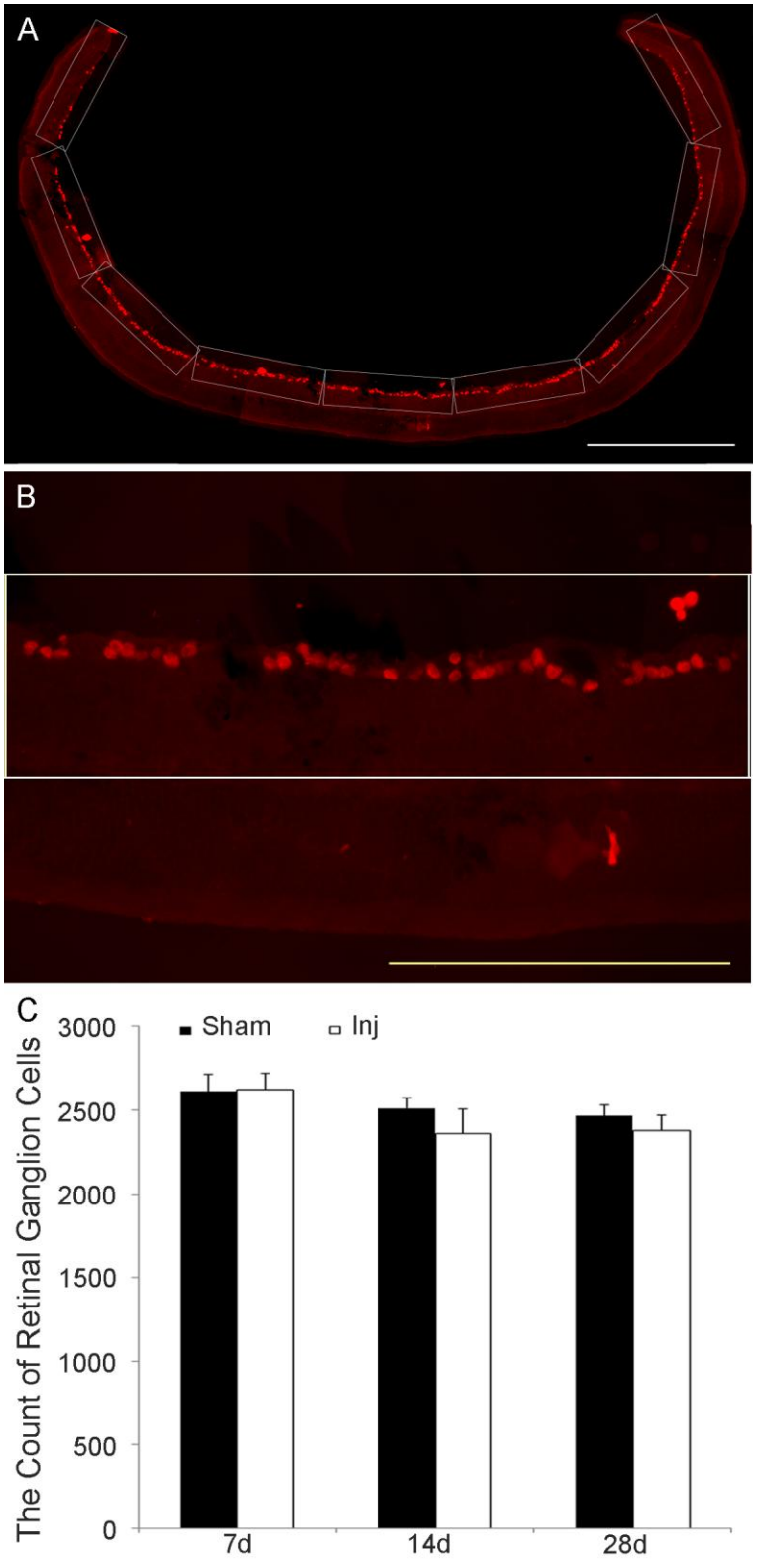

Figure 4.4 This figure shows quantitative analysis of the retinal ganglion cell (RGC) number following TAI. Figure A illustrates the images taken from side to side of the retinal section immunostained with antibodies to Brn3a. Figure B shows the placement of a grid (0.435mm x 0.115mm = 0.05mm^2) expanding along the image parallel to the alignment of the RGCs, and covering all the RGCs that were counted. Figure C shows the quantitative assessments that reveal a subtle time dependent decrease of RGCs in both sham and injured animals from 7 days to 14 days and 28 days post injury. Note that, however, at each specific time point, the number of RGC shows no difference between the sham and the injured groups. Scale bar: 500 μm in A; 200μm in B.

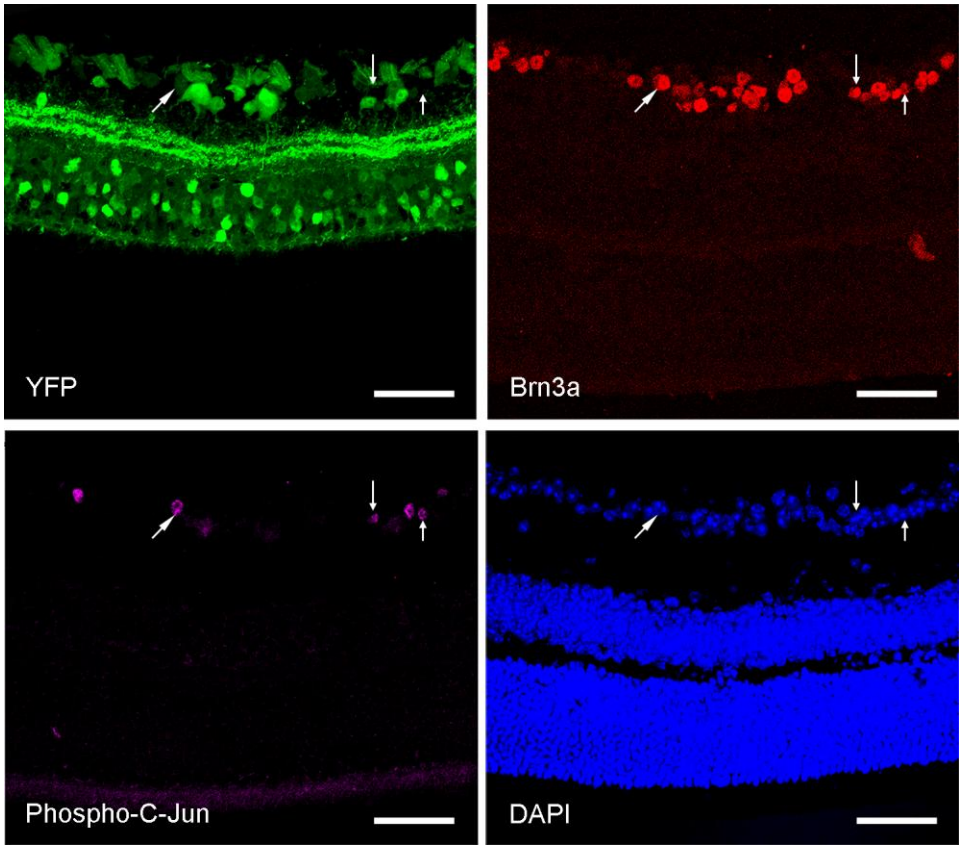

Figure 4.5 Note that an expression of phospho-c-Jun is found specifically within the retinal ganglion cell (RGC) layer, and colocalize with Brn3a positive RGCs (arrows). Also note that the phospho-c-Jun positive RGCs (purple) are scattered among adjacent phospho-c-Jun negative RGCs. Scale bar: 50μm.

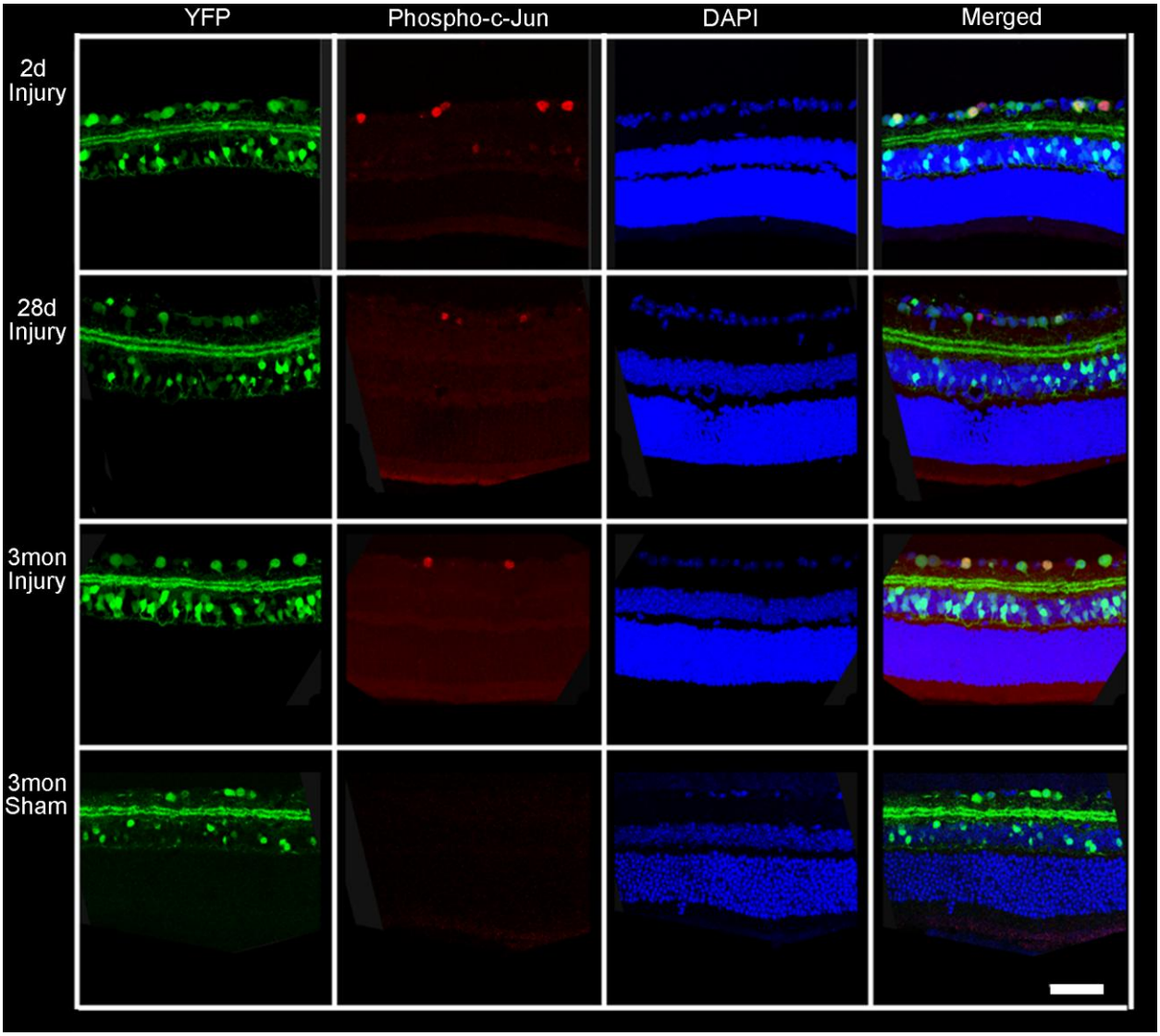

Figure 4.6 This figure reveals YFP positive retinal ganglion cell (RGC) layer with concomitant labeling with antibodies to phospho-c-Jun, a known regulator of neuronal repair and regeneration from 2 days to 90 days post injury. Note that, the phospho-c-Jun positive RGCs are scattered by other phospho-c-Jun negative RGCs. Also note that no phospho-c-Jun expression is seen in the RGCs from the sham animals. Scale bar: 50μm.

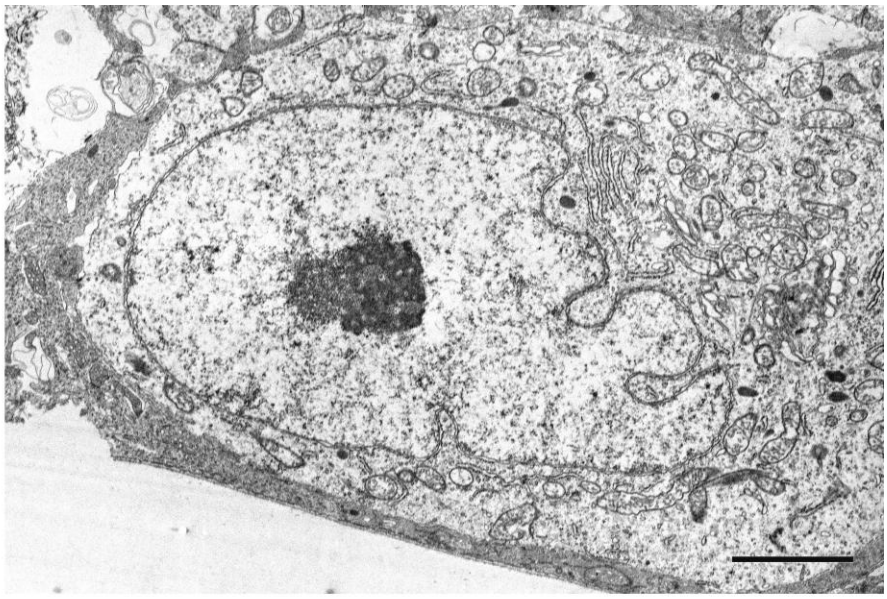

7d

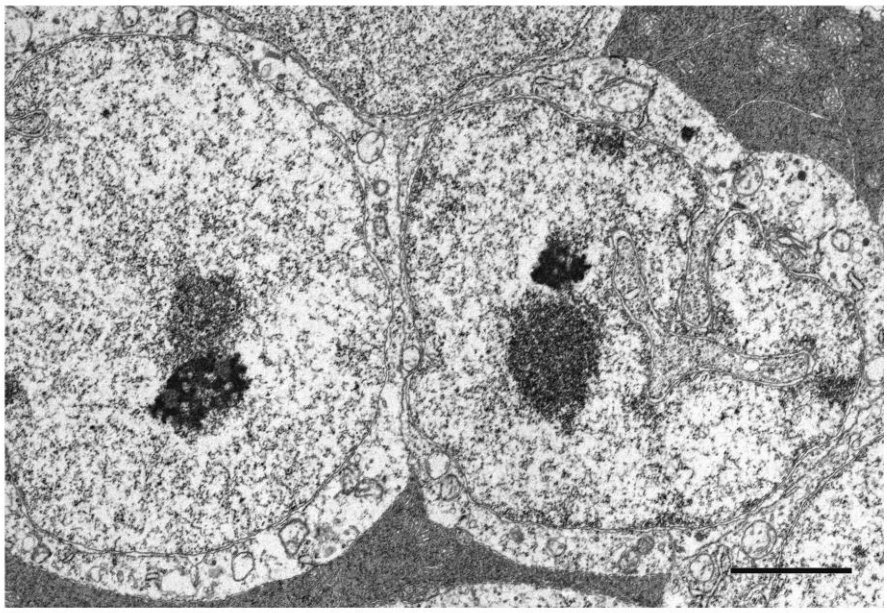

14d

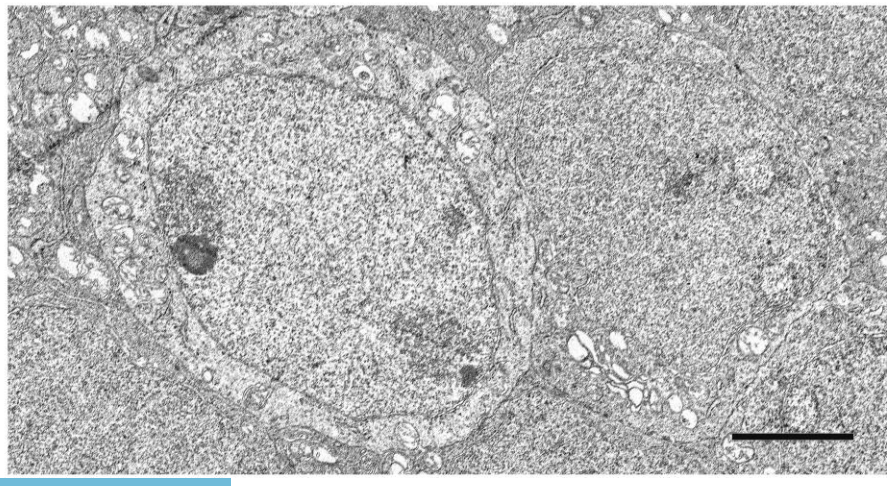

28d

Figure 4.7 These electron micrographs illustrate retinal ganglion cell ultrastructure at 7 days, 14 days and 28 days post injury. Note that at all time points the RGCs reveal normal ultrastructural detail, characteristic of the healthy neurons from the retinal ganglion cell. The only caveat here is that the RGCs visualized at 28 days post injury appear smaller, perhaps suggestive of atrophy. Scale bar, 2μm.

CHAPTER FIVE: APPENDIX I

DISTAL TRAUMATIC AXONAL DEGENERATION AND THE PROXIMAL AXONAL REORGANIZATION WITHIN THE INJURED OPTIC NERVE ARE ASSOCIATED WITH THE DIFFERENTIAL ACTIVATION OF MICROGLIA/MACROPHAGES

Introduction

Traumatic axonal injury (TAI) is a major feature of human traumatic brain injury (TBI) (Povlishock and Katz 2005), and has been associated with much of its morbidity (Graham et al., 2002). To date, significant insight has been gained into the initiating pathogenesis of TAI. However, the precise anterograde and retrograde sequelae of TAI have not been well characterized. Specifically once the axon disconnects, the continued changes in the proximal and the distal disconnected axonal segments, have not been comprehensively appreciated, nor have their causative mechanisms been fully probed.

Previously, axonal dieback, a phenomenon whereby axons retract from the initial site of injury, has been reported in spinal cord injury (SCI). For example, axonal dieback was observed in the rat and mice corticospinal tracts (CST) after thoracic spinal cord transection (Seif et al., 2007, Yoshimura et al., 2011). In addition to the initial mechanical separation, continued SCI axonal dieback has, in part, been linked to local macrophage activation (Busch et al., 2009; Busch et al., 2010; Horn et al., 2008), concomitant oligodendrocyte and microglia/macrophage death (Stirling et al., 2004) as well as myelin degeneration (McPhail et al., 2004). Of note,

distinct macrophage subsets, proinflammatory type (M1) and anti-inflammatory type (M2), have been described to be differentially activated following SCI (Kigerl et al., 2009).

Activation of microglia/macrophages has also been observed in relation to trauma induced axotomy following traumatic brain injury. Specifically, using a mouse midline closed skull injury model, which induces axonal injury in the corpus callosum, the activation of different subpopulations of microglia has been described in both the acute and chronic phases of injury (1 day – 28 days post injury) (Venkatesan et al., 2010). In such injuries, some activated microglia engulf injured axonal segments, consistent with the role of myelin phagocytosis during CNS inflammation (Reichert and Rotshenker, 1999, Venkatesan et al., 2010, Walther et al., 2000). At the same time, other activated microglia express nerve growth factors (Venkatesan et al., 2010), which can promote neuronal repair, axon sprouting and oligodendrocyte proliferation (Kromer, 1987, Althaus et al., 1992, Sofroniew et al., 2001, Frielingsdorf et al., 2007). Thus, although it is clear that microglia/macrophage activation is a consistent feature of CNS axonal damage and dieback, their precise role in terms of the events, occurring in either the proximal or distal disconnected axonal segments is not fully understood.

Previously, we utilized a model of traumatic brain injury evoking TAI within the mouse optic nerve, demonstrating highly localized, post-TBI axonal swelling and disconnection, with proximal and distal axonal dieback accompanied by the regression and reorganization of the proximal axonal swelling segments, and degeneration and delayed clearance of the distal swelling axonal segments (Wang et al., 2011). Given that our model is well characterized and in that the sequence of axonal disconnection and dieback on both the anterograde and retrograde fronts has been fully described within a well localized region of the optic nerve, we employed

these unique features to better understand the potential spatial-temporal relationship that exists between the microglia/macrophages and these axonal dynamic processes.

Material and Methods

Adult Thy1-YFP-16 transgenic mice, which expressed YFP under the promoter Thy1 within over 80% of the optic nerve fibers (Feng et al., 2000), were subjected to central fluid percussion injury as described in the General Methods Section (Chapter 2), and allowed to survive from 2 days to 28 days (at each time point, n = 3 in each injured group, n= 1 in the sham injured group). Animals (the same animal from Chapter 4) were perfused and the optic nerve was blocked and sectioned as described in Chapter 2 and Chapter 3 and processed for fluorescent immunohistochemistry.

Fluorescent Immunohistochemistry.

To study the relationship between the YFP-linked axonal dieback and the activation of microglia/macrophages, labeling of the optic nerve were performed utilizing an antibody targeting the microglia/macrophage population (Iba1). Specifically, YFP fluorescent optic nerve sections from 2 day to 28 day time point post injury were selected and rinsed 3 x 10 minutes in PBS, and pretreated with 10% NGS with 2% BSA and 0.5% Triton X in PBS at room temperature for 2 hours. Endogenous mouse IgG was blocked by primary antibodies derived from a mouse host (Mouse on Mouse Kit, MOM^{TM}; Vector Laboratories; Burlingame, CA). Then the sections were washed 3 x 10 minutes in 10% NGS with 2% BSA and 0.5% Triton X in PBS, and then incubated overnight at 4^{o}C with the primary antibody rabbit anti-Iba1 (1:1000; Zymed, San Francisco, CA). Next, the sections were washed 6 x 10 minutes with 1% NGS with

1% BSA and 0.2% Triton X in PBS at room temperature, followed by incubation with the secondary antibody Alexa 568-conjugated goat anti-rabbit IgG (1:500, Molecular probes, Invitrogen). The sections were then washed 4 x 5 minutes in PBS and 2 x 5 minutes in 0.1 M sodium phosphate buffer, and cover-slipped with Vectashield Hardset Mounting Medium with DAPI (Vector Laboratories) for analysis with a Leica TCS-SP2 AOBS confocal microscope (Leica Microsystems). For the study of the spatial-temporal relationship between the injured axons and their related macrophage/microglia, three-dimensional reconstructions were obtained with the Volocity Software package (Perkin Elmer; Waltham, MA).

Results

Sham Injury-General Findings and Cellular Phenotype

In the optic nerve of sham-injured animals, the YFP-positive axons maintained continuity without any evidence of axonal swellings through the length of the optic nerve. Along the length of the optic nerve, no activation of microglia/macrophages could be observed at any time post injury (Figure 5.1 A). Specifically, the microglia/macrophages demonstrated a resting morphology, with their processes paralleling normal, aligned optic nerve axons (Figure 5.1 B and 5.1 C).

Microglia/Macrophage Responses to Diffuse TAI within the Optic Nerve

Initial activation of microglia/macrophage within 2 days post injury

As early as 2 days post injury, in the optic nerve of injured animals, activated microglia/macrophages were found scattered among diffusely injured axons. At this time point, they were confined to the site of initial axonal separation and dieback (Figure 5.2 A). Of note, at

this post injury time frame, only limited evidence of direct microglia association with the disconnected, distal axonal segments was found (Figure 5.2 B). As previously described in Chapter 3, the proximal axonal segments, which were now truncated and apparently undergoing reorganization, were not associated with or attached to this microglia/macrophage population (Figure 5.2 C).

Activation of microglia/macrophage at 7 days post injury

By 7 days post injury, microglia/macrophage activation demonstrated a dramatic increase and now numerous activated microglia/macrophages could be easily identified in the injured optic nerve (Figure 5.3). As noted previously, the distal disconnected, swollen axonal segments retained their rounded/spheroidal shape (Chapter 3), and again, these distal, degenerating axonal segments were interspersed among adjacent intact fibers. In relation to these distal disconnected and degenerating axonal segments, however, the related microglia/macrophages revealed dramatic activation, with their cell bodies demonstrating rounded up profiles, consistent with their activation. These activated microglia/macrophages established direct contact with the degenerating distal axonal segments, with their processes attaching to and engulfing the swollen, rounded distal axonal profiles (Figure 5.4). Of note, no evidence of microglia/macrophage clustering was observed in relation to these degenerating axonal segments.

In contrast to this dramatic distal microglia/macrophage activation, the proximal axonal segments, which again revealed a truncated configuration (Figure 5.5) (as previously described in Chapter 3), retained an axonal profile distinct from the distal spheroid, degenerating axonal segments. These proximal segments revealed shrinkage and resorption, consistent with reorganization overtime. In relation to these proximal axonal segments, the

microglia/macrophages were significantly less active, with their processes paralleling but not engulfing these axonal profiles (Figure 5.5).

Persistent activation of microglia/macrophages in the distal degenerating axonal segments at 14 and 28 days post injury

Up to 14 to 28 days post injury, activated microglia/macrophages persisted within the distal disconnected, degenerating axonal segments (Figure 5.6 A and B). Again, their cell bodies were rounded, with their processes engulfing the distal, swollen degenerating axonal segments (Figure 5.6 A and B), consistent with their role in clearing these degenerating axonal segments.

The proximal axonal segments at 14 and 28 days post injury, manifested continued reorganization, with the microglia/macrophages again maintaining a resting state. Their cell bodies were compressed, and their processes paralleled the axonal profiles, without any evidence of the proximal axonal segment engulfment (Figure 5.6 C and D).

Discussion

In the current study following TAI in the optic nerve, activation of the microglia/macrophages was first observed at 2 days post injury, becoming dominant by 7 to 14 days and persisting up to 28 days post TBI. The distal, disconnected axonal segments, after the acute dieback, transitioned into a pattern of Wallerian degeneration, with the distal damaged axons encompassed by the processes of activated microglia/macrophages. In contrast, the proximal axonal segments underwent reorganization and their related microglia/macrophages remained markedly less active, with their processes paralleling but not enveloping these axonal profiles. These varied responses in the distal and the proximal axonal segments, most likely

speak to the fact that different signaling pathways were involved in these two regions and therefore translated to differential microglia/macrophages responses.

At the early hours to 2 days post injury, both the proximal axonal segment and the distal disconnected axonal segments underwent rapid dieback in both the rostral and caudal directions as previously described in Chapter 3. Specifically, the acute axonal dieback of the proximal axonal segment moved approximately 0.4-0.8mm within a 48 hours period following injury, while the distal axonal segment retracted rapidly toward the chiasm at a similar speed (Chapter 3). Because of the rapidity of these events, local calcium dysregulation and calpain activation are most likely involved in both of these acute axonal dieback processes during this early period post injury. Others have demonstrated that a rapid increase of intra-axonal calcium is associated with the initial axonal dieback following either *in vitro* laser-induced axonal damage (Hellman et al., 2010) or *in vivo* optic nerve crush (Knöferle et al., 2010). This increased intra-axonal calcium, activates calpain and overloads and damages mitochondria, which collectively promote axonal dieback. In spinal cord transection studies, calpain inhibitors effectively inhibited acute axonal dieback following cord transection in both the proximal and the distal directions (Kerschensteiner et al., 2005), confirming the function of calpain in this acute axonal dieback response. This is most likely related to calpain's capacity in degrading microtubules, neurofilaments and spectrin (Banik et al., 1997; Billger et al., 1988; Johnson et al., 1991; McGinn et al., 2009; Roberts-Lewis et al., 1994; Siman et al., 1984). In addition to calcium-activated, calpain-mediated cytoskeletal proteolysis, calcium overloading can also destroy mitochondria, resulting in ATP deficiency, compromising axonal transport, further facilitating axonal dieback.

After the rapid dieback, our proximal axonal segments manifested a rapid transition from swollen enlarged segments to a truncated morphology (Chapter 3), which persisted from 7 – 28 days post injury (the current chapter). Consistent with this proximal axonal segment reorganization and its attempt to repair, was the related finding that the associated microglia/macrophages maintained a resting state from the 7 – 28 days post injury. The underlining mechanisms for such phenomenon may be due to the rapid resealing of the axonal membrane, the conversion of anterograde transport to retrograde axonal transport and the continuity of these proximal axonal segments with viable RGCs (Chapter 4). The proximal axonal reorganization/repair maybe preceded by a rapid resealing of the axolemmal membrane (Liu et al., 2011, Meiri et al., 1983). Studies utilizing cockroach giant axon transection have demonstrated that at the cut end of the nerve fiber, the axonal membrane reseals within 5 to 30 minutes after the transection at 23^{o}C to 27^{o}C, and this resealing depends on the influx of calcium into the axoplasm and its subsequent activation of phospholipase A2 (Yawo and Kuno, 1983; Yawo and Kuno, 1985). Such axonal membrane resealing also involves the Ca^{2+} mediated calpain activity after the transection of the neurites of *in vitro* cultured rat septal neuron (Xie and Barrett, 1991) and after crayfish medial giant axon transection (Godell et al., 1997). Additionally, vesicle proteins, such as synaptotagmin, synaptobrevin and syntaxin, have also been demonstrated to play an important role in membrane resealing (Fishman and Bittner, 2003). Such axolemmal resealing could prevent the influx of extracellular molecules and inhibit the release of intra-axonal components into the extra-axonal environment. Besides the rapid resealing of the axolemmal membrane, anterograde axonal transport could be converted to retrograde axonal transport (Tuck and Cavalli, 2010, Bisby and Bulger, 1977) via local proteolysis (Sahenk and Lasek, 1988) and/or the modification of proteins on the transported

vesicles (Martz et al., 1989), facilitating the reorganization of the proximal axonal segment. Further, the proximal axonal segments, perhaps receive persistent support from viable RGC, attenuating/inhibiting degeneration and promoting axonal reorganization, without generating myelin debris. All these events most likely resulted in less dramatic alternation of the microenvironment, translating to the minimal stimulus to microglia/macrophage and their relatively resting status in the proximal axonal segments.

In contrast, in the distal disconnected, degenerating axonal segments, the microglia/macrophage manifested an activated phenotype from 7 to 28 days post injury, with their processes attaching to and encompassing the distal disconnected, degenerating axonal segments. The persistent activation of microglia/macrophage in this region is most likely linked to the persistent production of myelin debris during axonal degeneration (Kelley et al., 2007, Brück et al., 1995). Such microglia/macrophage activation is also consistent with their role in the clearance of the degenerating axonal segments previously described following the brain and spinal cord injury (Busch et al., 2009; Busch et al., 2010; Horn et al., 2008; Venkatesan et al., 2010). In SCI studies, Horn (2008) reported a spatial-temporal correlation between macrophage infiltration and the retraction of the injured ascending dorsal column sensory axon from 7 to 28 days after injury. Horn (2008) also demonstrated in an *in vitro* study direct adhesive contacts between activated macrophages and dystrophic axons, with extensive axonal retraction induced only when the macrophages were activated. Busch (2009) demonstrated the expression and secretion of MMP-9 by the activated macrophages, and the specific inhibition of MMP-9 block the macrophage-induced retraction of dystrophic axons. In addition to MMP-9, activated microglia/macrophages also secrete cytokines, such as interleukin-1 (IL-1), IL-6 and tumor necrosis factor-α (Gentleman et al., 2004; Kita et al., 2000; McClain et al., 1991). It has been

demonstrated that IL-6 can increase microglia/macrophage's phagocytotic activity (Shafer et al., 2002-2003). Such positive feedback may further facilitate their engulfment of the distal degenerating axonal segments and the clearance of myelin debris, and maybe associated with potential synaptic plasticity in the downstream target.

Such close association of the distal axonal degeneration and dieback and microglia/macrophage activation imply that blocking the activation of macrophage/microglia is a potential therapeutic approach to attenuate distal axonal degeneration. For example, minocycline, an anti-inflammatory and neuroprotective medication, inhibits microglial activation and attenuates MMPs (Brundula et al., 2002; Yrjänheikki et al., 1998). When administered intraperitoneally, minocycline is effective in reducing the number of activated microglia/macrophages, while also inhibiting axonal dieback, reducing lesion size and enhancing functional performance at both 7 and 14 days after SCI (Stirling et al., 2004).

The morphology of microglia/macrophage transforming from the activated state in the distal disconnected, degenerating axonal segments to the resting state in the proximal reorganized axonal segments, suggests that their status is most likely modified by the adjacent microenvironment. As discussed, it is possible that in the proximal axonal segments, the microenvironment was not dramatically altered. On the other hand, in the distal degenerating axonal segments, the microenvironment was obviously different due to the local generation of myelin debris and the secretion of cytokines.

While it is likely that the activity of microglia/macrophage can be modified by the local microenvironment, it is unclear whether distinct subtypes of microglia/macrophage reside in the injured optic nerve. Previous studies in SCI, however, demonstrate that two distinct macrophage subsets, namely proinflammatory type (M1) and anti-inflammatory type (M2), are activated

differentially following SCI (Kigerl et al., 2009). The M1 macrophages are activated rapidly and persist up to 28 days post SCI, in contrast to the M2 macrophages which are activated transiently and recover to the preinjury levels by 14 days post injury (Kigerl et al., 2009). Further, inducing macrophages to differentiate into the M2 phenotype by peroxisome proliferator activated receptor (PPAR) agonists, has been demonstrated to promote anatomical and functional repair after rodent SCI (McTigue et al., 2007; Odegaard et al., 2007; Vill Villanueva and Tontonoz, 2010). Although there is little evidence regarding the activation of M1 and M2 macrophage in optic nerve injury studies, this SCI study suggests that the induction of a microglia/macrophage transition into the resting phenotype, may be a potential therapeutic strategy to attenuate the distal, disconnected axonal degeneration in our current study.

All the above findings of the differential activity of microglia/macrophages in the disconnected proximal and distal axonal segments in the current communication were obtained based upon the morphological change of microglia/macrophages via the utilization of antibodies targeting Iba1 which label all microglia/macrophages. These results may further be confirmed via the utilization of other markers that specifically stain activated microglia/macrophages, affirming their activation at the disconnected distal axonal segments.

In summary, this study reveals differential microglia/macrophage response to the disconnected proximal and distal axonal segments. These observations within the optic nerve provide unique insight into the pathobiology associated with the TAI, particularly in terms of activated microglia/macrophages in the distal disconnected axonal segments versus the resting microglia/macrophages found in the proximal, reorganizing axonal segments.

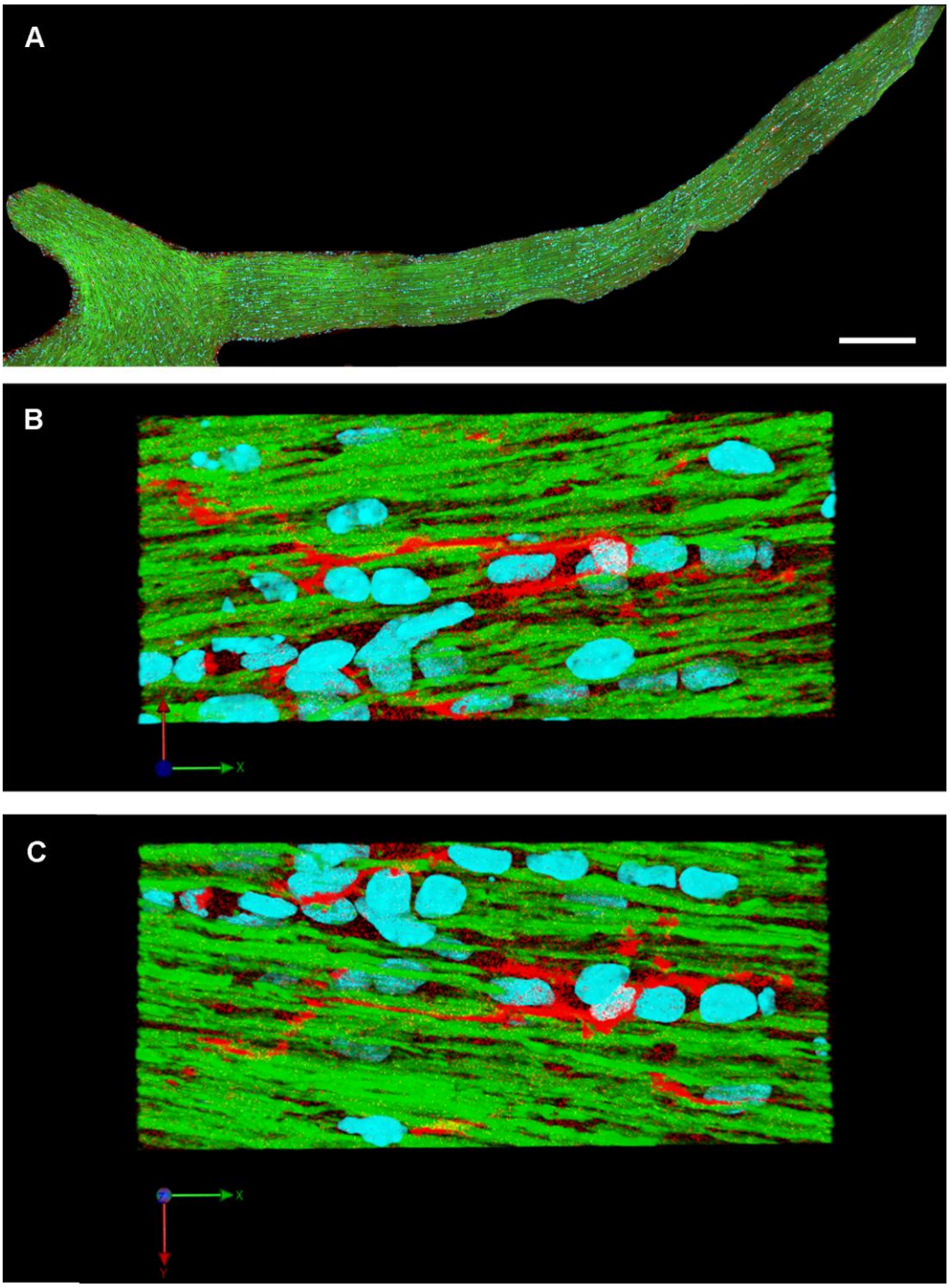

Figure 5.1 The microglia/macrophages maintain at a resting state throughout the length of the optic nerve 2 days after sham injury (A). Note that all the scattered microglia/macrophages reveal morphological features consistent with a resting state, with their processes paralleling the normal YFP expressing axons (B and C). (Blue: DAPI; YFP: axon; Red: microglia/macrophage). Scale bar: 300μm in A.

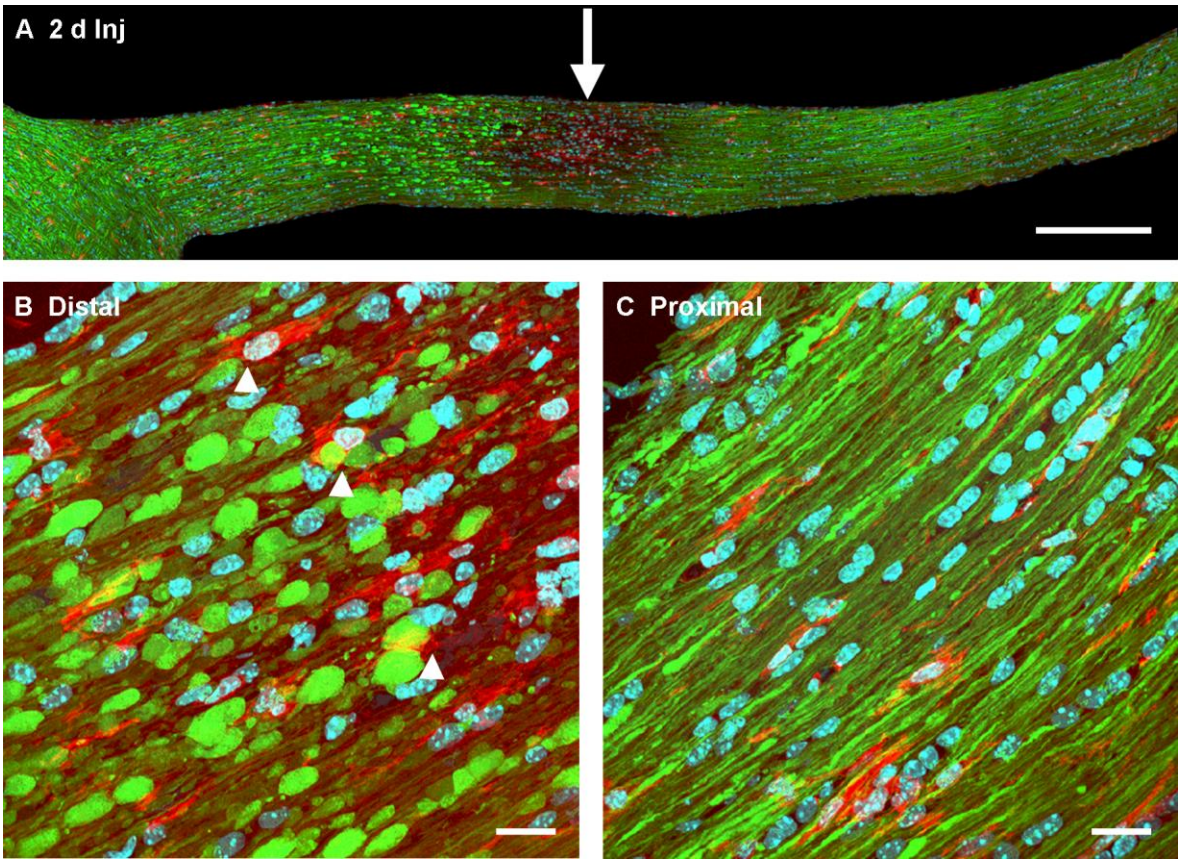

Figure 5.2 Activated microglia/macrophages can be recognized in the optic nerve at 2 days post TBI (A). Specifically, the activated microglia/macrophage can be seen scattered between injured axons at the site of initial axonal injury (A arrow). Note that a few activated microglia/macrophage lie adjacent to distal axonal segments in the process of dieback toward the chiasm (B arrowhead), however, in the proximal axonal segments, no association exists between microglia/macrophage and the reorganizing proximal axonal segments (C). Scale bar: 300µm in A, 20µm in B and C.

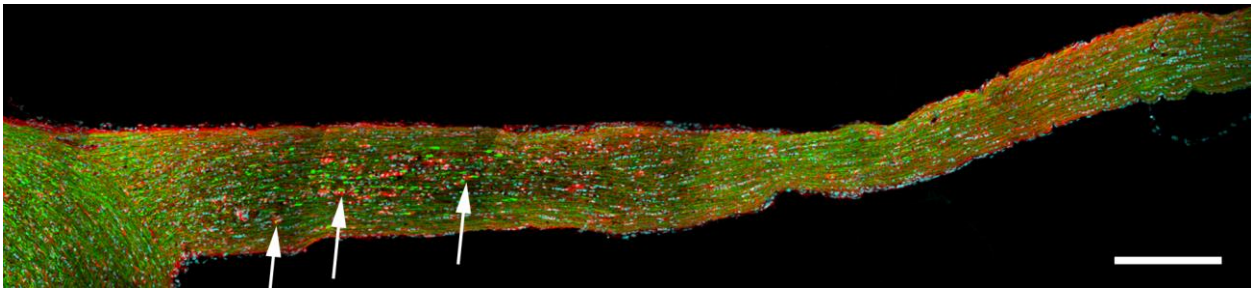

Figure 5.3 Activated microglia/macrophages predominate in the optic nerve at 7 days post TBI. Specifically, note that the activated microglia/macrophages attach/engulf the distal, disconnected degenerating axonal segments (arrow). (Red, Iba1 immunostaining, microglia/macrophage). Scale bar: 300µm.

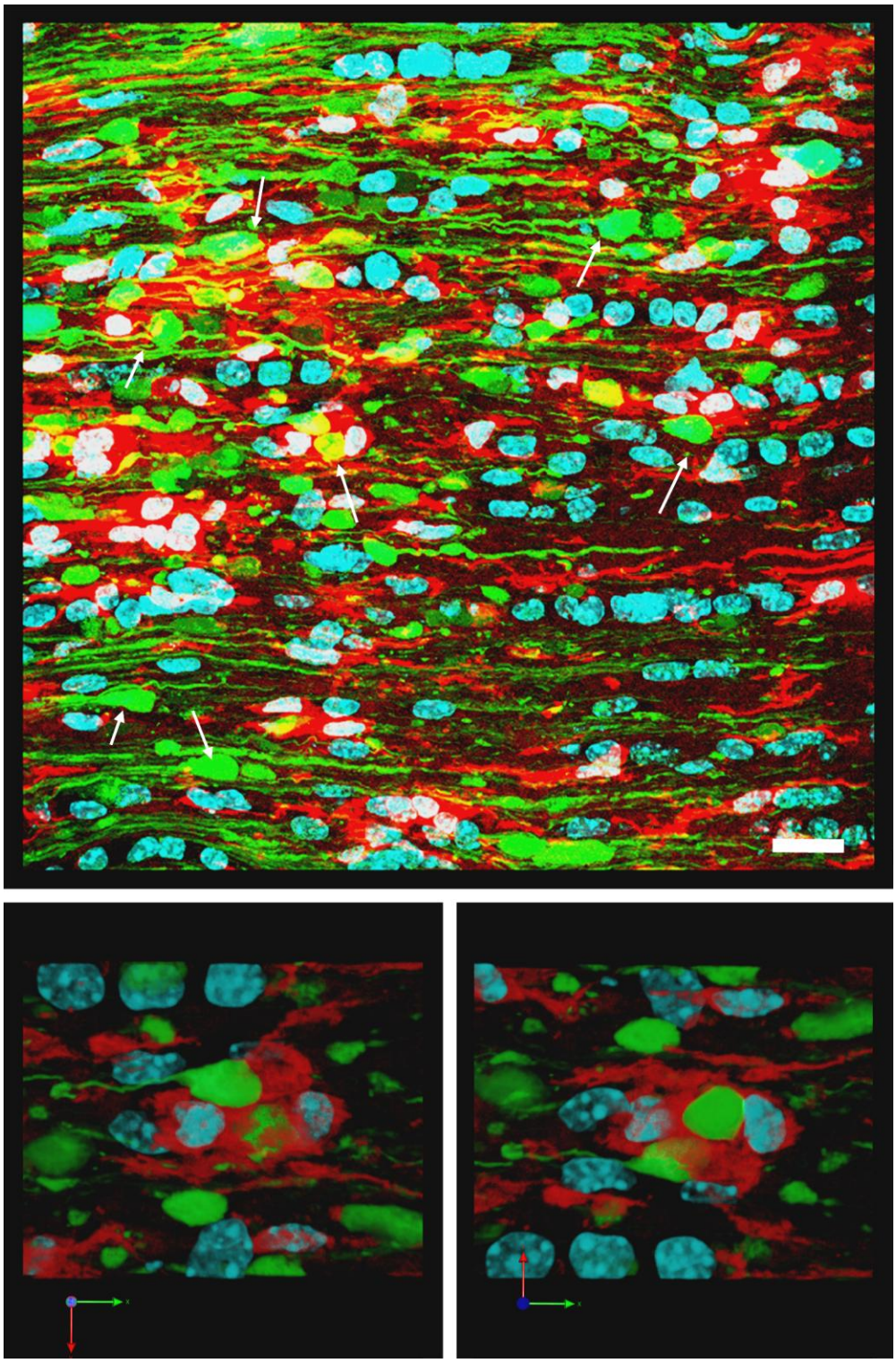

Figure 5.4 At higher magnification, the activated microglia/macrophages can be seen to approach and engulf the distal, disconnected swollen axonal segments within the optic nerve at 7 days post injury. The top image shows that at 7 days post injury, there are numerous persistent, disconnected distal swollen axonal segments (white arrows). The activated microglia/macrophages (red) appear reactive, and their related appendages contact and engulf the swollen axonal segments. The lower two images show at even higher magnification that the distal swollen axonal segments (YFP) are enveloped by the processes of activated microglia/macrophages. Scale bar: 20µm.

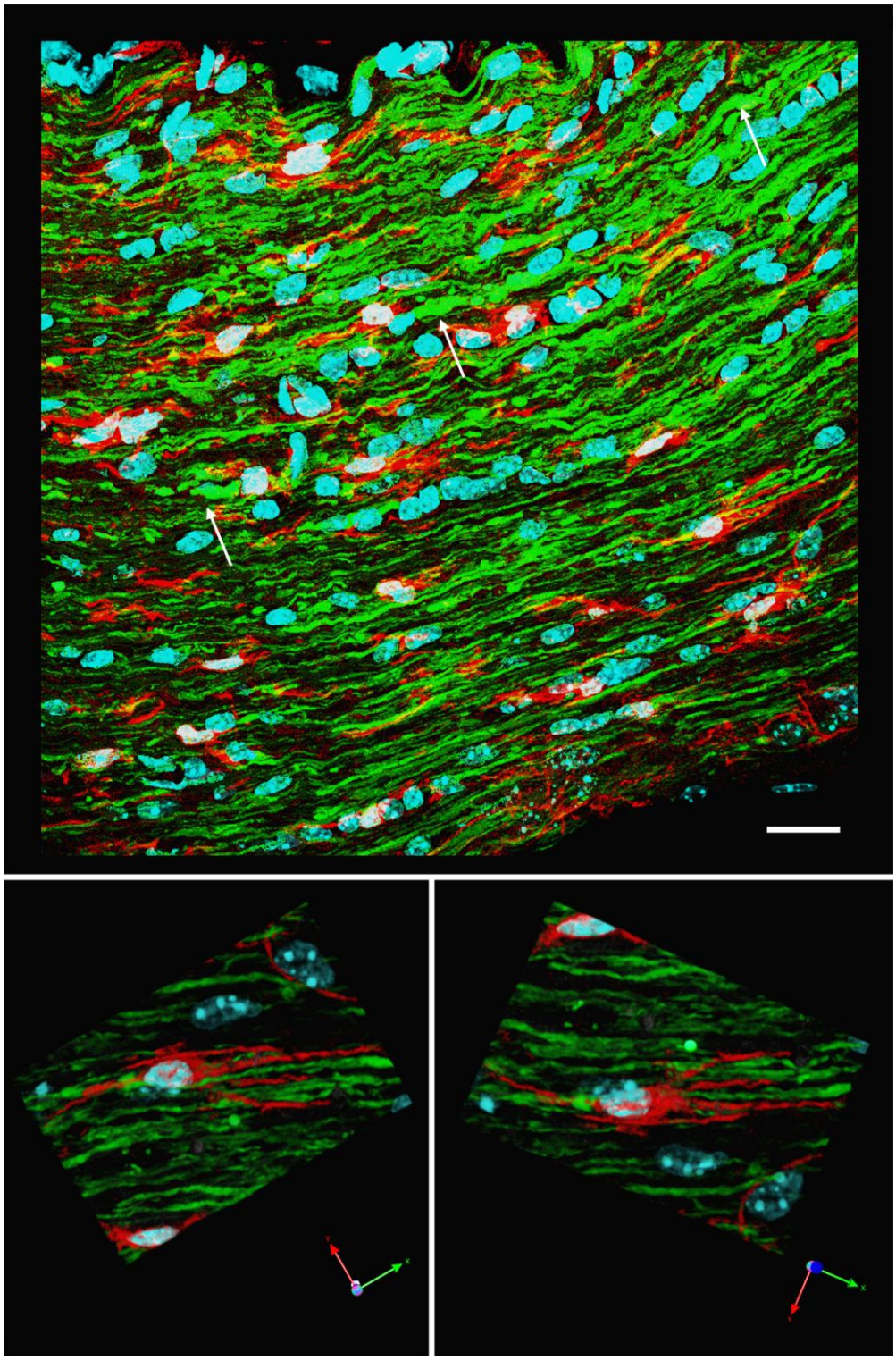

Figure 5.5 The microglia/macrophages appear less active in the proximal axonal segments of the optic nerve at 7 days post injury. The top image reveals at 7 days post injury, that the proximal axonal segments are truncated (white arrows), consistent with reorganization. Microglia/macrophages are scattered between these proximal axonal segments. The lower two images showed at a higher magnification, that in the proximal axonal segments, a microglia/macrophage (red) maintain a resting state with its processes paralleling the alignment of the axonal fibers. Scale bar: 20μm.

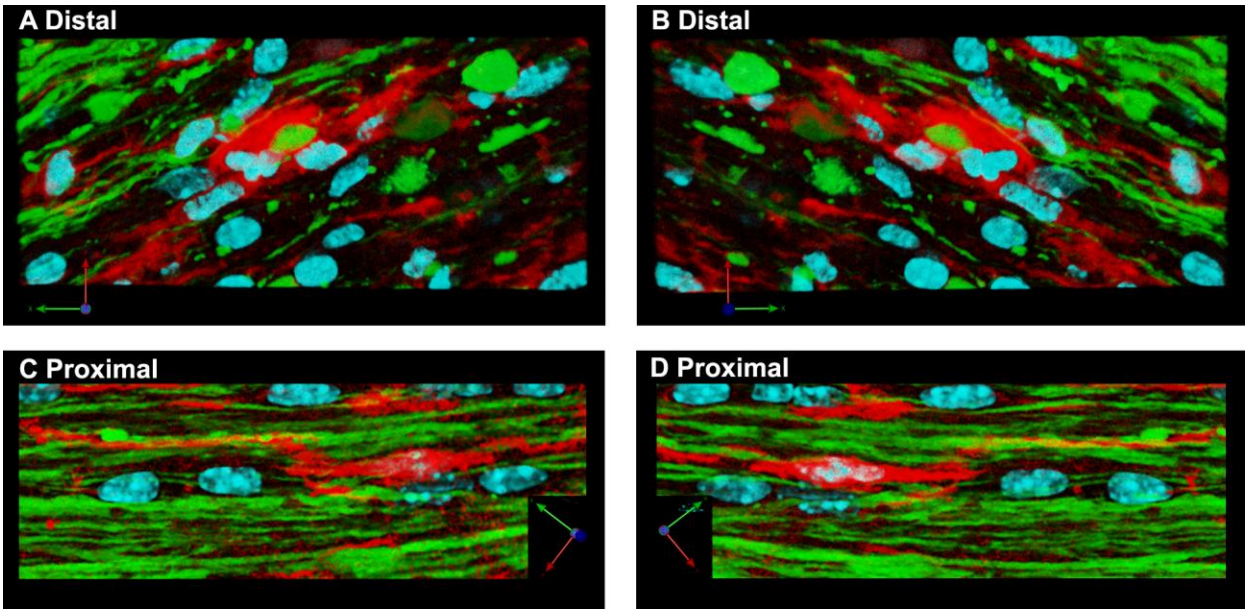

Figure 5.6 Activated microglia/macrophages predominate in the distal disconnected axonal segments of the optic nerve at 14 and 28 days post TBI. Specifically, activated microglia/macrophages (Red, Iba1 immunostaining) can be seen attaching to and engulfing the distal disconnected, degenerating axonal segments (A and B). In contrast, in the proximal axonal segments, the microglia/macrophage again retains a resting state, compressed between the axonal fibers, with their processes paralleling the aligned axonal profile (C and D).

CHAPTER SIX: APPENDIX II

THE CLEARANCE OF OPTIC NERVE EDEMA AND THE RECOVERY OF YFP FLUORESCENT AXONAL FIBERS OVERTIME POSTINJURY

Introduction

We have previously shown that our model of traumatic brain injury (TBI) evoked diffuse traumatic axonal injury (TAI) within the mouse optic nerve, with the TAI eliciting progressive axonal swelling and disconnection, together with proximal and distal axonal dieback (Chapter 3 and Wang et al., 2011). These processes were accompanied with an apparent focal loss of YFP fluorescence in the region between the detached proximal and distal axonal segments. This loss of YFP fluorescence was not the result of actual fiber dissolution. Rather it was due to local fluorescence quenching, a sequelae of local blood-brain barrier (BBB) disruption. The barrier disruption was demonstrated by the passage of immunoglobulin (IgG) into the optic nerve (Figure 3.10), which was most likely accompanied by the movement of water, with the formation of edema, consistent with previous electron microscopic (EM) observation of the expansion of the interstitium (Figure 3.3).

To date it has been demonstrated that water and solvent properties of water can lead to fluorescence quenching (Ebbesen and Ghiron, 1989; Oshima et al., 2006; Sadkowski and Fleming, 1980; Seliskar and Brand, 1971; Tobita et al., 2001). Since optic nerve edema involves significant generation of water, it is not unreasonable to hypothesize that this water can

participate in fluorescence quenching. The correctness of this hypothesis is further supported by previous observation of axonal profiles using antibodies to the endogenous YFP (Figure 3.11), confirming that the loss of fluorescence was most likely due to quenching, and not actual fiber loss.

In the current chapter, we employed the same YFP transgenic mice TBI model and evaluated optic nerve axons at the electron microscopic level overtime post injury to better appreciate the persistence of intact/unaltered axons and reconfirm the characteristics of diffuse axonal injury of this model. In these studies, the intact axons were not separated by an expanded interstitial space in later phases of injury, suggesting the clearance of edema overtime postinjury. Further, in concert with this observation, we observed at the confocal fluorescent microscopic level, the recovery of YFP fluorescent intact axons in the previously identified regions of fluorescence loss, confirming the correctness of our hypothesis that water participates in fluorescence quenching, as the clearance of edema apparently reversed fluorescence quenching.

Material and Methods

Adult Thy1-YFP-16 transgenic mice, which expressed YFP within the optic nerve fibers (Feng et al., 2000), were subjected to central fluid percussion injury as described in the General Methods Section (Chapter 2), and allowed to survive from 2 days to 90 days (at each time point, n = 3 in the injured group, n = 1 in the sham injured group). Animals (the same animal from Chapter 4/5) were perfused and the optic nerve was blocked and sectioned as described in Chapter 2 and Chapter 3. The optic nerves were processed for electron microscopic analysis and fluorescent confocal microscopic analysis.

Electron Microscopy

For electron microscopic (EM) analysis, the YFP-16 transgenic mice were first perfused with 100ml heparinized normal saline, followed by 200ml 2% paraformaldehyde and 2.5% glutaraldehyde in Millonig's buffer. Again, the brain and the optic nerves were post-fixed and blocked as described in Chapter 2. These prepared YFP optic nerves were osmicated in 1% OsO4, dehydrated, embedded in epoxy resins (Embed-812; Electron Microscopy Sciences, Hatfield, PA), mounted on plastic slides (Thomas Scientific Co., Swedesboro, NJ) and cover-slipped. After resin curing, the injured axonal segments including the locus of fluorescence quenching, were excised, mounted on plastic studs, and thick sectioned to the depth of the sites of interest using an ultramicrotome (Leica Ultracut R; Leica, Wien, Austria). Serial 40 nm sections were cut and mounted onto Formvar-coated single-slotted grids. The grids were then stained with 5% uranyl acetate in 50% methanol for 2 minutes and 0.5% lead citrate for 1 minutes, and visualized using a JEM 1230 electron microscope (JEOL Ltd., Tokyo, Japan).

Fluorescent Confocal Microscopy

The optic nerve sections from YFP-16 transgenic mice sustaining central fluid percussion injury or sham injury, were prepared as described previously (See Chapter 2 Animal perfusion and Optic nerve preparation). The cryo-dissected 10μm optic nerve sections were directly mounted on glass slides with ProLong-Gold antifade reagent (Invitrogen, Carlsbad, CA), and cover-slipped for image capture with a Leica TCS-SP2 AOBS confocal microscope (Leica Microsystems), at 2 days, 7 days, 14 days, 28 days and 3 months post injury. The evaluation of YFP fluorescent axonal fibers was specifically located at the locus of previous fluorescent loss, the same locus of initial TAI (approximately 1mm proximal to the chiasm).

Results

Electron microscopic observation of the optic nerve axon at the locus of fluorescence quenching

As early as 5 minutes to 1 hour post injury, the optic nerve revealed initial axonal swellings (see Chapter 3 Figure 3.3). This axonal injury was accompanied by the expansion of the interstitial space (see Chapter 3 Figure 3.3 asterisk), consistent with the presence of edema generated by the disruption of the blood-brain barrier (BBB) discussed before.

At 7 days (Figure 6.1) and 28 days (Figure 6.2) post injury, in the same locus of fluorescence quenching, numerous intact axonal fibers were observed via EM analysis. Specifically, at these time frames post injury, this region revealed numerous continuous linear/non-swollen axonal profiles spanning the field, which revealed only occasional Wallerian debris interspersed among the morphologically intact axons. Within the axonal cylinder of the intact axons, microtubules and neurofilaments paralleled the longitudinal orientation of the axon, with no evidence of microtubule misalignment or neurofilament compaction. Within these axons no accumulations of either mitochondria, smooth endoplasmic reticulum or vesicles were found. The intact mitochondria revealed normal morphology, with no findings of dilation or disorganized cristae. This ultrastructural analysis confirmed the maintenance of axonal integrity within the locus of fluorescence quenching, consistent with the characteristics of diffuse traumatic axonal injury.

Of note, at 7 days and 28 days post injury timeframe, these same loci of YFP fluorescence quenching, revealed no evidence of the expansion of the interstitial space (Figure 6.1 and Figure 6.2). This observation varied from previously described time frames in which the

expansion of the interstitial space within the optic nerve was routinely observed (See Chapter 3 Figure 3.3). Such reduction of the interstitial space at these more chronic phases post injury (7 days and 28 days) is consistent with the resolution of edema overtime.

Confocal microscopic observation of YFP fluorescent axons in the region of fluorescence quenching

Concomitant with our ultrastractural observation of intact axonal fibers and the clearance of edema overtime in the region of fluorescence quenching, was the finding of a recovery of YFP fluorescent axonal fibers within this same region.

At 2 days post injury, the optic nerve of the injured mice exhibited predominent axonal swellings and disconnection. The proximal axonal swellings were truncated and shifted toward the globe. The distal axonal swellings were rounded and redistributed toward the chiasm. These reactive axonal changes and dieback were accompanied by an apparent focal loss of fluorescence (Figure 6.3).

By 7 days post injury however, the optic nerve of the injured mice demonstrated an initial recovery of the YFP fluorescent fibers at the locus of original fluorescence quenching. Specifically, routine confocal analysis revealed more intact/unaltered YFP fluorescent axonal profiles, as well as detached and fragmented axonal profiles in the same locus of fluorescence loss described in the earlier time frame (Figure 6.3). Again, the proximal axonal swellings were truncated, consistent with their reorganization.

From 14 days and 28 days post injury, within the locus of original YFP fluorescence quenching, the restoration of YFP fluorescent axonal fibers continued (Figure 6.3), with more

YFP fluorescent fibers together with occasional scattered fragmented axonals profiles were revealed.

By 3 month post injury, this recovery of YFP fluorescent axons showed further improvement at the locus of original fluorescence quenching, which was now crossed by numerous linear/continuous unaltered YFP fluorescent axonal profiles, without evidence of swollen axonal segments or fragmented axons (Figure 6.3).

Discussion

In this current study, we provide at more chronic time points the ultrastructural evidence of numerous intact axonal fibers in the region of previously described YFP fluorescence quenching. This occurred together with the reduction of the interstitial space overtime post injury, consistent with the clearance of edema. This resolution of edema was also accompanied by the recovery of YFP fluorescent axonal fibers overtime post injury.

The existence of numerous intact axonal fibers at the locus of original YFP fluorescence loss confirmed that not all the axons within the optic nerve were injured by the initial traumatic injury. Rather, apparently only a sub-population of axons within the optic nerve was traumatically perturbed, an observation entirely consistent with the characteristics of diffuse traumatic axonal injury wherein injured axons are interspersed by other adjacent intact fibers (Buki and Povlishock, 2006; Greer et al., 2011).

Current observation of an initial expansion of the interstitial space followed by its closure over time is consistent with a transient opening of the blood-brain-barrier (BBB) following TAI. This observation is similar to previous research performed in a rat weight drop injury model in which edema occurred becoming maximal by 5 hours post injury, thereafter resolving (Vink et

al., 2003). Using the same rat weight drop model, Barzó (1997) observed that the water diffusion distance, increased up to 45 minutes postinjury and thereafter decreased. Since water diffusion distance is predominantly associated with the formation of vasogenic edema, which results from the compromise of BBB, this transient increase of water diffusion distance/vasogenic edema coincides with the BBB opening immediately upon brain trauma followed by a relatively rapid BBB closure at later time points (Barzó et al., 1996).

The currently described clearance of edema within the injured optic nerve, was accompanied by a recovery of YFP fluorescent axons in the same region of our previously reported fluorescence quenching. Previous studies have demonstrated the relationship between water and fluorescence quenching, through the hydrogen-bond interactions (Oshima et al., 2006), the transition to a close-lying energy level (Tobita et al., 2001) and other mechanisms. Accordingly, it is not unreasonable to assume that the reversal of fluorescence quenching could be achieved through the reduction of water, herein the clearance of edema. Besides the resolution of tissue water, other studies have also been demonstrated to recover fluorescence, such as the removal of the quenching reagent (Chen et al., 1999), the addition of anions (SO_3^{2-} and PO_4^{3-}, Xia et al., 2012) and the oxidation of ions (Kress et a., 2002). Whether these events are involved in our recovery of YFP fluorescent fibers over time, requires further investigation.

In summary, this study demonstrated the maintenance of intact axonal fibers in the region of YFP fluorescence quenching, consistent with the characteristic of TAI. The clearance of edema was accompanied by the recovery of YFP fluorescent axons overtime post injury, confirming the correctness of previous hypothesis that water result in fluorescence quenching.

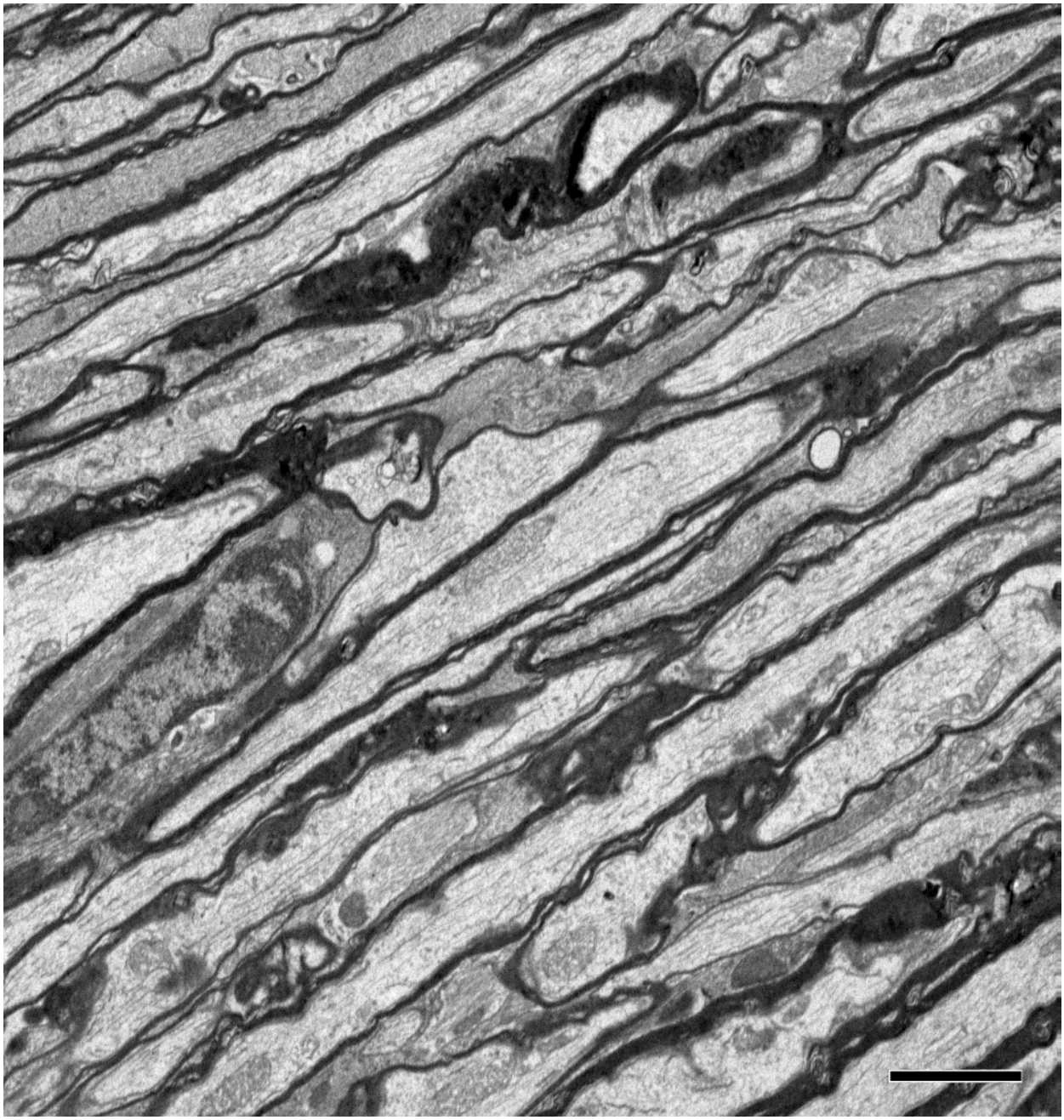

Figure 6.1 At 7 days post injury, the previous locus of fluorescent loss within the injured optic nerve, reveals numerous intact axonal fibers. The neurofilaments and microtubules parallel the long axis of axons. The mitochondria within the axons maintain normal morphology. Some Wallerian debris can be seen scattered between intact axons, a finding consistent with TAI. Also note that the interstitial space appears unremarkable at this time frame. Scale bar: 2µm.

Figure 6.2 At 28 days post TBI, the original locus of fluorescence quenching within the optic nerve again reveals numerous intact axonal fibers, without any swollen axonal segments. The microtubules parallel the alignment of the axon, and the mitochondria maintain normal morphology showing no dilation or disorganization of the mitochondrial cristae. Occasional electron dense Wallerian debris are found interspersed between these intact axonal fibers, consistent with TAI. Again, no expansion of the interstitial space is seen at this time point post injury. Scale bar: 2µm.

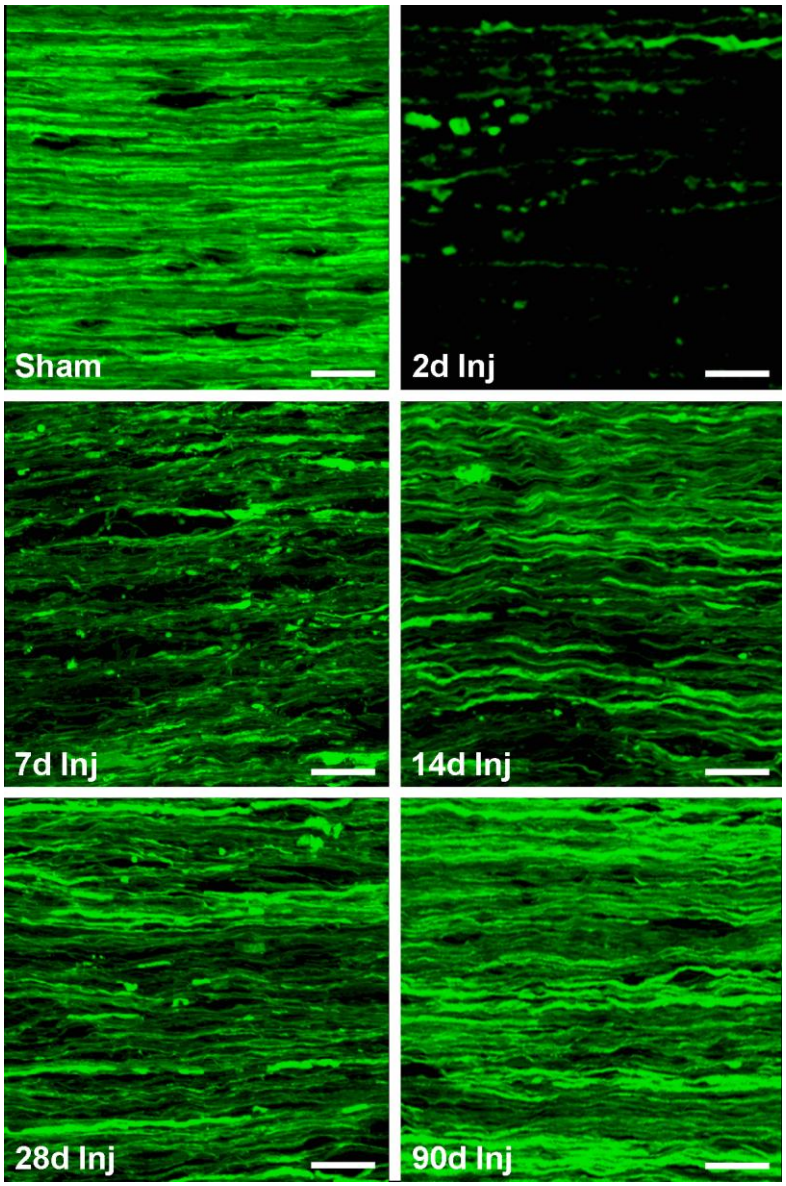

Figure 6.3 The recovery of the YFP fluorescent optic nerve fibers in the region of fluorescence quenching overtime post injury. The optic nerve of the sham-injured mice reveals a robust distribution of linear/continued YFP fluoresent axons, with no evidence of axonal swelling or YFP fluorescent loss. At 2 days post injury, the locus of initial traumatic axonal injury (TAI) within the optic nerve reveals disconnected axonal swellings and fragmented axonal profiles. Note that the dramatic YFP fluorescent loss at this 2 days post injury time frame. By 7 days post injury, initial recovery of YFP fluorescent axonal profiles can be seen at the same locus of YFP fluorescent loss, with fragmented axonal profiles scattered among the intact axons. At 14 days and 28 days post injury, the recovery of YFP fluorescent axonal fibers continues. By 3 months post injury, more linear/continued YFP fluorescent axons are revealed at the same locus of YFP fluorescence quenching, although recovery is not complete due to TAI and its attendent diffuse axonal damage. Scale bar: 20µm.

CHAPTER SEVEN

GENERAL DISCUSSION

Distinct from the discussion in each individual chapter, I integrate here the results of this thesis and discuss fully those issues relevant to the reported axonal damage in visual system, considering the pathological changes occurring both in the anterograde and retrograde directions, as well as their implications for therapeutic intervention and axonal repair.

Synopsis of the Current Work and its Implications

The current thesis presents the first characterization of a mouse model of diffuse traumatic axonal injury in the optic nerve following mild traumatic brain injury. By subjecting transgenic mice expressing endogenous YFP fluorescent protein in the optic nerve to central fluid percussion injury (cFPI), we consistently generated diffuse TAI in the optic nerve, demonstrating overtime progressive axonal swelling and disconnection. This ultimately led to proximal and distal axonal dieback, with regression and reorganization of the proximal swellings, and the persisting degeneration and dieback in the distal axonal segments. In concert with these development and characterization studies, we also demonstrated the limitations of traditional APP immunohistochemical staining to routinely detect axonal injury. Specifically, we convincingly demonstrated that antibodies targeting C-terminus of APP detect only the proximal swollen axonal segment, without distal mapping. Equally important, this same APP

immunostaining diminished dramatically within 3 days post injury in the proximal region (Chapter 3), further suggesting the more limited utility of this marker.

Of additional importance in this study was its finding that this diffuse TAI in the optic nerve following cFPI, did not induce significant death of retinal ganglion cells (RGC), as demonstrated by qualitative (TUNEL and caspase 3 immunostaining), quantitative (Brn3a immunostaining) and ultrastructural analysis. Of parallel importance was the finding that this RGC survival was accompanied by their persistent expression of phospho-c-Jun from 2 to 90 days post injury, which has been linked to neuronal survival and potential axonal repair in other injury paradigms (Chapter 4). Lastly, in light of the fact that the observed axonal dieback was not related to RGC death, other mechanisms must be evoked to explain this phenomenon.

In the early hours post injury, the acute axonal dieback observed in both the proximal and distal segments, is most likely linked to local calcium dysregulation and activation of proteinases. In the more chronic phases post injury, specifically 7 to 28 days post injury, the observation within the distal disconnected, degenerating axonal segments, that activated microglia/macrophages closely envelop/encompass these segments, suggests their potential role in delayed axonal degeneration and dieback. In contrast, the microglia/macrophage appeared less reactive in the proximal axonal segments, with their processes paralleling these axonal profiles undergoing reorganization/repair (Chapter 5 Appendix I).

In concert, with all the above this optic nerve injury was also associated with blood-brain barrier disruption and local edema formation that resolved overtime (Chapter 6 Appendix II). Although this barrier disruption did not appear to influence the pathogenesis in the optic nerve, the edema interfered with the observation of intact YFP expressing axons in the site of initial TAI (Chapter 3).

In the following passages we expand the above, providing a more thorough evaluation of our findings and their overall implications for the field of TBI research and its associated axonal injury, while also setting the stage for future investigations in this area. Specifically, for the purpose of this component of the thesis we organize this chapter around our central findings which include model characterization, its utility for studying TAI, the occurrence of anterograde and retrograde responses to injury, its association with blood-brain-barrier disruption as well as future directions focusing on therapeutic intervention, neuroplasticity and axonal regeneration.

Characterization of a Mouse Model of TAI within the Visual System

This optic nerve TAI model induced by TBI using YFP expressing mice provided unprecedented insight into the pathogenesis of TAI. The observed optic nerve TAI was generated from a common TBI model modified from rat (Dixon et al., 1987) to mice (Greer et al., 2011, Wang et al., 2011). In this model, optic nerve TAI occurred immediately following mild TBI, and was accompanied by concomitant scattered axonal damage in the neocortex, the dorsolateral thalamus and subcortical white matter, all of which were consistent with mild TBI (Greer et al., 2011; Greer et al., 2012). The site of the initiation of TAI in the optic nerve always approximated the optic nerve segment 1mm proximal to the chiasm, which made the critical assessment of this phenomenon all the more feasible. While unknown, the localization of the TAI to this region of the visual axis is most likely linked to brain deformation and compression of the optic nerve, occurring when the dorsal cortex was impacted by the fluid injury pulse.

Importantly, the described optic nerve TAI following cFPI replicates the optic nerve damage described in shaken baby syndrome, wherein the optic nerve from infants sustaining fatal whiplash shaking, reveals strong beta amyloid precursor protein (beta-APP)

immunoreactivity in swollen axonal segments within the optic nerve (Gleckman et al., 2000). Our optic nerve diffuse axonal swollen segments, specifically the proximal axonal segments, were also APP immunoreactive. Of note, the antibodies utilized in our research targeted the C-terminus of APP protein and only detected the proximal swollen axonal segments which lost immunoreactivity over 3 days post injury (Chapter 3). This accumulation of beta-APP, which undergoes anterograde axonal transport, is consistent with a trauma-induced impaired axonal transport. Ultrastructurally, these injured axonal segments revealed swollen mitochondria, misaligned neurofilaments and microtubules, as well as the accumulation of SER, mitochondria and vesicles (Chapter 3), all of which are consistent with focal axonal cytoskeletal damage/ disorganization with the compromise of axonal transport.

The reactive axonal changes seen within the optic nerve following cFPI, are also similar to those seen with optic nerve stretch. Previous to the development of the current optic nerve TAI model, optic nerve stretch has been utilized to study traumatic axonal injury, and has provided important insight into the pathogenesis of TAI (Gennarelli et al., 1989; Maxwell et al., 1990; Maxwell and Graham, 1997; Saatman et al., 2003; Serbest et al., 2007; Sulaiman et al., 2010). Gennarelli and colleagues (1989) created an optic nerve stretch injury model using albino guinea pigs via a rapid controlled elongation (tensile strain) of the optic nerve. This was achieved by placing a sling over the posterior pole of the globe. After the stretch injury, Gennarelli et al (1989) demonstrated that the anterograde axonal transport of horseradish peroxidase (HRP) was impaired from the RGC to the chiasm and superior colliculi. In these studies, the optic nerve demonstrated axonal swellings with the accumulation of organelles, sitting adjacent to axons revealing normal morphology. Importantly, however, this stretch injury model did not replicate the characteristics of either human or subhuman primate diffuse axonal injury because this model

failed to generate concomitant change within the brain parenchyma. Specifically, unlike fluid percussion injury, optic nerve stretch was not accompanied by TAI in either the brain or brain stem, which are typically involved in human and animal TBI. Utilizing guinea pig optic nerve stretch injury, Maxwell (2003) noted that traumatic axonal injury occurred approximately half way along the length of the nerve, with the site of axonal injury associated with axonal mitochondrial abnormalities and neurofilament compaction. Other injured axons demonstrated the loss of neurofilaments and microtubules (Maxwell et al., 2003). Saatman (2003) stretched the mouse optic nerve, and demonstrated a two phase calpain activation associated with TAI, with an early phase of calpain activation occurring within minutes to hours after injury, associated with intra-axonal structural damage. A later phase of calpain activation observed at 4 days post injury, was linked to axonal degeneration. In addition to calpain-mediated spectrin proteolysis, Serbest (2007) also observed the loss of neurofilaments and microtubules in optic nerve axons after stretch injury.

However, despite similarities between our model and those described above, important differences exist between these model systems. As discussed in Chapter 3, dissimilar to optic nerve stretch which induces TAI within the optic nerve alone, our cFPI model also evoked TAI throughout the related brain parenchyma, involving the neocortex, the dorsolateral thalamus and subcortical white matter, findings consistent with other reports from our laboratory (Kelley et al., 2006 and 2007, Buki and Povlishock, 2006, Greer et al, 2011). This characteristic diffuse/scattered axonal injury within the optic nerve as well as the brain parenchyma arguably makes our model more similar to human TBI, with the caveat that our model may offer the potential for preclinical drug screening to target TAI within the visual system and cerebrum given its more human-like pattern of axonal injury.

Utility of this mouse model of TAI within the optic nerve to probe TAI pathogenesis

Besides the relevance of our model to the pathobiology of mild TBI, our current utilization of the YFP-16 transgenic mice, expressing endogenous YFP fluorescent protein within the majority of retinal ganglion cells and the optic nerve (Feng et al., 2000), allowed for the detailed and ready observation of the events starting from the initiation of axonal swelling to ultimate axonal disconnection, as well as any subsequent proximal and distal axonal dieback overtime (Chapter 3). Our use of the YFP-16 transgenic mice obviated the limitations associated with the use of APP immunohistochemistry which detected only the proximal, swollen axonal segments which typically lost immunoreactivity over 3 days post injury (Greer et al., 2011, Wang et al., 2011). The advantage associated with the expression of the YFP fluorescent protein by the Thy1 promoter, resided in its complete transport throughout the axons of the optic nerve. Accordingly, any morphological change associated with axonal injury was reflected in an altered/abnormal YFP fluorescent signal, directly visualized via fluorescent microscopy in both the proximal and the distal axonal segments.

Distinct from our current YFP expressing approach, the above described optic nerve stretch models utilized guinea pigs or wild type mice (Gennarelli et al., 1989, Maxwell et al., 2003, Saatman et al., 2003, Serbest et al., 2007). In these studies, the identification of axonal swellings relied completely upon immunohistochemical approaches and ultrastructural analysis which as noted previously, posed limitations (Gennarelli et al., 1989, Maxwell et al., 2003, Saatman et al., 2003, Serberst et al., 2007). Further, these methods did not allow for the precise identification of either the proximal or distal origins of any observed axonal swellings.

Specifically once the axon disconnected, it was virtually impossible to determine if the axonal swellings occurred in the proximal vs. distal disconnected segments. Consequently, this model did not allow for the clear delineation of the pathological changes occurring either anterogradely or retrogradely.

Implications of the current TAI model for understanding the anterograde and retrograde sequelae of TAI

Utilizing YFP expressing mice, our current optic nerve TAI model allowed the ready comparison of the pathological differences seen in the disconnected axonal segments in both the anterograde and the retrograde directions.

1) ***Anterograde responses - distal axonal dieback/degeneration and microglia/macrophage activation***

As described in Chapter 3, once disconnected, the anterograde/downstream distal axonal segments, underwent acute dieback toward the chiasm overtime. Ultrastructually, the distal swollen axonal segments revealed increased electron density, an accumulation of vesicles and swollen degenerating mitochondria, as well as disorganized microtubules and neurofilaments, all of which were consistent with dieback and degeneration, as a prelude to Wallerian change.

The acute dieback of the distal disconnected axonal segments in the first hours post injury, is most likely due to an initial increase in intra-axonal calcium and sodium. *In vitro* laser-induced axonal damage studies demonstrate that calcium dysregulation plays an important role in the initial axonal dieback (Hellman et al., 2010). A rapid increase of intra-axonal calcium has also been observed in the acute axonal degeneration following optic nerve crush, with its inhibition by calcium channel inhibitors markedly attenuating axonal degeneration (Knöferle et

al., 2010). Similar to the increase of intra-axonal calcium, a rise in the intra-axonal sodium may also play a role in the acute axonal dieback. A close relationship has been demonstrated between the increase of intra-axonal calcium and the rise in the intra-axonal sodium, which is further supported by the findings that the sodium channel inhibitor, tetrodotoxin, can also block the increase of calcium (LoPachin and Lehning, 1997). Again, such sodium channel blockers, dramatically ameliorate the number of acute axonal swellings following optic nerve crush (Beirowski et al., 2010).

In addition to the role of calcium and sodium dysregulation in the acute axonal dieback, calpain mediated proteolytic damage to the axonal cytoskeleton may also promote and perhaps, accelerate the acute axonal dieback. Specifically, calpains have been demonstrated to participate in the degradation of axonal cytoskeleton spectrin, microtubules and neurofilaments (Buki and Povlishock, 2006; Buki et al., 1999; Saatman et al., 2003). Further, such calpain activity has been directly linked to the degeneration of the distal, disconnected downstream axonal segments, as demonstrated by the finding that calpain inhibition attenuates the degeneration of the distal, disconnected downstream optic nerve fibers after crush injury (Couto et al., 2004).

In addition to the involvement of calcium and sodium dysregulation, as well as the activation of the calpain protease, other factors must also be taken into consideration in the process of the acute axonal dieback. In the current study, we also frequently observed in the distal disconnected axonal segment, that the mitochondria remained swollen, in response to the injury. This mitochondrial damage was most likely related to calcium overloading and subsequent mitochondrial perturbation. Given the fact that mitochondria are the major source of ATP production which is essential for axonal transport and the maintenance of the axolemma,

the injured mitochondria may also be linked to an ATP deficit, causing a failure in axonal transport, thereby further promoting axonal dieback.

Some equate this acute distal axonal dieback with the initial phases of Wallerian degeneration, however, in the strict sense, Wallerian degeneration is a more delayed event. In the acute axonal dieback period, the currently used optic nerve TAI model revealed only singular distal axonal swelling in continuity with axons projecting toward the chiasm. This is distinctly different from the Wallerian degeneration, which is associated with multiple loci of axonal swelling and fragmentation along the axonal segment distal to optic nerve transection (Beirowski et al., 2010).

Although the acute axonal dieback as described in the current study differs from Wallerian degeneration, at least in its acute phase response, it is most likely followed by Wallerian degeneration, which occurs as a delayed event. Mechanistically, transgenic mice with the *slow Wallerian degeneration* (Wld^S) protein have provided insight into the basic molecular and cellular mechanisms of Wallerian degeneration (Coleman and Freeman, 2010). The Wld^S protein (slow Wallerian degeneration) consists of a fragment of the ubiquitin assembly protein UFD2a/UBE4B and nicotinamide mononucleotide adenylyl-transferase-1 (Nmnat1), which is an enzyme promoting the synthesis of nicotinamide mononucleotide adenine dinucleotide (NAD) (Conforti et al., 2000; Mack et al., 2001; Wang and He, 2009). The speed of Wallerian degeneration is slowed in the Wld^S mouse to one tenth of the speed in the wild type animal (Perry et al., 1990, Glass et al., 1993). Using Wld^S mouse, Kerschensteiner (2005) found in both the proximal and distal disconnected axonal segments, that the acute axonal degeneration was delayed following spinal cord transection. Similarly, utilizing the transgenic Wld^S rodents, Beirowski (2010) observed in the distal axonal segments that the axonal swellings and

dystrophic axons were substantially reduced in number following optic nerve crush or transection. Recent studies demonstrate that Wld^S prevents axonal degeneration via several mechanisms, including increasing nuclear NAD biosynthesis (Araki et al., 2004), increasing the Wld^S mitochondrial Ca^{2+} buffering capacity and improving basal mitochondrial motility in axons (Avery et al., 2012). These findings indirectly suggest that the mechanisms of Wallerian degeneration are related to mitochondrial dysfunction. It has been demonstrated that the activation of the mitochondrial permeability transition pore (mPTP) within the Wld^s axon triggers its degeneration, while the depletion of the mPTP protein cyclophilin D effectively inhibits axonal degeneration (Barrientos et al., 2011).

In addition to these described factors associated with the initial axonal dieback and delayed axonal degeneration, other factors are most likely involved in the continued pathological progression here reported in the distal axonal segments. At 2 days postinjury, an initial activation of microglia/macrophages occurred at the site of the initiation of axonal injury, suggesting their potential involvement in the subacute phase of axonal dieback. In the current study, from 7 days to 28 days post injury, the injured optic nerve revealed a close spatiotemporal relationship between the distal disconnected, degenerating axonal segments and activated microglia/macrophages (Chapter 5). During this time frame, the distal swollen axonal segments were routinely encompassed/engulfed by the processes of activated microglia/macrophages, consistent with a comparable phagocytic role of microglia/macrophages described following injury in the corpus callosum (Venkatesan et al., 2010) as well as the spinal cord (Busch et al., 2009; Busch et al., 2010; Horn et al., 2008).

A well-known stimulus for continued macrophage activation, is the onset of delayed Wallerian degeneration in the distal disconnected axonal segment (Brück et al., 1995; Kelley et

al., 2007). Here the breakdown products of Wallerian degeneration, such as the myelin debris, most likely contribute to the long term, persistent activation of microglia and macrophages. Such activated microglia/macrophages are known to release proinflammatory cytokines, including interleukin-1, interleukin-6 and tumor necrosis factor-α (Gentleman et al., 2004; McClain et al., 1991; Kita et al., 2000), with cytokines, such as interleukin-6, further upregulating the phagocytic activity of microglia/macrophage (Shafer et al., 2002-2003). These activated microglia/macrophages can also release MMP9, which has been linked with axonal retraction (Busch et al., 2009).

2) Retrograde responses - the reorganization / repair of the proximal axonal segments and the survival of retinal ganglion cells

In contrast to the continued degeneration of the disconnected, distal axonal segment, as noted in our study, the retrograde/upstream proximal axonal segments underwent rapid dieback toward the retina, yet then transitioned to reorganization/repair overtime. As described, the proximal axonal segment transitioned from a spheroidal swollen segment into a truncated appendage (Chapter 3). These distinct morphological differences in the distal and the proximal axonal segments suggest the involvement of different pathological signaling pathways in the anterograde vs. retrograde directions.

2.1) Acute dieback of the proximal axonal segment

Like the dieback of the distal segment in the first hours post injury, the proximal axonal segment also underwent retraction toward the retina. This acute axonal dieback of the proximal axonal segment spanned approximately 0.4 - 0.8mm within a 48 hours period following injury

(Chapter 3). In its initial phases, this process most likely shares similar mechanisms to those described for the acute dieback of the distal axonal segment, including local calcium dysregulation and calpain activation. It has been shown that in the presence of calpain inhibitors, the acute axonal dieback of the proximal axonal segments is blocked following spinal cord transection (Kerschensteiner et al., 2005). In addition to the influx of calcium and calpain activation, other processes such as the formation of autophagosomes are also induced by the initial Ca^{2+} influx after axonal injury, and as such, may also contribute to the acute proximal axonal dieback (Knöferle et al., 2010). This premise is been supported by Koch (2010) who demonstrated that inhibition of the formation of autophagosomes by the autophagy inhibitor can attenuate acute axonal dieback.

2.2) The proximal axonal segment reorganization/repair

In contrast to the persistent distal rounded, degenerating axonal segments, the proximal axonal segments evaluated in our studies underwent a relatively rapid transition from an enlarged and swollen segment into a thinned and truncated appendage. Ultrastructurally, these proximal truncated appendages contained normal / unaltered mitochondria and other organelles and vesicles, none of which were consistent with degeneration. Rather, their appearance suggested reorganization / repair of the proximal segment (Chapter 3). Accordingly, such morphological differences in the proximal vs. the distal axonal segments suggest the activation of different pathological signaling pathways.

A possible basis for this proximal vs. distal difference may be related to postinjury proximal axolemmal resealing and its ability to restore local ionic homeostasis. Some have suggested that rapid proximal axonal reorganization/repair is preceded by a rapid resealing of the

axolemma (Liu et al., 2011, Meiri et al., 1983). Studies utilizing guinea-pig spinal cord transection/compression demonstrate that axonal membrane resealing process is related to the influx of calcium through the voltage dependent calcium channels(VDCC) (Nehrt et al., 2007). Calcium triggered calpain activity has also been described in the process of axonal membrane resealing following neurite transection in cultured rat septal neurons (Xie and Barrett, 1991). Calcium can also facilitate axolemma resealing via the activation of vesicle proteins, such as synaptotagmin, synaptobrevin and syntaxin (Detrait et al., 2000; Fishman and Bittner, 2003). Squid and crayfish giant axon injury studies show that when axons are injected with an antibody to block synaptotagmin binding to Ca^{2+}, the severed axons do not seal (Detrait et al., 2000). Similarly, when axons are injected with an antibody to syntaxin, the severed axon also fails to seal (Detrait et al., 2000). In contrast, when axons are injected with either denatured antibody to synaptotagmin or denatured antibody to syntaxin, the severed axons seal (Detrait et al., 2000), supporting the premise that axolemmal resealing may be mediated by Ca^{2+}-induced fusion of vesicle proteins. On note, this rapid resealing of the axolemma also occurred in the disconnected distal axonal segments; however, it did not inhibit the degeneration process of these distal axonal segments. In contrast, this rapid axolemma resealing is required for the reorganization of the proximal axonal segment.

Besides this rapid resealing of the axolemma, the conversion of anterograde to retrograde axonal transport may also participate in the proximal axonal reorganization and recovery (Tuck and Cavalli, 2010). Early nerve crush studies demonstrate that upon injury, the anterograde intra-axonal organelle transport is converted to the retrograde direction (Bisby and Bulger, 1977). Such conversion could in part, be related to local proteolysis at the site of injury (Sahenk and Lasek, 1988), or the modification of proteins on the transported vesicles (Martz et al., 1989).

Through these mechanisms, it is most likely that the conversion of anterograde to retrograde axonal transport attenuates vesicle and organelle accumulation at the injured axonal tip, transforming the proximal axonal segment from the enlarged and swollen segment into a more thinned and truncated morphology reminiscent of that described in the current communication.

2.3) Resting microglia/macrophage in the proximal axonal segment

Consistent with the proximal axonal segment's attempt to reorganize/repair overtime, was our parallel finding that the microglia/macrophages found in relation to proximal axonal segments, retained at a resting state throughout our 7 - 28 days post injury observation, a response in contrast to the activated macrophages seen in the distal, degenerating segments (Chapter 5). The reasons for this different response in the proximal vs. distal segments are not entirely clear. However, rapid axolemmal closure of the proximal axonal segment may be a factor. Such rapid axolemmal resealing could prevent the influx of damaging extracellular molecules into the axonal segments, or alternatively it could inhibit the release of intra-axonal components into the extra-axonal environment, thus preserving the microenvironment. Further, the observed reorganization/repair of the proximal axonal segments, was not associated with sustained generation of myelin debris, a well-known stimulus for continued macrophage activation.

2.4) The survival of retinal ganglion cells following TAI within the optic nerve

The proximal axonal segment reorganization and repair/recovery described in the current study could also be partially related to the fact that axons maintained continuity with a viable neuronal cell body of origin within the RGCs. As described in Chapter 4, the multiple qualitative (TUNEL and Caspase-3 immunostaining) and quantitative (Brn3a immunostaining) as well as

ultrastructural studies performed in the current study did not demonstrate any evidence of RGC loss. Further their persistent expression of phospho-C-Jun, a marker associated with neuronal survival and axonal regeneration (Greer et al., 2011), was entirely consistent with RGC survival and the described proximal axonal repair/reorganization.

Our description of RGCs survival post TAI within the employed optic nerve injury model is strikingly different from previous studies following other forms of optic nerve injury, which all were followed by significant RGC loss. We believe that this difference resides primarily in the model systems themselves. Our optic nerve TAI evoked a secondary process that involved progressive axonal swelling and delayed disconnection. Such delayed axonal injury was interspersed among other morphologically intact fibers. Thus, we believe that the more subtle and secondary progressive axonal injury occurring in our model of TAI, did not lead to the massive ionic disruption thereby proving supportive of RGC survival. In contrast to our model, optic nerve transection and crush evoked primary axonal injury, in which the axons disconnected immediately, with all the axonal fibers sustaining comparable injury and disconnection. Such primary axonal injury immediately exposed the injured axons to the extracellular environment, followed by an avalanche of sodium and calcium influx and the activation of proteases which then overwhelms cellular defense mechanisms leading to neuronal death (Emery et al., 1991, Lucas et al., 1990, Rosenberg et al., 2001, Strautman et al., 1990, Leybaert and de Hemptinne, 1996).

In addition to the differences between our optic nerve TAI and transection/crush injury models, our description of RGCs survival following TAI, is also dissimilar from the dramatic RGCs loss previously described following optic nerve stretch injury. In our cFPI model, the globe was shielded from injury. However, in the optic nerve stretch model, which employs a

sling at the posterior pole of the globe, direct injury to the retina and its vasculature most likely occurs at the moment of stretch, thereby contributing to retinal damage and the RGC loss. (Gennarelli et al., 1989; Maxwell et al., 1990; Maxwell and Graham, 1997; Saatman et al., 2003; Serbest et al., 2007; Sulaiman et al., 2010).

Besides retinal sparing, our current TAI model offers additional differences from other models of injury involving either stretch or transection/crush injury. In our model, the TAI was generated approximately 1 mm proximal to the optic chiasm. In contrast, with optic nerve stretch, the axonal injury was found more rostrally, midway between the globe and the optic chiasm (Maxwell et al., 2003). Similarly, with the optic nerve crush or transection, the axonal injure was generated in the intraorbital segment, approximating the retina, wherein the neuronal cell bodies of the RGCs reside. This difference in the initial site of axonal injury, may influence neuronal fate in terms of either life or death. Evidence to support this premise is found in neocortical axonal and spinal cord transection studies, which demonstrate higher neuronal survival rates when the axotomy occurs more distant from its cell body of origin (Dale et al., 1995; Liu et al., 2003). Thus, in our current study, the relative long distance between the initial site of TAI and the RGC could explain the enhanced RGCs survival relative to that seen following optic nerve stretch, transection or crush.

The RGC survival described in the current study also bears similarities to the survival of neocortical neurons described following diffuse TAI (Greer et al., 2011; Lifshitz et al., 2007; Singleton et al., 2002). Utilizing the same rodent central fluid percussion injury model, Greer and colleagues demonstrated within the neocortex perisomatic diffuse traumatic axonal injury, that did not translate into cell death, but rather progressed to atrophy (Greer et al., 2011; Lifshitz et al., 2007; Singleton et al., 2002). Such surviving neocortical neurons upregulated the expression

of phospho-c-Jun (Greer et al., 2011). Similar to these studies following TAI in the neocortex, our surviving RGCs revealed persistent phospho-c-Jun expression up to 90 days following injury (Chapter 4), and the reorganization and attempt repair of the proximal axonal segments overtime (Chapter 3 and Chapter 5), consistent with other reports of the link of phospho-c-Jun to neuronal survival, axonal sprouting and regeneration (Fitzgerald et al., 2009 and 2010; Greer et al., 2011; Herdegen et al., 1993; Hull and Bahr, 1994; Lu et al., 2003; Robinson, 1994 and 1995).

Paradoxically, the activation of c-Jun has been related to not only axon regeneration but also neuronal death (Bessero et al., 2010; Biermann et al., 2011; Herdegen et al., 1997; Liu et al., 2011; Raivich, 2008; Ribas et al., 2011; Sun et al., 2011). Genetic inactivation of c-Jun reduces axotomy-induced neuronal death but decreases the axon regenerative potential for surviving neurons (Raivich et al., 2004). Importantly, in our studies ATF-3, another transcription factor associated with axonal regeneration, was also upregulated in the RGCs at early time points post injury (data not shown), an observation again consistent with ATF-3 activation in the neocortical neurons following TAI (Greer et al, 2011). It has been demonstrated that ATF3 cooperate with c-Jun to enhance neurite outgrowth (Pearson et al., 2003; Lindwall et al., 2004). Takeda (2000) observed the colocalization of ATF-3 with c-Jun mRNA 5 days after optic nerve crush injury, suggesting that the heterodimer formation of ATF-3 with C-Jun may support RGC survival and axonal regeneration. It has also been demonstrated that ATF-3 binds to c-Jun, and activates the expression of the anti-apoptotic factor - the heat shock protein 27 (Hsp27), which most likely activates Akt, accordingly probably inhibits apoptosis and promotes neuronal survival and nerve elongation (Brunet et al., 1999; Datta et al., 1997; Nakagomi et al., 2003**)**.

Other features of this model and their relevance to TAI

As described above, our current studies demonstrated that TBI-induced diffuse TAI within the optic nerve was not followed by dramatic RGC death/loss, but rather persistent RGC survival with the proximal axonal segment's reorganization and its attempt to repair. This unique feature of optic nerve TAI is similar to brain neocortical TAI that is also not followed by neocortical neuron death, but rather atrophy and persistent expression of phospho-c-Jun and reactive axonal sprouting and elongation (Greer et al., 2011). In addition to this unique characteristic, current optic nerve TAI model also revealed transient blood-brain barrier disruption, local edema formation and its association with YFP fluorescence quenching in the acute phase post injury, and thereafter the closure of blood-brain barrier, the resolution of edema and the recovery of YFP fluorescent fibers at the chronic phase post injury.

1) Transient blood-brain barrier disruption

In concert with all the above abnormalities occurring in our optic nerve injury model was the occurrence of focal non-hemorrhagic blood-brain barrier (BBB) disruption and local edema formation which clearly approximated the site of ongoing axonal change and dieback. As noted in Chapter 3, we observed the extravasation of IgG within the optic nerve at 1 hour to 3 hours post injury. This occurred together with the expansion of the interstitial space at these early time points post injury (Chapter 3, Wang et al., 2011), suggesting local edema formation. Because this barrier perturbation occurred at the site of initial optic nerve axonal damage, this suggested that both events were triggered by the same forces of injury most likely maximally distorting the axons and microvessels at this point along the optic nerve's length. By 7 and 28 day post injury, the interstitial space had decreased in diameter, taking on a more control-like appearance, consistent with the resolution of edema at these later time points (Chapter 6). Such

traumatic barrier disruption described within the optic nerve is consistent with the brain parenchymal barrier disruption seen following fluid-percussion brain injury that has been linked to concomitant brain deformation and compression (Povlishock, et al., 1978, Kelley et al., 2007).

2) Blood–brain barrier disruption and the retention of axons in the region of YFP fluorescence quenching.

As noted, the observed blood-brain barrier disruption and edema formation in the current optic nerve model of diffuse TAI was not linked to the presence of either overt or petechial hemorrhage, suggesting a more subtle form of BBB perturbation. However, although subtle, this blood-brain barrier disruption did interfere with the detection of intact YFP expressing axons at the site of axonal injury via local fluorescent quenching (Chapter 3). In our study, the relationship between BBB disruption and fluorescent quenching was confirmed by the observation that those regions of local fluorescence loss mapped precisely to those zones of increased vascular permeability, as assessed by the passage of the endogenous immunoglobulin IgG (Chapter 3). We further confirmed this premise by utilizing antibodies targeting endogenous YFP independent of its fluorescent properties, a strategy which revealed in the same locus of fluorescent quenching the existence of intact/unaltered axons. These events suggested that the parallel movement of water and other molecules (e.g. ions) with the IgG participated in the fluorescent quenching, which confounded YFP use in our model system. Previously, although not well appreciated in the literature, it has been shown that water and solvent properties of water can lead to fluorescence quenching by multiple mechanisms, including but not limited to, hydrogen-bond interactions (Oshima et al., 2006), photoionization (Sadkowski and Fleming, 1980), the transition to a close-lying energy level (Tobita et al., 2001), intersystem crossing

(Seliskar and Brand, 1971), and specific solute–solvent interactions (Ebbesen and Ghiron, 1989). A recent study has also demonstrated that mild acidic conditions can alter the structural arrangement of yellow fluorescent protein, leading to fluorescence quenching (Hsu et al., 2010). Thus, it is not unreasonable to posit that either one or several of the above-described mechanisms result in fluorescence quenching in our current optic nerve injury model.

3) The clearance of edema and the recovery of YFP fluorescent axons

As noted, the observed blood-brain barrier disruption was transient, with the edema in the interstitial space of the optic nerve resolving overtime (Chapter 6), in a fashion similar to the transient brain edema described following weight drop TBI (Vink et al., 2003, Barzó et al., 1997). Specifically, by diffusion-weighted imaging in the cerebral cortex, Barzó (1997) observed that water diffusion distance, predominantly associated with the formation of vasogenic edema, increased over 45minutes postinjury, and thereafter, decreased, reaching minimum values by 7 to 14 days post injury. Such a vasogenic edema profile coincides with a process in which the BBB opens immediately following TBI with its subsequent closure moments later (Barzó et al., 1996).

The observed rapid BBB closure most likely helped restore the microenvironment of both the injured and non-injured axonal segments, promoting the recovery of the YFP fluorescence of intact axonal fibers in the original region of fluorescence quenching. The closure of BBB most likely resulted in the resolution of edema via several mechanisms. It has been demonstrated that the extravasated plasma proteins, including but not limited to immunoglobulin, are rapidly taken up by the glial cells from the extracellular/interstitial space (Del Bigio et al., 2000; Jensen et al., 1997), and degraded by glia, consequently attenuating the interstitial osmotic force that has induced edema (Betz et al., 1989; Klatzo et al., 1980). These processes are accompanied with the

closure/restoration of BBB, creating a permissive osmotic gradient, for water to move from the interstitial space back into the blood (Duvdevani et al., 1995).

This resolution of water is most likely associated with the alteration of pH and other solvent content (e.g. ions and anions) in the microenvironment. Given the relationship between water, the acidic environment and fluorescence quenching described before, it is not unreasonable to assume that the resolution of water, the change of pH and other solvent could reverse fluorescence quenching. Previous studies have demonstrated that fluorescence quenching can be reversed by the removal of the quenching reagent (Chen et al., 1999), the addition of anions such as SO_3^{2-} and PO_4^{3-} (Xia et al., 2012), as well as the oxidation of ions (Kress et a., 2002). Whether these processes are involved in the recovery of YFP fluorescent fibers over time, or do other mechanisms participate in this reversal of YFP fluorescence quenching, requires further investigation.

Future directions targeting therapeutic intervention and neuroplasticity

In summary, our current studies demonstrate optic nerve TAI induced by TBI and provide new insight into the pathogenesis of diffuse traumatic axonal injury, particularly in terms of its progressive swelling, disconnection and dieback proximally and distally. This optic nerve TAI is also accompanied with diffuse traumatic axonal injury in the brain parenchyma, making our model comparable to human TBI, offering the potential for more rational preclinical drug screening to target TAI with the caveat that optic nerve axonal protection should translate into comparable axonal protection within the brain.

1) ***Potential utility of the optic nerve TAI model for therapeutic screening***

As noted above, a further benefit of our model system may reside in its usefulness for drug screening targeting axonal injury. The ability to treat the injured optic nerve via CSF and intraocular routes provides multiple portals for drugs that may not readily cross the BBB due to molecular weight, charge or protein binding. In this case, due to the bathing of the optic nerve by the CSF, neuroprotective drugs could be applied directly via intrathecal pathway, to obviate any difficulty sometimes encountered when penetrating blood-brain-barrier via intravenous or intraperitoneal routes (Gabathuler, 2010; Misra et al., 2003; Hossain et al., 2010; Okonkwo and Povlishock, 1999). Specifically, this model could allow us to reexamine various purported axonal protective drugs, such as poloxamer 188, mitochondrial permeability transition (MPT) inhibitors, calpain inhibitors, caspase inhibitors, calcineurin inhibitors and progesterone. For example, previous *in vitro* studies utilizing mechanical trauma to cultured neurons, have demonstrated that Poloxamer 188 promotes membrane resealing and reduces axonal injury (Kilinc et al., 2007, Maskarinec et al., 2005). Another axonal protective drug, Cyclosporine A, a mitochondrial permeability transition (MPT) inhibitor, has been shown to attenuate axonal damage following mild axonal stretch injury (Staal et al., 2007) while reducing rat traumatic axonal injury following experimental TBI (Okonkwo et al., 2003), and protecting compound action potentials in rats corpus callosum following experimental TBI (Colley et al., 2010). Further, the immunophilin ligand FK506, is not only able to reduce mitochondrial permeability transition (MPT), but also attenuate the activity of calcineurin. FK506 has been demonstrated to ameliorate axonal damage following diffuse TBI (Marmarou and Povlishock, 2006), and exert neuroprotective effect on both myelinated and unmyelinated axons (Reeves et al., 2007). Additionally, progesterone has been proven to have beneficial axonal protective effects in animal TBI studies and is now in Phase III ProTECT clinical trials which should be started within 4

hours of TBI (Espinoza and Wright, 2011; O'Connor et al., 2007; Hua et al., 2012). Besides these various drugs axonal protective effect, hypothermia has also been demonstrated to provide long term benefit to TAI if performed immediately post injury (Ma et al., 2009), and further the therapeutic window is effectively extended when the above described axonal protective drugs were combined with hypothermia (Fujita et al., 2011, Oda et al., 2011). Thus, it is possible to hypothesize that the therapeutic window of progesterone could also be prolonged when it is combined with hypothermia.

Lastly, our current optic nerve TAI model should readily allow the incorporation of various genetic modifications. Specifically, gene transfection or knockout paradigm can be utilized to upregulate the intrinsic growth pathway to enhance axonal regeneration. For example, the inhibition of the PTEN (phosphatase and tensin homologue), the activation of mTOR (mammalian target of rapamycin) pathway, and the deletion of SOCS3 (suppressor of cytokine signaling) pathway have been proven effective to promote optic nerve axonal regeneration after optic nerve lesion (Park et al., 2008, Sun et al., 2011). The potential optic nerve axonal regeneration will reinnervate the downstream target including lateral geniculate nucleus, help recover the retinal-geniculate projection.

2) ***Anterograde degeneration and potential downstream plasticity***

In addition to its therapeutic screening benefits, this optic nerve diffuse TAI model should also allow for the mapping of diffuse deafferentation of the downstream targets, such as the lateral geniculate nucleus (LGN) and superior colliculi, allowing a detailed assessment of the ensuing synaptic loss as well as any potential synaptic rearrangement. Previous studies have demonstrated following TAI a diffuse pattern of axon terminal degeneration and subsequent

deafferentation in the cat dorsal lateral vestibular nucleus (Erb and Povlishock, 1991). Specifically, following TAI a marked reduction occurred in the perisomatic vestibular nuclear terminals (Erb and Povlishock, 1991). Interestingly, this axon terminal loss and synaptic deafferentation were followed by the return of some puncta/terminals in the deafferented somata by 60 days postinjury, with these terminals reaching 75% of control values by 6 months postinjury, and virtually recovering by the 7 to 12 month postinjury period (Erb and Povlishock, 1991). These results suggest that mild to moderate TBI with its attendant TAI and associated diffuse deafferentation create a unique environment for adaptive synaptic recovery (Erb and Povlishock, 1991).

Although these studies suggested adaptive recovery, it remains to be seen if other forms of TAI elicit comparable synaptic repair. To this end, our model of TAI in the optic nerve should allow for a critical assessment of any terminal/synaptic loss in its target LGN, while considering any potential for synaptic recovery therein. In this approach LM silver salt, immunocytochemical and TEM studies can be used to follow the specific patterns of synaptic loss occurring in the LGN overtime. Then once the pattern of deafferentation is established, contemporary tracer approach could be used to map the LGN's synaptic reorganization and repair.

Conceivably, the domains originally occupied by the degenerating axon terminals, will be replaced by the regenerating synapses in an adaptive manner. Via the intra- vitreous injection of the anterograde tracer-cholera toxin beta conjugated with different fluorescent probes, the tracer can be moved along the optic nerve overtime, with the downstream targets of the retinal-projection mapped by the tracer. This technique should allow for a thorough assessment of downstream target deafferentation and potential synaptic plasticity following the diffuse TAI in the optic nerve.

Summary

In summary, this optic nerve TAI following diffuse brain injury model provides unique insight into the pathogenesis of diffuse traumatic axonal injury, from its progressive swelling and disconnection, to rapid axonal dieback in both the proximal and distal direction. Overtime, the anterograde/downstream disconnected distal axonal segments underwent persisting degeneration. In contrast, the retrograde/upstream proximal axonal segments transitioned rapidly to reorganization. Of note, this optic nerve TAI model was also accompanied with diffuse traumatic axonal injury in the brain parenchyma, indicating its utility for various treatment screening. In addition to these events, the optic nerve diffuse TAI was not followed by retrograde RGC death overtime. Moreover, these sustaining RGCs revealed the persistent expression of phospho-c-Jun, consistent with neuronal survival. Affirmaion that the RGCs survival was associated with the reorganization and potential repair of the proximal axonal segments, was provided by the finding that the microglia/macrophages maintained a resting state within this same segment. In contrast to these proximal axonal segment reorganization, the downstream distal disconnected axonal segment underwent continued dieback and degeneration, and spatial-temporally related to the activation of microglia/macrophage, suggesting that specific inhibition of microglia/macrophage would be a potential therapeutic strategy to prevent distal axonal degeneration and dieback. Collectively, we believe that our current model will allow the exploration of potential axonal regeneration and synaptic plasticity in future studies.

LIST OF REFERENCES

1. Abe N, Cavalli V. (2008). Nerve injury signaling. Curr Opin Neurobiol. 18(3): 276-283.

2. Adams JH, Graham DI, Scott G, Parker LS, Doyle D. (1980). Brain damage in fatal non-missile head injury. J Clin Pathol. 33:1132–1145.

3. Adams JH, Scott G, Parker LS, Graham DI, Doyle D. (1980). The contusion index: a quantitative approach to cerebral contusions in head injury. Neuropathol Appl Neurobiol. 6(4): 319-324.

4. Agudo M, Pérez-Marín MC, Lönngren U, Sobrado P, Conesa A, Cánovas I, Salinas-Navarro M, Miralles-Imperial J, Hallböök F, Vidal-Sanz M. (2008). Time course profiling of the retinal transcriptome after optic nerve transection and optic nerve crush. Mol Vis 14:1050-1063.

5. Aguayo AJ, Rasminsky M, Bray GM, Carbonetto S, McKerracher L, Villegas-Pérez MP, Vidal-Sanz M, Carter DA. (1991). Degenerative and regenerative responses of injured neurons in the central nervous system of adult mammals. Philos Trans R Soc Lond B Biol Sci. 331(1261): 337-343.

6. Aguilar HI, Botla R, Arora AS, Bronk SF, Gores GJ. (1996). Induction of the mitochondrial permeability transition by protease activity in rats: a mechanism of hepatocyte necrosis. Gastroenterology. 110(2): 558-566.

7. Ahmed SM, Rzigalinski BA, Willoughby KA, Sitterding HA, Ellis EF. (2000). Stretch-induced injury alters mitochondrial membrane potential and cellular ATP in cultured astrocytes and neurons. J Neurochem. 74(5): 1951-1960.

8. Alarcón-Martínez L, Avilés-Trigueros M, Galindo-Romero C, Valiente-Soriano J, Agudo-Barriuso M, Villa Pde L, Villegas-Pérez MP, Vidal-Sanz M. (2010). ERG changes in albino and pigmented mice after optic nerve transection. Vision Res. 50(21): 2176-2187.

9. Aldrich EF, Eisenberg HM, Saydjari C, Luerssen TG, Foulkes MA, Jane JA, Marshall LF, Marmarou A, Young HF. (1992). Diffuse brain swelling in severely head-injured children. A report from the NIH Traumatic Coma Data Bank. J Neurosurg. 76(3): 450-454.

10. Althaus HH, Klöppner S, Schmidt-Schultz T, Schwartz P. (1992). Nerve growth factor induces proliferation and enhances fiber regeneration in oligodendrocytes isolated from adult pig brain. Neurosci Lett. 135(2): 219-223.

11. Ambron RT, Walters ET. (1996). Priming events and retrograde injury signals. A new perspective on the cellular and molecular biology of nerve regeneration. Mol Neurobiol. 13(1): 61-79.

12. Anderson RL, Panje WR, Gross CE. (1982). Optic nerve blindness following blunt forehead trauma. Ophthalmology. 89(5): 445–455.

13. Araki T, Sasaki Y, Milbrandt J. (2004). Increased nuclear NAD biosynthesis and SIRT1 activation prevent axonal degeneration. Science. 305(5686): 1010-1013.

14. Araújo Couto L, Sampaio Narciso M, Hokoç JN, Blanco Martinez AM. (2004). Calpain inhibitor 2 prevents axonal degeneration of opossum optic nerve fibers. J Neurosci Res. 77(3): 410-419.

15. Arfanakis K, Haughton VM, Carew JD, Rogers BP, Dempsey RJ, Meyerand ME. (2002). Diffusion tensor MR imaging in diffuse axonal injury. AJNR Am J Neuroradiol. 23(5): 794-802.

16. Arrington DD, Van Vleet TR, Schnellmann RG. (2006). Calpain 10: a mitochondrial calpain and its role in calcium-induced mitochondrial dysfunction. Am J Physiol Cell Physiol. 291(6): C1159-1171.

17. Atalay B, Bavbek M, Cekinmez M, Ozen O, Nacar A, Karabay G, Gulsen S. (2007). Antibodies neutralizing Nogo-A increase pan-cadherin expression and motor recovery following spinal cord injury in rats. Spinal Cord. 45(12): 780-786.

18. Atkins EJ, Newman NJ, Biousse V. (2008). Post-traumatic visual loss. Rev. Neurol. Dis. 5(2): 73-81. Review.

19. Avery MA, Rooney TM, Pandya JD, Wishart TM, Gillingwater TH, Geddes JW, Sullivan PG, Freeman MR. (2012). WldS prevents axon degeneration through increased mitochondrial flux and enhanced mitochondrial Ca2+ buffering. Curr Biol. 22(7): 596-600.

20. Babcock DF, Hille B. (1998). Mitochondrial oversight of cellular Ca2+ signaling. Curr Opin Neurobiol. 8(3): 398-404.

21. Banik NL, Matzelle DC, Gantt-Wilford G, Osborne A, Hogan EL. (1997). Increased calpain content and progressive degradation of neurofilament protein in spinal cord injury. Brain Res. 752(1-2): 301-306.

22. Barker, WH and Mullooly, JP. (1997). Stroke in a defined elderly population, 1967-1985. A less lethal and disabling but no less common disease. Stroke 28, 284-290.

23. Barnat M, Enslen H, Propst F, Davis RJ, Soares S, Nothias F. (2010). Distinct roles of c-Jun N-terminal kinase isoforms in neurite initiation and elongation during axonal regeneration. J Neurosci. 30(23): 7804-7816.

24. Barrette B, Hébert MA, Filali M, Lafortune K, Vallières N, Gowing G, Julien JP, Lacroix S. (2008). Requirement of myeloid cells for axon regeneration. J Neurosci. 28(38): 9363-9376.

25. Barrientos SA, Martinez NW, Yoo S, Jara JS, Zamorano S, Hetz C, Twiss JL, Alvarez J, Court FA. (2011). Axonal degeneration is mediated by the mitochondrial permeability transition pore. J Neurosci. 31(3): 966-978.

26. Bartus RT, Elliott P, Hayward N, Dean R, McEwen EL, Fisher SK. (1996). Permeability of the blood brain barrier by the bradykinin agonist, RMP-7: evidence for a sensitive, auto-regulated, receptor-mediated system. Immunopharmacology. 33(1-3): 270-278.

27. Barzó P, Marmarou A, Fatouros P, Corwin F, Dunbar J. (1996). Magnetic resonance imaging-monitored acute blood-brain barrier changes in experimental traumatic brain injury. J Neurosurg. 85(6): 1113-1121.

28. Barzó P, Marmarou A, Fatouros P, Hayasaki K, Corwin F. (1997). Biphasic pathophysiological response of vasogenic and cellular edema in traumatic brain swelling. Acta Neurochir Suppl. 70: 119-122.

29. Beazley LD, Rodger J, Chen P, Tee LB, Stirling RV, Taylor AL, Dunlop SA. (2003). Training on a visual task improves the outcome of optic nerve regeneration. J Neurotrauma. 20(11): 1263–1270.

30. Beirowski B, Nógrádi A, Babetto E, Garcia-Alias G, Coleman MP. (2010). Mechanisms of axonal spheroid formation in central nervous system Wallerian degeneration. J.Neuropathol. Exp. Neurol. 69(5): 455–472.

31. Belanger HG, Vanderploeg RD, Curtiss G, Warden DL. (2007). Recent neuroimaging techniques in mild traumatic brain injury. J. Neuropsychiatry Clin. Neurosci. 19(1): 5–20.

32. Ben-Yaakov K, Fainzilber M. (2009). Retrograde injury signaling in lesioned axons. Results Probl Cell Differ. 48: 327-338.

33. Benowitz LI, Yin Y. (2010). Optic nerve regeneration. Arch Ophthalmol. 128(8): 1059-1064.

34. Berkelaar M, Clarke DB, Wang YC, Bray GM, Aguayo AJ. (1994). Axotomy results in delayed death and apoptosis of retinal ganglion cells in adult rats. J Neurosci. 14(7): 4368-4374.

35. Bessero AC, Chiodini F, Rungger-Brändle E, Bonny C, Clarke PG. (2010). Role of the c-Jun N-terminal kinase pathway in retinal excitotoxicity, and neuroprotection by its inhibition. J Neurochem. 113(5): 1307-1318.

36. Betz AL, Iannotti F, Hoff JT. (1989). Brain edema: a classification based on blood-brain barrier integrity. Cerebrovasc Brain Metab Rev. 1(2): 133-154.

37. Bezprozvanny I. (2009). Calcium signaling and neurodegenerative diseases. Trends Mol Med. 15(3): 89–100.

38. Bie X, Chen Y, Zheng X, Dai H. (2011). The role of crocetin in protection following cerebral contusion and in the enhancement of angiogenesis in rats. Fitoterapia. 82(7): 997-1002.

39. Biermann J, Lagrèze WA, Schallner N, Schwer CI, Goebel U. (2011). Inhalative preconditioning with hydrogen sulfide attenuated apoptosis after retinal ischemia/reperfusion injury. Mol Vis. 1275-1286.

40. Billger M, Wallin M, Karlsson JO. (1988). Proteolysis of tubulin and microtubule-associated proteins 1 and 2 by calpain I and II. Difference in sensitivity of assembled and disassembled microtubules. Cell Calcium. 9(1): 33-44.

41. Bisby MA, Bulger VT. (1977). Reversal of axonal transport at a nerve crush. J Neurochem. 29(2): 313-320.

42. Block ML, Zecca L, Hong JS. (2007). Microglia-mediated neurotoxicity: uncovering the molecular mechanisms. Nat Rev Neurosci. 8(1): 57-69.

43. Blumbergs PC, Jones NR, North JB. (1989). Diffuse axonal injury in head trauma. J. Neurol. Neurosurg. Psychiatry 52(7): 838–841.

44. Blumbergs PC, Scott G, Manavis J, Wainwright H, Simpson DA, McLean AJ. (1995). Topography of axonal injury as defined by amyloid precursor protein and the sector scoring method in mild and severe closed head injury. J. Neurotrauma. 12(4): 565–572.

45. Bogoyevitch MA. (2006). The isoform-specific functions of the c-Jun N-terminal Kinases (JNKs): differences revealed by gene targeting. Bioessays. 28(9): 923-934.

46. Bomze HM, Bulsara KR, Iskandar BJ, Caroni P, Skene JH. (2001). Spinal axon regeneration evoked by replacing two growth cone proteins in adult neurons. Nat Neurosci. 4(1): 38-43.

47. Bonatz H, Röhrig S, Mestres P, Meyer M, Giehl KM. (2000). An axotomy model for the induction of death of rat and mouse corticospinal neurons in vivo. J Neurosci Methods. 100(1-2): 105-115.

48. Bouquet C, Soares S, von Boxberg Y, Ravaille-Veron M, Propst F, Nothias F. (2004). Microtubule-associated protein 1B controls directionality of growth cone migration and axonal branching in regeneration of adult dorsal root ganglia neurons. J Neurosci. 24(32): 7204-7213.

49. Boyd JG, Gordon T. (2003). Neurotrophic factors and their receptors in axonal regeneration and functional recovery after peripheral nerve injury. Mol Neurobiol. 27(3): 277-324.

50. Broude E, McAtee M, Kelley MS, Bregman BS. (1997). c-Jun expression in adult rat dorsal root ganglion neurons: differential response after central or peripheral axotomy. Exp Neurol. 148(1): 367-377.

51. Brück W, Brück Y, Maruschak B, Friede RL. (1995). Mechanisms of macrophage recruitment in Wallerian degeneration. Acta Neuropathol. 89(4): 363-367.

52. Brundula V, Rewcastle NB, Metz LM, Bernard CC, Yong VW. (2002). Targeting leukocyte MMPs and transmigration: minocycline as a potential therapy for multiple sclerosis. Brain. 125(Pt 6): 1297-1308.

53. Brunet A, Bonni A, Zigmond MJ, Lin MZ, Juo P, Hu LS, Anderson MJ, Arden KC, Blenis J, Greenberg ME. (1999). Akt promotes cell survival by phosphorylating and inhibiting a Forkhead transcription factor. Cell. 96(6): 857-868.

54. Brustovetsky N, Brustovetsky T, Purl KJ, Capano M, Crompton M, Dubinsky JM. (2003). Increased susceptibility of striatal mitochondria to calcium-induced permeability transition. J Neurosci. 23(12): 4858-4867.

55. Büki A, Farkas O, Doczi T, Povlishock JT. (2003). Preinjury administration of the calpain inhibitor MDL-28170 attenuates traumatically induced axonal injury. J Neurotrauma. 20(3): 261-268.

56. Büki A, Okonkwo DO, Povlishock JT. (1999). Postinjury cyclosporin A administration limits axonal damage and disconnection in traumatic brain injury. J Neurotrauma. 16(6): 511-521.

57. Büki A, Okonkwo DO, Wang KK, Povlishock JT. (2000). Cytochrome c release and caspase activation in traumatic axonal injury. J Neurosci. 20(8): 2825-2834.

58. Büki A, Povlishock JT. (2006). All roads lead to disconnection?--Traumatic axonal injury revisited. Acta Neurochir (Wien) 148:181-193; discussion 193-194.

59. Büki A, Siman R, Trojanowski JQ, Povlishock JT. (1999). The role of calpain-mediated spectrin proteolysis in traumatically induced axonal injury. J Neuropathol Exp Neurol. 58(4): 365-375.

60. Bulsara KR, Iskandar BJ, Villavicencio AT, Skene JH. (2002). A new millenium for spinal cord regeneration: growth-associated genes. Spine (Phila Pa 1976). 27(17): 1946-1949.

61. Busch SA, Horn KP, Cuascut FX, Hawthorne AL, Bai L, Miller RH, Silver J. (2010). Adult NG2+ cells are permissive to neurite outgrowth and stabilize sensory axons during macrophage-induced axonal dieback after spinal cord injury. J Neurosci. 30(1): 255-265.

62. Busch SA, Horn KP, Silver DJ, Silver J. (2009). Overcoming macrophage-mediated axonal dieback following CNS injury. J Neurosci. 29(32): 9967-9976.

63. Cai D, Deng K, Mellado W, Lee J, Ratan RR, Filbin MT. (2002). Arginase I and polyamines act downstream from cyclic AMP in overcoming inhibition of axonal growth MAG and myelin in vitro. Neuron. 35(4): 711-719.

64. Callahan MP, Mensinger AF. (2007). Restoration of visual function following optic nerve regeneration in bluegill (Lepomis macrochirus) x pumpkinseed (Lepomis gibbosus) hybrid sunfish. Vis Neurosci. 24(3): 309-317.

65. Campbell G, Hutchins K, Winterbottom J, Grenningloh G, Lieberman AR, Anderson PN. (2005). Upregulation of activating transcription factor 3 (ATF3) by intrinsic CNS neurons regenerating axons into peripheral nerve grafts. Exp Neurol. 192(2): 340-347.

66. Cao Z, Gao Y, Bryson JB, Hou J, Chaudhry N, Siddiq M, Martinez J, Spencer T, Carmel J, Hart RB, Filbin MT. (2006). The cytokine interleukin-6 is sufficient but not necessary to mimic the peripheral conditioning lesion effect on axonal growth. J Neurosci. 26(20): 5565-5573.

67. Capó-Aponte JE, Urosevich TG, Temme LA, Tarbett AK, Sanghera NK. (2012). Visual dysfunctions and symptoms during the subacute stage of blast-induced mild traumatic brain injury. Mil Med. 177(7): 804-813.

68. Casaccia-Bonnefil P, Carter BD, Dobrowsky RT, Chao MV. (1996). Death of oligodendrocytes mediated by the interaction of nerve growth factor with its receptor p75. Nature. 383(6602): 716-719.

69. Catrinescu MM, Chan W, Mahammed A, Gross Z, Levin LA. (2012). Superoxide signaling and cell death in retinal ganglion cell axotomy: effects of metallocorroles. Exp Eye Res. 97(1): 31-35.

70. Cavalli V, Kujala P, Klumperman J, Goldstein LS. (2005). Sunday Driver links axonal transport to damage signaling. J Cell Biol. 168(5): 775-787.

71. Chen XH, Johnson VE, Uryu K, Trojanowski JQ, Smith DH. (2009). A lack of amyloid beta plaques despite persistent accumulation of amyloid beta in axons of long-term survivors of traumatic brain injury. Brain Pathol. 19(2): 214-223.

72. Chen L, McBranch DW, Wang HL, Helgeson R, Wudl F, Whitten DG. (1999). Highly sensitive biological and chemical sensors based on reversible fluorescence quenching in a conjugated polymer. Proc Natl Acad Sci U S A. 96(22): 12287-12292.

73. Chen YH, Lin SZ, Chiang YH, Ju DT, Liu MY, Chen GJ. (2004). Supraorbital keyhole surgery for optic nerve decompression and dura repair. J Neurotrauma. 21(7): 976-981.

74. Chen M, Ona VO, Li M, Ferrante RJ, Fink KB, Zhu S, Bian J, Guo L, Farrell LA, Hersch SM, Hobbs W, Vonsattel JP, Cha JH, Friedlander RM. (2000). Minocycline inhibits caspase-1 and caspase-3 expression and delays mortality in a transgenic mouse model of Huntington disease. Nat Med. 6(7): 797-801.

75. Chinopoulos C, Adam-Vizi V. (2010). Mitochondrial Ca2+ sequestration and precipitation revisited. FEBS J. 277(18): 3637–3651.

76. Christman CW, Grady MS, Walker SA, Holloway KL, Povlishock JT. (1994). Ultrastructural studies of diffuse axonal injury in humans. J. Neurotrauma 11(2): 173-186.

77. Chu ZG, Yang ZG, Dong ZH, Chen TW, Zhu ZY, Shao H. (2011). Comparative study of earthquake-related and non-earthquake-related head traumas using multidetector computed tomography. Clinics (Sao Paulo). 66(10): 1735-1742.

78. Clark RS, Kochanek PM, Watkins SC, Chen M, Dixon CE, Seidberg NA, Melick J, Loeffert JE, Nathaniel PD, Jin KL, Graham SH. (2000). Caspase-3 mediated neuronal death after traumatic brain injury in rats. J Neurochem. 74(2): 740-753.

79. Cockerham GC, Goodrich GL, Weichel ED, Orcutt JC, Rizzo JF, Bower KS, Schuchard RA. (2009). Eye and visual function in traumatic brain injury. J Rehabil Res Dev. 46(6): 811-818.

80. Coleman MP, Freeman MR. (2010). Wallerian degeneration, wld(s), and nmnat. Annu Rev Neurosci. 33: 245-267. Review.

81. Colley BS, Phillips LL, Reeves TM. (2010). The effects of cyclosporin-A on axonal conduction deficits following traumatic brain injury in adult rats. Exp Neurol. 224(1): 241-251.

82. Comley LH, Wishart TM, Baxter B, Murray LM, Nimmo A, Thomson D, Parson SH, Gillingwater TH. (2011). Induction of cell stress in neurons from transgenic mice expressing yellow fluorescent protein: implications for neurodegeneration research. PLoS One. 6(3): e17639.

83. Conforti L, Tarlton A, Mack TG, Mi W, Buckmaster EA, Wagner D, Perry VH, Coleman MP. (2000). A Ufd2/D4Cole1e chimeric protein and overexpression of Rbp7 in the slow Wallerian degeneration (WldS) mouse. Proc Natl Acad Sci U S A. 97(21): 11377-11382.

84. Connern CP, Halestrap AP. (1992). Purification and N-terminal sequencing of peptidyl-prolyl cis-trans-isomerase from rat liver mitochondrial matrix reveals the existence of a distinct mitochondrial cyclophilin. Biochem J. 284 (Pt 2): 381-385.

85. Coronado, McGuire, Faul, Sugerman, Pearson. The Epidemiology and Prevention of TBI (in press) 2012.

86. Crompton M, Costi A. (1988). Kinetic evidence for a heart mitochondrial pore activated by Ca2+, inorganic phosphate and oxidative stress. A potential mechanism for mitochondrial dysfunction during cellular Ca2+ overload. Eur J Biochem. 178(2): 489-501.

87. Crompton M, Costi A. (1990). A heart mitochondrial Ca2(+)-dependent pore of possible relevance to re-perfusion-induced injury. Evidence that ADP facilitates pore interconversion between the closed and open states. Biochem J. 266(1): 33-39.

88. Crompton M, Costi A, Hayat L. (1987). Evidence for the presence of a reversible Ca2+-dependent pore activated by oxidative stress in heart mitochondria. Biochem J. 245(3): 915-918.

89. Crompton M, Moser R, Lüdi H, Carafoli E. (1978). The interrelations between the transport of sodium and calcium in mitochondria of various mammalian tissues. Eur J Biochem. 82(1): 25–31.

90. Dajas-Bailador F, Jones EV, Whitmarsh AJ. (2008). The JIP1 scaffold protein regulates axonal development in cortical neurons. Curr Biol. 18(3): 221-226.

91. Dakin SG, Werling D, Hibbert A, Abayasekara DR, Young NJ, Smith RK, Dudhia J. (2012). Macrophage Sub-Populations and the Lipoxin A(4) Receptor Implicate Active Inflammation during Equine Tendon Repair. PLoS One. 7(2): e32333.

92. Dale SM, Kuang RZ, Wei X, Varon S. (1995). Corticospinal motor neurons in the adult rat: degeneration after intracortical axotomy and protection by ciliary neurotrophic factor (CNTF). Exp Neurol. 135(1): 67-73.

93. Datta SR, Dudek H, Tao X, Masters S, Fu H, Gotoh Y, Greenberg ME. (1997). Akt phosphorylation of BAD couples survival signals to the cell-intrinsic death machinery. Cell. 91(2): 231-241.

94. Del Bigio MR, Deck JH, Davidson GS. (2000). Glial swelling with eosinophilia in human post-mortem brains: a change indicative of plasma extravasation. Acta Neuropathol.100(6): 688-694.

95. Deng-Bryant Y, Singh IN, Carrico KM, Hall ED. (2008). Neuroprotective effects of tempol, a catalytic scavenger of peroxynitrite-derived free radicals, in a mouse traumatic brain injury model. J. Cereb. Blood Flow Metab. 28(6): 1114–1126.

96. Deonarine K, Panelli MC, Stashower ME, Jin P, Smith K, Slade HB, Norwood C, Wang E, Marincola FM, Stroncek DF. (2007). Gene expression profiling of cutaneous wound healing. J Transl Med. 5:11.

97. Detrait E, Eddleman CS, Yoo S, Fukuda M, Nguyen MP, Bittner GD, Fishman HM. (2000). Axolemmal repair requires proteins that mediate synaptic vesicle fusion. J Neurobiol. 44(4): 382-391.

98. Dibas A, Oku H, Fukuhara M, Kurimoto T, Ikeda T, Patil RV, Sharif NA, Yorio T. (2010). Changes in ocular aquaporin expression following optic nerve crush. Mol Vis. 16: 330-340.

99. Dietrich WD, Alonso O, Halley M. (1994). Early microvascular and neuronal consequences of traumatic brain injury: a light and electron microscopic study in rats. J Neurotrauma. 11(3): 289-301.

100. Ding JY, Kreipke CW, Speirs SL, Schafer P, Schafer S, Rafols JA. (2009). Hypoxia-inducible factor-1alpha signaling in aquaporin upregulation after traumatic brain injury. Neurosci Lett. 453(1): 68-72.

101. Ding Y, Yao B, Lai Q, McAllister JP. (2001). Impaired motor learning and diffuse axonal damage in motor and visual systems of the rat following traumatic brain injury. Neurol Res. 23(2-3): 193-202.

102. Dixon CE, Lyeth BG, Povlishock JT, Findling RL, Hamm RJ, Marmarou A, Young HF, Hayes RL. (1987). A fluid percussion model of experimental brain injury in the rat. J. Neurosurg. 67(1): 110–119.

103. Donkin JJ, Vink R. (2010). Mechanisms of cerebral edema in traumatic brain injury: therapeutic developments. Curr. Opin. Neurol. 23(3): 293–299.

104. Dua RK, Devi BI, Yasha TC. (2010). Increased expression of Aquaporin-4 and its correlation with contrast enhancement and perilesional edema in brain tumors. Br J Neurosurg. 24(4): 454-459.

105. Duvdevani R, Roof RL, Fülöp Z, Hoffman SW, Stein DG. (1995). Blood-brain barrier breakdown and edema formation following frontal cortical contusion: does hormonal status play a role? J Neurotrauma. 12(1): 65-75.

106. Ebbesen TW, Ghiron CA. (1989). Role of specific solvation in the fluorescence sensitivity of 1,8-ANS to water. J. Phys. Chem. 93, 7139–7143.

107. Emery DG, Lucas JH, Gross GW. (1991). Contributions of sodium and chloride to ultrastructural damage after dendrotomy. Exp Brain Res. 86(1): 60-72.

108. Erb DE, Povlishock JT. (1991). Neuroplasticity following traumatic brain injury: a study of GABAergic terminal loss and recovery in the cat dorsal lateral vestibular nucleus. Exp Brain Res. 83(2): 253-267.

109. Espinoza TR, Wright DW. (2011). The role of progesterone in traumatic brain injury. J Head Trauma Rehabil. 26(6): 497-499.

110. Farkas O, Lifshitz J, Povlishock JT. (2006). Mechanoporation induced by diffuse traumatic brain injury: an irreversible or reversible response to injury? J Neurosci. 26(12): 3130-3140.

111. Farkas O, Polgár B, Szekeres-Barthó J, Dóczi T, Povlishock JT, Büki A. (2005). Spectrin breakdown products in the cerebrospinal fluid in severe head injury--preliminary observations. Acta Neurochir (Wien). 147(8): 855-861.

112. Farkas O, Povlishock JT. (2007). Cellular and subcellular change evoked by diffuse traumatic brain injury: a complex web of change extending far beyond focal damage. Prog Brain Res. 161: 43-59.

113. Faul M, Xu L, Wald MM, Coronado VG. Traumatic brain injury in the United States: emergency department visits, hospitalizations, and deaths. Atlanta (GA): Centers for Disease Control and Prevention, National Center for Injury Prevention and Control; 2010

114. Fearnside, MR and Simpson, DA. (1997). Part One: the Injury, Chapter1: Epidemiology, in Head Injury: Pathophysiology and management of severe closed injury, (eds P. Reilly and R. Bullock), Chapman & Hall USA, New York, pp. 3-23. Available at: http://www.neurotraumasociety.org/Portals/150619/docs/Chap01.pdf. Accessed November 8, 2012.

115. Feng G, Mellor RH, Bernstein M, Keller-Peck C, Nguyen QT, Wallace M, Nerbonne JM, Lichtman JW, Sanes JR. (2000). Imaging neuronal subsets in transgenic mice expressing multiple spectral variants of GFP. Neuron 28(1): 41–51.

116. Fenrich K, Gordon T. (2004). Canadian Association of Neuroscience review: axonal regeneration in the peripheral and central nervous systems--current issues and advances. Can J Neurol Sci.31 (2): 142-156. Review.

117. Fernandes KJ, Fan DP, Tsui BJ, Cassar SL, Tetzlaff W. (1999). Influence of the axotomy to cell body distance in rat rubrospinal and spinal motoneurons: differential regulation of GAP-43, tubulins, and neurofilament-M. J Comp Neurol. 414(4): 495-510.

118. Feringa ER, Vahlsing HL, Smith BE. (1983). Retrograde transport in corticospinal neurons after spinal cord transection. Neurology. 33(4): 478-482.

119. Fineman I, Hovda DA, Smith M, Yoshino A, Becker DP. (1993). Concussive brain injury is associated with a prolonged accumulation of calcium: a 45Ca autoradiographic study. Brain Res. 624(1-2): 94-102.

120. Finkelstein E, Corso P, Miller T and associates. The Incidence and Economic Burden of Injuries in the United States. New York (NY): Oxford University Press; 2006.

121. Fishman HM, Bittner GD. (2003). Vesicle-mediated restoration of a plasmalemmal barrier in severed axons. News Physiol Sci. 18: 115-118.

122. Fitzgerald M, Bartlett CA, Harvey AR, Dunlop SA. (2010). Early events of secondary degeneration after partial optic nerve transection: an immunohistochemical study. J Neurotrauma. 27(2): 439-452.

123. Fitzgerald M, Payne SC, Bartlett CA, Evill L, Harvey AR, Dunlop SA. (2009). Secondary retinal ganglion cell death and the neuroprotective effects of the calcium channel blocker lomerizine. Invest Ophthalmol Vis Sci. 50(11): 5456-5462.

124. Foda MA, Marmarou A. (1994). A new model of diffuse brain injury in rats. Part II: Morphological characterization. J Neurosurg. 80(2): 301-313.

125. Frade JM, Rodríguez-Tébar A, Barde YA. (1996). Induction of cell death by endogenous nerve growth factor through its p75 receptor. Nature. 383(6596):166-168.

126. Frielingsdorf H, Simpson DR, Thal LJ, Pizzo DP. (2007). Nerve growth factor promotes survival of new neurons in the adult hippocampus. Neurobiol Dis. 26(1): 47-55.

127. Fujita M, Oda Y, Wei EP, Povlishock JT. (2011). The combination of either tempol or FK506 with delayed hypothermia: implications for traumatically induced microvascular and axonal protection. J Neurotrauma. 28(7): 1209-1218.

128. Funakoshi H, Frisén J, Barbany G, Timmusk T, Zachrisson O, Verge VM, Persson H. (1993). Differential expression of mRNAs for neurotrophins and their receptors after axotomy of the sciatic nerve. J Cell Biol. 123(2): 455-465.

129. Gabathuler R. (2010). Approaches to transport therapeutic drugs across the blood-brain barrier to treat brain diseases. Neurobiol Dis. 37(1): 48-57.

130. Galindo-Romero C, Avilés-Trigueros M, Jiménez-López M, Valiente-Soriano FJ, Salinas-Navarro M, Nadal-Nicolás F, Villegas-Pérez MP, Vidal-Sanz M, Agudo-Barriuso M. (2011). Axotomy-induced retinal ganglion cell death in adult mice: quantitative and topographic time course analyses. Exp Eye Res. 92(5): 377-387.

131. Gamblin TC, Chen F, Zambrano A, Abraha A, Lagalwar S, Guillozet AL, Lu M, Fu Y, Garcia-Sierra F, LaPointe N, Miller R, Berry RW, Binder LI, Cryns VL. (2003). Caspase cleavage of tau: linking amyloid and neurofibrillary tangles in Alzheimer's disease. Proc Natl Acad Sci U S A. 100(17): 10032-10037.

132. Gao Y, Deng K, Hou J, Bryson JB, Barco A, Nikulina E, Spencer T, Mellado W, Kandel ER, Filbin MT. (2004). Activated CREB is sufficient to overcome inhibitors in myelin and promote spinal axon regeneration in vivo. Neuron. 44(4): 609-621.

133. Gao G, Oda Y, Wei EP, Povlishock JT. (2010). The adverse pial arteriolar and axonal consequences of traumatic brain injury complicated by hypoxia and their therapeutic modulation with hypothermia in rat. J. Cereb. Blood Flow Metab. 30(3): 628–637.

134. Gasche Y, Fujimura M, Morita-Fujimura Y, Copin JC, Kawase M, Massengale J, Chan PH. (1999). Early appearance of activated matrix metalloproteinase-9 after focal cerebral ischemia in mice: a possible role in blood-brain barrier dysfunction. J Cereb Blood Flow Metab. 19(9): 1020-1028.

135. Gennarelli TA, Thibault LE. (1985). Biomechanics of head injury, in Neurosurgery, (eds R. H. Wilkins and S. S. Rengachary), McGraw-Hill, New York, vol. 2, pp. 1531–1535.

136. Gennarelli TA. (1993). Mechanisms of brain injury. J Emerg Med 11 Suppl 1:5–11.

137. Gennarelli TA, Thibault LE, Graham DI. (1998). Diffuse Axonal Injury: An Important Form of Traumatic Brain Damage. The Neuroscientist 4:202–215

138. Gennarelli TA, Thibault LE, Tipperman R, Tomei G, Sergot R, Brown M, Maxwell WL, Graham DI, Adams JH, Irvine A, et al. (1989). Axonal injury in the optic nerve: a model simulating diffuse axonal injury in the brain. J Neurosurg. 71(2): 244-253.

139. Gentleman SM, Leclercq PD, Moyes L, Graham DI, Smith C, Griffin WS, Nicoll JA. (2004). Long-term intracerebral inflammatory response after traumatic brain injury. Forensic Sci Int. 146(2-3): 97-104.

140. Giehl KM, Tetzlaff W. (1996). BDNF and NT-3, but not NGF, prevent axotomy-induced death of rat corticospinal neurons in vivo. Eur J Neurosci. 8(6): 1167-1175.

141. Giger RJ, Venkatesh K, Chivatakarn O, Raiker SJ, Robak L, Hofer T, Lee H, Rader C. (2008). Mechanisms of CNS myelin inhibition: evidence for distinct and neuronal cell type specific receptor systems. Restor Neurol Neurosci. 26(2-3): 97-115.

142. Glass JD, Brushart TM, George EB, Griffin JW. (1993). Prolonged survival of transected nerve fibres in C57BL/Ola mice is an intrinsic characteristic of the axon. J Neurocytol. 22(5): 311-321.

143. Gleckman AM, Bell MD, Evans RJ, Smith TW. (1999). Diffuse axonal injury in infants with nonaccidental craniocerebral trauma: Enhanced detection by beta-amyloid precursor protein immunohistochemical staining. Arch. Pathol. Lab. Med. 123(2): 146 - 151.

144. Gleckman AM, Evans RJ, Bell MD, Smith TW. (2000). Optic nerve damage in shaken baby syndrome: detection by beta-amyloid precursor protein immunohistochemistry. Arch Pathol Lab Med. 124(2): 251-256.

145. Godell CM, Smyers ME, Eddleman CS, Ballinger ML, Fishman HM, Bittner GD. (1997). Calpain activity promotes the sealing of severed giant axons. Proc Natl Acad Sci U S A. 94(9): 4751-4756.

146. Goll DE, Thompson VF, Li H, Wei W, Cong J. (2003). The calpain system. Physiol Rev. 83(3): 731–801.

147. Gordon T. Dependence of peripheral nerves on their target organs. In Burnstock G, Vrbova G, O'Brien R (Eds). Somatic and Autonomic Nerve-Muscle Interactions. New York, NY: Elsevier Science Publishers, 1983, pp 289-325.

148. Graham DI, Gennarelli TA: Pathology of brain damage after head injury, in Head Injury. Edited by Cooper PR, Golfinos JG. New York, McGraw-Hill, 2000, pp 133-153.

149. Graham DI, Gennarelli TA, McIntosh TK. (2002). Trauma, in: Greenfield's Neuropathology. D.I. Graham, and P.L. Lantos, (eds). London: Arnold Publishers. pps. 823-898.

150. Granacher RP. (2007). Traumatic Brain Injury: Methods for Clinical & Forensic Neuropsychiatric Assessment, Second Edition. Boca Raton: CRC. pp. 26-33.

151. Greer JE, McGinn MJ, Povlishock JT. (2011). Diffuse traumatic axonal injury in the mouse induces atrophy, c-Jun activation, and axonal outgrowth in the axotomized neuronal population. J Neurosci. 31(13): 5089-5105.

152. Greer JE, Povlishock JT, Jacobs KM. (2012). Electrophysiological abnormalities in both axotomized and nonaxotomized pyramidal neurons following mild traumatic brain injury. J Neurosci. 32(19): 6682-6687.

153. Griffiths EJ, Halestrap AP. (1995).Mitochondrial non-specific pores remain closed during cardiac ischaemia, but open upon reperfusion. Biochem J. 307 (Pt 1): 93-98.

154. Gurdjian, ES. (1976). Cerebral contusions: Re-evaluation of the mechanism of their development. Journal of Trauma. 16(1): 35–51.

155. Hai TW, Liu F, Coukos WJ, Green MR. (1989). Transcription factor ATF cDNA clones: an extensive family of leucine zipper proteins able to selectively form DNA-binding heterodimers. Genes Dev. 3(12B): 2083-2090.

156. Hains BC, Black JA, Waxman SG. (2003). Primary cortical motor neurons undergo apoptosis after axotomizing spinal cord injury. J Comp Neurol. 462(3): 328-341.

157. Halestrap AP. (2009). What is the mitochondrial permeability transition pore? J Mol Cell Cardiol. 46(6): 821-831.

158. Halestrap AP, Clarke SJ, Javadov SA. (2004). Mitochondrial permeability transition pore opening during myocardial reperfusion--a target for cardioprotection. Cardiovasc Res. 61(3): 372-385.

159. Halestrap AP, Kerr PM, Javadov S, Woodfield KY. (1998). Elucidating the molecular mechanism of the permeability transition pore and its role in reperfusion injury of the heart. Biochim Biophys Acta. 1366(1-2): 79-94.

160. Halestrap AP, Pasdois P. (2009). The role of the mitochondrial permeability transition pore in heart disease. Biochim Biophys Acta. 1787(11): 1402-415.

161. Hall ED, Vaishnav RA, Mustafa AG. (2010). Antioxidant therapies for traumatic brain injury. Neurotherapeutics 7(1): 51–61.

162. Hall SM. (1999). The biology of chronically denervated Schwann cells. Ann N Y Acad Sci. 883: 215-233.

163. Hannila SS, Filbin MT. (2008). The role of cyclic AMP signaling in promoting axonal regeneration after spinal cord injury. Exp Neurol. 209(2): 321-332.

164. Hanz S, Fainzilber M. (2004). Integration of retrograde axonal and nuclear transport mechanisms in neurons: implications for therapeutics. Neuroscientist.10(5): 404-408.

165. Hanz S, Perlson E, Willis D, Zheng JQ, Massarwa R, Huerta JJ, Koltzenburg M, Kohler M, van-Minnen J, Twiss JL, Fainzilber M. (2003). Axoplasmic importins enable retrograde injury signaling in lesioned nerve. Neuron. 40(6): 1095-1104.

166. Hardman JM, Manoukian A. (2002). "Pathology of Head Trauma". Neuroimaging Clinics of North America 12 (2): 175–187.

167. Haworth RA, Hunter DR. (1979). The Ca2+-induced membrane transition in mitochondria. II. Nature of the Ca2+ trigger site. Arch Biochem Biophys. 195(2): 460-467.

168. Hawthorne AL, Hu H, Kundu B, Steinmetz MP, Wylie CJ, Deneris ES, Silver J. (2011). The unusual response of serotonergic neurons after CNS Injury: lack of axonal dieback and enhanced sprouting within the inhibitory environment of the glial scar. J Neurosci. 31(15): 5605-5616.

169. He XS, Xiang Z, Zhou F, Fu LA, Shuang W. (2004). Calcium overloading in traumatic axonal injury by lateral head rotation: a morphological evidence in rat model. J Clin Neurosci. 11(4): 402-407.

170. Heather NL, Derraik JG, Brennan C, Jefferies C, Hofman PL, Kelly P, Jones RG, Rowe DL, Cutfield WS. (2012). Cortisol response to synacthen stimulation is attenuated following abusive head trauma. Clin Endocrinol (Oxf). 10.1111/j.1365-2265.

171. Hellman AN, Vahidi B, Kim HJ, Mismar W, Steward O, Jeon NL, Venugopalan V. (2010). Examination of axonal injury and regeneration in micropatterned neuronal culture using pulsed laser microbeam dissection. Lab. Chip. 10, 2083–2092.

172. Hellström M, Pollett MA, Harvey AR. (2011). Post-injury delivery of rAAV2-CNTF combined with short-term pharmacotherapy is neuroprotective and promotes extensive axonal regeneration after optic nerve trauma. J Neurotrauma. 28(12): 2475-2483.

173. Herdegen T, Bastmeyer M, Bähr M, Stuermer C, Bravo R, Zimmermann M. (1993). Expression of JUN, KROX, and CREB transcription factors in goldfish and rat retinal ganglion cells following optic nerve lesion is related to axonal sprouting. J Neurobiol. 24(4): 528-543.

174. Herdegen T, Brecht S, Mayer B, Leah J, Kummer W, Bravo R, Zimmermann M. (1993). Long-lasting expression of JUN and KROX transcription factors and nitric oxide synthase in intrinsic neurons of the rat brain following axotomy. J Neurosci. 13(10): 4130-4145.

175. Herdegen T, Skene P, Bähr M. (1997). The c-Jun transcription factor--bipotential mediator of neuronal death, survival and regeneration. Trends Neurosci. 20(5): 227-231.

176. Hiebert GW, Dyer JK, Tetzlaff W, Steeves JD. (2000). Immunological myelin disruption does not alter expression of regeneration-associated genes in intact or axotomized rubrospinal neurons. Exp Neurol. 163(1): 149-156.

177. Hinzman JM, Thomas TC, Burmeister JJ, Quintero JE, Huettl P, Pomerleau F, Gerhardt GA, Lifshitz J. (2010). Diffuse brain injury elevates tonic glutamate levels and potassium-evoked glutamate release in discrete brain regions at two days post-injury: an enzyme-based microelectrode array study. J Neurotrauma. 27(5): 889–899.

178. Höke A, Gordon T, Zochodne DW, Sulaiman OA. (2002). A decline in glial cell-line-derived neurotrophic factor expression is associated with impaired regeneration after long-term Schwann cell denervation. Exp Neurol. 173(1): 77-85.

179. Holmberg E, Zhang SX, Sarmiere PD, Kluge BR, White JT, Doolen S. (2008). Statins decrease chondroitin sulfate proteoglycan expression and acute astrocyte activation in central nervous system injury. Exp Neurol. 214(1): 78-86.

180. Horn KP, Busch SA, Hawthorne AL, van Rooijen N, Silver J. (2008). Another barrier to regeneration in the CNS: activated macrophages induce extensive retraction of dystrophic axons through direct physical interactions. J Neurosci. 28(38): 9330-9341.

181. Hortobágyi T, Wise S, Hunt N, Cary N, Djurovic V, Fegan-Earl A, Shorrock K, Rouse D, Al-Sarraj S. (2007). Traumatic axonal damage in the brain can be detected using beta-APP immunohistochemistry within 35 min after head injury to human adults. Neuropathol. Appl. Neurobiol. 33(2): 226–237.

182. Hossain S, Akaike T, Chowdhury EH. (2010). Current approaches for drug delivery to central nervous system. Curr Drug Deliv. 7(5): 389-397.

183. Hoyt CS. (2007). Brain injury and the eye. Eye (Lond). 21, 1285-1289. Review

184. Hsu ST, Blaser G, Behrens C, Cabrita LD, Dobson CM, Jackson SE. (2010). Folding study of Venus reveals a strong ion dependence of its yellow fluorescence under mildly acidic conditions. J Biol Chem. 285(7): 4859-4869.

185. Hu Y, Park KK, Yang L, Wei X, Yang Q, Cho KS, Thielen P, Lee AH, Cartoni R, Glimcher LH, Chen DF, He Z. (2012). Differential effects of unfolded protein response pathways on axon injury-induced death of retinal ganglion cells. Neuron. 73(3): 445-452.

186. Hua F, Reiss JI, Tang H, Wang J, Fowler X, Sayeed I, Stein DG. (2012). Progesterone and low-dose vitamin D hormone treatment enhances sparing of memory following traumatic brain injury. Horm Behav. 61(4): 642-651.

187. Huang AP, Lee CW, Hsieh HJ, Yang CC, Tsai YH, Tsuang FY, Kuo LT, Chen YS, Tu YK, Huang SJ, Liu HM, Tsai JC. (2011). Early Parenchymal Contrast Extravasation Predicts Subsequent Hemorrhage Progression, Clinical Deterioration, and Need for Surgery in Patients With Traumatic Cerebral Contusion. J Trauma. 71(6): 1593-1599.

188. Huebner EA, Strittmatter SM. (2009). Axon regeneration in the peripheral and central nervous systems. Results Probl Cell Differ. 48: 339-351.

189. Hüll M, Bähr. (1994). Differential regulation of c-JUN expression in rat retinal ganglion cells after proximal and distal optic nerve transection. Neurosci Lett. 178(1): 39-42.

190. Hüll M, Bähr M. (1994). Regulation of immediate-early gene expression in rat retinal ganglion cells after axotomy and during regeneration through a peripheral nerve graft. J Neurobiol. 25(1): 92-105.

191. Igarashi M, Li WW, Sudo Y, Fishman MC. (1995). Ligand-induced growth cone collapse: amplification and blockade by variant GAP-43 peptides. J Neurosci. 15(8): 5660-5667.

192. Ito M, Natsume A, Takeuchi H, Shimato S, Ohno M, Wakabayashi T, Yoshida J. (2009). Type I interferon inhibits astrocytic gliosis and promotes functional recovery after spinal cord injury by deactivation of the MEK/ERK pathway. J Neurotrauma. 26(1): 41-53.

193. Ito Y, Yamamoto M, Li M, Doyu M, Tanaka F, Mutch T, Mitsuma T, Sobue G. (1998). Differential temporal expression of mRNAs for ciliary neurotrophic factor (CNTF), leukemia inhibitory factor (LIF), interleukin-6 (IL-6), and their receptors (CNTFR alpha, LIFR beta, IL-6R alpha and gp130) in injured peripheral nerves. Brain Res. 793(1-2): 321-327.

194. Itoh A, Horiuchi M, Wakayama K, Xu J, Bannerman P, Pleasure D, Itoh T. (2011). ZPK/DLK, a mitogen-activated protein kinase kinase kinase, is a critical mediator of programmed cell death of motoneurons. J Neurosci. 31(20): 7223-7228.

195. Iwata A, Stys PK, Wolf JA, Chen XH, Taylor AG, Meaney DF, Smith DH. (2004). Traumatic axonal injury induces proteolytic cleavage of the voltage-gated sodium channels modulated by tetrodotoxin and protease inhibitors. J Neurosci. 24(19): 4605-4613.

196. Iwamura A, Taoka T, Fukusumi A, Sakamoto M, Miyasaka T, Ochi T, Akashi T, Okuchi K, Kichikawa K. (2012). Diffuse vascular injury: convergent-type hemorrhage in the supratentorial white matter on susceptibility-weighted image in cases of severe traumatic brain damage. Neuroradiology. 54(4): 335-343.

197. Jamieson, KG, Yelland, JN. (1968). Extradural haematoma: report of 167 cases. Journal of Neurosurgery. 29(1): 13–23.

198. Jayakumar AR, Panickar KS, Curtis KM, Tong XY, Moriyama M, Norenberg MD. (2011). Na-K-Cl cotransporter-1 in the mechanism of cell swelling in cultured astrocytes after fluid percussion injury. J Neurochem. 117(3): 437-448.

199. Jensen MB, Finsen B, Zimmer J. (1997). Morphological and immunophenotypic microglial changes in the denervated fascia dentata of adult rats: correlation with blood-brain barrier damage and astroglial reactions. Exp Neurol. 143(1): 103-116.

200. Johnson N, Khan A, Virji S, Ward JM, Crompton M. (1999). Import and processing of heart mitochondrial cyclophilin D. Eur J Biochem. 263(2): 353-359.

201. Johnson GV, Litersky JM, Jope RS. (1991). Degradation of microtubule-associated protein 2 and brain spectrin by calpain: a comparative study. J Neurochem. 56(5): 1630-1638.

202. Kelley BJ, Farkas O, Lifshitz J, Povlishock JT. (2006). Traumatic axonal injury in the perisomatic domain triggers ultrarapid secondary axotomy and Wallerian degeneration. Exp Neurol. 198(2): 350-360.

203. Kelley, B.J., Lifshitz, J., Povlishock, J.T. (2007). Neuroinflammatory responses after experimental diffuse traumatic brain injury. J. Neuropathol. Exp. Neurol. 66(11): 989–1001.

204. Kenney AM, Kocsis JD. (1998). Peripheral axotomy induces long-term c-Jun amino-terminal kinase-1 activation and activator protein-1 binding activity by c-Jun and junD in adult rat dorsal root ganglia in vivo. J Neurosci. 18(4): 1318-1328.

205. Kerschensteiner M, Schwab ME, Lichtman JW, Misgeld T. (2005). In vivo imaging of axonal degeneration and regeneration in the injured spinal cord. Nat Med. 11(5): 572-577.

206. Kielczewski JL, Pease ME, Quigley HA. (2005). The effect of experimental glaucoma and optic nerve transection on amacrine cells in the rat retina. Invest Ophthalmol Vis Sci. 46(9): 3188-3196.

207. Kigerl KA, Gensel JC, Ankeny DP, Alexander JK, Donnelly DJ, Popovich PG. (2009). Identification of two distinct macrophage subsets with divergent effects causing either neurotoxicity or regeneration in the injured mouse spinal cord. J Neurosci. 29(43): 13435-13444.

208. Kilinc D, Gallo G, Barbee K. (2007). Poloxamer 188 reduces axonal beading following mechanical trauma to cultured neurons. Conf Proc IEEE Eng Med Biol Soc. 2007: 5395-5398.

209. Kilinc D, Gallo G, Barbee KA. (2008). Mechanically-induced membrane poration causes axonal beading and localized cytoskeletal damage.Exp Neurol. 212(2): 422-430.

210. Kilinc D, Gallo G, Barbee KA. (2009). Mechanical membrane injury induces axonal beading through localized activation of calpain.Exp Neurol. 219(2): 553-561.

211. Kim JJ, Gean AD. (2011). Imaging for the Diagnosis and Management of Traumatic Brain Injury. Neurotherapeutics. 8(1): 39–53.

212. Kita T, Tanaka T, Tanaka N, Kinoshita Y. (2000). The role of tumor necrosis factor-alpha in diffuse axonal injury following fluid-percussive brain injury in rats. Int J Legal Med. 113(4): 221-228.

213. Klatzo I, Chui E, Fujiwara K, Spatz M. (1980). Resolution of vasogenic brain edema. Adv Neurol. 28:359-373.

214. Knöferle J, Koch JC, Ostendorf T, Michel U, Planchamp V, Vutova P, Tönges L, Stadelmann C, Brück W, Bähr M, Lingor P. (2010). Mechanisms of acute axonal degeneration in the optic nerve in vivo. Proc Natl Acad Sci U S A. 107(13): 6064-6069.

215. Koch JC, Knöferle J, Tönges L, Ostendorf T, Bähr M, Lingor P. (2010). Acute axonal degeneration in vivo is attenuated by inhibition of autophagy in a calcium-dependent manner. Autophagy. 6(5): 658-659.

216. Koizumi, H, Povlishock, JT. (1998). Posttraumatic hypothermia in the treatment of axonal damage in an animal model of traumatic axonal injury. J. Neurosurg. 89(2): 303–309.

217. Kondo K, Maruishi M, Ueno H, Sawada K, Hashimoto Y, Ohshita T, Takahashi T, Ohtsuki T, Matsumoto M. (2010). The pathophysiology of prospective memory failure after diffuse axonal injury--lesion-symptom analysis using diffusion tensor imaging. BMC Neurosci. Nov 20; 11: 147.

218. Kress GJ, Dineley KE, Reynolds IJ. (2002). The relationship between intracellular free iron and cell injury in cultured neurons, astrocytes, and oligodendrocytes. J Neurosci. 22(14): 5848-5855.

219. Kreutzberg GW. (1996). Principles of neuronal regeneration. Acta Neurochir Suppl. 66: 103-106.

220. Kreutzberg GW. Reaction of the cell body to axonal damage. In: Waxman SG, Kocsis JD, Stys PK, (Eds). The Axon. New York, Oxford: Oxford University Press, 1995; 355-374.

221. Kromer LF. (1987). Nerve growth factor treatment after brain injury prevents neuronal death. Science. 235(4785): 214-216.

222. Kumar R, Saksena S, Husain M, Srivastava A, Rathore RK, Agarwal S, Gupta RK. (2010). Serial changes in diffusion tensor imaging metrics of corpus callosum in moderate traumatic brain injury patients and their correlation with neuropsychometric tests: a 2-year follow-up study. J. Head Trauma Rehabil. 25(1): 31–42.

223. Kupina NC, Nath R, Bernath EE, Inoue J, Mitsuyoshi A, Yuen PW, Wang KK, Hall ED. (2001). The novel calpain inhibitor SJA6017 improves functional outcome after delayed administration in a mouse model of diffuse brain injury. J Neurotrauma. 18(11): 1229-1240.

224. Kurimoto T, Yin Y, Omura K, Gilbert HY, Kim D, Cen LP, Moko L, Kügler S, Benowitz LI. (2010). Long-distance axon regeneration in the mature optic nerve: contributions of oncomodulin, cAMP, and pten gene deletion. J Neurosci. 30(46): 15654-15663.

225. Lambert JM, Lopez EF, Lindsey ML. (2008). Macrophage roles following myocardial infarction. Int J Cardiol. 130(2): 147-158.

226. Lang DA, Teasdale GM, Macpherson P, Lawrence A. (1994). Diffuse brain swelling after head injury: more often malignant in adults than children? J Neurosurg. 80(4): 675-680.

227. LaPlaca MC, Thibault LE. (1998). Dynamic mechanical deformation of neurons triggers an acute calcium response and cell injury involving the N-methyl-D-aspartate glutamate receptor. J Neurosci Res. 52(2): 220-229.

228. Lee AC, Ou Y, Fong D. (2003). Depressed skull fractures: a pattern of abusive head injury in three older children. Child Abuse Negl. 27(11): 1323-1329.

229. Leung AW, Halestrap AP. (2008). Recent progress in elucidating the molecular mechanism of the mitochondrial permeability transition pore. Biochim Biophys Acta. 1777(7-8): 946-952.

230. Levkovitch-Verbin H, Dardik R, Vander S, Nisgav Y, Kalev-Landoy M, Melamed S. (2006). Experimental glaucoma and optic nerve transection induce simultaneous upregulation of proapoptotic and prosurvival genes. Invest Ophthalmol Vis Sci. 47(6): 2491-2497.

231. Levkovitch-Verbin H, Quigley HA, Martin KR, Harizman N, Valenta DF, Pease ME, Melamed S. (2005). The transcription factor c-jun is activated in retinal ganglion cells in experimental rat glaucoma. Exp Eye Res. 80(5): 663-670.

232. Leybaert L, de Hemptinne A. (1996). Changes of intracellular free calcium following mechanical injury in a spinal cord slice preparation. Exp Brain Res. 112(3): 392-402.

233. Li XY, Feng DF. (2009). Diffuse axonal injury: novel insights into detection and treatment. J Clin Neurosci. 16(5): 614–619.

234. Li J, Li XY, Feng DF, Pan DC. (2010). Biomarkers associated with diffuse traumatic axonal injury: exploring pathogenesis, early diagnosis, and prognosis. J Trauma. 69(6): 1610-1618.

235. Liang D, Bhatta S, Gerzanich V, Simard JM. (2007). Cytotoxic edema: mechanisms of pathological cell swelling. Neurosurg Focus. 22 (5):E2.

236. Lieven CJ, Hoegger MJ, Schlieve CR, Levin LA. (2006). Retinal ganglion cell axotomy induces an increase in intracellular superoxide anion. Invest Ophthalmol Vis Sci. 47(4): 1477-1485.

237. Lifshitz J, Kelley BJ, Povlishock JT. (2007). Perisomatic thalamic axotomy after diffuse traumatic brain injury is associated with atrophy rather than cell death. J Neuropathol Exp Neurol. 66(3): 218-229.

238. Lindwall C, Dahlin L, Lundborg G, Kanje M. (2004). Inhibition of c-Jun phosphorylation reduces axonal outgrowth of adult rat nodose ganglia and dorsal root ganglia sensory neurons. Mol Cell Neurosci. 27(3): 267-279.

239. Lindwall C, Kanje M. (2005). Retrograde axonal transport of JNK signaling molecules influence injury induced nuclear changes in p-c-Jun and ATF3 in adult rat sensory neurons. Mol Cell Neurosci. 29(2): 269-282.

240. Lipton ML, Gellella E, Lo C, Gold T, Ardekani BA, Shifteh K, Bello JA, Branch CA. (2008). Multifocal white matter ultrastructural abnormalities in mild traumatic brain injury with cognitive disability: a voxel-wise analysis of diffusion tensor imaging. J Neurotrauma. 25(11): 1335-1342.

241. Liu H, Sun H, Liu C. (2011). Interference of the apoptotic signaling pathway in RGC stress response by SP600125 in moderate ocular hypertensive rats. Chin J Physiol. 54(2): 124-132.

242. Liu K, Tedeschi A, Park KK, He Z. (2011). Neuronal intrinsic mechanisms of axon regeneration. Annu Rev Neurosci. 34:131-152.

243. Liu PH, Tsai HY, Chung YW, Wang YJ, Tseng GF. (2004). The proximity of the lesion to cell bodies determines the free radical risk induced in rat rubrospinal neurons subjected to axonal injury. Anat Embryol (Berl). 207(6): 439-451.

244. Liu PH, Wang YJ, Tseng GF. (2003). Close axonal injury of rubrospinal neurons induced transient perineuronal astrocytic and microglial reaction that coincided with their massive degeneration. Exp Neurol. 179(1): 111-126.

245. LoPachin RM, Lehning EJ. (1997). Mechanism of calcium entry during axon injury and degeneration. Toxicol Appl Pharmacol. 143(2): 233-244.

246. Lu Q, Cui Q, Yip HK, So KF. (2003). c-Jun expression in surviving and regenerating retinal ganglion cells: effects of intravitreal neurotrophic supply. Invest Ophthalmol Vis Sci. 44(12): 5342-5348.

247. Lucas JH, Emery DG, Higgins ML, Gross GW. (1990). Neuronal survival and dynamics of ultrastructural damage after dendrotomy in low calcium. J Neurotrauma. 7(3): 169-192.

248. Lukas TJ, Wang AL, Yuan M, Neufeld AH. (2009). Early cellular signaling responses to axonal injury. Cell Commun Signal. 7:5.

249. Ma M, Matthews BT, Lampe JW, Meaney DF, Shofer FS, Neumar RW. (2009). Immediate short-duration hypothermia provides long-term protection in an in vivo model of traumatic axonal injury. Exp Neurol. 215(1): 119-127.

250. MacAskill AF, Atkin TA, Kittler JT. (2010). Mitochondrial trafficking and the provision of energy and calcium buffering at excitatory synapses. Eur J Neurosci. 32(2): 231-240.

251. Mack TG, Koester MP, Pollerberg GE. (2000). The microtubule-associated protein MAP1B is involved in local stabilization of turning growth cones. Mol Cell Neurosci. 15(1): 51-65.

252. Mack TG, Reiner M, Beirowski B, Mi W, Emanuelli M, Wagner D, Thomson D, Gillingwater T, Court F, Conforti L, Fernando FS, Tarlton A, Andressen C, Addicks K, Magni G, Ribchester RR, Perry VH, Coleman MP. (2001). Wallerian degeneration of injured axons and synapses is delayed by a Ube4b/Nmnat chimeric gene. Nat Neurosci. 4(12): 1199-1206.

253. Mandolesi G, Madeddu F, Bozzi Y, Maffei L, Ratto GM. (2004). Acute physiological response of mammalian central neurons to axotomy: ionic regulation and electrical activity. FASEB J. 18(15): 1934-1936.

254. Manser C, Stevenson A, Banner S, Davies J, Tudor EL, Ono Y, Leigh PN, McLoughlin DM, Shaw CE, Miller CC. (2008). Deregulation of PKN1 activity disrupts neurofilament organisation and axonal transport. FEBS Lett. 582(15): 2303-2308.

255. Marmarou A. (2007) A review of progress in understanding the pathophysiology and treatment of brain edema. Neurosurg Focus. 22(5): E1.

256. Marmarou CR, Povlishock JT. (2006). Administration of the immunophilin ligand FK506 differentially attenuates neurofilament compaction and impaired axonal transport in injured axons following diffuse traumatic brain injury. Exp Neurol. 197(2): 353-362.

257. Maskarinec SA, Wu G, Lee KY. (2005). Membrane sealing by polymers. Ann N Y Acad Sci. 1066: 310-320.

258. Martz D, Garner J, and Lasek RJ. (1989). Protein changes during anterograde-to-retrograde conversion of axonally transported vesicles. Brain Res. 476(1): 199–203.

259. Mata M, Honegger P, Fink DJ. (1997). Modulation of phosphorylation of neuronal cytoskeletal proteins by neuronal depolarization. Cell Mol Neurobiol. 17(1): 129-140.

260. Matsuzaki H, Kunita M, Kawai K. (1982). Optic nerve damage in head trauma: clinical and experimental studies. Jpn J Ophthalmol. 26(4): 447-461.

261. Maxwell WL, Domleo A, McColl G, Jafari SS, Graham DI. (2003). Post-acute alterations in the axonal cytoskeleton after traumatic axonal injury. J Neurotrauma. 20(2): 151-168.

262. Maxwell WL, Graham DI. (1997). Loss of axonal microtubules and neurofilaments after stretch-injury to guinea pig optic nerve fibers. J. Neurotrauma. 14(9): 603-614.

263. Maxwell WL, Irvine A, Adams JH, Graham DI, Gennarelli TA. (1988). Response of cerebral microvasculature to brain injury. J Pathol. 155(4): 327-335.

264. Maxwell WL, Irvine A, Strang RH, Graham DI, Adams JH, Gennarelli TA. (1990). Glycogen accumulation in axons after stretch injury. J. Neurocytol. 19(2): 235–241.

265. Maxwell WL, Irvine A, Watt C, Graham DI, Adams JH, Gennarelli TA. (1991). The microvascular response to stretch injury in the adult guinea pig visual system. J Neurotrauma. Winter; 8(4): 271-279.

266. Maxwell WL, Islam MN, Graham DI, Gennarelli TA. (1994). A qualitative and quantitative analysis of the response of the retinal ganglion cell soma after stretch injury to the adult guinea-pig optic nerve. J Neurocytol. 23(6): 379-392.

267. Maxwell WL, Povlishock JT, Graham DL. (1997). A mechanistic analysis of nondisruptive axonal injury: a review. J. Neurotrauma. 14(7): 419–440.

268. Maxwell WL, Watson A, Queen R, Conway B, Russell D, Neilson M, Graham DI. (2005). Slow, medium, or fast re-warming following post-traumatic hypothermia therapy? An ultrastructural perspective. J. Neurotrauma. 22(8): 873–884.

269. Mbye LH, Singh IN, Carrico KM, Saatman KE, Hall ED. (2009). Comparative neuroprotective effects of cyclosporin A and NIM811, a nonimmunosuppressive cyclosporin A analog, following traumatic brain injury. J Cereb Blood Flow Metab. 29(1): 87-97.

270. McBride RL, Feringa ER, Garver MK, Williams JK Jr. (1990). Retrograde transport of fluoro-gold in corticospinal and rubrospinal neurons 10 and 20 weeks after T-9 spinal cord transection. Exp Neurol. 108(1): 83-85.

271. McClain C, Cohen D, Phillips R, Ott L, Young B. (1991). Increased plasma and ventricular fluid interleukin-6 levels in patients with head injury.J Lab Clin Med. 118(3): 225-231.

272. McCracken E, Hunter AJ, Patel S, Graham DI, Dewar D. (1999). Calpain activation and cytoskeletal protein breakdown in the corpus callosum of head-injured patients. J Neurotrauma. 16(9): 749-761.

273. McDonald CL, Bandtlow C, Reindl M. (2011). Targeting the Nogo receptor complex in diseases of the central nervous system. Curr Med Chem. 18(2): 234-244.

274. McGinn MJ, Kelley BJ, Akinyi L, Oli MW, Liu MC, Hayes RL, Wang KK, Povlishock JT. (2009). Biochemical, structural, and biomarker evidence for calpain-mediated cytoskeletal change after diffuse brain injury uncomplicated by contusion. J Neuropathol Exp Neurol. 68(3): 241-249.

275. McPhail LT, Stirling DP, Tetzlaff W, Kwiecien JM, Ramer MS. (2004). The contribution of activated phagocytes and myelin degeneration to axonal retraction/dieback following spinal cord injury. Eur J Neurosci. 20(8): 1984-1994.

276. McTigue DM, Tripathi R, Wei P, Lash AT. (2007)/ The PPAR gamma agonist Pioglitazone improves anatomical and locomotor recovery after rodent spinal cord injury. Exp Neurol. 205(2): 396-406.

277. Meiri H, Dormann A, Spira ME. (1983). Comparison of ultrastructural changes in proximal and distal segments of transected giant fibers of the cockroach Periplaneta americana. Brain Res. 1263(1): 1-14.

278. Merline M, Kalil K. (1990). Cell death of corticospinal neurons is induced by axotomy before but not after innervation of spinal targets. J Comp Neurol. 296(3): 506-516.

279. Meyer M, Matsuoka I, Wetmore C, Olson L, Thoenen H. (1992). Enhanced synthesis of brain-derived neurotrophic factor in the lesioned peripheral nerve: different mechanisms are responsible for the regulation of BDNF and NGF mRNA. J Cell Biol. 119(1): 45-54.

280. Misra A, Ganesh S, Shahiwala A, Shah SP. (2003). Drug delivery to the central nervous system: a review. J Pharm Pharm Sci. 6(2):252-273. Review.

281. Mohammed Sulaiman A, Denman N, Buchanan S, Porter N, Vesi S, Sharpe R, Graham DI, Maxwell WL. (2011). Stereology and ultrastructure of chronic phase axonal and cell soma pathology in stretch-injured central nerve fibers. J Neurotrauma. 28(3): 383-400.

282. Mondello S, Robicsek SA, Gabrielli A, Brophy GM, Papa L, Tepas J, Robertson C, Buki A, Scharf D, Jixiang M, Akinyi L, Muller U, Wang KK, Hayes RL. (2010). αII-spectrin breakdown products (SBDPs): diagnosis and outcome in severe traumatic brain injury patients. J Neurotrauma. 27(7): 1203-1213.

283. Monnier PP, D'Onofrio PM, Magharious M, Hollander AC, Tassew N, Szydlowska K, Tymianski M, Koeberle PD. (2011). Involvement of caspase-6 and caspase-8 in neuronal apoptosis and the regenerative failure of injured retinal ganglion cells. J Neurosci. 31(29): 10494-10505.

284. Montero M, Alonso MT, Carnicero E, Cuchillo-Ibanez I, Albillos A, Garcia AG, Garcia-Sancho J , Alvarez J. (2000). Chromaffin-cell stimulation triggers fast millimolar mitochondrial Ca2+ transients that modulate secretion. Nat Cell Biol. 2(2): 57–61.

285. Nadal-Nicolás FM, Jiménez-López M, Sobrado-Calvo P, Nieto-López L, Cánovas-Martínez I, Salinas-Navarro M, Vidal-Sanz M, Agudo M. (2009). Brn3a as a marker of retinal ganglion cells: qualitative and quantitative time course studies in naive and optic nerve-injured retinas. Invest Ophthalmol Vis Sci. 50(8): 3860-3868.

286. Nag S, Manias JL, Stewart DJ. (2009). Pathology and new players in the pathogenesis of brain edema. Acta Neuropathol. 118(2): 197-217.

287. Nahrendorf M, Swirski FK, Aikawa E, Stangenberg L, Wurdinger T, Figueiredo JL, Libby P, Weissleder R, Pittet MJ. (2007). The healing myocardium sequentially mobilizes two monocyte subsets with divergent and complementary functions. J Exp Med. 204(12): 3037-3047.

288. Nakagomi S, Suzuki Y, Namikawa K, Kiryu-Seo S, Kiyama H. (2003). Expression of the activating transcription factor 3 prevents c-Jun N-terminal kinase-induced neuronal death by promoting heat shock protein 27 expression and Akt activation. J Neurosci. 23(12): 5187-5196.

289. Naveilhan P, ElShamy WM, Ernfors P. (1997). Differential regulation of mRNAs for GDNF and its receptors Ret and GDNFR alpha after sciatic nerve lesion in the mouse. Eur J Neurosci. 9(7): 1450-1460.

290. Nehrt A, Rodgers R, Shapiro S, Borgens R, Shi R. (2007). The critical role of voltage-dependent calcium channel in axonal repair following mechanical trauma. Neuroscience. 146(4): 1504-1512.

291. Neve LD, Savage AA, Koke JR, García DM. (2012). Activating transcription factor 3 and reactive astrocytes following optic nerve injury in zebrafish. Comp Biochem Physiol C Toxicol Pharmacol. 155(2): 213-218.

292. Newcombe V, Chatfield D, Outtrim J, Vowler S, Manktelow A, Cross J, Scoffings D, Coleman M, Hutchinson P, Coles J, Carpenter TA, Pickard J, Williams G, Menon D. (2011). Mapping traumatic axonal injury using diffusion tensor imaging: correlations with functional outcome. PLoS One. 6(5): e19214.

293. Ng I, Yeo TT, Tang WY, Soong R, Ng PY, Smith DR. (2000). Apoptosis occurs after cerebral contusions in humans. Neurosurgery. 46(4): 949-956.

294. Nicholls DG. (2005). Mitochondria and calcium signaling. Cell Calcium. 38(3-4): 311-317.

295. Nikolaeva MA, Mukherjee B, Stys PK. (2005). Na+-dependent sources of intra-axonal Ca2+ release in rat optic nerve during in vitro chemical ischemia. J Neurosci. 25(43): 9960-9967.

296. O'Connor CA, Cernak I, Johnson F, Vink R. (2007). Effects of progesterone on neurologic and morphologic outcome following diffuse traumatic brain injury in rats. Exp Neurol. 205(1): 145-153.

297. Oda, Y., Gao, G., Wei, E.P., and Povlishock, J.T. (2011). Combinational therapy using hypothermia and the immunophilin ligand FK506 to target altered pial arteriolar

reactivity, axonal damage, and blood–brain barrier dysfunction after traumatic brain injury in rat. J. Cereb. Blood Flow Metab. 31(4): 1143-1154.

298. Odegaard JI, Ricardo-Gonzalez RR, Goforth MH, Morel CR, Subramanian V, Mukundan L, Red Eagle A, Vats D, Brombacher F, Ferrante AW, Chawla A. (2007). Macrophage-specific PPARgamma controls alternative activation and improves insulin resistance. Nature. 447(7148): 1116-1120.

299. Okonkwo DO, Büki A, Siman R, Povlishock JT. (1999). Cyclosporin A limits calcium-induced axonal damage following traumatic brain injury. Neuroreport. 10(2): 353–358.

300. Okonkwo DO, Melon DE, Pellicane AJ, Mutlu LK, Rubin DG, Stone JR, Helm GA. (2003). Dose-response of cyclosporin A in attenuating traumatic axonal injury in rat. Neuroreport. 14(3): 463-466.

301. Okonkwo DO, Pettus EH, Moroi J, Povlishock JT. (1998). Alteration of the neurofilament sidearm and its relation to neurofilament compaction occurring with traumatic axonal injury. Brain Res. 784(1-2): 1-6.

302. Okonkwo DO, Povlishock JT. (1999). An intrathecal bolus of cyclosporin A before injury preserves mitochondrial integrity and attenuates axonal disruption in traumatic brain injury. J Cereb Blood Flow Metab. 19(4): 443-451.

303. Oshima J, Yoshihara T, Tobita S. (2006). Water-induced fluorescence quenching of mono- and dicyanoanilines. Chem. Physics Lett. 423, 306–311.

304. Ouardouz M, Coderre E, Basak A, Chen A, Zamponi GW, Hameed S, Rehak R, Yin X, Trapp BD, Stys PK. (2009a). Glutamate receptors on myelinated spinal cord axons: I. GluR6 kainate receptors. Ann Neurol. 65(2): 51-159.

305. Ouardouz M, Coderre E, Zamponi GW, Hameed S, Yin X, Trapp BD, Stys PK. (2009b). Glutamate receptors on myelinated spinal cord axons: II. AMPA and GluR5 receptors.Ann Neurol. 65(2): 160-166.

306. Oudega M, Vargas CG, Weber AB, Kleitman N, Bunge MB. (1999). Long-term effects of methylprednisolone following transection of adult rat spinal cord. Eur. J. Neurosci. 11, 2453–2464.

307. Palmer HS, Garzon B, Xu J, Berntsen EM, Skandsen T, Håberg AK. (2010). Reduced fractional anisotropy does not change the shape of the hemodynamic response in survivors of severe traumatic brain injury. J Neurotrauma. 27(5): 853-862.

308. Pan S, Ryu SY, Sheu SS. (2011). Distinctive characteristics and functions of multiple mitochondrial Ca2+ influx mechanisms. Sci China Life Sci. 54(8): 763-769.

309. Park KK, Liu K, Hu Y, Smith PD, Wang C, Cai B, Xu B, Connolly L, Kramvis I, Sahin M, He Z. (2008). Promoting axon regeneration in the adult CNS by modulation of the PTEN/mTOR pathway. Science. 322(5903): 963-966.

310. Park SY, Ferreira A. (2005). The generation of a 17 kDa neurotoxic fragment: an alternative mechanism by which tau mediates beta-amyloid-induced neurodegeneration. J Neurosci. 25(22): 5365-5375.

311. Pearson AG, Gray CW, Pearson JF, Greenwood JM, During MJ, Dragunow M. (2003). ATF3 enhances c-Jun-mediated neurite sprouting. Brain Res Mol Brain Res. 120(1): 38-45.

312. Peinado-Ramon P, Salvador M, Villegas-Perez MP, Vidal-Sanz M. (1996). Effects of axotomy and intraocular administration of NT-4, NT-3, and brain-derived neurotrophic factor on the survival of adult rat retinal ganglion cells. A quantitative in vivo study. Invest Ophthalmol Vis Sci. 37(4): 489–500.

313. Perlson E, Hanz S, Medzihradszky KF, Burlingame AL, Fainzilber M. (2004). From snails to sciatic nerve: Retrograde injury signaling from axon to soma in lesioned neurons. J Neurobiol. 58(2): 287-294.

314. Perry VH, Brown MC, Lunn ER, Tree P, Gordon S. (1990). Evidence that Very Slow Wallerian Degeneration in C57BL/Ola Mice is an Intrinsic Property of the Peripheral Nerve. Eur J Neurosci. 2(9): 802-808.

315. Pettus EH, Christman CW, Giebel ML, Povlishock JT. (1994). Traumatically induced altered membrane permeability: its relationship to traumatically induced reactive axonal change. J Neurotrauma. 11(5): 507-522.

316. Pettus EH, Povlishock JT. (1996). Characterization of a distinct set of intra-axonal ultrastructural changes associated with traumatically induced alteration in axolemmal permeability. Brain Res. 722(1-2): 1-11.

317. Piehl F, Hammarberg H, Tabar G, Hökfelt T, Cullheim S. (1998). Changes in the mRNA expression pattern, with special reference to calcitonin gene-related peptide, after axonal injuries in rat motoneurons depends on age and type of injury. Exp Brain Res. 119(2): 191-204.

318. Phillips LL, Lyeth BG, Hamm RJ, Povlishock JT. (1994). Combined fluid percussion brain injury and entorhinal cortical lesion: a model for assessing the interaction between neuroexcitation and deafferentation. J Neurotrauma. 11(6): 641-656.

319. Phillips LL, Reeves TM. (2001). Interactive pathology following traumatic brain injury modifies hippocampal plasticity. Restor Neurol Neurosci. 19(3-4): 213-235.

320. Pike BR, Flint J, Dutta S, Johnson E, Wang KK, Hayes RL. (2001). Accumulation of non-erythroid alpha II-spectrin and calpain-cleaved alpha II-spectrin breakdown products in cerebrospinal fluid after traumatic brain injury in rats. J Neurochem. 78(6): 1297-1306.

321. Pineda JA, Lewis SB, Valadka AB, Papa L, Hannay HJ, Heaton SC, Demery JA, Liu MC, Aikman JM, Akle V, Brophy GM, Tepas JJ, Wang KK, Robertson CS, Hayes RL. (2007). Clinical significance of alphaII-spectrin breakdown products in cerebrospinal fluid after severe traumatic brain injury. J Neurotrauma. 24(2): 354-366.

322. Pittella JE, Gusmao SN. (2003). Diffuse vascular injury in fatal road traffic accident victims: its relationship to diffuse axonal injury. J Forensic Sci 48: 626–630.

323. Pivovarova NB, Andrews SB. (2010). Calcium-dependent mitochondrial function and dysfunction in neurons. FEBS J. 277(18): 3622-3636.

324. Pivovarova NB, Hongpaisan J, Andrews SB, Friel DD. (1999). Depolarization-induced mitochondrial Ca accumulation in sympathetic neurons: spatial and temporal characteristics. J Neurosci. 19(15): 6372–6384.

325. Plunet W, Kwon BK, Tetzlaff W. (2002). Promoting axonal regeneration in the central nervous system by enhancing the cell body response to axotomy. J Neurosci Res. 68(1): 1-6.

326. Povlishock JT. (1992). Traumatically induced axonal injury: pathogenesis and pathobiological implications. Brain Pathol. 2(1): 1-12.

327. Povlishock JT, Becker DP, Cheng CL, Vaughan GW. (1983). Axonal change in minor head injury. J. Neuropathol. Exp. Neurol. 42(3): 225-242.

328. Povlishock JT, Becker DP, Sullivan HG, Miller JD. (1978). Vascular permeability alterations to horseradish peroxidase in experimental brain injury. Brain Res. 153, 223–239.

329. Povlishock JT, Christman CW. (1995). The pathobiology of traumatically induced axonal injury in animals and humans: a review of current thoughts. J. Neurotrauma 12(4), 555-564.

330. Povlishock JT, Erb DE, Astruc J. (1992). Axonal response to traumatic brain injury: reactive axonal change, deafferentation, and neuroplasticity. J Neurotrauma. 9 Suppl 1:S189-200.

331. Povlishock JT, Katz DI. (2005). Update of neuropathology and neurological recovery after traumatic brain injury. J. Head Trauma Rehabil. 20(1): 76–94.

332. Povlishock JT, Kontos HA. (1985). Continuing axonal and vascular change following experimental brain trauma. Cent. Nerv. Syst. Trauma 2(4): 285–298.

333. Povlishock JT, Marmarou A, McIntosh T, Trojanowski JQ, Moroi J. (1997). Impact acceleration injury in the rat: evidence for focal axolemmal change and related neurofilament sidearm alteration. J Neuropathol Exp Neurol. 56(4): 347-59.

334. Pozzo-Miller LD, Pivovarova NB, Leapman RD, Buchanan RA, Reese TS, Andrews SB. (1997). Activity- dependent calcium sequestration in dendrites of hippocampal neurons in brain slices. J Neurosci 17(22): 8729-8738.

335. Prilloff S, Henrich-Noack P, Kropf S, Sabel BA. (2010). Experience-dependent plasticity and vision restoration in rats after optic nerve crush. J Neurotrauma. 27(12): 2295-2307.

336. Qiu J, Cai D, Dai H, McAtee M, Hoffman PN, Bregman BS, Filbin MT. (2002). Spinal axon regeneration induced by elevation of cyclic AMP. Neuron. 34(6): 895-903.

337. Quigley HA, Cone FE, Gelman SE, Yang Z, Son JL, Oglesby EN, Pease ME, Zack DJ. (2011). Lack of neuroprotection against experimental glaucoma in c-Jun N-terminal kinase 3 knockout mice. Exp Eye Res. 92(4): 299-305.

338. Raivich G. (2008). c-Jun expression, activation and function in neural cell death, inflammation and repair. J Neurochem. 107(4): 898-906.

339. Raivich G, Bohatschek M, Da Costa C, Iwata O, Galiano M, Hristova M, Nateri AS, Makwana M, Riera-Sans L, Wolfer DP, Lipp HP, Aguzzi A, Wagner EF, Behrens A. (2004). The AP-1 transcription factor c-Jun is required for efficient axonal regeneration. Neuron. 43(1): 57-67.

340. Ramon y Cajal S. Degeneration and Regeneration of the Nervous System. Vol. 5. New York: Oxford University Press; 1991.

341. Reeves TM, Greer JE, Vanderveer AS, Phillips LL. (2010). Proteolysis of submembrane cytoskeletal proteins ankyrin-G and αII-spectrin following diffuse brain injury: a role in white matter vulnerability at Nodes of Ranvier. Brain Pathol. 20(6): 1055-1068.

342. Reeves TM, Phillips LL, Lee NN, Povlishock JT. (2007). Preferential neuroprotective effect of tacrolimus (FK506) on unmyelinated axons following traumatic brain injury. Brain Res. 1154: 225-236.

343. Reeves TM, Phillips LL, Povlishock JT. (2005). Myelinated and unmyelinated axons of the corpus callosum differ in vulnerability and functional recovery following traumatic brain injury. Exp Neurol. 196(1): 126-137.

344. Reeves TM, Prins ML, Zhu J, Povlishock JT, Phillips LL. (2003). Matrix metalloproteinase inhibition alters functional and structural correlates of deafferentation-induced sprouting in the dentate gyrus. J Neurosci. 23(32): 10182-10189.

345. Reichard RR, Smith C, Graham DI. (2005). The significance of beta-APP immunoreactivity in forensic practice. Neuropathol. Appl. Neurobiol. 31(3): 304–313.

346. Reichert F, Rotshenker S. (1999). Galectin-3/MAC-2 in experimental allergic encephalomyelitis. Exp Neurol. 160(2): 508-514.

347. Ribas VT, Arruda-Carvalho M, Linden R, Chiarini LB. (2011). Early c-Jun N-terminal kinase-dependent phosphorylation of activating transcription factor-2 is associated with degeneration of retinal ganglion cells. Neuroscience. 180:64-74.

348. Richard M. Rubin. (2005). Chapter 26: Traumatic optic neuropathy. Neuro-ophthalmology: the practical guide By Leonard A. Levin. And Anthony C. Arnold. Thieme Medical Publishers, Inc. PP246-252.

349. Ringger NC, O'Steen BE, Brabham JG, Silver X, Pineda J, Wang KK, Hayes RL, Papa L. (2004). A novel marker for traumatic brain injury: CSF alphaII-spectrin breakdown product levels. J Neurotrauma. 21(10): 1443-1456.

350. Roberts-Lewis JM, Savage MJ, Marcy VR, Pinsker LR, Siman R. (1994). Immunolocalization of calpain I-mediated spectrin degradation to vulnerable neurons in the ischemic gerbil brain. J. Neurosci. 14(6): 3934-3944.

351. Robinson GA. (1994). Immediate early gene expression in axotomized and regenerating retinal ganglion cells of the adult rat. Brain Res Mol Brain Res. 24(1-4): 43-54.

352. Robinson GA. (1995). Axotomy-induced regulation of c-Jun expression in regenerating rat retinal ganglion cells. Brain Res Mol Brain Res. 30(1): 61-69.

353. Rosenberg LJ, Emery DG, Lucas JH. (2001). Effects of sodium and chloride on neuronal survival after neurite transection. J Neuropathol Exp Neurol. 60(1): 33-48.

354. Rosenberg GA, Yang Y. (2007). Vasogenic edema due to tight junction disruption by matrix metalloproteinases in cerebral ischemia. Neurosurg Focus. 22(5): E4. Review.

355. Ross DE. (2011). Review of longitudinal studies of MRI brain volumetry in patients with traumatic brain injury. Brain Inj. 25(13-14): 1271-1278.

356. Rousseau V, Engelmann R, Sabel BA. (1999). Restoration of vision III: Soma swelling dynamics predicts neuronal death or survival after optic nerve crush in vivo. Neuroreport, 10(16): 3387–3391.

357. Rousseau V, Sabel BA. (2001). Restoration of vision IV: Compensatory soma size increase of retinal ganglion cells predicts recovery of vision after partial optic nerve crush. Restorative Restor Neurol Neurosci.18(4): 177–189.

358. Rumiantsev IuV, Bessmertnyĭ MZ, Vinogradov EV, Khisametdinova AI. (1981). Unilateral lesion of the optic nerve in cranio-cerebral injuries. [Article in Russian] Zh Vopr Neirokhir Im N N Burdenko. Jan-Feb; (1): 8-12.

359. Sahenk Z, Lasek RJ. (1988). Inhibition of proteolysis blocks anterograde-retrograde conversion of axonally transported vesicles. Brain Res. 460(1): 199–203.

360. Saatman KE, Abai B, Grosvenor A, Vorwerk CK, Smith DH, Meaney DF. (2003).Traumatic axonal injury results in biphasic calpain activation and retrograde transport impairment in mice. J Cereb Blood Flow Metab. 23(1): 34-42.

361. Saatman KE, Bozyczko-Coyne D, Marcy V, Siman R, McIntosh TK. (1996). Prolonged calpain-mediated spectrin breakdown occurs regionally following experimental brain injury in the rat. J Neuropathol Exp Neurol. 55(7): 850-860.

362. Saatman KE, Creed J, Raghupathi R. (2010). Calpain as a therapeutic target in traumatic brain injury. Neurotherapeutics. 7(1): 31-42.

363. Saatman KE, Graham DI, McIntosh TK. (1998). The neuronal cytoskeleton is at risk after mild and moderate brain injury. J Neurotrauma. 15(12): 1047-1058.

364. Saatman KE, Serbest G, Burkhardt MF. (2009). Axonal damage due to traumatic brain injury, in: Handbook of Neurochemistry and Molecular Neurobiology: Brain and Spinal Cord Trauma. N.L. Banik, A. Lajtha, S.K. Ray (eds). New York: Springer, pps. 343–361.

365. Sabel BA, Henrich-Noack P, Fedorov A, Gall C. (2011).Vision restoration after brain and retina damage: the "residual vision activation theory".Prog Brain Res. 192:199-262.

366. Sadkowski PJ, Fleming GR. (1980). The influence of solvent-solute interaction on radiationless processes: excited state dynamics of anilinonaphthalene sulphonate and related molecules. Chem. Phys. 54, 79–89.

367. Sahenk Z, Lasek RJ. (1988). Inhibition of proteolysis blocks anterograde-retrograde conversion of axonally transported vesicles. Brain Res. 460(1): 199–203.

368. Saijilafu, Hur EM, Zhou FQ. (2011). Genetic dissection of axon regeneration via in vivo electroporation of adult mouse sensory neurons. Nat Commun. 2: 543.

369. Samsam M, Mi W, Wessig C, Zielasek J, Toyka KV, Coleman MP, Martini R. (2003). The Wlds mutation delays robust loss of motor and sensory axons in a genetic model for myelin-related axonopathy. J Neurosci. 23(7): 2833-2839.

370. Sarkies N. (2004). Traumatic optic neuropathy. Eye (Lond). 18(11): 1122-1125.

371. Saul KE, Koke JR, García DM. (2010). Activating transcription factor 3 (ATF3) expression in the neural retina and optic nerve of zebrafish during optic nerve regeneration. Comp Biochem Physiol A Mol Integr Physiol. 155(2): 172-182.

372. Schonberg DL, Popovich PG, McTigue DM. (2007). Oligodendrocyte generation is differentially influenced by toll-like receptor (TLR) 2 and TLR4-mediated intraspinal macrophage activation. J Neuropathol Exp Neurol. 66(12): 1124-1135.

373. Schumacher PA, Siman RG, Fehlings MG. (2000). Pretreatment with calpain inhibitor CEP-4143 inhibits calpain I activation and cytoskeletal degradation, improves neurological function, and enhances axonal survival after traumatic spinal cord injury. J Neurochem. 74(4): 1646-1655.

374. Seif GI, Nomura H, Tator CH. (2007). Retrograde axonal degeneration "dieback" in the corticospinal tract after transection injury of the rat spinal cord: a confocal microscopy study. J Neurotrauma. 24(9): 1513-1528.

375. Seijffers R, Mills CD, Woolf CJ. (2007). ATF3 increases the intrinsic growth state of DRG neurons to enhance peripheral nerve regeneration. J Neurosci. 27(30): 7911-7920.

376. Seliskar CJ, Brand L. (1971). Electronic spectra of 2-aminonaphthalene-6-sulfonate and related molecules. I. General properties and excited-state reactions. J. Am. Chem. Soc. 93, 5405–5414.

377. Seniuk N, Altares M, Dunn R, Richardson PM. (1992). Decreased synthesis of ciliary neurotrophic factor in degenerating peripheral nerves. Brain Res. 572(1-2): 300-302.

378. Serbest G, Burkhardt MF, Siman R, Raghupathi R, Saatman KE. (2007). Temporal profiles of cytoskeletal protein loss following traumatic axonal injury in mice. Neurochem Res. 32(12): 2006-2014.

379. Serbest G, Horwitz J, Barbee K. (2005). The effect of poloxamer-188 on neuronal cell recovery from mechanical injury. J Neurotrauma. 22(1): 119-132.

380. Serbest G, Horwitz J, Jost M, Barbee K. (2006). Mechanisms of cell death and neuroprotection by poloxamer 188 after mechanical trauma. FASEB J. 20(2): 308-310.

381. Shadiack AM, Sun Y, Zigmond RE. (2001). Nerve growth factor antiserum induces axotomy-like changes in neuropeptide expression in intact sympathetic and sensory neurons. J Neurosci. 21(2): 363-371.

382. Shafer LL, McNulty JA, Young MR. (2002-2003). Brain activation of monocyte-lineage cells: involvement of interleukin-6. Neuroimmunomodulation. 10(5): 295-304.

383. Shagin DA, Barsova EV, Yanushevich YG, Fradkov AF, Lukyanov KA, Labas YA, Semenova TN, Ugalde JA, Meyers A, Nunez JM, Widder EA, Lukyanov SA, Matz MV.

(2004). GFP-like proteins as ubiquitous metazoan superfamily: evolution of functional features and structural complexity. Mol. Biol. Evol. 21(5): 841–850.

384. Sherriff FE, Bridges LR, Gentleman SM, Sivaloganathan S, Wilson S. (1994a). Markers of axonal injury in post mortem human brain. Acta Neuropathol. 88(5): 433–439.

385. Sherriff FE, Bridges LR, Sivaloganathan S. (1994b). Early detection of axonal injury after human head trauma using immunocytochemistry for beta-amyloid precursor protein. Acta Neuropathol. 87(1): 55–62.

386. Signoretti S, Marmarou A, Tavazzi B, Lazzarino G, Beaumont A, Vagnozzi R. (2001). N-Acetylaspartate reduction as a measure of injury severity and mitochondrial dysfunction following diffuse traumatic brain injury. J Neurotrauma. 18(10): 977-991.

387. Siman R, Baudry M, Lynch G. (1984). Brain fodrin: substrate for calpain I, an endogenous calcium-activated protease. Proc Natl Acad Sci U S A. 81(11): 3572-3576.

388. Singleton RH, Povlishock JT. (2004). Identification and characterization of heterogeneous neuronal injury and death in regions of diffuse brain injury: evidence for multiple independent injury phenotypes. J Neurosci. 24(14): 3543-3553.

389. Singleton RH, Stone JR, Okonkwo DO, Pellicane AJ, Povlishock JT. (2001). The immunophilin ligand FK506 attenuates axonal injury in an impact-acceleration model of traumatic brain injury. J Neurotrauma. 18(6): 607-614.

390. Singleton RH, Zhu J, Stone JR, Povlishock JT. (2002). Traumatically induced axotomy adjacent to the soma does not result in acute neuronal death. J Neurosci. 22(3): 791-802.

391. Sofroniew MV, Howe CL, Mobley WC. (2001). Nerve growth factor signaling, neuroprotection, and neural repair. Annu Rev Neurosci. 24: 1217-1281.

392. Sprecher SG, Desplan C. (2008). Switch of rhodopsin expression in terminally differentiated Drosophila sensory neurons. Nature. 454(7203), 533–537.

393. Springer JE, Azbill RD, Kennedy SE, George J, Geddes JW. (1997). Rapid calpain I activation and cytoskeletal protein degradation following traumatic spinal cord injury: attenuation with riluzole pretreatment. J Neurochem. 69(4): 1592-600.

394. Staal JA, Dickson TC, Chung RS, Vickers JC. (2007). Cyclosporin-A treatment attenuates delayed cytoskeletal alterations and secondary axotomy following mild axonal stretch injury. Dev Neurobiol. 67(14): 1831-1842.

395. Starkov AA. (2010). The molecular identity of the mitochondrial Ca2+ sequestration system. FEBS J 277: 3652–3663.

396. Stirling DP, Khodarahmi K, Liu J, McPhail LT, McBride CB, Steeves JD, Ramer MS, Tetzlaff W. (2004). Minocycline treatment reduces delayed oligodendrocyte death, attenuates axonal dieback, and improves functional outcome after spinal cord injury. J Neurosci. 24(9): 2182-2190.

397. Stirling DP, Stys PK. (2010). Mechanisms of axonal injury: internodal nanocomplexes and calcium deregulation. Trends Mol Med. 16(4): 160-170.

398. Stone JR, Singleton RH, Povlishock JT. (2000). Antibodies to the C-terminus of the beta-amyloid precursor protein (APP): A site specific marker for the detection of traumatic axonal injury. Brain Res. 871(2): 288–302.

399. Stone JR, Walker SA, Povlishock JT. (1999). The visualization of a new class of traumatically injured axons through the use of a modified method of microwave antigen retrieval. Acta Neuropathol. 97(4): 335–345.

400. Strautman AF, Cork RJ, Robinson KR. (1990). The distribution of free calcium in transected spinal axons and its modulation by applied electrical fields. J Neurosci. 10(11): 3564-3575.

401. Strich SJ. (1956). Diffuse degeneration of the cerebral white matter in severe dementia following head injury.J Neurol Neurosurg Psychiatry. 19(3): 163-185.

402. Strittmatter SM, Igarashi M, Fishman MC. (1994). GAP-43 amino terminal peptides modulate growth cone morphology and neurite outgrowth. J Neurosci. 14(9): 5503-5513.

403. Stys PK. (2005). General mechanisms of axonal damage and its prevention. J Neurol Sci. 233(1-2): 3-13.

404. Sun F, Park KK, Belin S, Wang D, Lu T, Chen G, Zhang K, Yeung C, Feng G, Yankner BA, He Z. (2011). Sustained axon regeneration induced by co-deletion of PTEN and SOCS3. Nature. 480(7377): 372-375.

405. Sun H, Wang Y, Pang IH, Shen J, Tang X, Li Y, Liu C, Li B. (2011). Protective effect of a JNK inhibitor against retinal ganglion cell loss induced by acute moderate ocular hypertension. Mol Vis. 17: 864-875.

406. Susarla BT, Laing ED, Yu P, Katagiri Y, Geller HM, Symes AJ. (2011). Smad proteins differentially regulate transforming growth factor-β-mediated induction of chondroitin sulfate proteoglycans. J Neurochem. 119(4): 868-878.

407. Sutton RL, Lescaudron L, Stein DG. (1993). Unilateral cortical contusion injury in the rat: vascular disruption and temporal development of cortical necrosis. J Neurotrauma. Summer; 10(2): 135-149.

408. Taft WC, Yang K, Dixon CE, Hayes RL. (1992). Microtubule-associated protein 2 levels decrease in hippocampus following traumatic brain injury. J Neurotrauma. 9(3): 281-290.

409. Takeda M, Kato H, Takamiya A, Yoshida A, Kiyama H. (2000). Injury-specific expression of activating transcription factor-3 in retinal ganglion cells and its colocalized expression with phosphorylated c-Jun. Invest Ophthalmol Vis Sci. 41(9): 2412-2421.

410. Tetzlaff W, Alexander SW, Miller FD, Bisby MA.(1991).Response of facial and rubrospinal neurons to axotomy: changes in mRNA expression for cytoskeletal proteins and GAP-43. J Neurosci. 11(8): 2528-2544.

411. Thiagarajan P, Ciuffreda KJ, Ludlam DP. (2011). Vergence dysfunction in mild traumatic brain injury (mTBI): a review. Ophthalmic Physiol Opt. 31(5): 456-468.

412. Thompson SN, Gibson TR, Thompson BM, Deng Y, Hall ED. (2006). Relationship of calpain-mediated proteolysis to the expression of axonal and synaptic plasticity markers following traumatic brain injury in mice. Exp Neurol. 201(1): 253-265.

413. Thomas Zampieri. Blinded veterans association testimony. 2007 Oct. 4. P2.

414. Tobita S, Ida K, Shiobara S. (2001). Water-induced fluorescence quenching of aniline and its derivatives in aqueous solution. Res. Chem. Intermed. 27, 205–218.

415. Tokushige H, Waki M, Takayama Y, Tanihara H. (2011). Effects of Y-39983, a selective Rho-associated protein kinase inhibitor, on blood flow in optic nerve head in rabbits and axonal regeneration of retinal ganglion cells in rats. Curr Eye Res. 36(10): 964-970.

416. Tomaiuolo F, Bivona U, Lerch JP, Di Paola M, Carlesimo A, Ciurli P, Matteis M, Cecchetti L, Forcina A, Silvestro D, Azicnuda E, Sabatini U, Di Giacomo D, Caltagirone C, Petrides M, Formisano R. (2012). Memory and anatomical change in severe traumatic brain injury: ~1 vs. ~8yr follow-up. Brain Res Bull. 87(4-5): 373-382.

417. Toyooka T, Nawashiro H, Shinomiya N, Shima K. (2011). Down-regulation of glial fibrillary acidic protein and vimentin by RNA interference improves acute urinary dysfunction associated with spinal cord injury in rats. J Neurotrauma. 28(4): 607-618.

418. Traumatic Brain Injury in the United States: Emergency Department Visits, Hospitalizations and Deaths 2002-2006. Available at: http://www.cdc.gov/traumaticbraininjury/tbi_ed.html. Accessed by November 10, 2012

419. Traumatic Brain Injury: Pages 307–353; Chapter 9. Rehabilitation and Management of Visual Dysfunction Following Traumatic Brain Injury 2010. Edited by Mark J . Ashley Sc.D CRC Press 2010. Print ISBN: 978-1-4200-7194-8

420. Tuck E, Cavalli V. (2010). Roles of membrane trafficking in nerve repair and regeneration. Commun Integr Biol. 3(3): 209-214.

421. Unterberg AW, Stover J, Kress B, Kiening KL. (2004). Edema and brain trauma. Neuroscience. 129(4): 1021-1029.

422. Vallières N, Berard JL, David S, Lacroix S. (2006). Systemic injections of lipopolysaccharide accelerates myelin phagocytosis during Wallerian degeneration in the injured mouse spinal cord. Glia. 53(1): 103-113.

423. Venkatesan C, Chrzaszcz M, Choi N, Wainwright MS. (2010). Chronic upregulation of activated microglia immunoreactive for galectin-3/Mac-2 and nerve growth factor following diffuse axonal injury. J Neuroinflammation. 7: 32.

424. Vidal-Sanz M, Bray GM, Villegas-Pérez MP, Thanos S, Aguayo AJ. (1987). Axonal regeneration and synapse formation in the superior colliculus by retinal ganglion cells in the adult rat. J Neurosci. 7(9): 2894-2909.

425. Villanueva CJ, Tontonoz P. (2010). Licensing PPARγ to work in macrophages. Immunity. 33(5): 647-649.

426. Vinit S, Darlot F, Aoulaïche H, Boulenguez P, Kastner A. (2011). Distinct expression of c-Jun and HSP27 in axotomized and spared bulbospinal neurons after cervical spinal cord injury. J Mol Neurosci. 45(2): 119-133.

427. Vink R, Young A, Bennett CJ, Hu X, Connor CO, Cernak I, Nimmo AJ. (2003). Neuropeptide release influences brain edema formation after diffuse traumatic brain injury. Acta Neurochir Suppl. 86: 257-260.

428. von Reyn CR, Spaethling JM, Mesfin MN, Ma M, Neumar RW, Smith DH, Siman R, Meaney DF. (2009). Calpain mediates proteolysis of the voltage-gated sodium channel alpha-subunit. J Neurosci. 29(33): 10350-10356.

429. Waldmeier PC, Feldtrauer JJ, Qian T, Lemasters JJ. (2002). Inhibition of the mitochondrial permeability transition by the nonimmunosuppressive cyclosporin derivative NIM811. Mol Pharmacol. 62(1): 22-29.

430. Walther M, Kuklinski S, Pesheva P, Guntinas-Lichius O, Angelov DN, Neiss WF, Asou H, Probstmeier R. (2000). Galectin-3 is upregulated in microglial cells in response to ischemic brain lesions, but not to facial nerve axotomy. J Neurosci Res. 61(4): 430-435.

431. Wang JY, Bakhadirov K, Devous MD Sr, Abdi H, McColl R, Moore C, Marquez de la Plata CD, Ding K, Whittemore A, Babcock E, Rickbeil T, Dobervich J, Kroll D, Dao B, Mohindra N, Madden CJ, Diaz-Arrastia R. (2008). Diffusion tensor tractography of traumatic diffuse axonal injury. Arch. Neurol. 65(5): 619–626.

432. Wang J, Hamm RJ, Povlishock JT. (2011).Traumatic axonal injury in the optic nerve: evidence for axonal swelling, disconnection, dieback, and reorganization. J Neurotrauma. 28(7):1185-1198.

433. Wang J, He Z. (2009). NAD and axon degeneration: from the Wlds gene to neurochemistry. Cell Adh Migr. 3(1):77-87.

434. Wang KK, Posmantur R, Nath R, McGinnis K, Whitton M, Talanian RV, Glantz SB, Morrow JS.(1998). Simultaneous degradation of alphaII- and betaII-spectrin by caspase 3 (CPP32) in apoptotic cells. J Biol Chem. 273(35): 22490-22497.

435. Wang MS, Davis AA, Culver DG, Wang Q, Powers JC, Glass JD. (2004). Calpain inhibition protects against Taxol-induced sensory neuropathy. Brain. 127(Pt 3): 671-679.

436. Warner MA, Youn TS, Davis T, Chandra A, Marquez de la Plata C, Moore C, Harper C, Madden CJ, Spence J, McColl R, Devous M, King RD, Diaz-Arrastia R. (2010). Regionally selective atrophy after traumatic axonal injury. Arch Neurol. 67(11): 1336-1344.

437. Weber JT, Rzigalinski BA, Ellis EF. (2001). Traumatic injury of cortical neurons causes changes in intracellular calcium stores and capacitative calcium influx. J Biol Chem. 276(3): 1800-1807.

438. Weber JT, Rzigalinski BA, Willoughby KA, Moore SF, Ellis EF. (1999). Alterations in calcium-mediated signal transduction after traumatic injury of cortical neurons. Cell Calcium. 26(6): 289-299.

439. What are the Leading Causes of TBI? Available at: http://www.cdc.gov/traumaticbraininjury/causes.html. Accessed by November 10, 2012.

440. Whitmarsh AJ, Kuan CY, Kennedy NJ, Kelkar N, Haydar TF, Mordes JP, Appel M, Rossini AA, Jones SN, Flavell RA, Rakic P, Davis RJ. (2001). Requirement of the JIP1 scaffold protein for stress-induced JNK activation. Genes Dev. 15(18):2421-2432.

441. Wolf JA, Stys PK, Lusardi T, Meaney D, Smith DH. (2001). Traumatic axonal injury induces calcium influx modulated by tetrodotoxin-sensitive sodium channels. J Neurosci. 21(6):1923-1930.

442. Wong J, Hoe NW, Zhiwei F, Ng I. (2005). Apoptosis and traumatic brain injury. Neurocrit Care. 3(2):177-182. Review.

443. Wu HY, Lynch DR. (2006). Calpain and synaptic function. Mol Neurobiol. 33(3): 215–236.

444. Xia Y, Wang J, Zhang Y, Song L, Ye J, Yang G, Tan K. (2012). Quantum dot based turn-on fluorescent probes for anion sensing. Nanoscale. 4(19): 5954-5959.

445. Xiang M, Zhou L, Macke JP, Yoshioka T, Hendry SH, Eddy RL, Shows TB, Nathans J. (1995). The Brn-3 family of POU-domain factors: primary structure, binding specificity, and expression in subsets of retinal ganglion cells and somatosensory neurons. J Neurosci. 15(7 Pt 1): 4762-4785.

446. Xie XY, Barrett JN. (1991). Membrane resealing in cultured rat septal neurons after neurite transection: evidence for enhancement by Ca(2+)-triggered protease activity and cytoskeletal disassembly. J Neurosci. 11(10): 3257-3267.

447. Yaghmai A, Povlishock J. (1992). Traumatically induced reactive change as visualized through the use of monoclonal antibodies targeted to neurofilament subunits. J. Neuropathol. Exp. Neurol. 51(2): 158-176.

448. Yang Y, Rosenberg GA. (2011). MMP-mediated disruption of claudin-5 in the blood-brain barrier of rat brain after cerebral ischemia. Methods Mol Biol. 762:333-345.

449. Yasuda J, Whitmarsh AJ, Cavanagh J, Sharma M, Davis RJ. (1999). The JIP group of mitogen-activated protein kinase scaffold proteins. Mol Cell Biol. 19(10): 7245-7254.

450. Yawo H, Kuno M. (1985). Calcium dependence of membrane sealing at the cut end of the cockroach giant axon. J Neurosci. 5(6): 1626-1632.

451. Yin Y, Cui Q, Li Y, Irwin N, Fischer D, Harvey AR, Benowitz LI. (2003). Macrophage-derived factors stimulate optic nerve regeneration. J Neurosci. 23(6): 2284-2293.

452. Yin Y, Henzl MT, Lorber B, Nakazawa T, Thomas TT, Jiang F, Langer R, Benowitz LI. (2006). Oncomodulin is a macrophage-derived signal for axon regeneration in retinal ganglion cells. Nat Neurosci. 9(6): 843-852.

453. Yoshimura K, Ueno M, Lee S, Nakamura Y, Sato A, Yoshimura K, Kishima H, Yoshimine T, Yamashita T. (2011).C-Jun N-terminal kinase induces axonal degeneration and limits motor recovery after spinal cord injury in mice. Neurosci Res. 71(3): 266-277.

454. Yrjänheikki J, Keinänen R, Pellikka M, Hökfelt T, Koistinaho J. (1998). Tetracyclines inhibit microglial activation and are neuroprotective in global brain ischemia. Proc Natl Acad Sci U S A. 95(26): 15769-15774.

455. Yune TY, Lee JY, Jung GY, Kim SJ, Jiang MH, Kim YC, Oh YJ, Markelonis GJ, Oh TH. (2007). Minocycline alleviates death of oligodendrocytes by inhibiting pro-nerve growth factor production in microglia after spinal cord injury. J Neurosci. 27(29): 7751-7761.

456. Zampieri T. Blinded veterans association testimony. October 4, 2007. Available at: http://www.eyeresearch.org/pdf/1004_zampieri_testimony.pdf. Accessed July 28, 2012.

457. Zemlan FP, Rosenberg WS, Luebbe PA, Campbell TA, Dean GE, Weiner NE, Cohen JA, Rudick RA, Woo D. (1999). Quantification of axonal damage in traumatic brain injury: affinity purification and characterization of cerebrospinal fluid tau proteins. J Neurochem. 72(2): 741-750.

458. Zhang XP, Ambron RT. (2000). Positive injury signals induce growth and prolong survival in Aplysia neurons. J. Neurobiol. 45(2): 84 - 94.

459. Zhilin G, Huoniu O, Zhihua C, Guorong D. (2011). Wide optic nerve canal decompression for the treatment of blindness resulting from an indirect optic nerve injury. J Craniofac Surg. 22(4):1463-1465.

460. Zimmerman R A, Bilaniuk LI. (1982). Computed tomographic staging of traumatic epidural bleeding. Radiology, 144(4): 809–812.

Vita

Jiaqiong Wang was born on January 26, 1980, in Huangzhou, Hubei, China, and is a Chinese citizen. She graduated from Huanggang Middle School, Huangzhou, Hubei, China in 1998. She received her Bachelor of Medicine in China from Tongji Medical College of Huazhong University of Science and Technology in 2003. She subsequently received her Master of Science in China from Nanjing Medical University in 2006.